Universität Rostock

Traditio et Innovatio

PH.D. THESIS ON THE SUBJECT OF

ARM ENERGY BALANCING TECHNIQUES FOR MODULAR MULTILEVEL CONVERTER FOR BOTH EQUAL AND UNEQUAL FREQUENCIES OPERATIONS

Dissertation

zur

Erlangung des akademischen Grades

Doktor-Ingenieur (Dr.-Ing.)

der Fakultät für Informatik und Elektrotechnik

der Universität Rostock

vorgelegt von

M.Sc. Gyanendra Kumar Sah

aus Rostock

Rostock, 15.12.2023

https://doi.org/10.18453/rosdok_id00004850

Chair of Power Electronics and Electrical Drives
Institute of Electrical Power Engineering
Faculty of Computer Science and Electrical Engineering
University of Rostock

1. Gutachter:
Prof. Dr.-Ing Hans-Günter Eckel,
Institut für Elektrische Energietechnik,
University of Rostock, Germany

2. Gutachter:
Prof. Dr.-Ing. Marc Hiller,
Power Electronic Systems (PES),
Elektrotechnisches Institut (ETI)
Karlsruher Institut für Technologie (KIT), Germany

3. Gutachter:
Dr. Rainer Gruber,
Siemens Mobility GmbH,
Erlangen, Germany

Datum der Einreichung: 15.12.2023

Datum der Verteidigung: 21.06.2024

Acknowledgment

I would like to take this opportunity to show my gratitude to God (Radhe Govind), Prof. Eckel, Mr. Schütt, Prof. P Meena, Dr. Nand Kishor Singh, other mentors, family members, and friends who gave me opportunities and made me capable of growing and expanding my knowledge and professional research career.

A special thanks to my role model: My mother. She lost her husband when I was in 1st standard in school. She worked day and night nonstop without holidays and vacations to feed her four children, including me, and helped us get a good education. I should admit that what I am today is all because of you, Mother. This thesis is for you, only for you. I am also thankful to have a very hardworking big brother and his wife who take care of the whole family in my hometown in my absence and never let me worry about any bad situations there.

God has been very kind to me and helped me connect with good mentors and friends since childhood. I would like to thank all my high school teachers. I especially thank Mr. Lalbabu Yadav (my math teacher) and Mr. Manish Singh, who always guided me in every step during my school days. Immediately after high school, I met Dr. Nand Kishor Singh, a senior electrical research scientist who motivated me to start a career in electrical engineering.

Prof. P Meena, Prof. L Venkatesha, and Dr. Jagwani helped me theoretically and experimentally learn and explore power electronics in detail during my bachelor's study. They even gave me keys to access two power electronics laboratories and expensive equipment during my bachelor's study, which was exceptional even for master students then. I should say that the freedom you all gave me and your trust made me capable of further pursuing a research career in power electronics.

Mr. Schütt and Prof. Eckel are my academic guides during my master's and Ph.D. studies. Apart from being excellent supervisors, they are very supportive, friendly, and understanding personalities. They trusted me and provided me necessary freedoms to further increase my knowledge of controls. Mr. Schütt primarily taught me the discrete converter controls, which is very interesting and helpful for my professional career. I would like to thank further all my colleagues, especially Mr. Christian Neumann, Mr. Vishwas Acharya Nayampalli, Mr. Till-Mathis Plötz, and Mr. Loknadh Salagamsetty who helped me in various stages during my master's and Ph.D. studies.

Last but not least, I am grateful to my beautiful wife (Sudha), who kept me motivated and provided enough time to write this document even during her pregnancy.

Abstract

Modular Multilevel Converter (MMC) has gained popularity in medium and high voltage industrial applications like HVDC, statcom, electric drives, etc., due to its modular submodule design. MMC can be used for either DC-AC, AC-AC with equal frequency, or AC-AC with unequal frequency applications. Due to the modular submodule design, an additional controller is required to regulate the MMC's arm energies. MMC provides numerous degrees of freedom to exchange energies among its arms. The main objective of this work is to investigate and present all possible degrees of freedom to exchange energies between the arms of MMC for both equal and unequal single-phase and three-phase system frequency operations.

Further, different arm energies regulation techniques of MMC (derived from a suitable combination of degrees of freedom) and their stability analysis for different single-phase and three-phase frequency operations are presented. In normal operation, it could be desired not to inject harmonics into the MMC's source and load side currents. Only four average arm energy controllers are found to be possible, which do not inject harmonics into the source and load currents. Of these four methods, only two are stable for equal frequency operation. A generalized analytical toolchain is proposed to mathematically analyze and compare the performance of all discussed arm energy regulation techniques during various load conditions.

Almost all power converters are controlled using digital controllers; hence, accurately designing the controllers in the discrete-time domain is essential. The direct discrete-time plant model is assumed to be the most accurate, but its inaccuracy because of the incapability to accurately sample the average voltage at the *Point of Common Coupling* (PCC) is investigated. A possible correction using a deadbeat-based observer is proposed to tune the closed-loop bandwidth of the discrete-time current controller accurately.

This work also presents how to design the average arm energy control loops from the arm power equations for a selected arm energy strategy. Command tracking obtained from the simulation is used to validate the design and tuning of the controllers.

A new seven-arm direct AC-AC MMC topology is proposed to increase the converter's power density if the source does not allow reactive power flow for equal frequency operation of MMC. Further, if the source allows exchanging the reactive power, a simple strategy to reduce the MMC's current stress for equal frequency operation by compensating the load reactive power with the source reactive power is presented.

Zusammenfassung

Der Modular Multilevel Converter (MMC) hat aufgrund seines modularen Submoduldesigns an Popularität in mittel- und hochspannungsindustriellen Anwendungen wie HGÜ, Statcom, elektrischen Antrieben usw. gewonnen. Der MMC kann für Gleichstrom-Wechselstrom-, Wechselstrom-Wechselstrom-Anwendungen mit gleicher Frequenz oder Wechselstrom-Wechselstrom-Anwendungen mit ungleicher Frequenz verwendet werden. Aufgrund des modularen Submoduldesigns ist ein zusätzlicher Regler erforderlich, um die Armenergien des MMC zu regulieren. Der MMC bietet zahlreiche Freiheitsgrade, um Energien zwischen seinen Armen auszutauschen. Das Hauptziel dieser Arbeit ist es, alle möglichen Freiheitsgrade zum Austausch von Energien zwischen den Armen des MMC für gleich- und ungleichfrequente Einphasen- und Dreiphasensysteme zu untersuchen und darzustellen.

Darüber hinaus werden verschiedene Regelungstechniken der Armenergien des MMC (abgeleitet aus einer geeigneten Kombination der Freiheitsgrade) und ihre Stabilitätsanalyse für verschiedene Einphasen- und Dreiphasen-Frequenzoperationen vorgestellt. Im Normalbetrieb könnte es gewünscht sein, keine Oberwellen in die Quell- und Lastströme des MMC einzuspeisen. Es wurden nur vier Durchschnitts-Armenergieregler gefunden, die keine Oberwellen in die Quellen- und Lastströme einspeisen. Von diesen vier Methoden sind nur zwei für den Betrieb mit gleicher Frequenz stabil. Eine allgemeine analytische Toolchain wird vorgeschlagen, um mathematisch die Leistungsfähigkeit aller besprochenen Armenergien-Regelungstechniken unter verschiedenen Lastbedingungen zu analysieren und zu vergleichen.

Fast alle Stromrichter werden heutzutage mit digitalen Reglern gesteuert; daher ist die genaue Auslegung der Regler im zeitdiskreten Bereich wesentlich. Das direkt-zeitdiskrete Anlagenmodell wird als das genaueste angenommen (Lösung der Differentialgleichungen, statt Approximationsmodell), aber seine Ungenauigkeit aufgrund der Unfähigkeit, die durchschnittliche Spannung am Netzanschlusspunkt (PCC – Point of Common Coupling) genau zu erfassen, wird untersucht. Eine mögliche Korrektur mittels eines Deadbeat-basierten Beobachters wird vorgeschlagen, um die geschlossene Bandbreite des zeitdiskreten Stromreglers genau abzustimmen.

Diese Arbeit zeigt auch, wie man die Regelkreise der Durchschnitts-Armenergiern aus den Armleistungsgleichungen für eine ausgewählte Armenergiestrategie entwirft. Die

Sollwertverfolgung, die aus der Simulation erhalten wird, wird verwendet, um die Auslegung und Abstimmung der Regler zu validieren.

Eine neue sieben-arm direkt Wechselstrom-Wechselstrom-MMC-Topologie wird vorgeschlagen, um die Leistungsdichte des Wandlers zu erhöhen, falls die Quelle keinen Blindleistungsfluss für den Betrieb des MMC mit gleicher Frequenz zulässt. Darüber hinaus wird, falls die Quelle den Austausch von Blindleistung ermöglicht, eine einfache Strategie vorgestellt, um die Strombelastung des MMC für den Betrieb mit gleicher Frequenz zu reduzieren, indem die Blindleistung der Last mit der Blindleistung der Quelle kompensiert wird.

Author

Gyanendra Kumar Sah represented Nepal at the 45th *International Physics Olympiad* (45th IPHO) in Astana in 2014. He earned a B.Sc. degree in Electrical and Electronics Engineering from BMS College of Engineering, India, in 2018, and subsequently, he obtained an M.Sc. degree in Electrical Engineering from the University of Rostock, Germany, in 2020.

From September 2020 to September 2023, he worked as a research assistant and doctoral candidate at the Institute of Electrical Power Engineering at the University of Rostock, Germany. His topics of interest include the digital converter control design, passivity investigation, and arm energy balancing control design for *Modular Multilevel Converter* (MMC).

Since October 2023, he has been working as a Specialist Converter Control Engineer at Siemens Mobility in Erlangen, Germany. His work includes designing and validating the controls of MMC and investigating the passivity of the power converters.

Table of Contents

List of Figures

List of Tables

List of Abbreviations

AC	Alternative Current
CT	Command Tracking
CCSFb	Cross-Coupling State Feedback
DCCSFb	Decoupled Cross-Coupling State Feedback
DC	Direct Current
DIC	Disturbance Input Decoupling
DID	Disturbance Input Decoupling
DOF	Degree of Freedom
FRF	Frequency Response Function
FB	Full Bridge
FC	Flying Capacitor
HB	Half Bridge
ICC	Inner Current Controller
IGBT	Insulated-Gate Bipolar Transistor
KVL	Kirchhoff's Voltage Law
MMC	Modular Multilevel Converter
MI	Manipulated Input
MIC	Manipulated Input Coupling
MID	Manipulated Input Decoupling
NPC	Neutral Point Clamped
OEL	Outer Energy Loop
P	Proportional Controller
PI	Proportional Integral Controller
PR	Proportional Resonant Controller
R	Resonant Controller

List of Symbols

C_{SM}	Submodule's DC-link capacitance
f_a	Three-phase frequency
f_b	Single-phase frequency
f_{cm}	Common-mode frequency
f_{Mean}	Mean calculation frequency
f_1, f_2	Eigenvalues
f_{br}	Closed-loop bandwidth
f_s	Sampling Frequency
f_{sw}	Switching frequency
i_{a123}	Instantaneous three-phase current
i_{b123}	Circulating currents
i_{p123}	Upper arm currents
i_{n123}	Lower arm currents
i_b	Instantaneous single-phase current
i_{cm}	Instantaneous common-mode current
i_{by}	Instantaneous circulating current for phase y of MMC
i_{ay}	Instantaneous three-phase current for phase y of MMC
$i_{b\alpha\beta 0}$	Instantaneous circulating currents in the αβ0-frame
$i_{a\alpha\beta}$	Instantaneous three-phase currents in the αβ-frame
i_{bdq+}	Positive sequence circulating currents in the dq-frame
i_{bdq-}	Negative sequence circulating currents in the dq-frame
i_{adq+}	Positive sequence three-phase currents in the dq-frame
i_{adq-}	Negative sequence three-phase currents in the dq-frame
$\overset{b}{i}_{b\alpha\beta}$	Circulating currents in phase with v_b
$\overset{b}{i}_{a\alpha\beta}$	Three-phase currents in phase with v_b

$i_{b\alpha\beta}^{cm}$	Circulating currents in phase with v_{cm}
$i_{a\alpha\beta}^{cm}$	Three-phase currents in phase with v_{cm}
K_p	Proportional gain
K_i	Integral gain
K_{ir}	Resonant controller's gain
N	Number of submodules
p_{p123}	Upper arm powers
p_{n123}	Lower arm powers
v_{a123}	Instantaneous three-phase voltage
v_b	Instantaneous single-phase voltage
v_{cm}	Instantaneous common-mode voltage
v_{p123}	Upper arm voltages
v_{n123}	Lower arm voltages
w_{p123}	Upper arm energies
w_{n123}	Lower arm energies
$\overline{w}$	Average arm energy
ω_c	Resonant controller's cutoff frequency
$Z_{Trf\text{-}a}$	Three-phase transformer impedance
$Z_{Trf\text{-}b}$	Single-phase transformer impedance
Z_{arm}	Arm impedance
Σ	Summation system
Δ	Difference system
θ_b	Single-phase voltage angle
θ_a	Three-phase voltage angle
θ_{cm}	Common-mode voltage angle

1 Introduction

Due to the development of high-power semiconductors over recent years, various multilevel voltage source inverters have emerged, enabling better line-side behavior (high power quality and high efficiency) than conventionally used converter topologies [GLI03b, KNA11]. A multilevel converter topology is extensively used for medium or high-voltage applications like HVDC, statcom, electric drives, etc. The multilevel *Voltage Source Inverter* (VSI) can be realized by the cascaded connection of the switches or the full-bridge (H-bridge) inverter cells. The cascaded connection of switches or inverter cells helps to reduce voltage stress on the individual switching devices (IGBT, MOSFET, etc.) and capacitors. However, a central multi-winding phase-shifted line-frequency transformer is required to deliver electric power to each floating H-bridge inverter cell when a multilevel inverter is realized by the cascaded connection of H-bridge inverter cells [AKA10, THI13, AKA17]. A central DC-link capacitor is required when the cascaded connection of the switches realizes a conventional multilevel converter.

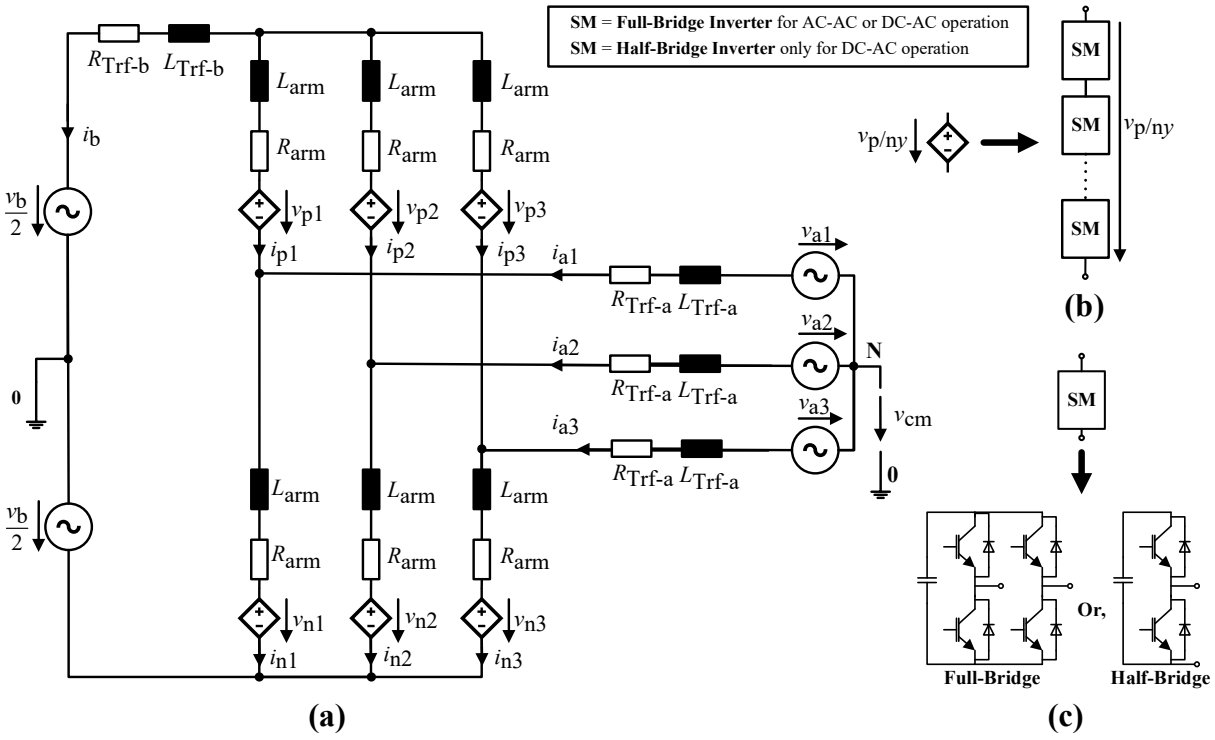

Figure 1.1: Electrical circuit diagram of *Modular Multilevel Converter* (MMC).

In 2003, Prof. Marquardt and his coauthors proposed another revolutionary multilevel power converter, "*Modular Multilevel Converter* (MMC)," and its fundamental operating principles [LES03a, LES03b, GLI03a, GLI03b, GLI05]. MMC topology eliminates the additional "central" components (multi-winding phase-shifted line-frequency transformer and DC-link capacitors) for stringent modular and scalable realization.

Fig. 1.1a shows the average circuit diagram of MMC. It has three phases (y = 1, 2, 3). Each phase consists of two arms: the upper arm (py) and the lower arm (ny). Each arm consists of an L-filter (L_{arm}) and a controlled voltage source ($v_{\text{p/n}y}$) connected in series. Here, $v_{\text{p/n}y} = v_{\text{p}y}$ or $v_{\text{n}y}$, and R_{arm} represents the internal resistance of the L-filter. Fig. 1.1b illustrates the realization of a controlled voltage source in an arm by connecting multiple Sub-Modules (SMs) in series. A submodule can be realized by (a) the full-bridge (FB), (b) the half-bridge (HB), (c) the clamp-double, (d) the three-level *Flying Capacitor* (FC), (e) the three-level *Neutral Point Clamped* (NPC), (f) the five-level cross-connected SM, etc. [DEB15]. Fig. 1.1c considers only basic full-bridge (FB) and half-bridge (HB) submodules. The FB submodule can be universally used for all applications, but the HB submodule can only be used for the DC-AC operation of MMC [MAR10].

The single-phase grid (v_{b}) or the single-phase load is connected to MMC via the neutral points of the upper (p123) and lower (n123) arms. And the three-phase grid (v_{a123}) or the three-phase load is connected to MMC via the central point of the three phases of MMC. $Z_{\text{Trf-a}}$ ($= R_{\text{Trf-a}} + \text{j}\omega L_{\text{Trf-a}}$) and $Z_{\text{Trf-b}}$ ($= R_{\text{Trf-b}} + \text{j}\omega L_{\text{Trf-b}}$) represents the equivalent three-phase and single-phase transformer impedances, respectively. The zero sequence three-phase voltage (v_{a0}) with respect to the central point (0) of the single-phase system is termed as common-mode voltage (v_{cm}) [KOL15a], thus $v_{\text{a0}} = v_{\text{cm}}$.

The three-phase voltage source's neutral point (N) can be floating or grounded. To reduce complexity in deriving the governing voltage equations, generally, one considers the neutral point (N) of the three-phase system to be connected to the central point of the single-phase voltage source [KOL15a] (also see Fig. 3.2). Here, a floating neutral point is considered to analyze the accuracy of the derived governing voltage equations even when the three-phase neutral point is floating.

The number of submodules can be decided based on the three-phase, single-phase, and common-mode voltage magnitudes. Submodules are floating hence scaling the converter dimensioning is comparatively simpler than the conventional multilevel converters. A central DC-link capacitor is eliminated, making MMC a feasible converter topology for HVDC, high

voltage, and medium voltage applications. The central DC-link capacitor is actually distributed among the converter's floating submodules. Therefore, an additional effort is required to regulate the individual arm ($W_{\mathrm{p/n123}}$) and submodule energies.

Fig. 1.2 illustrates the general control structure of MMC [KOL14, PER14, KAR16, DIE20]. The arm energy controllers regulate the six arm energies of MMC. The arm energy controllers generate the suitable reference arm ($i^{*}_{\mathrm{p/n123}}$) and source side (i^{*}_{a123} or i^{*}_{b}) currents as the output. MMC can draw energy either from the three-phase or the single-phase system. Thus, the arm energy controllers provide a three-phase reference current (i^{*}_{a123}) when the MMC draws active power from the three-phase system. And they give a single-phase reference current (i^{*}_{b}) when the single-phase side of MMC behaves like a source.

The current controllers regulate the currents according to the arm energy controller's command and generate the reference arm voltages ($v^{*}_{\mathrm{p/n123}}$) as the output signals. The reference arm voltage ($v^{*}_{\mathrm{p/n123}}$) can be realized by switching the submodules of each arm. Since the submodules are floating, an additional sorting algorithm is essential in distributing the arm energies uniformly among their corresponding submodules. The sorting algorithm is independent; hence any sorting method can be chosen to uniformly distribute the submodule's energies [KAR16], which is out of this work's scope. This work only focuses on exploring various possible methods in regulating the energies of the six arms of MMC (also see Fig. 1.2). Therefore, the average equivalent circuit diagram of MMC (shown in Fig. 1.1a) is used to validate the proposed control concepts.

The three-phase and the single-phase system frequencies can be either the same or different. Hence, MMC can be used for either DC-AC, AC-AC with unequal frequency or AC-AC with equal frequency operation. A DC-AC MMC topology can be used for applications like (a) HVDC [GUA11, GUA12, KNA11], (b) powering DC traction networks, (c) variable speed motor drive [KOL15a], (d) wind energy storage systems [NOV17], (e) battery energy storage systems (BESS) [BAR11a], and many more.

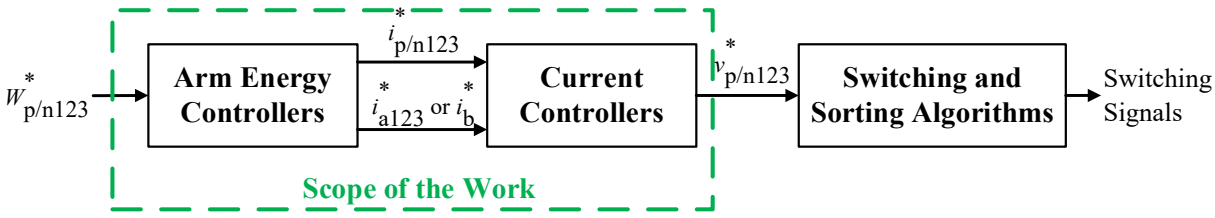

Figure 1.2: General control structure of MMC.

The railway traction system in Germany, Switzerland, Austria, Norway, and Sweden is based on a 16.7 Hz AC system. The frequency (16.7 Hz) used here has historical significance. In another European countries, 50 Hz AC or DC systems are used [BEC21]. In China and Japan, the 50 Hz single-phase railway network is used [SON18]. The operation of direct AC-AC MMC for powering a 16.7 Hz single-phase railway network from a three-phase 50 Hz grid is presented in [WIN10, ÄNG11b]. Direct AC-AC MMC with equal frequency operation causes significant energy variation in a phase's upper and lower arms due to the coupling between the three-phase and the single-phase systems. Application of the direct AC-AC MMC with equal frequency operation is discussed in [LEI18b, QIN19, SON18].

MMC provides many possibilities to regulate the arm energies of MMC. Many researchers have proposed various strategies for regulating the arm energies for DC-AC and AC-AC operations. Extensive research work can be found for DC-AC and AC-AC with $f_b = f_a/3$ operations during normal and abnormal conditions. Here, f_b and f_a are the single-phase and three-phase frequencies. On the other hand, only a few studies discuss the direct AC-AC MMC topology under equal frequency ($f_b = f_a$) operation [SON18].

None of the research works are found that have proposed and analyzed all possible ways to regulate the arm energies of MMC for DC-AC, AC-AC with unequal frequency and AC-AC with equal frequency operations. Further, the literature does not present a stability analysis for the proposed arm energy controllers, which is more critical during equal frequency ($f_b = f_a$) operation of MMC. Hence, the primary objective of this work is to present different possible methods to regulate the arm energies of MMC for DC-AC and AC-AC operations and analyze their stability for equal and unequal frequency operations. Further, this work discusses the stability analysis of the controllers during the three-phase and the single-phase failure conditions. A generalized analytical toolchain is also proposed, which can help analyze the converter's performance during normal and abnormal conditions.

It is recommended to keep Appendix A.9 (auxiliary sheets) as a separately printed handout and look at this handout while you are reading the upcoming chapters. Although the auxiliary sheets are not mandatory to understand the thesis, but they can help save time and assist you in understanding a few sections with less effort. The auxiliary sheets mainly contain the main findings of Chapter 2. The figure, equation, and table numbers are kept the same as they are in the chapters to quickly locate the position of a figure, equation, or table of auxiliary sheets in the thesis chapter.

Chapter 2 illustrates the analytical approach to identify numerous possible degrees of freedom for regulating the arm energies of MMC. The chapter further derives different possible arm energy balancing methods by suitable combinations of all degrees of freedom. An analytical toolchain is proposed to analyze and check the stability of the arm energy controllers for various single-phase and three-phase system frequency operations. Additionally, the proposed toolchain can help investigate the converter's performance during normal and abnormal conditions. At last, the presented arm energy-balancing methods are compared with the proposed arm energy-balancing methods in the literature.

Chapter 3 proposes a discrete-time current controller to control the circulating and the three-phase (or single-phase) currents. The limitation of the direct discrete-time plant model is investigated with the help of an open-loop bode plot. The tuning of the current controllers is validated with the help of the closed-loop *Command Tracking* (CT) plots.

Chapter 4 proposes the generalized steps in designing the discrete-time average arm energy control loops with the help of the average arm power equations in the αβ0-frame. The necessary changes in the controllers with the changes in the single-phase and three-phase system frequencies are also highlighted. The tuning of the controller is again investigated with the help of closed-loop bode or command tracking plots.

Chapter 5 presents the simulation and analytical results of MMC for DC-AC, AC-AC with unequal, and AC-AC with equal frequency operations during normal operations. The performance of MMC with poor power quality of load is also presented. The analytical results are compared with the simulation results.

Chapter 6 proposes a seven-arm direct AC-AC MMC topology to significantly reduce the conventional six-arm MMC's current stress for equal frequency operation. Further, the overall dimensioning of the system can be reduced, or the power rating of the converter can be increased using the proposed seven-arm topology for equal frequency operation.

2 Arm Energy Balancing Methods of MMC

The dc-link capacitors of the submodules are floating in *Modular Multilevel Converter* (MMC). Thus, the dc-link capacitor voltages or the energies should be regulated with the help of controllers. The general control structure of MMC is already shown in Fig. 1.2 in Chapter 1. This chapter intends to identify many possible ways to regulate the arm energies of MMC. Further, the controller's steady-state stability for the various single-phase (f_b) and three-phase (f_b) system frequencies are investigated during normal and abnormal conditions. An analytical toolchain is proposed to analyze the performance of MMC mathematically. The analytical toolchain facilitates mathematically analyzing the controller's performance, saving time, staffing, and money. At last, the arm energies balancing methods in the literature are compared with the discussed energy balancing methods in this work.

Fig. 2.1a illustrates the average equivalent circuit diagram of MMC. The three-phase neutral point (N) is considered floating; hence the zero-sequence component of the three-phase current ($i_{a0} = 0$) is always zero. An arm current ($i_{p/ny}$) of phase y of MMC can be decomposed into two components: (a) the circulating current (i_{by}) and the three-phase current (0.5 i_{ay}). (2.1) shows the decomposition of the arm currents for phase y of MMC [KOL15a]. (2.2) illustrates that the zero-sequence component of the circulating current (i_{b0}) is proportional to the single-phase current (i_b).

$$i_{py} = i_{by} - \frac{i_{ay}}{2}, \text{ and } i_{ny} = i_{by} + \frac{i_{ay}}{2} \tag{2.1}$$

$$i_{b0} = i_{p0} = \frac{i_{p1} + i_{p2} + i_{p3}}{3} = i_{n0} = \frac{i_{n1} + i_{n2} + i_{n3}}{3} = \frac{i_{b1} + i_{b2} + i_{b3}}{3} = -\frac{i_b}{3} \tag{2.2}$$

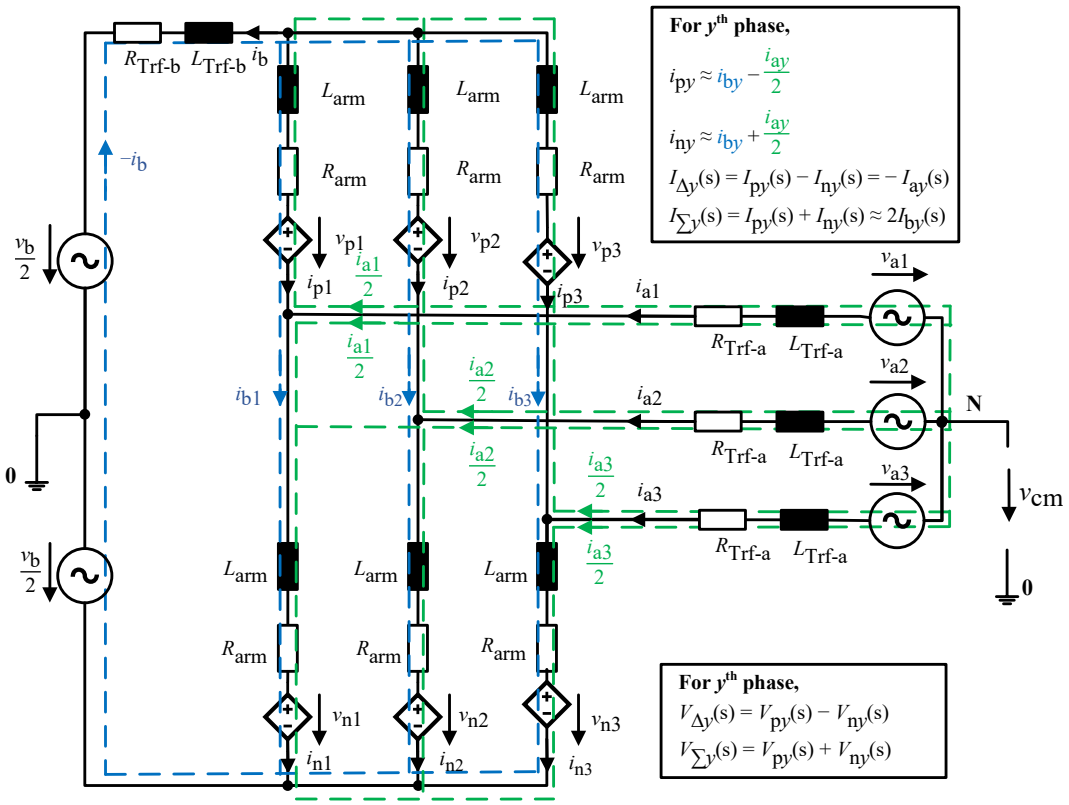

(a) Average Equivalent Circuit Diagram of MMC

1. Total Arm Energy Regulation $(w_{\Sigma 0})$
2. Total Upper and Lower Arm Energies Regulation $(w_{\Delta 0})$
3. Summation Phase Energies Regulation $(w_{\Sigma \alpha\beta})$
4. Difference Phase Energies Regulation $(w_{\Delta \alpha\beta})$

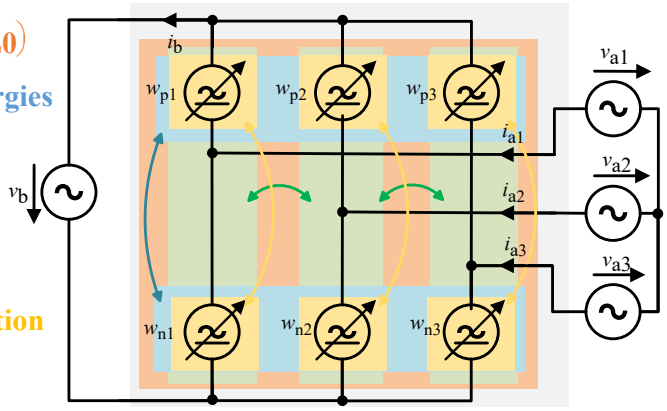

(b) Arm energy Model

Figure. 2.1: Electrical circuit diagram of *Modular Multilevel Converter* (MMC).

2.1 Summation and Difference Arm Power Equations in the αβ0-Frame

MMC provides numerous degrees of freedom and many ways to regulate its six-arm energies. The general expressions of the six arm powers of MMC can help determine numerous degrees of freedom and arm energy balancing methods. Derivation of the six arm power equations in the αβ0-frame is selected because it helps to identify a few additional degrees of freedom (e.g.,

negative sequence circulating and three-phase currents), which are difficult to notice in the abc-frame. Further, the arm power equations in the αβ0-frame facilitate an easier understanding of which degree of freedom influences which arm powers or energies.

Fig. 2.1b shows the simplified arm energy circuit diagram that will be used to derive the simplified arm power equations of MMC. Here, all arm impedances ($Z_{\text{arm}} = R_{\text{arm}} + j\omega L_{\text{arm}}$), the three-phase transformer impedance ($Z_{\text{Trf-a}} = R_{\text{Trf-a}} + j\omega L_{\text{Trf-a}}$), and the single-phase transformer impedance ($Z_{\text{Trf-b}} = R_{\text{Trf-b}} + j\omega L_{\text{Trf-b}}$) are neglected to reduce the small value power terms in the equations. The six controlled voltage sources ($v_{\text{p/n123}}$) in Fig 2.1a are replaced with the corresponding arm energy components ($w_{\text{p/n123}}$). The zero sequence three-phase voltage (v_{a0}) with respect to the central point (0) of the single-phase system is termed as common-mode voltage (v_{cm}) [KOL15a], thus $v_{\text{a0}} = v_{\text{cm}}$.

Referring to Fig. 2.1b (also see Appendix A.3.1), (2.3) represents the upper arm ($v_{\text{p}y}$) and lower arm ($v_{\text{n}y}$) voltages of phase y of MMC. Derivation of the arm power equations in the αβ0-frame is shown step by step in Appendix A.5. In this section, the derivation steps are discussed briefly.

$$v_{\text{p}y} = \frac{v_{\text{b}}}{2} - v_{\text{a}y}\text{ , and } v_{\text{n}y} = \frac{v_{\text{b}}}{2} + v_{\text{a}y} \tag{2.3}$$

Chapter 3 will prove that the single-phase (i_{b}), circulating ($i_{\text{b}\alpha\beta}$), and three-phase ($i_{\text{a}\alpha\beta}$) currents can be decoupled and controlled independently in the summation (Σ) and the difference (Δ) systems. Therefore, it is also advisable to derive the arm power equations and design the arm energy controllers in the summation (Σ) and the difference (Δ) systems. (2.4) shows the general definition of the summation and difference system. (2.5) and (2.6) represent the arm currents and voltages in the summation and difference systems for phase y of MMC, respectively. (2.7) and (2.8) illustrate the arm powers for phase y of MMC in the summation and difference systems, respectively, (also see Appendix A.5.1). It should be noted that the summation and difference arm power expressions are indifferent if the three-phase neutral point (N) is floating or grounded.

$$F_{\Sigma y} = F_{\text{p}y} + F_{\text{n}y} \;\; ; \;\; F_{\Delta y} = F_{\text{p}y} - F_{\text{n}y} \tag{2.4}$$

$$i_{\Sigma y} = i_{\text{p}y} + i_{\text{n}y} = 2\, i_{\text{b}y} \;\; ; \;\; i_{\Delta y} = i_{\text{p}y} - i_{\text{n}y} = -\, i_{\text{a}y} \tag{2.5}$$

$$v_{\Sigma y} = v_{\text{p}y} + v_{\text{n}y} = v_{\text{b}} \;\; ; \;\; v_{\Delta y} = v_{\text{p}y} - v_{\text{n}y} = -\, 2\, v_{\text{a}y} \tag{2.6}$$

$$p_{\Sigma y} = p_{\text{p}y} + p_{\text{n}y} = v_{\text{p}y}\, i_{\text{p}y} + v_{\text{n}y}\, i_{\text{n}y} = v_{\text{b}}\, i_{\text{b}y} + v_{\text{a}y}\, i_{\text{a}y} \tag{2.7}$$

$$p_{\Delta y} = p_{\text{p}y} - p_{\text{n}y} = v_{\text{p}y}\, i_{\text{p}y} - v_{\text{n}y}\, i_{\text{n}y} = -\, 2\, v_{\text{a}y}\, i_{\text{b}y} - \frac{i_{\text{a}y}}{2}\, v_{\text{b}} \tag{2.8}$$

(2.9) and (2.10) illustrate the governing equations for Clarke's (abc to αβ0) and inverse Clarke's (αβ0 to abc) transformations. The voltage (v_{ay}) and currents (i_{by}, and i_{ay}) in (2.7) and (2.8) are in the abc-frame. The expressions of the voltage ($v_{ay} = f(v_{a\alpha}, v_{a\beta}, v_{a0})$) and currents ($i_{ay} = f(i_{a\alpha}, i_{a\beta}, i_{a0})$, and $i_{by} = f(i_{b\alpha}, i_{b\beta}, i_{b0})$) in the abc-frame as a function of their corresponding components in the αβ0-frame can be obtained with the help of inverse Clarke transformation ($F_{abc} = C^{-1} F_{\alpha\beta0}$). (2.11) to (2.16) represent the six arm power equations of MMC in the abc-frame, which are obtained after replacing the currents ($i_{ay} = f(i_{a\alpha}, i_{a\beta}, i_{a0})$, and $i_{by} = f(i_{b\alpha}, i_{b\beta}, i_{b0})$) and voltage ($v_{ay} = f(v_{a\alpha}, v_{a\beta}, v_{a0})$) in the abc-frame in (2.7) and (2.8) with their corresponding expressions as a function of the αβ0-frame components (see Appendix A5.2). Here, the three-phase zero sequence current ($i_{a0} = 0$) equals zero because the three-phase neutral point is floating, and the zero-sequence three-phase voltage ($v_{a0} = v_{cm}$) is defined as the common-mode voltage (v_{cm}). Clarke's transformation of the arm powers expressions from (2.11) to (2.16) and simplifications gives the summation ($p_{\Sigma\alpha\beta0}$) and difference ($p_{\Delta\alpha\beta0}$) arm power expressions in the αβ0-frame ((2.17) to (2.22)) (see Appendix A.5.3). Here, all the currents, voltages, and powers are now given in the αβ0-frame.

$$\mathrm{F}_{\alpha\beta0} = C\,\mathrm{F}_{abc} \;\; ; \;\; \mathrm{F}_{abc} = C^{-1}\,\mathrm{F}_{\alpha\beta0} \tag{2.9}$$

$$C = \frac{2}{3}\begin{pmatrix} 1 & -\frac{1}{2} & -\frac{1}{2} \\ 0 & \frac{\sqrt{3}}{2} & -\frac{\sqrt{3}}{2} \\ \frac{1}{2} & \frac{1}{2} & \frac{1}{2} \end{pmatrix} \; ; \; C^{-1} = \begin{pmatrix} 1 & 0 & 1 \\ -\frac{1}{2} & \frac{\sqrt{3}}{2} & 1 \\ -\frac{1}{2} & -\frac{\sqrt{3}}{2} & 1 \end{pmatrix} \tag{2.10}$$

$$p_{\Sigma1} = v_b\left(i_{b\alpha} + i_{b0}\right) + \left(v_{a\alpha} + v_{cm}\right) i_{a\alpha} \tag{2.11}$$

$$p_{\Sigma2} = v_b\left(-\frac{1}{2} i_{b\alpha} + \frac{\sqrt{3}}{2} i_{b\beta} + i_{b0}\right) + \left(-\frac{1}{2} v_{a\alpha} + \frac{\sqrt{3}}{2} v_{a\beta} + v_{cm}\right)\left(-\frac{1}{2} i_{a\alpha} + \frac{\sqrt{3}}{2} i_{a\beta}\right) \tag{2.12}$$

$$p_{\Sigma3} = v_b\left(-\frac{1}{2} i_{b\alpha} - \frac{\sqrt{3}}{2} i_{b\beta} + i_{b0}\right) + \left(-\frac{1}{2} v_{a\alpha} - \frac{\sqrt{3}}{2} v_{a\beta} + v_{cm}\right)\left(-\frac{1}{2} i_{a\alpha} - \frac{\sqrt{3}}{2} i_{a\beta}\right) \tag{2.13}$$

$$p_{\Delta1} = -2\left(v_{a\alpha} + v_{cm}\right)\left(i_{b\alpha} + i_{b0}\right) - \frac{v_b\, i_{a\alpha}}{2} \tag{2.14}$$

$$p_{\Delta2} = -2\left(-\frac{1}{2} v_{a\alpha} + \frac{\sqrt{3}}{2} v_{a\beta} + v_{cm}\right)\left(-\frac{1}{2} i_{b\alpha} + \frac{\sqrt{3}}{2} i_{b\beta} + i_{b0}\right) - \frac{v_b}{2}\left(-\frac{1}{2} i_{a\alpha} + \frac{\sqrt{3}}{2} i_{a\beta}\right) \tag{2.15}$$

$$p_{\Delta3} = -2\left(-\frac{1}{2} v_{a\alpha} - \frac{\sqrt{3}}{2} v_{a\beta} + v_{cm}\right)\left(-\frac{1}{2} i_{b\alpha} - \frac{\sqrt{3}}{2} i_{b\beta} + i_{b0}\right) - \frac{v_b}{2}\left(-\frac{1}{2} i_{a\alpha} - \frac{\sqrt{3}}{2} i_{a\beta}\right) \tag{2.16}$$

$$p_{\Sigma0} = v_b\, i_{b0} + \frac{v_{a\alpha}\, i_{a\alpha} + v_{a\beta}\, i_{a\beta}}{2} \tag{2.17}$$

$$p_{\Delta 0} = -2\, v_{cm}\, i_{b0} - v_{a\alpha}\, i_{b\alpha} - v_{a\beta}\, i_{b\beta} \tag{2.18}$$

$$p_{\Sigma\alpha} = v_b\, i_{b\alpha} + v_{cm}\, i_{a\alpha} + \frac{v_{a\alpha}\, i_{a\alpha} - v_{a\beta}\, i_{a\beta}}{2} \tag{2.19}$$

$$p_{\Sigma\beta} = v_b\, i_{b\beta} + v_{cm}\, i_{a\beta} - \frac{v_{a\alpha}\, i_{a\beta} + v_{a\beta}\, i_{a\alpha}}{2} \tag{2.20}$$

$$p_{\Delta\alpha} = -\frac{v_b\, i_{a\alpha}}{2} - 2\, v_{a\alpha}\, i_{b0} - 2\, v_{cm}\, i_{b\alpha} - v_{a\alpha}\, i_{b\alpha} + v_{a\beta}\, i_{b\beta} \tag{2.21}$$

$$p_{\Delta\beta} = -\frac{v_b\, i_{a\beta}}{2} - 2\, v_{a\beta}\, i_{b0} - 2\, v_{cm}\, i_{b\beta} + v_{a\alpha}\, i_{b\beta} + v_{a\beta}\, i_{b\alpha} \tag{2.22}$$

2.2 Degrees of Freedom

The discussed arm energy controllers would try to control the average (not instantaneous) arm energies ($\overline{w}_{p/n123}$) by varying the average arm powers ($\bar{p}_{p/n123}$) to decouple the couplings between the *Manipulated Inputs* (MIs). The average arm energies ($\overline{w}_{p/n123}$ = constant) are regulated in a steady state if the average arm power is zero ($\bar{p}_{p/n123}$ = 0). If the average summation ($\bar{p}_{\Sigma\alpha\beta0}$ = 0) and difference ($\bar{p}_{\Delta\alpha\beta0}$ = 0) arm powers are zero in the αβ0-frame then the average arm energies ($\overline{w}_{p/n123}$) in the abc frame are automatically regulated because $\bar{p}_{p/n123}$ = 0. Therefore, all possible *Degrees of Freedom* (DOF) and arm energies balancing methods of MMC can be derived using the arm power equations from (2.17) to (2.22). It can be noted that the arm power expressions consist of three general power terms: (a) $v_{a\alpha}\, i_{x\alpha} + v_{a\beta}\, i_{x\beta}$, (b) $v_{a\alpha}\, i_{x\alpha} - v_{a\beta}\, i_{x\beta}$, and (c) $v_{a\alpha}\, i_{x\beta} + v_{a\beta}\, i_{x\alpha}$. Here, x = a or b. Identifying the average value expression of these three power terms is essential to identify all degrees of freedom.

(2.23) illustrates the three-phase (θ_a), single-phase (θ_b), and common-mode (θ_{cm}) voltage phase angles definition. Here, ω_a, ω_b, and ω_{cm} represent the three-phase, single-phase, and common-mode angular frequencies. The single-phase angle leads to the three-phase angle by ϕ_b. (2.24) represents the expressions of the instantaneous three-phase ($v_{a\alpha\beta}$), single-phase (v_b), and common-mode (v_{cm}) voltages. V_a, V_b, and V_{cm} represent the three-phase, single-phase, and common-mode RMS voltages. It is assumed that the three-phase voltage does not contain the negative sequence component.

$$\theta_a = \omega_a t\ ;\ \theta_b = \omega_b t + \phi_b\ ;\ \theta_{cm} = \omega_{cm} t + \phi_{cm} \tag{2.23}$$

$$v_{a\alpha} = \sqrt{2} V_a \cos(\theta_a),\ v_{a\beta} = \sqrt{2} V_a \sin(\theta_a),\ v_b = \sqrt{2} V_b \cos(\theta_b) \text{ and } v_{cm} = \sqrt{2} V_{cm} \cos(\theta_{cm}) \tag{2.24}$$

In this work, I_x and V_x represents the RMS quantities, and i_x and v_x represent the instantaneous quantities. (2.25) shows the inverse Park's transformation (dq to αβ) matrices for the positive ($D(\theta_a)$) and the negative ($D^{-1}(\theta_a)$) sequences current components [KOL15a]. The three-phase angle (θ_a) is used for Park and inverse Park's transformation. Assuming the current (i_{x123}) has both positive ($\boldsymbol{i}_{xdq+}$) and negative ($\boldsymbol{i}_{xdq-}$) sequence components, (2.26) shows the overall current in the αβ-frame, including its positive ($\boldsymbol{i}_{xdq+}$) and negative ($\boldsymbol{i}_{xdq-}$) sequence components in the dq-frame. Here, $\boldsymbol{i}_{xdq+}$ is the DC value in the positive sequence dq-frame ($\boldsymbol{F}_{dq+} = e^{-j\theta_a}\boldsymbol{F}_{\alpha\beta}$) and i_{xdq-} is the DC value in the negative sequence dq-frame ($\boldsymbol{F}_{dq-} = e^{j\theta_a}\boldsymbol{F}_{\alpha\beta}$). Note: $\boldsymbol{F}_{\alpha\beta} = F_\alpha + j\,F_\beta$, $\boldsymbol{F}_{dq-} = F_{d-} + j\,F_{q-}$, and $\boldsymbol{F}_{dq+} = F_{d+} + j\,F_{q+}$ are complex variables.

$$D(\theta_a) = \begin{pmatrix} \cos(\theta_a) & -\sin(\theta_a) \\ \sin(\theta_a) & \cos(\theta_a) \end{pmatrix} \; ; \; D^{-1}(\theta_a) = \begin{pmatrix} \cos(\theta_a) & \sin(\theta_a) \\ -\sin(\theta_a) & \cos(\theta_a) \end{pmatrix} \tag{2.25}$$

$$i_{x\alpha\beta} = D(\theta_a)\, i_{xdq+} + D^{-1}(\theta_a)\, i_{xdq-} \rightarrow \begin{pmatrix} i_{x\alpha} \\ i_{x\beta} \end{pmatrix} = \begin{pmatrix} \cos(\theta_a)\left(i_{xd+} + i_{xd-}\right) + \sin(\theta_a)\left(i_{xq-} - i_{xq+}\right) \\ \cos(\theta_a)\left(i_{xq+} + i_{xq-}\right) + \sin(\theta_a)\left(i_{xd+} - i_{xd-}\right) \end{pmatrix} \tag{2.26}$$

$$\overline{\cos(2\,\theta_a)} = \overline{\sin(2\,\theta_a)} = \overline{\cos(\theta_a)} = \overline{\sin(\theta_a)} = 0 \tag{2.27}$$

$$\overline{v_{a\alpha}\, i_{x\alpha} + v_{a\beta}\, i_{x\beta}} = \sqrt{2}\, V_a\, i_{xd+} \tag{2.28}$$

$$\overline{v_{a\alpha}\, i_{x\alpha} - v_{a\beta}\, i_{x\beta}} = \sqrt{2}\, V_a\, i_{xd-} \tag{2.29}$$

$$\overline{v_{a\alpha}\, i_{x\beta} + v_{a\beta}\, i_{x\alpha}} = \sqrt{2}\, V_a\, i_{xq-} \tag{2.30}$$

Now, the average of the above mentioned three power terms ((a) $v_{a\alpha}\, i_{x\alpha} + v_{a\beta}\, i_{x\beta}$, (b) $v_{a\alpha}\, i_{x\alpha} - v_{a\beta}\, i_{x\beta}$, and (c) $v_{a\alpha}\, i_{x\beta} + v_{a\beta}\, i_{x\alpha}$) can be solved with the help of (2.24), (2.26), and (2.27). (2.28), (2.29), and (2.30) represent the general expressions of the average of the power terms: (a) $v_{a\alpha}\, i_{x\alpha} + v_{a\beta}\, i_{x\beta}$, (b) $v_{a\alpha}\, i_{x\alpha} - v_{a\beta}\, i_{x\beta}$, and (c) $v_{a\alpha}\, i_{x\beta} + v_{a\beta}\, i_{x\alpha}$, respectively. It is clear from (2.29) and (2.30) that even the negative sequence current components (i_{xd-}, and i_{xq-}) can influence the average arm powers ($\overline{v_{a\alpha}\, i_{x\alpha} - v_{a\beta}\, i_{x\beta}}$, and $\overline{v_{a\alpha}\, i_{x\beta} + v_{a\beta}\, i_{x\alpha}}$). And only positive sequence d-axis current (i_{xd+}) affects the average power term $\overline{v_{a\alpha}\, i_{x\alpha} + v_{a\beta}\, i_{x\beta}}$ (see (2.28)). But the positive sequence q-axis current (i_{xq+}) does not make average arm power in the MMC's arm power expressions and only increases oscillations in the arm energies [KOL15a].

Apart from the three general power terms ((a) $v_{a\alpha}\, i_{x\alpha} + v_{a\beta}\, i_{x\beta}$, (b) $v_{a\alpha}\, i_{x\alpha} - v_{a\beta}\, i_{x\beta}$, and (c) $v_{a\alpha}\, i_{x\beta} + v_{a\beta}\, i_{x\alpha}$), the six arm power expressions ((2.17) to (2.22)) also consists of several power terms which can be generalized as the product of voltage v_g and current $i_{x\alpha/\beta/0}$ ($v_g\, i_{x\alpha/\beta/0}$). Here,

(a) $i_{x\alpha/\beta/0} = i_{x\alpha}$, $i_{x\beta}$ or i_{x0}, (b) x = a or b, and (c) g = a, b, or cm. The voltage (v_g) and current ($i^g_{x\alpha/\beta/0}$) with the same frequency only can make average power. $i^g_{x\alpha/\beta/0}$ represents the component of the current $i_{x\alpha/\beta/0}$ in phase with the voltage v_g. (2.31) represents the average of the product of v_g and $i^g_{x\alpha/\beta/0}$. Here, V_g and $I^g_{x\alpha/\beta/0}$ are the RMS voltage and current values, respectively.

$$\overline{v_g\, i^g_{x\alpha/\beta/0}} = V_g\, I^g_{x\alpha/\beta/0} \tag{2.31}$$

The summation arm power in the 0-frame ($p_{\Sigma 0}$), (2.17), can help regulate the total arm energy ($w_{p1} + w_{p2} + w_{p3} + w_{n1} + w_{n2} + w_{n3}$) (also see Fig. 2.1b). The difference arm power in the 0-frame ($p_{\Delta 0}$), (2.18), can help regulate the difference between the total upper and lower arms energies ($(w_{p1} + w_{p2} + w_{p3}) - (w_{n1} + w_{n2} + w_{n3})$). The summation arm power ($p_{\Sigma\alpha\beta}$) in the αβ-frame, (2.19) and (2.20), help regulate the summation phase energies ($(w_{p1} + w_{n1})$, $(w_{p2} + w_{n2})$, and $(w_{p3} + w_{n3})$). And the difference arm power ($p_{\Delta\alpha\beta}$) equations in the αβ-frame, (2.21) and (2.22), help to control the difference of the upper and lower arm (or the difference phase) energies ($(w_{p1} - w_{n1})$, $(w_{p2} - w_{n2})$, and $(w_{p3} - w_{n3})$) of all three phases of MMC (also see Fig. 2.1).

The summation arm power in the 0-frame ($p_{\Sigma 0}$), (2.17), consists of two power terms (0.5 ($v_{a\alpha}\, i_{a\alpha} + v_{a\beta}\, i_{a\beta}$), and $v_b\, i_{b0}$). Thus, the average summation arm power in the 0-frame ($\bar{p}_{\Sigma 0}$) can be varied by controlling the average power term $0.5\ \overline{(v_{a\alpha}\, i_{a\alpha} + v_{a\beta}\, i_{a\beta})}$, or $\overline{v_b\, i_{b0}}$. The average power term $\left(0.5\ \overline{(v_{a\alpha}\, i_{a\alpha} + v_{a\beta}\, i_{a\beta})} = V_a\, i_{ad+}/\sqrt{2}\right)$ can be varied by controlling the three-phase positive sequence current in the d-axis (i_{ad+}) (also see (2.28)), and the average power term ($\overline{v_b\, i_{b0}} = V_b\, I^b_{b0}$) can be altered by changing the zero-sequence circulating current (i^b_{b0}) in phase with the single-phase voltage (v_b). Here, i^b_{b0} ($= -i^b_b/3$) is equivalent to the minus of the single-phase current in phase with v_b (i^b_b) (also see (2.2)). Thus, two degrees of freedom ($DOF_1 = i_{ad+}$ and $DOF_2 = I^b_{b0}$) are possible to control total arm energy of MMC ($\bar{w}_{\Sigma 0}$) by varying $\bar{p}_{\Sigma 0}$.

Also, the difference arm power in the 0-frame ($p_{\Delta 0}$), (2.18), consists of two power terms ($v_{a\alpha}\, i_{b\alpha} + v_{a\beta}\, i_{b\beta}$, and $2\, v_{cm}\, i_{b0}$). Therefore, the average difference arm power in the 0-frame ($\bar{p}_{\Delta 0}$) can be controlled by varying the average power term $\overline{v_{a\alpha}\, i_{b\alpha} + v_{a\beta}\, i_{b\beta}}$, or $\overline{2\, v_{cm}\, i_{b0}}$. The average power term $\left(\overline{v_{a\alpha}\, i_{b\alpha} + v_{a\beta}\, i_{b\beta}} = \sqrt{2}\, V_a\, i_{bd+}\right)$ can be adjusted by controlling the positive sequence circulating current in the d-axis (i_{bd+}) (also see (2.28)), and the average power term ($\overline{2\, v_{cm}\, i_{b0}} = 2\, V_{cm}\, I^{cm}_{b0}$) can be varied by changing the zero-sequence circulating current (i^{cm}_{b0}) in

phase with the common-mode voltage (v_{cm}). Therefore, two degrees of freedom ($DOF_3 = i_{bd+}$, and $DOF_4 = I_{b0}^{cm}$) are possible to regulate the total upper and total lower arm energies of MMC ($\overline{w}_{\Delta 0}$) by varying $\bar{p}_{\Delta 0}$.

Table 2.1: *Degrees of Freedom* (DOF) and six *Manipulated Inputs* ($MI_{1,2,3,4,5\&6}$) for regulating the corresponding arm energies of MMC.

1. Total Arm Energy ($\overline{w_{\Sigma 0}}$) Regulation using MI_1	**2. Total Upper and Lower Arms Energies ($\overline{w_{\Delta 0}}$) Regulation using MI_2**
DOF_1: Positive sequence three-phase currents in the d-axis $\left(i_{ad+}\right)$.	**DOF_3**: Positive sequence circulating currents in the d-axis $\left(i_{bd+}\right)$.
DOF_2: Zero sequence circulating current in phase with v_b $\left(i_{b0}^{b}\right)$.	**DOF_4**: Zero sequence circulating current in phase with v_{cm} $\left(i_{b0}^{cm}\right)$.
3. Summation Phase Energies ($\overline{w_{\Sigma\alpha\beta}}$) Regulation using $MI_{3\&4}$	**4. Difference Phase Energies ($\overline{w_{\Delta\alpha\beta}}$) Regulation using $MI_{5\&6}$**
$DOF_{5\&6}$: Circulating currents in phase with v_b $\left(i_{b\alpha\beta}^{b}\right)$.	**$DOF_{11\&12}$**: Three-phase currents in phase with v_b $\left(i_{a\alpha\beta}^{b}\right)$.
$DOF_{7\&8}$: Three-phase currents in phase with v_{cm} $\left(i_{a\alpha\beta}^{cm}\right)$.	**$DOF_{13\&14}$**: Single-phase currents in phase with $v_{a\alpha\beta}$ $\left(i_{b0}^{a\text{-}\alpha\beta}\right)$.
$DOF_{9\&10}$: Negative sequence three-phase currents $\left(i_{adq-}\right)$.	**$DOF_{15\&16}$**: Circulating currents in phase with v_{cm} $\left(i_{b\alpha\beta}^{cm}\right)$.
Note: $i_{b0} = -\frac{i_b}{3}$	**$DOF_{17\&18}$**: Negative sequence circulating currents $\left(i_{bdq-}\right)$.

The summation arm power in the α-frame ($p_{\Sigma\alpha}$), (2.19), consists of three power terms ($v_b\, i_{b\alpha}$, $v_{cm}\, i_{a\alpha}$, and 0.5 ($v_{a\alpha}\, i_{a\alpha} - v_{a\beta}\, i_{a\beta}$)). Thus, the average summation arm power in the α-frame ($\bar{p}_{\Sigma\alpha}$) can be varied by controlling the average power term $\overline{v_b\, i_{b\alpha}}$, $\overline{v_{cm}\, i_{a\alpha}}$, or $\overline{0.5\,(v_{a\alpha}\, i_{a\alpha} - v_{a\beta}\, i_{a\beta})}$. The average power term ($\overline{v_b\, i_{b\alpha}} = V_b\, I_{b\alpha}^{b}$) can be altered by changing the circulating current in the α-frame ($i_{b\alpha}^{b}$) in phase with the single-phase voltage (v_b), the average power term ($\overline{v_{cm}\, i_{a\alpha}} = V_{cm}\, I_{a\alpha}^{cm}$) can be altered by changing the three-phase current in the α-frame ($i_{a\alpha}^{cm}$) in phase with the common-mode voltage (v_{cm}) and the average power term

$\left(\overline{0.5\,(v_{a\alpha}\,i_{a\alpha} - v_{a\beta}\,i_{a\beta})} = V_a\,i_{ad-}/\sqrt{2}\right)$ can be varied by controlling the negative sequence three-phase current in the d-axis (i_{ad-}) (also see (2.29)). Thus, three degrees of freedom ($DOF_5 = I^{b}_{b\alpha}$, $DOF_7 = I^{cm}_{a\alpha}$, and $DOF_9 = i_{ad-}$) are possible to regulate the summation phase energy of MMC in the α-frame ($\overline{w}_{\Delta\Sigma\alpha}$) by varying $\bar{p}_{\Sigma\alpha}$.

Similarly, the summation arm power in the β-frame ($p_{\Sigma\beta}$), (2.20), consists of three power terms ($v_b\,i_{b\beta}$, $v_{cm}\,i_{a\beta}$, and $0.5\,(v_{a\alpha}\,i_{a\beta} + v_{a\beta}\,i_{a\alpha})$). Thus, the average summation arm power in the β-frame ($\bar{p}_{\Sigma\beta}$) can be controlled by varying the average power term $\overline{v_b\,i_{b\beta}}$, $\overline{v_{cm}\,i_{a\beta}}$, or $\overline{0.5\,(v_{a\alpha}\,i_{a\beta} + v_{a\beta}\,i_{a\alpha})}$. The average power term ($\overline{v_b\,i_{b\beta}} = V_b I^{b}_{b\beta}$) can be controlled by changing the circulating current in the β-frame ($i^{b}_{b\beta}$) in phase with the single-phase voltage (v_b), the average power term ($\overline{v_{cm}\,i_{a\beta}} = V_{cm} I^{cm}_{a\beta}$) can be altered by changing the three-phase current in the β-frame ($i^{cm}_{a\beta}$) in phase with the common-mode voltage (v_{cm}) and the average power term $\left(\overline{0.5\,(v_{a\alpha}\,i_{a\beta} + v_{a\beta}\,i_{a\alpha})} = V_a\,i_{aq-}/\sqrt{2}\right)$ can be varied by controlling the negative sequence three-phase current in the q-axis (i_{ad-}) (also see (2.30)). Thus, additional three degrees of freedom ($DOF_6 = I^{b}_{b\beta}$, $DOF_8 = I^{cm}_{a\beta}$, and $DOF_{10} = i_{aq-}$) are possible to regulate the summation phase energy of MMC in the β-frame ($\overline{w}_{\Sigma\beta}$) by varying $\bar{p}_{\Sigma\beta}$.

The difference arm power in the α-frame ($p_{\Delta\alpha}$), (2.21), consists of four power terms ($0.5\,v_b\,i_{a\alpha}$, $2\,v_{a\alpha}\,i_{b0}$, $2\,v_{cm}\,i_{b\alpha}$, and $v_{a\alpha}\,i_{b\alpha} - v_{a\beta}\,i_{b\beta}$). Thus, the average difference arm power in the α-frame ($\bar{p}_{\Delta\alpha}$) can be varied by controlling the average power term $\overline{0.5\,v_b\,i_{a\alpha}}$, $\overline{2\,v_{a\alpha}\,i_{b0}}$, $\overline{2\,v_{cm}\,i_{b\alpha}}$, or $\overline{v_{a\alpha}\,i_{b\alpha} - v_{a\beta}\,i_{b\beta}}$. The average power term ($\overline{0.5\,v_b\,i_{a\alpha}} = 0.5\,V_b I^{b}_{a\alpha}$) can be altered by changing the three-phase current in the α-frame ($i^{b}_{a\alpha}$) in phase with the single-phase voltage (v_b), the average power term ($\overline{2\,v_{a\alpha}\,i_{b0}} = 2\,V_a I^{a\text{-}\alpha}_{b0}$) can be varied by changing the zero-sequence circulating current ($i^{a\text{-}\alpha}_{b0}$) in phase with the three-phase voltage in the α-frame ($v_{a\alpha}$), the average power term ($\overline{2\,v_{cm}\,i_{b\alpha}} = 2\,V_{cm} I^{cm}_{b\alpha}$) can be adjusted with the help of the circulating current in the α-frame ($i^{cm}_{b\alpha}$) in phase with the common-mode voltage (v_{cm}) and the average power term $\left(\overline{v_{a\alpha}\,i_{b\alpha} - v_{a\beta}\,i_{b\beta}} = \sqrt{2}\,V_a\,i_{bd-}\right)$ can be modified by controlling the negative sequence circulating current in the d-axis (i_{bd-}) (also see (2.29)). Thus, four degrees of freedom ($DOF_{11} = I^{b}_{a\alpha}$, $DOF_{13} = I^{a\text{-}\alpha}_{b0}$, $DOF_{15} = I^{cm}_{b\alpha}$, and $DOF_{17} = i_{bd-}$) are possible to regulate the difference phase energy of MMC in the α-frame ($\overline{w}_{\Delta\alpha}$) by varying $\bar{p}_{\Delta\alpha}$.

Table 2.2: Stability analysis of all arm energies regulation techniques for direct AC-AC and DC-AC MMC topologies when no harmonics are injected into the load side of MMC. Here, n = integer, f_{cm} = Max(f_o, $3f_a$) if $f_b \neq 3f_a$, $f_{cm} = f_x$ if $f_b = 3f_a$, and $V_b = V_{dc}$ if $f_b = 0$. **Note**: v_{cm} can also be DC for AC-AC applications. Refer to section 2.4 to know about Matrix A and |A|.

Method	**Manipulated Inputs** (MI_1,MI_2,$MI_{3\&4}$, $MI_{5\&6}$)	**Determinant (|A|)** (Unstable if |A| = 0, otherwise stable)	
		$f_a = f_b \neq 0$	$f_a = n f_b, f_b = n f_a$, ($f_b = 0$ & $f_a \neq 0$).
1	i_{ad+}, i_{bd+}, $i^{b}_{b\alpha\beta}$, i_{bdq-}	0	$2\,V_a^4\,V_b^2$
2	i_{ad+}, i_{bd+}, $i^{b}_{b\alpha\beta}$, $i^{b}_{a\alpha\beta}$	$\frac{V_a^2}{16}\left(\cos^2(3\phi_b)\,V_a^2\,V_b^2 - \left(2V_a^2 - V_b^2\right)^2\right)$	$-\frac{1}{4}\,V_a^2\,V_b^4$
3	i_{ad+}, i_{bd+}, i_{adq-}, i_{bdq-}	$-V_a^2\left(V_a^2 - \frac{V_b^2}{4}\right)^2$	$-V_a^6$
4	i_{ad+}, i_{bd+}, i_{adq-}, $i^{b}_{a\alpha\beta}$	0	$\frac{1}{8}\,V_a^4\,V_b^2$
5	i^{b}_{b0}, i_{bd+}, $i^{b}_{b\alpha\beta}$, i_{bdq-}	0	$2\sqrt{2}\,V_a^3\,V_b^3$
6	i^{b}_{b0}, i_{bd+}, $i^{b}_{b\alpha\beta}$, $i^{a\text{-}\alpha\beta}_{b0}$	0	$-4\sqrt{2}\,V_a^3\,V_b^3$
7	i_{ad+}, i_{bd+}, $i^{b}_{b\alpha\beta}$, $i^{cm}_{b\alpha\beta}$	$-2\,V_a^2\,V_b^2\,V_{cm}^2$	$-4\,V_a^2\,V_b^2\,V_{cm}^2$
8	i_{ad+}, i_{bd+}, $i^{cm}_{a\alpha\beta}$, $i^{b}_{a\alpha\beta}$	$-\frac{1}{8}\,V_a^2\,V_b^2\,V_{cm}^2$	$-\frac{1}{4}\,V_a^2\,V_b^2\,V_{cm}^2$
9	i_{ad+}, i_{bd+}, $i^{cm}_{a\alpha\beta}$, $i^{cm}_{b\alpha\beta}$	$-4\,V_a^2\,V_{cm}^4$	$-4\,V_a^2\,V_{cm}^4$
10	i_{ad+}, i_{bd+}, $i^{cm}_{a\alpha\beta}$, i_{bdq-}	$2\,V_a^4\,V_{cm}^2$	$2\,V_a^4\,V_{cm}^2$
11	i_{ad+}, i_{bd+}, i_{adq-}, $i^{cm}_{b\alpha\beta}$	$2\,V_a^4\,V_{cm}^2$	$2\,V_a^4\,V_{cm}^2$
12	i^{b}_{b0}, i_{bd+}, $i^{b}_{b\alpha\beta}$, $i^{cm}_{b\alpha\beta}$	$-2\sqrt{2}\,V_a\,V_b^3\,V_{cm}^2$	$-4\sqrt{2}\,V_a\,V_b^3\,V_{cm}^2$
13	i^{b}_{b0}, i^{cm}_{b0}, $i^{b}_{b\alpha\beta}$, $i^{a\text{-}\alpha\beta}_{b0}$	0	$-8\,V_a^2\,V_b^3\,V_{cm}$
14	i^{b}_{b0}, i^{cm}_{b0}, $i^{b}_{b\alpha\beta}$, $i^{cm}_{b\alpha\beta}$	$-8\,V_b^3\,V_{cm}^3$	$-8\,V_b^3\,V_{cm}^3$
15	i^{b}_{b0}, i^{cm}_{b0}, $i^{b}_{b\alpha\beta}$, i_{bdq-}	$V_a^2\,V_b^3\,V_{cm}$	$4V_a^2\,V_b^3\,V_{cm}$

Similarly, the difference arm power in the β-frame ($p_{\Delta\beta}$), (2.22), consists of four power terms ($0.5\ v_b\ i_{a\beta}$, $2\ v_{a\beta}\ i_{b0}$, $2\ v_{cm}\ i_{b\beta}$, and $v_{a\alpha}\ i_{b\beta} + v_{a\beta}\ i_{b\alpha}$). Thus, the average difference arm power in the β-frame ($\bar{p}_{\Delta\beta}$) can be varied by controlling the average power term $\overline{0.5\ v_b\ i_{a\beta}}$, $\overline{2\ v_{a\beta}\ i_{b0}}$, $\overline{2\ v_{cm}\ i_{b\beta}}$, or $\overline{v_{a\alpha}\ i_{b\beta} + v_{a\beta}\ i_{b\alpha}}$. The average power term ($\overline{0.5\ v_b\ i_{a\beta}} = 0.5\ V_b\ I^{b}_{a\beta}$) can be altered by changing the three-phase current in the β-frame ($i^{b}_{a\beta}$) in phase with the single-phase voltage (v_b), the average power term ($\overline{2\ v_{a\beta}\ i_{b0}} = 2\ V_a\ I^{a\text{-}\beta}_{b0}$) can be adjusted with the help of the zero-sequence circulating current ($i^{a\text{-}\beta}_{b0}$) in phase with the three-phase voltage in the β-frame ($v_{a\beta}$), the average power term ($\overline{2\ v_{cm}\ i_{b\beta}} = 2\ V_{cm}\ I^{cm}_{b\beta}$) can be altered by changing the circulating current in the β-frame ($i^{cm}_{b\beta}$) in phase with the common-mode voltage (v_{cm}) and the average power term $\left(\overline{v_{a\alpha}\ i_{b\beta} + v_{a\beta}\ i_{b\alpha}} = \sqrt{2}\ V_a\ i_{bq-}\right)$ can be varied by controlling the negative sequence circulating current in the q-axis (i_{bq-}) (also see (2.30)). Thus, four degrees of freedom ($DOF_{12} = I^{b}_{a\beta}$, $DOF_{14} = I^{a\text{-}\beta}_{b0}$, $DOF_{16} = I^{cm}_{b\beta}$, and $DOF_{18} = i_{bq-}$) are possible to regulate the difference phase energy of MMC in the β-frame ($\overline{w}_{\Delta\beta}$) by varying $\bar{p}_{\Delta\beta}$.

All discussed possible degrees of freedom corresponding to their energy controllers (also see Fig. 2.1b) are listed in Table 2.1. Like the positive sequence three-phase current in the q-axis (i_{aq+}), the positive sequence circulating current in the q-axis (i_{bq+}) makes only reactive power in MMC. Thus, i_{bq+} is not considered as a degree of freedom to regulate the arm energies of MMC [KOL15a]. Simply put, three-phase (i_{ad+}, i_{adq-}, $i^{b}_{a\alpha\beta}$, and $i^{cm}_{a\alpha\beta}$), circulating (i_{bd+}, i_{bdq-}, $i^{b}_{b\alpha\beta}$, and $i^{cm}_{b\alpha\beta}$), and single-phase ($i^{a\text{-}\alpha\beta}_{b0}$, i^{b}_{b0}, i^{cm}_{b0}) currents in phase with three-phase ($v_{a\alpha\beta}$), single-phase (v_b), and common-mode (v_{cm}) voltages are listed as degrees of freedom in Table 2.1. The common-mode voltage (v_{cm}) also acts like a degree of freedom, which makes average arm power with the current components in phase with it.

2.3 Arm Energies Balancing Methods

Only six degrees of freedom are necessary for designing the six energy-balancing controllers to regulate the six-arm energies of MMC. The selected six degrees of freedom are termed as *Manipulated Inputs* (*MI*s). Referring to Table 2.1, the manipulated input MI_1, MI_2, $MI_{3\&4}$, and $MI_{5\&6}$ help to control the total energy ($\overline{w}_{\Sigma 0}$), total upper and total lower arms energies ($\overline{w}_{\Delta 0}$), the summation phase energies ($\overline{w}_{\Sigma\alpha\beta}$), and the difference phase energies ($\overline{w}_{\Delta\alpha\beta}$), respectively. All possible arm energy balancing methods can be derived by finding all combinations of six

degrees of freedom from the Table. 2.1. There are 48 valid combinations of six degrees of freedom, or the arm energies of MMC can be controlled in 48 different ways.

Table 2.2 and Table 2.3 present all these possible arm energy balancing methods. The second column of both tables represents the selected six degrees of freedom or manipulated inputs (MI_1, MI_2, $MI_{3\&4}$ and $MI_{5\&6}$). The single-phase or the three-phase systems can act as a source or load. When the three-phase system is the source, $MI_1 = DOF_1 = i_{ad+}$ and if the single-phase is the source, $MI_1 = DOF_2 = I_{b0}^{b}$. No harmonics are injected into the load current by the arm energy controllers listed in Table 2.2. In other words, controlling only the source current is enough to regulate the arm energies. In contrast, both source and load currents should be controlled to regulate the arm energies using the methods listed in Table 2.3. Thus, harmonics are injected into the load current for the energy balancing methods in Table 2.3.

If $DOF_4 = I_{b0}^{cm}$, $DOF_{13} = I_{b0}^{a\text{-}\alpha}$ or $DOF_{14} = I_{b0}^{a\text{-}\beta}$ is selected as a manipulated input, harmonics are injected into the single-phase current. Similarly, the harmonic is injected into the three-phase current if $DOF_{11} = I_{a\alpha}^{b}$, $DOF_{12} = I_{a\beta}^{b}$, $DOF_7 = I_{a\alpha}^{cm}$, $DOF_8 = I_{a\beta}^{cm}$, $DOF_9 = i_{ad-}$ or $DOF_{10} = i_{aq-}$ is selected as a manipulated input.

Only four energy balancing methods (Method-1, 5, 7 & 12) are possible, which do not inject harmonics into both load and source currents. The three-phase acts like a source if Method-1, or Method-7 is selected and the single-phase behaves like a source if Method-5 or Method-12 is selected. In the upcoming section 2.4, it will be proved that only two methods (Method-7 and 12), which do not inject harmonics into source and load currents, are stable for equal three-phase and single-phase frequency operation ($f_b = f_a \neq 0$), and the common-mode voltage (v_{cm}) is a must for equal frequency operation. And the other two methods (Method-1 and 5) are only stable for unequal frequency ($f_b \neq f_a$) operations.

2.4 Stability Analysis of the Arm Energy Balancing Methods

Stability analysis of the arm energy controller of MMC is essential, especially for the equal frequency operation ($f_b = f_a \neq 0$). f_b and f_a are single-phase and three-phase frequencies. (2.32) to (2.36) represent the general expression of the instantaneous three-phase current ($i_{a\alpha\beta}$), circulating current in the αβ-frame ($i_{b\alpha\beta}$), and circulating current in the 0-frame (i_{b0}), including all degrees of freedom. Each current ($i_{a\alpha\beta}$, $i_{b\alpha\beta}$, and i_{b0}) consists of components in phase with the three-phase ($v_{a\alpha\beta}$), single-phase (v_b), and common-mode (v_{cm}) voltages. The three-phase current ($i_{a\alpha\beta}$) also includes the positive sequence three-phase current in the q-axis (i_{aq+}), which is responsible for the reactive power in the three-phase system (Q_a). Also, the circulating current

in the 0-frame (i_{b0}) or the single-phase current ($i_b = -3\, i_{b0}$) includes the reactive power component ($i_{b0}^{\perp b}$). $i_{b0}^{\perp b}$ is perpendicular to v_b. (2.37) represents the relations between the reactive powers and the corresponding reactive current components. V_{aq} is assumed to equal zero, which can be achieved using a three-phase *Phase Locked Loop* (PLL).

$$i_{a\alpha} = \cos(\theta_a)\left(i_{ad+} + i_{ad-}\right) + \sin(\theta_a)\left(i_{aq-} - i_{aq+}\right) + \sqrt{2} I_{a\alpha}^{cm} \cos(\theta_{cm}) + \sqrt{2} I_{a\alpha}^{b} \cos(\theta_b) \quad (2.32)$$

$$i_{a\beta} = \cos(\theta_a)\left(i_{aq+} + i_{aq-}\right) + \sin(\theta_a)\left(i_{ad+} - i_{ad-}\right) + \sqrt{2} I_{a\beta}^{cm} \cos(\theta_{cm}) + \sqrt{2}\, I_{a\beta}^{b} \cos(\theta_b) \quad (2.33)$$

$$i_{b\alpha} = \cos(\theta_a)\left(i_{bd+} + i_{bd-}\right) + \sin(\theta_a)\, i_{bq-} + \sqrt{2} I_{b\alpha}^{cm} \cos(\theta_{cm}) + \sqrt{2} I_{b\alpha}^{b} \cos(\theta_b) \quad (2.34)$$

$$i_{b\beta} = \cos(\theta_a) i_{bq-} + \sin(\theta_a)\left(i_{bd+} - i_{bd-}\right) + \sqrt{2} I_{b\beta}^{cm} \cos(\theta_{cm}) + \sqrt{2}\, I_{b\beta}^{b} \cos(\theta_b) \quad (2.35)$$

$$i_{b0} = \sqrt{2} I_{b0}^{\perp b} \sin(\theta_b) + \sqrt{2} I_{b0}^{b} \cos(\theta_b) + \sqrt{2} I_{b0}^{cm} \cos(\theta_{cm}) + \sqrt{2} I_{b0}^{a\text{-}\alpha} \cos(\theta_a) + \sqrt{2} I_{b0}^{a\text{-}\beta} \sin(\theta_a) \quad (2.36)$$

$$I_{b0}^{\perp b} = -\frac{Q_b}{3\, V_b} \;;\; i_{aq+} = -\frac{2\, Q_a}{3\, V_{ad}} \quad (2.37)$$

Table 2.3: Stability analysis of all arm energies regulation techniques for direct AC-AC and DC-AC MMC topologies when harmonics are injected into the load side of MMC. Here, n = integer, $f_{cm} = \text{Max}(f_o, 3f_a)$ if $f_b \neq 3f_a$, $f_{cm} = f_x$ if $f_b = 3f_a$ and $V_b = V_{dc}$ if $f_b = 0$. **Note**: v_{cm} can also be DC for AC-AC applications. Refer to section 2.4 to know about Matrix A and |A|.

Method	**Manipulated Inputs** (MI_1,MI_2,$MI_{3\&4}$, $MI_{5\&6}$)	**Determinant (|A|)** (Unstable if |A| = 0, otherwise stable)	
		$f_a = f_b \neq 0$	$f_a = n f_b, f_b = n f_a$, ($f_b = 0$ & $f_a \neq 0$).
16	i_{ad+}, i_{bd+}, $i_{b\alpha\beta}^{b}$, $i_{b0}^{a\text{-}\alpha\beta}$	$-2\, V_a^2\, V_b^2 \left(V_a^2 - \frac{V_b^2}{4}\right)$	$-4\, V_a^4\, V_b^2$
17	i_{ad+}, i_{bd+}, $i_{a\alpha\beta}^{cm}$, $i_{b0}^{a\text{-}\alpha\beta}$	$-4\, V_a^2\, V_{cm}^2 \left(V_a^2 - \frac{V_b^2}{4}\right)$	$-4\, V_a^4\, V_{cm}^2$
18	i_{ad+}, i_{bd+}, i_{adq-}, $i_{b0}^{a\text{-}\alpha\beta}$	$2\, V_a^4 \left(V_a^2 - \frac{V_b^2}{4}\right)$	$2\, V_a^6$
19	i_{ad+}, i_{b0}^{cm}, $i_{b\alpha\beta}^{b}$, $i_{a\alpha\beta}^{b}$	$-\frac{\sqrt{2}}{4} V_a\, V_{cm} \left(V_a^2 - \frac{V_b^2}{2}\right)\left(V_a^2 - V_b^2\right)$	$-\frac{1}{4}\sqrt{2}\, V_a\, V_b^4\, V_{cm}$

20	$i_{\mathrm{ad}+}, i_{\mathrm{b0}}^{\mathrm{cm}}, i_{\mathrm{b}\alpha\beta}^{\mathrm{b}}, i_{\mathrm{b0}}^{\mathrm{a}-\alpha\beta}$	$-4\sqrt{2}\,V_{\mathrm{a}}\,V_{\mathrm{b}}^{2}\,V_{\mathrm{cm}}\left(V_{\mathrm{a}}^{2}-\frac{V_{\mathrm{b}}^{2}}{4}\right)$	$-4\sqrt{2}\,V_{\mathrm{a}}^{3}\,V_{\mathrm{b}}^{2}\,V_{\mathrm{cm}}$
21	$i_{\mathrm{ad}+}, i_{\mathrm{b0}}^{\mathrm{cm}}, i_{\mathrm{b}\alpha\beta}^{\mathrm{b}}, i_{\mathrm{b}\alpha\beta}^{\mathrm{cm}}$	$-4\sqrt{2}\,V_{\mathrm{a}}\,V_{\mathrm{b}}^{2}\,V_{\mathrm{cm}}^{3}$	$-4\sqrt{2}\,V_{\mathrm{a}}\,V_{\mathrm{b}}^{2}\,V_{\mathrm{cm}}^{3}$
22	$i_{\mathrm{ad}+}, i_{\mathrm{b0}}^{\mathrm{cm}}, i_{\mathrm{b}\alpha\beta}^{\mathrm{b}}, i_{\mathrm{bdq}-}$	$\frac{\sqrt{2}}{2}\,V_{\mathrm{a}}^{3}\,V_{\mathrm{b}}^{2}\,V_{\mathrm{cm}}$	$2\sqrt{2}\,V_{\mathrm{a}}^{3}\,V_{\mathrm{b}}^{2}\,V_{\mathrm{cm}}$
23	$i_{\mathrm{ad}+}, i_{\mathrm{b0}}^{\mathrm{cm}}, i_{\mathrm{a}\alpha\beta}^{\mathrm{cm}}, i_{\mathrm{a}\alpha\beta}^{\mathrm{b}}$	$-\frac{\sqrt{2}}{8}\,V_{\mathrm{a}}\,V_{\mathrm{b}}^{2}\,V_{\mathrm{cm}}^{3}$	$-\frac{1}{4}\sqrt{2}\,V_{\mathrm{a}}\,V_{\mathrm{b}}^{2}\,V_{\mathrm{cm}}^{3}$
24	$i_{\mathrm{ad}+}, i_{\mathrm{b0}}^{\mathrm{cm}}, i_{\mathrm{a}\alpha\beta}^{\mathrm{cm}}, i_{\mathrm{b0}}^{\mathrm{a}-\alpha\beta}$	$-4\sqrt{2}\,V_{\mathrm{a}}\,V_{\mathrm{cm}}^{3}\left(V_{\mathrm{a}}^{2}-\frac{V_{\mathrm{b}}^{2}}{4}\right)$	$-4\sqrt{2}\,V_{\mathrm{a}}^{3}\,V_{\mathrm{cm}}^{3}$
25	$i_{\mathrm{ad}+}, i_{\mathrm{b0}}^{\mathrm{cm}}, i_{\mathrm{a}\alpha\beta}^{\mathrm{cm}}, i_{\mathrm{b}\alpha\beta}^{\mathrm{cm}}$	$-4\sqrt{2}\,V_{\mathrm{a}}\,V_{\mathrm{cm}}^{5}$	$-4\sqrt{2}\,V_{\mathrm{a}}\,V_{\mathrm{cm}}^{5}$
26	$i_{\mathrm{ad}+}, i_{\mathrm{b0}}^{\mathrm{cm}}, i_{\mathrm{a}\alpha\beta}^{\mathrm{cm}}, i_{\mathrm{bdq}-}$	$2\sqrt{2}\,V_{\mathrm{a}}^{3}\,V_{\mathrm{cm}}^{3}$	$2\sqrt{2}\,V_{\mathrm{a}}^{3}\,V_{\mathrm{cm}}^{3}$
27	$i_{\mathrm{ad}+}, i_{\mathrm{b0}}^{\mathrm{cm}}, i_{\mathrm{adq}-}, i_{\mathrm{a}\alpha\beta}^{\mathrm{b}}$	0	$\frac{1}{8}\sqrt{2}\,V_{\mathrm{a}}^{3}\,V_{\mathrm{b}}^{2}\,V_{\mathrm{cm}}$
28	$i_{\mathrm{ad}+}, i_{\mathrm{b0}}^{\mathrm{cm}}, i_{\mathrm{adq}-}, i_{\mathrm{b0}}^{\mathrm{a}-\alpha\beta}$	$2\sqrt{2}\,V_{\mathrm{a}}^{3}\,V_{\mathrm{cm}}\left(V_{\mathrm{a}}^{2}-\frac{V_{\mathrm{b}}^{2}}{4}\right)$	$2\sqrt{2}\,V_{\mathrm{a}}^{5}\,V_{\mathrm{cm}}$
29	$i_{\mathrm{ad}+}, i_{\mathrm{b0}}^{\mathrm{cm}}, i_{\mathrm{adq}-}, i_{\mathrm{b}\alpha\beta}^{\mathrm{cm}}$	$2\sqrt{2}\,V_{\mathrm{a}}^{3}\,V_{\mathrm{cm}}^{3}$	$2\sqrt{2}\,V_{\mathrm{a}}^{3}\,V_{\mathrm{cm}}^{3}$
30	$i_{\mathrm{ad}+}, i_{\mathrm{b0}}^{\mathrm{cm}}, i_{\mathrm{adq}-}, i_{\mathrm{bdq}-}$	$-\sqrt{2}\,V_{\mathrm{a}}\,V_{\mathrm{cm}}\left(V_{\mathrm{a}}^{2}-\frac{V_{\mathrm{b}}^{2}}{4}\right)^{2}$	$-\sqrt{2}\,V_{\mathrm{a}}^{5}\,V_{\mathrm{cm}}$
31	$i_{\mathrm{b0}}^{\mathrm{b}}, i_{\mathrm{bd}+}, i_{\mathrm{b}\alpha\beta}^{\mathrm{b}}, i_{\mathrm{a}\alpha\beta}^{\mathrm{b}}$	$-\frac{\sqrt{2}}{8}V_{\mathrm{a}}V_{\mathrm{b}}\left(2\sin^{2}(3\phi_{\mathrm{b}})V_{\mathrm{a}}^{4}+\left(V_{\mathrm{a}}^{2}-V_{\mathrm{b}}^{2}\right)\left(4V_{\mathrm{a}}^{2}-V_{\mathrm{b}}^{2}\right)\right)$	$-\frac{1}{4}\sqrt{2}\,V_{\mathrm{a}}\,V_{\mathrm{b}}^{5}$
32	$i_{\mathrm{b0}}^{\mathrm{b}}, i_{\mathrm{bd}+}, i_{\mathrm{a}\alpha\beta}^{\mathrm{cm}}, i_{\mathrm{a}\alpha\beta}^{\mathrm{b}}$	$\frac{\sqrt{2}}{2}\,V_{\mathrm{a}}\,V_{\mathrm{b}}\,V_{\mathrm{cm}}^{2}\left(V_{\mathrm{a}}^{2}-\frac{V_{\mathrm{b}}^{2}}{2}\right)$	$-\frac{1}{4}\sqrt{2}\,V_{\mathrm{a}}\,V_{\mathrm{b}}^{3}\,V_{\mathrm{cm}}^{2}$
33	$i_{\mathrm{b0}}^{\mathrm{b}}, i_{\mathrm{bd}+}, i_{\mathrm{a}\alpha\beta}^{\mathrm{cm}}, i_{\mathrm{b0}}^{\mathrm{a}-\alpha\beta}$	0	$-4\sqrt{2}\,V_{\mathrm{a}}^{3}\,V_{\mathrm{b}}\,V_{\mathrm{cm}}^{2}$
34	$i_{\mathrm{b0}}^{\mathrm{b}}, i_{\mathrm{bd}+}, i_{\mathrm{a}\alpha\beta}^{\mathrm{cm}}, i_{\mathrm{b}\alpha\beta}^{\mathrm{cm}}$	$-4\sqrt{2}\,V_{\mathrm{a}}\,V_{\mathrm{b}}\,V_{\mathrm{cm}}^{4}$	$-4\sqrt{2}\,V_{\mathrm{a}}\,V_{\mathrm{b}}\,V_{\mathrm{cm}}^{4}$
35	$i_{\mathrm{b0}}^{\mathrm{b}}, i_{\mathrm{bd}+}, i_{\mathrm{a}\alpha\beta}^{\mathrm{cm}}, i_{\mathrm{bdq}-}$	$2\sqrt{2}\,V_{\mathrm{a}}^{3}\,V_{\mathrm{b}}\,V_{\mathrm{cm}}^{2}$	$2\sqrt{2}\,V_{\mathrm{a}}^{3}\,V_{\mathrm{b}}\,V_{\mathrm{cm}}^{2}$

36	$i^{b}_{b0}, i_{bd+}, i_{adq-}, i^{b}_{a\alpha\beta}$	$-\frac{\sqrt{2}}{8} V_a^3 V_b \left(V_a^2 - \frac{V_b^2}{4}\right)$	$\frac{1}{8}\sqrt{2} V_a^3 V_b^3$
37	$i^{b}_{b0}, i_{bd+}, i_{adq-}, i^{a\text{-}\alpha\beta}_{b0}$	0	$2\sqrt{2} V_a^5 V_b$
38	$i^{b}_{b0}, i_{bd+}, i_{adq-}, i^{cm}_{b\alpha\beta}$	$2\sqrt{2} V_a^3 V_b V_{cm}^2$	$2\sqrt{2} V_a^3 V_b V_{cm}^2$
39	$i^{b}_{b0}, i_{bd+}, i_{adq-}, i_{bdq-}$	$-\sqrt{2} V_a V_b \left(V_a^2 - \frac{V_b^2}{4}\right)^2$	$-\sqrt{2} V_a^5 V_b$
40	$i^{b}_{b0}, i^{cm}_{b0}, i^{b}_{b\alpha\beta}, i^{b}_{a\alpha\beta}$	$-\frac{3}{2} V_b V_{cm} \left(V_a^2 - \frac{V_b^2}{3}\right)\left(V_a^2 - V_b^2\right)$	$-\frac{1}{2} V_b^5 V_{cm}$
41	$i^{b}_{b0}, i^{cm}_{b0}, i^{cm}_{a\alpha\beta}, i^{b}_{a\alpha\beta}$	$V_b V_{cm}^3 \left(V_a^2 - \frac{V_b^2}{2}\right)$	$-\frac{1}{2} V_b^3 V_{cm}^3$
42	$i^{b}_{b0}, i^{cm}_{b0}, i^{cm}_{a\alpha\beta}, i^{a\text{-}\alpha\beta}_{b0}$	0	$-8 V_a^2 V_b V_{cm}^3$
43	$i^{b}_{b0}, i^{cm}_{b0}, i^{cm}_{a\alpha\beta}, i^{cm}_{b\alpha\beta}$	$-8 V_b V_{cm}^5$	$-8 V_b V_{cm}^5$
44	$i^{b}_{b0}, i^{cm}_{b0}, i^{cm}_{a\alpha\beta}, i_{bdq-}$	$4 V_a^2 V_b V_{cm}^3$	$4 V_a^2 V_b V_{cm}^3$
45	$i^{b}_{b0}, i^{cm}_{b0}, i_{adq-}, i^{b}_{a\alpha\beta}$	$-\frac{1}{4} V_a^2 V_b V_{cm} \left(V_a^2 - \frac{V_b^2}{4}\right)$	$\frac{1}{4} V_a^2 V_b^3 V_{cm}$
46	$i^{b}_{b0}, i^{cm}_{b0}, i_{adq-}, i^{a\text{-}\alpha\beta}_{b0}$	0	$4 V_a^4 V_b V_{cm}$
47	$i^{b}_{b0}, i^{cm}_{b0}, i_{adq-}, i^{cm}_{b\alpha\beta}$	$4 V_a^2 V_b V_{cm}^3$	$4 V_a^2 V_b V_{cm}^3$
48	$i^{b}_{b0}, i^{cm}_{b0}, i_{adq-}, i_{bdq-}$	$-2 V_b V_{cm} \left(V_a^2 - \frac{V_b^2}{4}\right)^2$	$-2 V_a^4 V_b V_{cm}$

(2.38) and (2.39) show the average arm power equations, including all *Degrees of Freedom* (DOF) using matrix notation. The residual matrix $\overline{P_{6x1}}$ contains the power terms corresponding to the reactive current components. Derivation of the general average arm power equations considering all degrees o are shown step by step in Appendix A.6. The general expressions of

the elements of the matrix a_{6x18} are documented in Table A.6.1, and Table A.6.2. And the general expressions of the elements of the matrix $\overline{P_{6x1}}$ are listed in Table A.6.3.

The elements of the matrices a_{6x18} and $\overline{P_{6x1}}$ for equal frequency operation ($f_b = f_a \neq 0$) are tabulated in Table A.6.4 and Table A.6.5, respectively. Similarly, the elements of matrices a_{6x18} and $\overline{P_{6x1}}$ for unequal frequency operations ($f_a = n f_b$, $f_b = n f_a$, ($f_b = 0$ & $f_a \neq 0$)) are tabulated in Table A.6.6, and Table A.6.7, respectively. Here, n = integer, and $f_{cm} = \text{Max}(f_o, 3f_a)$ if $f_b \neq 3f_a$, or $f_{cm} = f_x$ if $f_b = 3f_a$ ($x \neq$ a & $x \neq$ b). The frequency for mean calculation is $f_{Mean} = f_a$ if $f_b = f_a \neq 0$, $f_{Mean} = f_a$ if $f_b = 0$ & $f_a \neq 0$, $f_{Mean} = \text{Min}(f_a, f_b)$ if $f_b \neq 0$, and $f_{Mean} = f_{cm}$ if $f_b = f_a = 0$. The f_{Mean} and f_{cm} ($f_{cm} \neq f_a$ & $f_{cm} \neq f_b$) are selected to reduce additional coupling between the systems. During a particular case, DC-DC operation of MMC, while the starting of the three-phase AC machine, the common-mode frequency (f_{cm}) is saturated at a minimum value (f_o) for the stable operation of MMC [KOL15a].

$$\left(\overline{P_{\Sigma/\Delta\alpha\beta0}}\right)_{6x1} = a_{6x18}\, DOF_{18x1} + \overline{P_{6x1}} \tag{2.38}$$

$$\left(\overline{P_{\Sigma/\Delta\alpha\beta0}}\right)_{6x1} = \left(\overline{P_{\Sigma0}} \quad \overline{P_{\Delta0}} \quad \overline{P_{\Sigma\alpha}} \quad \overline{P_{\Sigma\beta}} \quad \overline{P_{\Delta\alpha}} \quad \overline{P_{\Delta\beta}}\right)^{T} \tag{2.39}$$

$$\left(\overline{P_{\Sigma/\Delta\alpha\beta0}}\right)_{6x1} = A_{6x6}\, MI_{6x1} + \overline{P_{rem(6x1)}} = 0_{6x1} \tag{2.40}$$

$$MI_{6x1} = -A_{6x6}^{-1}\, \overline{P_{rem(6x1)}} \tag{2.41}$$

$$A_{6x6} = a_{6x18}(:, MI\_index) \tag{2.42}$$

$$MI\_index = [1, 3, 5, 6, 17, 18] \text{ for Method-1} \tag{2.43}$$

$$MI\_index = [1, 3, 5, 6, 15, 16] \text{ for Method-7} \tag{2.44}$$

(2.40) represents the average arm power equation for an arm energy balancing method in a steady state. In the steady state, the average arm powers ($\overline{P_{\Sigma/\Delta\alpha\beta0}} = 0_{6x1}$) should equal zero to keep the average arm energies constant. $\overline{P_{rem(6x1)}}$ represents the remaining power terms matrix, which consists of the power terms corresponding to the reactive power current components $\left(i_{aq+} \text{ and } i_{b0}^{\perp b}\right)$ and the active power load current component $\left(i_{ad+} \text{ or } i_{b0}^{\parallel b}\right)$. (2.41) illustrates the solution of (2.40). It suggests that a valid solution only exists if the inverse of the matrix A_{6x6} is possible, or its determinant is nonzero ($|A| \neq 0$). The matrices A_{6x6} for all energy balancing methods given in Table 2.2, are shown in Table A.7.1 and Table A.7.2 for equal and unequal frequency operations, respectively. The matrix A_{6x6} can be derived from the matrix a_{6x18} by

knowing which six degrees of freedom are selected. (2.42) shows the relation between the matrix A_{6x6} and a_{6x18}. Here, *MI_index* represents a row matrix with elements equal to the index numbers of the selected six degrees of freedom.

Let us consider two arm energy balancing methods (Method-1 and Method-7) to understand the general steps used in analyzing the stability of a selected arm energy controller. Method-1 and Method-7 are selected because they are the only two possible arm energy balancing methods that do not inject harmonics into source and load currents when the three-phase acts like a source. Referring to Table 2.1 and Table 2.2, (2.43) and (2.44) represent the matrix *MI_index* for the energy balancing Method-1 and Method-7, respectively. The matrix A_{6x6} for Method-1 consists of the elements of columns 1, 3, 5, 6, 17, and 18 of the matrix a_{6x18}. Similarly, the matrix A_{6x6} for Method-7 consists of the elements of columns 1, 3, 5, 6, 15, and 16 of the matrix a_{6x18}. Referring to Table A.6.4, (2.42), (2.43), and (2.44), the matrices A_{6x6} for Method-1 and Method-7 for equal frequency ($f_b = f_a \neq 0$) operation are shown in (2.45) and (2.46), respectively (also see Table A.7.1). The matrix A_{6x6} is a non-diagonal matrix; hence the manipulated inputs are naturally coupled in equal frequency operation. (2.47) shows the determinant (|A|) of matrix A_{6x6} for Method-1 and Method-7 for equal frequency ($f_b = f_a \neq 0$) operation. Maple software is used to compute all determinants. The determinant |A| equals zero for Method-1; hence Method-1 is unstable for equal frequency operation. On the other hand, Method-7 has a nonzero determinant; thus, the arm energy balancing Method-7 is stable for equal frequency operation.

$$A_{6x6} = \begin{pmatrix} \frac{\sqrt{2}V_a}{2} & 0 & 0 & 0 & 0 & 0 \\ 0 & -\sqrt{2}\,V_a & -V_a\cos(\phi_b) & V_a\sin(\phi_b) & 0 & 0 \\ 0 & \frac{\sqrt{2}\,V_b\cos(\phi_b)}{2} & V_b & 0 & \frac{\sqrt{2}\,V_b\cos(\phi_b)}{2} & -\frac{\sqrt{2}\,V_b\sin(\phi_b)}{2} \\ 0 & -\frac{\sqrt{2}\,V_b\sin(\phi_b)}{2} & 0 & V_b & \frac{\sqrt{2}\,V_b\sin(\phi_b)}{2} & \frac{\sqrt{2}\,V_b\cos(\phi_b)}{2} \\ -\frac{\sqrt{2}\,V_b\cos(\phi_b)}{4} & 0 & -V_a\cos(\phi_b) & -V_a\sin(\phi_b) & -\sqrt{2}\,V_a & 0 \\ \frac{\sqrt{2}\,V_b\sin(\phi_b)}{4} & 0 & -V_a\sin(\phi_b) & V_a\cos(\phi_b) & 0 & \sqrt{2}\,V_a \end{pmatrix} \text{ for Method-1} \quad (2.45)$$

$$A_{6x6} = \begin{pmatrix} \frac{\sqrt{2}}{2}V_a & 0 & 0 & 0 & 0 & 0 \\ 0 & -\sqrt{2}\,V_a & -V_a\cos(\phi_b) & V_a\sin(\phi_b) & 0 & 0 \\ 0 & \frac{\sqrt{2}}{2}V_b\cos(\phi_b) & V_b & 0 & 0 & 0 \\ 0 & -\frac{\sqrt{2}}{2}V_b\sin(\phi_b) & 0 & V_b & 0 & 0 \\ -\frac{\sqrt{2}}{4}V_b\cos(\phi_b) & 0 & -V_a\cos(\phi_b) & -V_a\sin(\phi_b) & -2\,V_{cm} & 0 \\ \frac{\sqrt{2}}{4}V_b\sin(\phi_b) & 0 & -V_a\sin(\phi_b) & V_a\cos(\phi_b) & 0 & -2\,V_{cm} \end{pmatrix} \text{ for Method-7} \quad (2.46)$$

$$|A| = 0 \text{ for Method-1 and } |A| = -2\,V_a^2\,V_b^2\,V_{cm}^2 \text{ for Method-7} \tag{2.47}$$

Similarly, (2.48) and (2.49) represent the matrix A_{6x6} for Method-1 and Method-7 for unequal frequency ($f_a = n\,f_b, f_b = n\,f_a$, or ($f_b = 0$ & $f_a \neq 0$)) operations, and their determinants (|A|) are given in (2.50). Here, n = integer, and $V_b = V_{dc}$ if the single-phase side of MMC is DC ($f_b = 0$). The determinant |A| is nonzero for Method-1 and method-7; hence, both methods can regulate the arm energies for unequal frequency operations. Further, the matrix A_{6x6} is a diagonal matrix representing that the manipulated inputs are naturally decoupled for the unequal frequency operations. For unequal frequency operations, the manipulated inputs only need to compensate for the losses in the converter; therefore, their magnitude is low in a steady state.

$$A_{6x6} = \begin{pmatrix} \frac{\sqrt{2}}{2}V_a & 0 & 0 & 0 & 0 & 0 \\ 0 & -\sqrt{2}\,V_a & 0 & 0 & 0 & 0 \\ 0 & 0 & V_b & 0 & 0 & 0 \\ 0 & 0 & 0 & V_b & 0 & 0 \\ 0 & 0 & 0 & 0 & -\sqrt{2}\,V_a & 0 \\ 0 & 0 & 0 & 0 & 0 & \sqrt{2}\,V_a \end{pmatrix} \text{ for Method-1} \tag{2.48}$$

$$A_{6x6} = \begin{pmatrix} \frac{\sqrt{2}}{2}V_a & 0 & 0 & 0 & 0 & 0 \\ 0 & -\sqrt{2}\,V_a & 0 & 0 & 0 & 0 \\ 0 & 0 & V_b & 0 & 0 & 0 \\ 0 & 0 & 0 & V_b & 0 & 0 \\ 0 & 0 & 0 & 0 & -2\,V_{cm} & 0 \\ 0 & 0 & 0 & 0 & 0 & -2\,V_{cm} \end{pmatrix} \text{ for Method-7} \tag{2.49}$$

$$|A| = 2\,V_a^4\,V_b^2 \text{ for Method-1 and } |A| = -4\,V_a^2\,V_b^2\,V_{cm}^2 \text{ for Method-7} \tag{2.50}$$

$$V_b = V_{dc} \text{ if } f_b = 0 \tag{2.51}$$

The general expressions of determinant |A| for all possible arm energy balancing methods are also listed in Table 2.2 and Table 2.3. Determinant |A| is nonzero for all methods for unequal frequency ($f_a = n\,f_b, f_b = n\,f_a$, or ($f_b = 0$ & $f_a \neq 0$)) operations; therefore, all methods are stable for unequal frequency operations. Referring to Table A.7.2, matrix A_{6x6} is found to be diagonal for all arm energy balancing methods for unequal frequency operations; hence naturally, all manipulated inputs are decoupled. On the other hand, several methods are found unstable for equal frequency operation due to the coupling between the manipulated inputs. Further, all

energy balancing methods without having current components in phase with the common-mode voltage (v_{cm}) are unstable for equal frequency operation. Thus, common-mode voltage is a must to regulate the arm energies for equal frequency operation of MMC.

All energy balancing methods having factor $(4V_a^2 - V_b^2)$, $(3V_a^2 - V_b^2)$, $(2V_a^2 - V_b^2)$, $(V_a^2 - V_b^2)$, $\cos^2(3\phi_b)$, or $\sin^2(3\phi_b)$ in the determinant |A|, can also become unstable during *Low Voltage Ride Through* (LVRT) or *High Voltage Ride Through* (HVRT); hence those methods are also not advisable to implement on the actual system for equal frequency operation. It can be further noted that out of the four energy balancing methods (Method-1, 5, 7, and 12), which do not inject harmonics into both source and load currents, only two energy balancing methods (Method-7 and 12) are found stable for equal frequency operation. Method-7can be used if the three-phase is the source, and Method-12 can be used if the single-phase is the source.

2.4.1 Stability Analysis during Failure Conditions

During a hard single-phase failure condition ($V_b = 0$), all stable methods with V_b as a factor in |A| become unstable because |A| becomes zero. Only Method-9, 10, 11, 25, 26, and 29 are stable for the hard short-circuit condition on the single-phase side for equal frequency operations. And only Method-14 and Method-43 are stable for equal frequency operation during the hard three-phase short circuit condition ($V_a = 0$). Method-14 or method-43 can also be used for a special operating condition (DC-DC operation) of MMC during the starting of the three-phase electric machine in variable drive applications. DC-DC operation of MMC can also be analyzed as equal frequency operation of MMC ($f_b = f_a = 0$).

Many methods (Method-3, 9, 10, 11, 17, 18, 24, 25, 26, 28, 29, and 30) are stable for the single-phase hard short-circuit conditions for unequal frequency operations. But, only four methods (Method-14, 40, 41, and 43) are stable for the hard three-phase short-circuit conditions. Only the energy balancing methods that inject harmonics into the source, load, or both side currents are stable during the hard short circuit conditions. Since the failure conditions last only a few hundred milliseconds, these energy balancing methods can be switched from one to another for stable operation of MMC during the failure or a particular (DC-DC) operating condition. Otherwise, MMC should be disconnected if the controller becomes unstable during the failure conditions.

2.5 Analytical Toolchain to Analyze MMC's Performance

Table 2.2 and Table 2.3 suggest that MMC arm energies can be regulated using various methods for both equal and unequal frequency operations. But, the performance of MMC would vary

with energy balancing methods. Thus, a suitable energy balancing method that meets the boundary conditions and guarantees stable operation during normal and abnormal conditions should be selected. The best way to analyze and compare the performance of MMC is to test the energy balancing methods in simulation, including the existing system and controllers. But it is time taking and requires more staffing and cost. The performance of MMC can be quickly analyzed and compared mathematically, which would save a significant amount of time and money. Hence, a mathematical analytical toolchain is proposed to facilitate analyzing and comparing the performance of MMC in the steady state for the stable arm energy balancing methods.

The following steps can be followed to mathematically compute the MMC, three-phase, and single-phase parameters for a selected stable arm energy balancing method.

Step-1: System definition

1. Identification of the load and the source side of MMC. It helps to select the first manipulated input (MI_1) to regulate the total energy of MMC (see Table 2.1).
2. Identification of the three-phase (f_a) and single-phase (f_b) system frequencies.
3. Defining the three-phase ($v_{a\alpha\beta}$), single-phase (v_b), and common-mode (v_{cm}) voltages.

$$\theta_a = \omega_a t \; ; \; \theta_b = \omega_b t + \phi_b \; ; \; \theta_{cm} = \omega_{cm} t + \phi_{cm} \tag{2.52}$$

$$v_{a\alpha} = \sqrt{2} V_a \cos(\theta_a), \; v_{a\beta} = \sqrt{2} V_a \sin(\theta_a), \; v_b = \sqrt{2} V_b \cos(\theta_b) \text{ and } v_{cm} = \sqrt{2} V_{cm} \cos(\theta_{cm}) \tag{2.53}$$

Table 2.4: Load active and reactive current components.

	If the three-phase is a load	If the single-phase is a load
Reactive Power Component	$i_{aq+} = -\frac{2\,Q_a}{3\,V_{ad}}$	$I_{b0}^{\perp b} = -\frac{Q_b}{3\,V_b}$
Active Power Component	$i_{ad+} = \frac{2\,P_a}{3\,V_{ad}}$	$I_{b0}^{b} = -\frac{P_b}{3\,V_b}$

4. Defining the active load power (P_a or P_b) and the reactive load power (Q_a or Q_b) according to Table 2.4.

Step-2: Solving Manipulated Inputs (MI_{6x1}) and System Currents

(2.32) to (2.36) show the general expression of the three-phase current ($i_{a\alpha\beta}$), the circulating current in the αβ-frame ($i_{b\alpha\beta}$), and the circulating current in the 0-frame (i_{b0}) or the single-phase current ($i_b = -3\,i_{b0}$), including all 18 degrees of freedom and reactive current components $\left(i_{aq+} \text{ and } i_{b0}^{\perp b}\right)$. The general current expressions retain only the reactive current components

(i_{aq+} and $i^{\perp b}_{b0}$), active load power component (i_{ad+} or i^{b}_{b0}), and the selected six degrees of freedom or manipulated inputs for an energy balancing method. The remaining 12 degrees of freedom are ignored or set to zero. For a better understanding, let us consider two energy balancing methods (Method-7 and Method-12). Table 2.5 represents the parameters corresponding to Method-7 and Method- 12. The single-phase acts as a load for Method-7, and the three-phase behaves like a load for Method-12. (2.54) to (2.58) show the instantaneous current expressions for Method-7 or Method-12.

Table 2.5: Parameters for the energy balancing Method-7 and Method-12.

Method	Load	Selected Manipulated Inputs	*MI_index*	A_{6x6}
7	Single-phase	i_{ad+}, i_{bd+}, $i^{b}_{b\alpha\beta}$, $i^{cm}_{b\alpha\beta}$	[1, 3, 5, 6, 15, 16]	$a_{6x18}(:, MI\_index)$
12	Three-phase	i^{b}_{b0}, i_{bd+}, $i^{b}_{b\alpha\beta}$, $i^{cm}_{b\alpha\beta}$	[2, 3, 5, 6, 15, 16]	$a_{6x18}(:, MI\_index)$

$$i_{a\alpha} = \cos(\theta_a)\, i_{ad+} - \sin(\theta_a)\, i_{aq+} \tag{2.54}$$

$$i_{a\beta} = \cos(\theta_a)\, i_{aq+} + \sin(\theta_a)\, i_{ad+} \tag{2.55}$$

$$i_{b\alpha} = \cos(\theta_a)\, i_{bd+} + \sqrt{2} I^{cm}_{b\alpha} \cos(\theta_{cm}) + \sqrt{2} I^{b}_{b\alpha} \cos(\theta_b) \tag{2.56}$$

$$i_{b\beta} = \sin(\theta_a)\, i_{bd+} + \sqrt{2} I^{cm}_{b\beta} \cos(\theta_{cm}) + \sqrt{2}\, I^{b}_{b\beta} \cos(\theta_b) \tag{2.57}$$

$$i_{b0} = \sqrt{2} I^{\perp b}_{b0} \sin(\theta_b) + \sqrt{2} I^{b}_{b0} \cos(\theta_b) \tag{2.58}$$

$$\left(\overline{P_{\Sigma/\Delta\alpha\beta0}}\right)_{6x1} = A_{6x6}\, MI_{6x1} + \overline{P_{rem(6x1)}} = 0_{6x1} \tag{2.59}$$

$$MI_{6x1} = -\, A^{-1}_{6x6}\, \overline{P_{rem(6x1)}} \tag{2.60}$$

$$(MI_{6x1}) = \left(i_{ad+}\ \ i_{bd+}\ \ I^{b}_{b\alpha}\ \ I^{b}_{b\beta}\ \ I^{cm}_{b\alpha}\ \ I^{cm}_{b\beta}\right)^{T} \text{ for Method-7} \tag{2.61}$$

$$(MI_{6x1}) = \left(I^{b}_{b0}\ \ i_{bd+}\ \ I^{b}_{b\alpha}\ \ I^{b}_{b\beta}\ \ I^{cm}_{b\alpha}\ \ I^{cm}_{b\beta}\right)^{T} \text{ for Method-12} \tag{2.62}$$

$$A_{6x6} = a_{6x18}(:, MI\_index) \tag{2.63}$$

$$A_{6x6} = \begin{pmatrix} \frac{\sqrt{2}}{2} V_a & 0 & 0 & 0 & 0 & 0 \\ 0 & -\sqrt{2}\, V_a & -V_a \cos(\phi_b) & V_a \sin(\phi_b) & 0 & 0 \\ 0 & \frac{\sqrt{2}}{2} V_b \cos(\phi_b) & V_b & 0 & 0 & 0 \\ 0 & -\frac{\sqrt{2}}{2} V_b \sin(\phi_b) & 0 & V_b & 0 & 0 \\ -\frac{\sqrt{2}}{4} V_b \cos(\phi_b) & 0 & -V_a \cos(\phi_b) & -V_a \sin(\phi_b) & -2\, V_{cm} & 0 \\ \frac{\sqrt{2}}{4} V_b \sin(\phi_b) & 0 & -V_a \sin(\phi_b) & V_a \cos(\phi_b) & 0 & -2\, V_{cm} \end{pmatrix} \text{ for Method-7} \quad (2.64)$$

(2.59) uses matrix notation to show the average arm power equation in the steady state. (2.60) represents the solution of (2.59). The matrix MI_{6x1} for Method-7 and Method-12 are given in (2.61) and (2.62), respectively. Matrix A_{6x6} can be derived from the matrix a_{6x18} using the general relation shown in (2.63). The frequency for mean calculation is $f_{Mean} = f_a$ if $f_b = f_a \neq 0$, $f_{Mean} = f_a$ if $f_b = 0$ & $f_a \neq 0$, $f_{Mean} = \text{Min}(f_a, f_b)$ if $f_b \neq 0$, and $f_{Mean} = f_{cm}$ if $f_b = f_a = 0$. The matrix A_{6x6} for the energy balancing techniques from Method-1 to Method-15 are documented in Appendix A.7 for equal and unequal frequency operations. The matrices A_{6x6} for Method-7 and Method-12 for equal frequency operation ($f_b = f_a$) are given in (2.64) and (2.65).

$$A_{6x6} = \begin{pmatrix} V_b & 0 & 0 & 0 & 0 & 0 \\ 0 & -\sqrt{2}\, V_a & -V_a \cos(\phi_b) & V_a \sin(\phi_b) & 0 & 0 \\ 0 & \frac{\sqrt{2}}{2} V_b \cos(\phi_b) & V_b & 0 & 0 & 0 \\ 0 & -\frac{\sqrt{2}}{2} V_b \sin(\phi_b) & 0 & V_b & 0 & 0 \\ -2\, V_a \cos(\phi_b) & 0 & -V_a \cos(\phi_b) & -V_a \sin(\phi_b) & -2\, V_{cm} & 0 \\ 2\, V_a \sin(\phi_b) & 0 & -V_a \sin(\phi_b) & V_a \cos(\phi_b) & 0 & -2\, V_{cm} \end{pmatrix} \text{ for Method-12} \quad (2.65)$$

The remaining power matrix $\overline{P_{rem(6x1)}}$ differs based on which side (three-phase or single-phase) of MMC behaves like a load. (2.66) shows a general expression for the remaining matrix $\overline{P_{rem(6x1)}}$ when the single-phase acts like a load ($MI_1 = i_{ad+}$) , and (2.67) represents $\overline{P_{rem(6x1)}}$ when the three-phase acts like a load ($MI_1 = \overset{b}{i}_{b0}$). Table 2.6 shows the elements of the residual matrix $\overline{P_{6x1}}$ for equal and unequal frequency operations. For unequal frequency operation, the $\overline{P_{6x1}}$ is a zero matrix because the three-phase voltage ($v_{a\alpha\beta}$) and single-phase current ($i_b = -3\, i_{b0}$) do not make average power together, and the three-phase current ($i_{a\alpha\beta}$) and single-phase voltage (v_b) do not make average power. In other words, the three-phase and single-phase systems are naturally decoupled in the average arm power plant model for unequal frequency operations.

But the three-phase and the single-phase currents and voltages can make average power with each other for equal frequency operation; hence the matrix $\overline{P_{6x1}}$ is nonzero. The first element of the matrix $\overline{P_{6x1}}$ is zero but the first element of $\overline{P_{rem(6x1)}}$ is nonzero because the elements $a_{6x18}(1,1)$ and $a_{6x18}(2,1)$ are nonzero (see (2.66), (2.67) and Table A.6.4), it means the first manipulated input, MI_1, has to compensate for the load active power and system losses. The second to fourth elements of the matrix $\overline{P_{6x1}}$ and $\overline{P_{rem(6x1)}}$ are zero, which means that the manipulated inputs (MI_2, and $MI_{3\&4}$) only have to compensate for the losses in the system. But the last two elements of the matrix $\overline{P_{6x1}}$ is nonzero; hence, the last two manipulated inputs ($MI_{5\&6}$) have to compensate for the additional average terms and losses in the system for equal frequency operation. The last two elements of the matrix $\overline{P_{6x1}}$ are nonzero only because of the load and source reactive powers.

The matrix $\overline{P_{6x1}}$ could also be made zero for equal frequency operation by compensating load reactive power with the source reactive power with the help of (2.68) or (2.69). (2.68) is used when the single-phase is load and (2.69) is used when the three-phase is load. But it should be remembered that (2.68) and (2.69) can only be realized if it is allowed to supply reactive power to the source. If the source only allows exchanging active power, then (2.68) and (2.69) cannot be realized, and the source reactive current component should be set to zero.

Table 2.6: $\overline{P_{6\times1}}$ for equal ($f_b = f_a \neq 0$) and unequal ($f_a = n f_b$, $f_b = n f_a$, or ($f_b = 0$ & $f_a \neq 0$)) frequency operations.

		Residual Arm powers ($\overline{P_{6\times1}}$)	
		$f_a = f_b \neq 0$	$f_a = n f_b$, $f_b = n f_a$, or ($f_b = 0$ & $f_a \neq 0$)
$\overline{P_{\Sigma 0}}$	P_1	0	0
$\overline{P_{\Delta 0}}$	P_2	0	0
$\overline{P_{\Sigma \alpha}}$	P_3	0	0
$\overline{P_{\Sigma \beta}}$	P_4	0	0
$\overline{P_{\Delta \alpha}}$	P_5	$-\left(\frac{V_b\, i_{aq+}}{2\sqrt{2}} + 2\, V_a\, I_{b0}^{\perp b}\right)\sin(\phi_b)$	0
$\overline{P_{\Delta \beta}}$	P_6	$-\left(\frac{V_b\, i_{aq+}}{2\sqrt{2}} + 2\, V_a\, I_{b0}^{\perp b}\right)\cos(\phi_b)$	0

$$\overline{P_{\text{rem(6x1)}}} = \overline{P_{\text{6x1}}} + \text{a}_{\text{6x18}}(:,2)\, I_{\text{b0}}^{\text{b}} \text{ if } MI_1 = i_{\text{ad+}} \text{ (Method-7)} \tag{2.66}$$

$$\overline{P_{\text{rem(6x1)}}} = \overline{P_{\text{6x1}}} + \text{a}_{\text{6x18}}(:,1)\, i_{\text{ad+}} \text{ if } MI_1 = I_{\text{b0}}^{\text{b}} \text{ (Method-12)} \tag{2.67}$$

$$i_{\text{aq+}} = -\frac{4\sqrt{2}\, V_{\text{a}}\, I_{\text{b0}}^{\perp\text{b}}}{V_{\text{b}}} \text{ if } MI_1 = i_{\text{ad+}} \text{ (Method-7)} \tag{2.68}$$

$$I_{\text{b0}}^{\perp\text{b}} = -\frac{V_{\text{b}}\, i_{\text{aq+}}}{4\sqrt{2}\, V_{\text{a}}} \text{ if } MI_1 = I_{\text{b0}}^{\text{b}} \text{ (Method-12)} \tag{2.69}$$

$$i_{\text{p123}} = i_{\text{b123}} - \frac{i_{\text{a123}}}{2} \;;\; i_{\text{n123}} = i_{\text{b123}} + \frac{i_{\text{a123}}}{2} \tag{2.70}$$

Solving (2.60) with the help of the derived matrices $\overline{P_{\text{rem(6x1)}}}$ and A_{6x6} would give the solution of the manipulated input matrix MI_{6x1}. The instantaneous value of the three-phase current ($i_{\text{a}\alpha\beta}$), the single-phase current ($i_{\text{b}} = -3\, i_{\text{b0}}$), and the circulating current in the αβ-frame ($i_{\text{b}\alpha\beta}$) can be obtained by substituting the elements of the matrix MI_{6x1} and reactive current components $\left(i_{\text{aq+}} \text{ and } i_{\text{b0}}^{\perp\text{b}}\right)$ in (2.54) to (2.58). Inverse Clarke's transformation can transfer the three-phase ($i_{\text{a}\alpha\beta}$) and the circulating current ($i_{\text{b}\alpha\beta0}$) components from the αβ0-frame to the abc-frame (i_{a123}, and i_{b123}). The instantaneous upper (i_{p123}) and lower (i_{n123}) arm currents of MMC can be computed using (2.70).

Step-3: Solving the Arm Power and the Ripple Arm Energy

The instantaneous arm power expression in the αβ0-frame using the summation and difference notation are given from (2.17) to (2.22) in Section 2.1. Substituting the instantaneous voltages ($v_{\text{a}\alpha\beta}$, v_{b} and v_{cm}) from step-1 and the instantaneous currents ($i_{\text{a}\alpha\beta}$, $i_{\text{b}\alpha\beta}$ and i_{b0}) from step-2 in the arm power equations would provide the instantaneous arm power ($p_{\Sigma/\Delta\alpha\beta0}$) values in the αβ0-frame. $p_{\Sigma/\Delta\alpha\beta0}$ is converted into the abc-frame ($p_{\Sigma/\Delta123}$) using the inverse Clarke's transformation. The upper (p_{p123}) and lower (p_{n123}) instantaneous arm power values can be obtained by solving the summation ($p_{\Sigma123}$) and difference ($p_{\Delta123}$) arm powers using (2.71). The arm powers are integrated to obtain the instantaneous arm energies in the steady state, as shown in (2.72). The initial condition of the arm energies ($w_{\text{p/n123}}(t = 0)$) is an unknown parameter, but it can be assumed equal to the set point of the arm energy controller for simplicity. The arm ripple energy ($\Delta w_{\text{p/n123}}$) can be computed independently of the initial condition of the arm energies. $\Delta w_{\text{p/n123}}$ only depends on the instantaneous arm powers.

$$p_{\mathrm{p123}} = \frac{p_{\Sigma 123} + p_{\Delta 123}}{2} \;;\; p_{\mathrm{n123}} = \frac{p_{\Sigma 123} - p_{\Delta 123}}{2} \tag{2.71}$$

$$w_{\mathrm{p123}} = w_{\mathrm{p123}}(t=0) + \int_0^T p_{\mathrm{p123}}\,\mathrm{d}t \;;\; w_{\mathrm{n123}} = w_{\mathrm{n123}}(t=0) + \int_0^T p_{\mathrm{n123}}\,\mathrm{d}t \tag{2.72}$$

Therefore, the proposed analytical toolchain can help to compute the MMC, single-phase, and three-phase parameters mathematically for a selected arm energy balancing method. The load parameters can easily be modified to solve the system voltages, currents, powers, and energies during various normal and abnormal conditions. Hence, this toolchain can save significant time and money in analyzing and comparing the performance of MMC for different arm energy balancing methods. In Chapter 5, the results of the proposed analytical toolchain are presented and compared with the simulation results.

2.6 Comparison of the Arm Energy Balancing Methods in the Literature

This section compares the existing arm energy controllers in the literature with the energy balancing methods listed in Table 2.2 and Table 2.3. Common-mode voltage (v_{cm}) is generally used to increase the fundamental three-phase voltage magnitude. The magnitude of v_{cm} is limited by the single-phase, three-phase, and total arm dc-link voltage magnitudes. In [KAR16, DIE20], v_{cm} is further decomposed into several components to have additional degrees of freedom. Decomposing v_{cm} can further increase the couplings in the system, and the dimensioning of MMC should be increased to realize several common-mode voltage components at once. Therefore, it is recommended to use the common-mode voltage with only one dominating frequency component so that it does not increase MMC's dimensioning and does not introduce additional couplings in the system.

Further, [LIZ16b, PER14] uses v_{cm} as one degree of freedom and computes the magnitude (V_{cm}) of v_{cm} based on the single-phase current magnitude (I_{b0}), which is not a stable approach for all load conditions. At the light load or no-load condition, the computed V_{cm} would be very high. The controller using V_{cm} ($\propto I^{-1}$) as a degree of freedom can only survive using a saturation block to limit V_{cm} to a safe value during a light load or no-load condition. Thus, V_{cm} should not be computed by dividing the current magnitude. Instead, the current magnitude in phase with v_{cm} is recommended to be calculated by dividing V_{cm}.

[KOL14, KOL15a] have proposed two energy regulation techniques for DC-AC MMC for variable-speed electric drive applications. Following the sign convention in this work, Table 2.7

represents the summary of two proposed energy controllers in [KOL14, KOL15a] according to the speed or frequency of the machine. The summation (Σ) power controllers for both (*high frequency* (hf) and *low frequency* (*l*f)) modes are the same, but the difference (Δ) power controllers differ for high frequency and low frequency modes. In high frequency mode, the three-phase voltage is AC hence the positive (i_{bd+}) and the negative (i_{bdq-}) sequence circulating currents can make average power with the three-phase voltages ($v_{a\alpha\beta}$). But when the speed of the machine is zero or low, the three-phase voltage behaves like a DC signal. If $f_a \approx f_b = 0$, additional coupling exists between the single-phase and three-phase systems because it is also equal frequency operation. Therefore, common-mode voltage is a must for the stable operation of MMC, according to the conclusion of Section 2.4.

Table 2.7: Arm energy balancing methods proposed by Mr. Kolb [KOL15a].

	Power	**Voltage**	**Current (*MI*s)**	**Frequency**
Horizontal (Σ)	$\overline{P_{\Sigma 0}}$	V_b	$MI_1 = I^b_{b0}$	DC
	$\overline{P_{\Sigma \alpha}}$	V_b	$MI_3 = I^b_{b\alpha}$	DC
	$\overline{P_{\Sigma \beta}}$	V_b	$MI_4 = I^b_{b\beta}$	DC
Vertical (Δ) (High Frequency (hf))	$\overline{P_{\Delta 0}}$	$-\sqrt{2}\,V_a$	$MI_2 = I_{bd+}$	ω_a
	$\overline{P_{\Delta \alpha}}$	$-\sqrt{2}\,V_a$	$MI_5 = I_{bd-}$	ω_a
	$\overline{P_{\Delta \beta}}$	$\sqrt{2}\,V_a$	$MI_6 = I_{bq-}$	ω_a
Vertical (Δ) (Low Frequency (*l*f))	$\overline{P_{\Delta\alpha\beta 0}}$	$-2\,V_{cm}$	$MI_{2,5\&6} = I^{cm}_{b\alpha\beta 0}$	ω_{cm}

Thus, Dr. Kolb has used common-mode voltage (v_{cm}) and the manipulated inputs ($i^{cm}_{b\alpha\beta 0}$), which make average power with v_{cm}, to regulate MMC energies for the low-frequency (*l*f) operation of the machine. The dominating frequency of v_{cm} (f_{cm}) equals three times the three-phase frequency ($f_{cm} = 3f_a$) for high frequency mode. But f_{cm} is set to an arbitrary value (f_o) in the low frequency mode because by setting $f_{cm} \approx 0$, v_{cm} will introduce additional couplings in the system. Harmonics is injected into the single-phase currents in the low frequency operation mode. Referring to Table 2.2, Mr. Kolb has used Method-5, and Method-14 to regulate the arm energies of MMC during the *high frequency* (hf) and *low frequency* (*l*f) modes, respectively. The stability analysis of both methods is missing in the literature.

Considering the neutral point (N) of the three-phase system is connected to the center of the single-phase voltage (also see Fig. 3.2), (2.18) can be modified to (2.73). Here, the zero-sequence three-phase current (i_{a0}) is also considered because the neutral point is no longer floating. i_{a0} provides an additional degree of freedom to regulate the total upper and total lower arms energies ($\overline{w_{\Delta 0}}$); thus, another 48-arm energy balancing methods are possible. But the existing system where N is connected to the middle point of v_b is rare or absent for high or medium voltage systems. [LIZ16b, PER14] have used i_{a0} as a manipulated input to regulate $\overline{w_{\Delta 0}}$ when N is grounded.

$$p_{\Delta 0} = -\frac{v_b\, i_{a0}}{2} - 2\, v_{cm}\, i_{b0} - v_{a\alpha}\, i_{b\alpha} - v_{a\beta}\, i_{b\beta} \tag{2.73}$$

Table 2.8: Arm energy balancing methods proposed by [LIZ16b, PER14].

	Power	**Voltage**	**Current (*MI*s)**	**Frequency**
Horizontal (Σ)	$\overline{P_{\Sigma 0}}$	V_b	$MI_1 = I^b_{b0}$	DC
	$\overline{P_{\Sigma \alpha}}$	V_b	$MI_3 = I^b_{b\alpha}$	DC
	$\overline{P_{\Sigma \beta}}$	V_b	$MI_4 = I^b_{b\beta}$	DC
Vertical ($\Delta\alpha\beta$)	$\overline{P_{\Delta \alpha}}$	$-\frac{V_b}{2}$	$MI_5 = I^b_{a\alpha}$	DC
	$\overline{P_{\Delta \beta}}$	$-\frac{V_b}{2}$	$MI_6 = I^b_{a\beta}$	DC
Vertical ($\Delta 0$) **(N = grounded)**	$\overline{P_{\Delta 0}}$	$-\frac{V_b}{2}$	$\boldsymbol{MI_2} = I^b_{a0}$	DC
Vertical ($\Delta 0$) **(N = floating)**	$\overline{P_{\Delta 0}}$	$\boldsymbol{MI_2} = -2\, V^{b0}_{cm}$	I_{b0}	DC

The overview of the proposed two energy balancing methods in [LIZ16b, PER14] for DC-AC MMC topology is shown in Table 2.8. When N is grounded, the i_{a0} regulates $\overline{w_{\Delta 0}}$. And when N is floating, the common-mode voltage magnitude (V_{cm}) obtained by dividing the single-phase current magnitude ($I_b = -3\, I_{b0}$) is used as the manipulated input (MI_2). Both methods are impractical. Controlling i_{a0} could violate some safety guidelines. Division by the current magnitude can lead to a very high value when the current magnitude is low; hence, it cannot guarantee the controller's stability for all load conditions. The controller might have only worked because V_{cm} was saturated in the controller. Further, the three-phase and single-phase

currents are controlled together to regulate the arm energies for both modes (N = grounded, or floating); hence harmonics are injected into the load (three-phase) and source (single-phase) currents. The energy balancing controllers in Table 2.8 can be linked to Method-40 in Table 2.3 by replacing i_{b0}^{cm} with i_{a0}^{b} when N is grounded and replacing i_{b0}^{cm} with v_{cm}^{b} when N is floating.

[KAR16, DIE20] have proposed arm energy balancing techniques using more than six DOF simultaneously. Using many degrees of freedom simultaneously would increase coupling between the arm power equations and could even lead to instability, especially for equal frequency operation of MMC. Further, the common-mode voltage is decomposed into several components, and the magnitude of a few common-mode voltages is computed by dividing the corresponding current magnitudes like in [LIZ16b, PER14]. Therefore, further complexity and coupling are introduced in the controller by using several degrees of freedom simultaneously. It also requires increasing the dimensioning of the converter to realize several common-mode voltages at once.

[DIN22a, DIN22b] uses four degrees of freedom ($P_{\Sigma 0}$, $i_{b\alpha\beta,}$ and $v_{cm)}$ and weighing functions to regulate the six arm energies of DC-AC MMC topology. The proposed arm energy method may lead to drifting in the arm energies over some time. The drift would increase with the converter impedance, asymmetry, and losses. The controller seems to work because the average arm power is naturally zero for DC-AC operation; thus, the manipulated inputs only need to compensate for the losses. But the controller cannot work for equal frequency operation because the additional average arm power has to be compensated using the manipulated inputs hence an additional two degrees of freedom should be selected.

Very few energy balancing controllers for equal frequency operation are found in the literature. [SON18] has proposed an energy balancing method using manipulated inputs i_{ad+}, $I_{b\alpha\beta 0}^{dc}$, and $I_{b\alpha\beta 0}^{cm}$ for equal frequency operation in traction applications. The dc circulating current ($I_{b\alpha\beta 0}^{dc}$) is used for phase energy balancing, which is irrelevant because the dc circulating current cannot make average power with the single-phase AC voltage (also see (2.19) and (2.20)). The controller would have survived because the residual power is naturally zero for the summation arm powers ($\overline{P_{\Sigma\alpha\beta 0}}$) in the αβ0-frame (also see Table 2.6). Further, the controller injects harmonics into the load current.

3 Design of the Discrete-Time Current Controllers of MMC

The general control structure of MMC is shown in Fig. 1.2 in Chapter 1. The arm energy controllers calculate the desired arm ($i^*_{p/n123}$) and source (i^*_{a123} or i^*_b) currents which would help balance the arm energies of MMC. The arm energy controllers provide i^*_{a123} as the output if the three-phase system acts like a source. And it gives i^*_b as the output if the single-phase system behaves like a source. The current controllers are necessary to control the arm ($i_{p/n123}$) and source (i_{a123} or i_b) currents according to the command of the arm energy controllers. Mainly digital controllers are used to control power converters these days; hence it is necessary to design the controllers in the discrete-time domain accurately. Tustin or Forward Euler approximation models are commonly used to obtain the discrete-time plant model from the

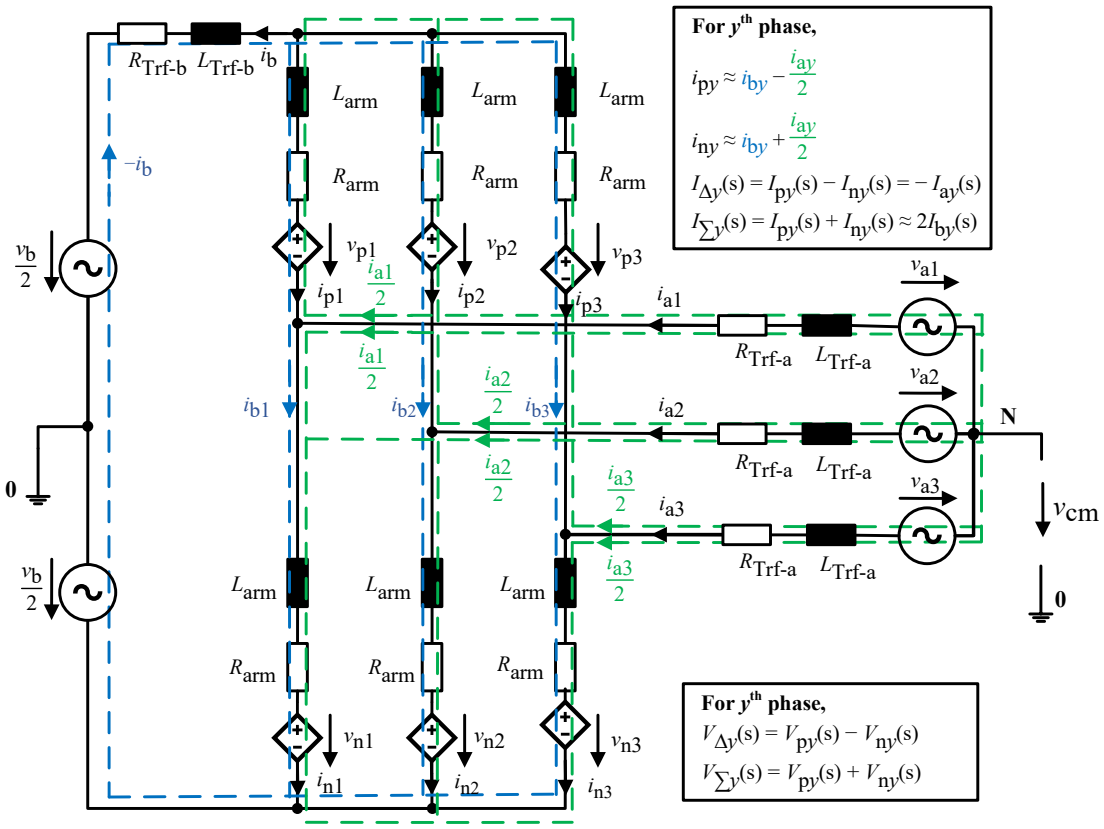

Figure 3.1: Average equivalent electrical circuit diagram of MMC when N is floating.

continuous-time domain plant model [SCH22]. The discrete-time plant model obtained using these approximations fails to represent the actual system for all the cases, especially for the lower sampling rate and the lower converter's switching frequency. Further, tuning the digital controllers with the help of these approximations can even lead to instability of the controller [SCH22, SAH20]. Therefore, a direct discrete-time plant model is essential in designing and tuning a discrete-time controller more accurately [SCH17].

The main objective of this chapter is to propose direct discrete-time current controllers for MMC and analyze their performance with the help of *Command Tracking* (CT) or closed-loop bode plots.

3.1 Summation and Difference Arm Voltage Equations in the s-Domain

Fig. 3.1 illustrates the average equivalent electrical circuit diagram of MMC. The three-phase voltage (v_{a123}) and single-phase voltage (v_b) sources are connected to the MMC via three-phase (Trf-a) and single-phase (Trf-b) transformers, respectively. If either single-phase, three-phase, or both transformers are absent, the corresponding impedances can be considered zero. The neutral point of the three-phase system (N) is considered floating.

An arm current ($i_{p/ny}$) of phase y of MMC can be decomposed into two components: (a) circulating current (i_{by}) and (b) three-phase current (0.5 i_{ay}) [KOL15a]. The same circulating current (i_{by}) flows in both the upper (py) and the lower (ny) arms of phase y of MMC. (3.1) illustrates the decomposition of the upper (i_{py}) and the lower (i_{ny}) arm currents in terms of i_{by} and 0.5i_{ay}. The system could be transferred into a summation (Σ) and a difference (Δ) system to decouple the single-phase and three-phase currents [SCH17]. The expressions for the summation and difference arm voltages and currents in the Laplace domain are shown in (3.2) and (3.3), respectively.

$$i_{py} = i_{by} - \frac{i_{ay}}{2}, \text{ and } i_{ny} = i_{by} + \frac{i_{ay}}{2} \tag{3.1}$$

$$V_{\sum y}(s) = V_{py}(s) + V_{ny}(s), \text{ and } V_{\Delta y}(s) = V_{py}(s) - V_{ny}(s) \tag{3.2}$$

$$I_{\sum y}(s) = I_{py}(s) + I_{ny}(s) = 2I_{by}(s), \text{ and } I_{\Delta y}(s) = I_{py}(s) - I_{ny}(s) = -I_{ay}(s) \tag{3.3}$$

(3.4) illustrates the governing summation arm voltage equation for phase y of MMC in the Laplace (s) domain. (3.4) is obtained by applying Kirchhoff's voltage law in a loop consisting of the single-phase transformer impedance ($Z_{Trf\text{-}b}(s) = R_{Trf\text{-}b} + s\,L_{Trf\text{-}b}$), the single-phase voltage

(v_b), and the lower (ny) and the upper (py) arms of phase y of MMC. The summation arm voltage expression in the abc-frame can be obtained by substituting $y = 1$, 2, and 3 in (3.4). (3.5) represents the governing expression of the summation arm voltage in the 0-frame, which is obtained using the transformation $F_0 = (F_1+F_2+F_3)/3$. The relation between the summation current in the 0-frame and the single-phase load current is illustrated in (3.6). Substituting (3.6) in (3.5) gives (3.7). Substituting $R_{b\text{-}0} = 2R_{arm}/3 + R_{Trf\text{-}b}$, and $L_{b\text{-}0} = 2L_{arm}/3 + L_{Trf\text{-}b}$ in (3.7) gives (3.8). $V_{\sum\text{-}0}(s) = V_b^*(s)$ can be modified to operate the single-phase system in either the grid forming or the grid flowing mode. In the grid-forming mode, $V_{\sum\text{-}0}(s) = V_b^*(s)$ is set to obtain the desired single-phase output voltage, and in the grid-flowing mode, $V_{\sum\text{-}0}(s) = V_b^*(s)$ is obtained from the single-phase current control loop.

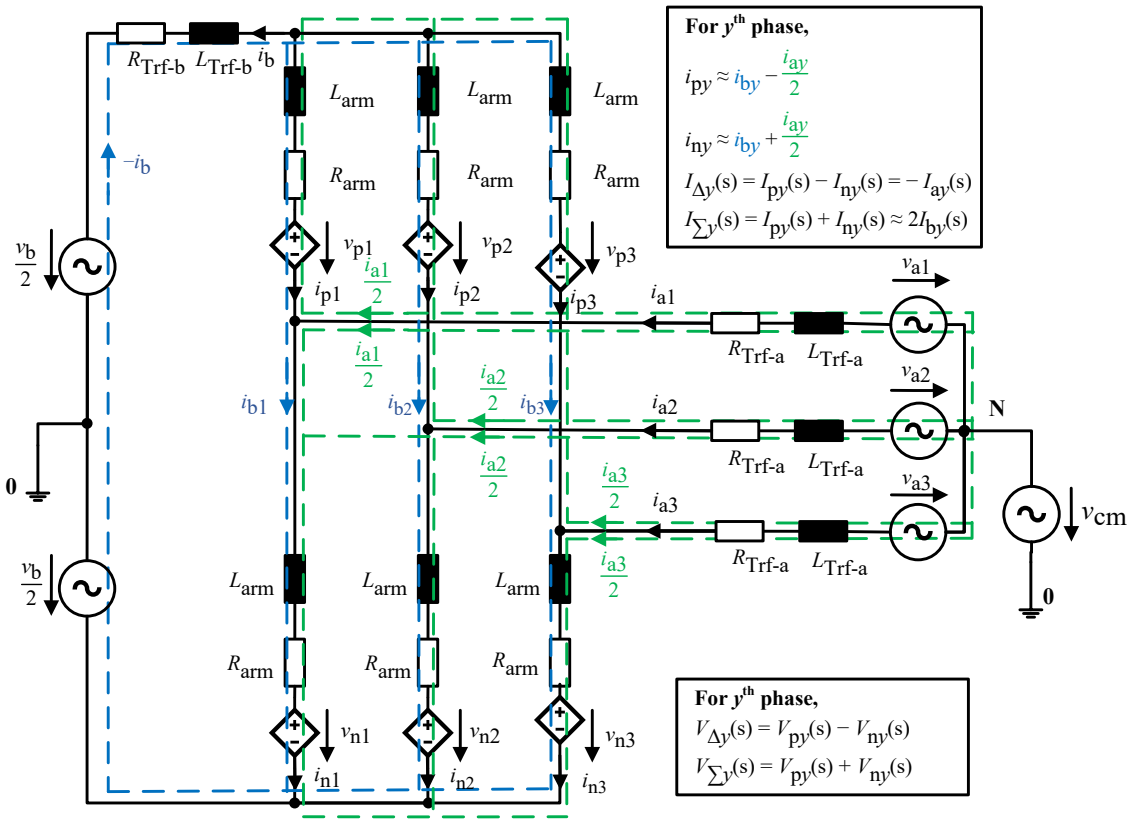

Figure 3.2: Average equivalent electrical circuit diagram of MMC when N is grounded.

$$V_b(s) = \left(R_{arm} + sL_{arm}\right) I_{\sum y}(s) + V_{\sum y}(s) - \left(R_{Trf\text{-}b} + sL_{Trf\text{-}b}\right) I_b(s) \tag{3.4}$$

$$V_b(s) = \left(R_{arm} + sL_{arm}\right) I_{\sum\text{-}0}(s) + V_{\sum\text{-}0}(s) - \left(R_{Trf\text{-}b} + sL_{Trf\text{-}b}\right) I_b(s) \tag{3.5}$$

$$I_{\sum\text{-}0}(s) = \frac{2I_{b1}(s) + 2I_{b2}(s) + 2I_{b3}(s)}{3} = -\frac{2}{3} I_b(s) \tag{3.6}$$

$$V_{\sum\text{-}0}(s) = V_b(s) + \left(\left(R_{Trf\text{-}b} + \frac{2}{3} R_{arm}\right) + s\left(L_{Trf\text{-}b} + \frac{2}{3} L_{arm}\right)\right) I_b(s) \tag{3.7}$$

$$V_{\sum\text{-}0}(s) = \overset{*}{V}_{b}(s) = V_{b}(s) + \left(R_{b\text{-}0} + sL_{b\text{-}0}\right) I_{b}(s) \tag{3.8}$$

$$\left(R_{arm} + sL_{arm}\right) \boldsymbol{I}_{\sum\alpha\beta}(s) + \boldsymbol{V}_{\sum\alpha\beta}(s) = 0 \tag{3.9}$$

$$\left(R_{arm} + L_{arm}\left(s + j\omega_{a}\right)\right) \boldsymbol{I}_{\sum\text{-}dq}(s) + \boldsymbol{V}_{\sum\text{-}dq}(s) = 0 \tag{3.10}$$

$$\left(R_{b\text{-}dq} + L_{b\text{-}dq}\left(s + j\omega_{a}\right)\right) \boldsymbol{I}_{\sum\text{-}dq}(s) + \boldsymbol{V}_{\sum\text{-}dq}(s) = 0 \tag{3.11}$$

Referring to Appendix A.1, Clarke's (abc to αβ) transformation of (3.4) using the complex vector notation ($\boldsymbol{F}_{\alpha\beta} = F_{\alpha} + jF_{\beta}$) is shown in (3.9). Here, the single-phase voltage ($V_{b}(s)$) and single-phase current ($I_{b}(s)$) are absent because these are common for all three summation arm voltage equations in the abc-frame. Referring to Appendix A.2, (3.10) represents the transformation of (3.9) in the dq-frame using the complex vector notation ($\boldsymbol{F}_{dq} = F_{d} + jF_{q}$). Substituting $R_{b\text{-}dq} = R_{arm}$, $L_{b\text{-}dq} = L_{arm}$ gives (3.11).

Usually, the neutral terminal (N) of the three-phase voltage source is assumed to be connected to the center (0) of the single-phase grid voltage source (also see Fig. 3.2) for the more straightforward derivation of the difference arm voltage equation of MMC [SCH17, KOL15a]. The assumption is only hypothetical and does not represent the actual system. Referring to Fig. 3.2 and following the steps in [SCH17, KOL15a], (3.12) represents the difference arm voltage equation for the phase *y* of MMC. Here, $R_{a} = R_{arm} + 2R_{Trf\text{-}a}$, and $L_{a} = L_{arm} + 2L_{Trf\text{-}a}$ (also see Appendix A.3). And (3.13) represents the difference voltage equation in the 0-frame. $V_{\Delta\text{-}0}(s) = -2V_{cm}(s)$ indicates that the zero-sequence difference arm voltage ($V_{\Delta\text{-}0}(s)$) can virtually implement the system's three-phase common-mode voltage ($V_{cm}(s)$).

In this work, the neutral terminal (N) is considered floating to represent the actual system (also see Fig. 3.1). Referring to Appendix A.3, (3.14) represents the generalized difference arm voltage equation for the phase *y* of MMC and (3.15) represents the difference arm voltage equation in the 0-frame when the neutral point (N) of a three-phase system is floating. Here, the zero sequence three-phase voltage with respect to the central point (0) of single-phase voltage ($V_{a\text{-}0}(s) = V_{cm}(s)$) is defined as the common-mode voltage ($V_{cm}(s)$). Transformation of (3.12) or (3.14) into the αβ-frame using the complex vector notation gives (3.16). Hence, the same difference voltage equation in the αβ-frame is obtained when the three-phase neutral pointed is floating or grounded to the central point of the single-phase voltage. But, the difference arm voltage equations differ in the 0-frame. Although, $V_{cm}(s) = -0.5\ V_{\Delta\text{-}0}(s)$ cannot be guaranteed when the three-phase neutral point is floating but it is still true that $V_{\Delta\text{-}0}(s)$ can help realize $V_{cm}(s)$ for the regulation of the arm energies of MMC. The mismatch ($X_{o}(s)$)

between $V_{cm}(s)$ and $V_{\Delta\text{-}0}(s)$ would not affect the overall performance of MMC because the three-phase neutral current ($I_{a\text{-}0}(s) = 0$) is always zero. (3.17) represents the transformation of (3.16) in the dq-frame using the complex vector notation.

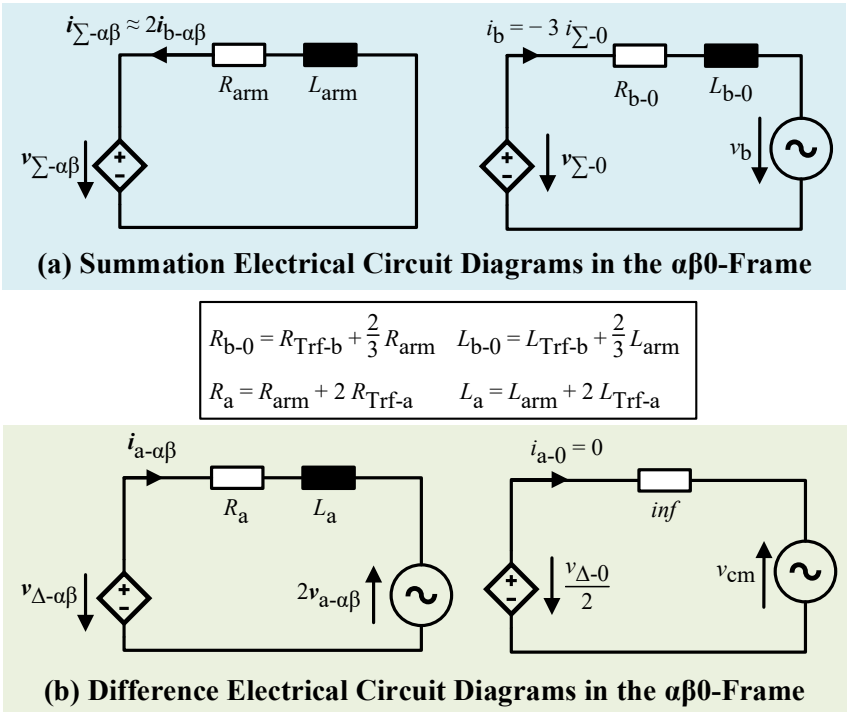

Figure 3.3: Average equivalent electrical circuit diagram of MMC in the αβ0-frame using the summation (∑) and the difference (Δ) notations.

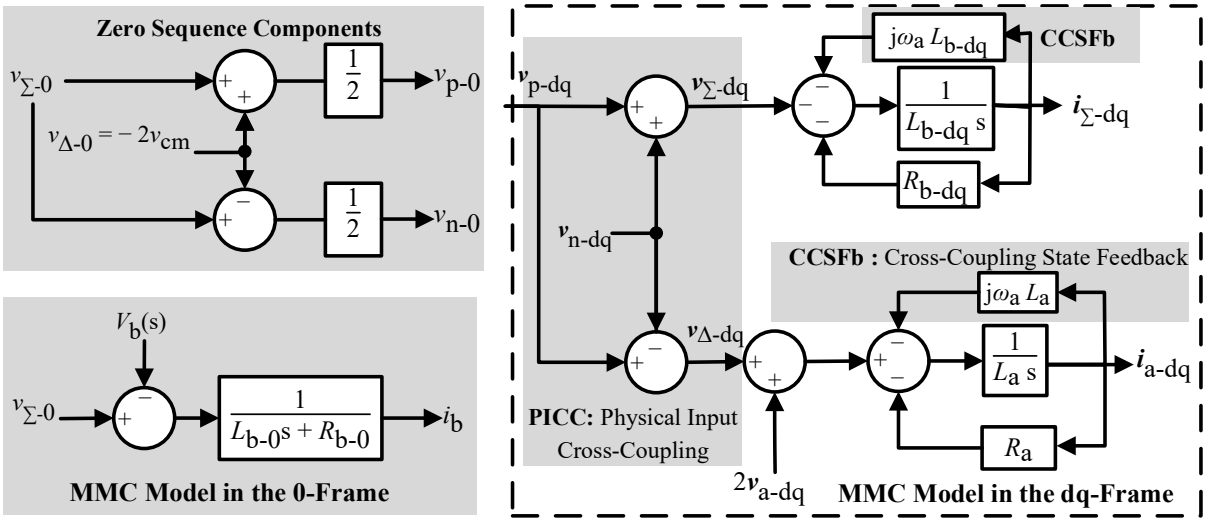

$R_{b\text{-}0} = \frac{2}{3} R_{arm} + R_{Trf\text{-}b}$ $L_{b\text{-}0} = \frac{2}{3} L_{arm} + L_{Trf\text{-}b}$ $R_{b\text{-}dq} = R_{arm}$ $L_{b\text{-}dq} = L_{arm}$

$R_a = R_{arm} + 2\, R_{Trf\text{-}a}$ $L_a = L_{arm} + 2\, L_{Trf\text{-}a}$

Figure 3.4. Continuous-time plant model of MMC in the dq0-frame.

$$-\left(R_a + L_a s\right) I_{ay}(s) + V_{\Delta y}(s) + 2V_{ay}(s) = 0 \tag{3.12}$$

$$V_{\Delta\text{-}0}(\mathrm{s}) + 2V_{\mathrm{cm}}(\mathrm{s}) = 0 \tag{3.13}$$

$$-\left(R_{\mathrm{a}} + L_{\mathrm{a}}\mathrm{s}\right) I_{\mathrm{a}y}(\mathrm{s}) + V_{\Delta y}(\mathrm{s}) + 2V_{\mathrm{a}y}(\mathrm{s}) = V_{\Delta\text{-}0}(\mathrm{s}) + 2V_{\mathrm{cm}}(\mathrm{s}) \tag{3.14}$$

$$V_{\Delta\text{-}0}(\mathrm{s}) + 2V_{\mathrm{cm}}(\mathrm{s}) = X_0(\mathrm{s}) \neq 0 \tag{3.15}$$

$$-\left(R_{\mathrm{a}} + L_{\mathrm{a}}\mathrm{s}\right) \boldsymbol{I}_{\mathrm{a}\text{-}\alpha\beta}(\mathrm{s}) + \boldsymbol{V}_{\Delta\text{-}\alpha\beta}(\mathrm{s}) + 2\boldsymbol{V}_{\mathrm{a}\text{-}\alpha\beta}(\mathrm{s}) = 0 \tag{3.16}$$

$$-\left(R_{\mathrm{a}} + L_{\mathrm{a}}\mathrm{s} + \mathrm{j}\omega_{\mathrm{a}}L_{\mathrm{a}}\right) \boldsymbol{I}_{\mathrm{a}\text{-}\mathrm{dq}}(\mathrm{s}) + \boldsymbol{V}_{\Delta\text{-}\mathrm{dq}}(\mathrm{s}) + 2\boldsymbol{V}_{\mathrm{a}\text{-}\mathrm{dq}}(\mathrm{s}) = 0 \tag{3.17}$$

$\boldsymbol{V}_{\Delta\text{-}\alpha\beta}(\mathrm{s})$ can also be modified to operate the three-phase system in either the grid forming or the grid following mode. In the grid-forming mode, $\boldsymbol{V}_{\Delta\text{-}\alpha\beta}(\mathrm{s})$ is set to obtain the desired three-phase output voltage of MMC, and in the grid-following mode, the $\boldsymbol{V}_{\Delta\text{-}\alpha\beta}(\mathrm{s})$ is obtained from the three-phase current control loop. It should be noted that the single-phase or the three-phase system can work in a grid-forming or a grid-following mode, irrespective of which system behaves like a source.

Referring to (3.8), (3.9), (3.13), and (3.16), Fig. 3.3 represents the average plant model circuit diagrams of MMC in the αβ0-frame using the summation (∑) and the difference (Δ) notations. The summation arm voltage in the αβ-frame ($\boldsymbol{v}_{\Sigma\text{-}\alpha\beta}$) only affects the circulating current in the αβ-frame ($\boldsymbol{i}_{\mathrm{b}\text{-}\alpha\beta}$), and $v_{\Sigma\text{-}0}$ only affects the single-phase (i_{b}) current. Similarly, the difference arm voltage in the αβ-frame ($\boldsymbol{v}_{\Delta\text{-}\alpha\beta}$) only affects the three-phase current ($\boldsymbol{i}_{\mathrm{a}\text{-}\alpha\beta}$), and $v_{\Delta\text{-}0}$ virtually implements v_{cm}. Hence, the single-phase (i_{b}), circulating ($\boldsymbol{i}_{\mathrm{b}\text{-}\alpha\beta}$), and three-phase ($\boldsymbol{i}_{\mathrm{a}\text{-}\alpha\beta}$) current controllers are naturally decoupled in the summation (∑) and the difference (Δ) systems [SCH17].

3.2 Design of the Current Controllers in the Continuous-Time Domain

Understanding the steps used for designing the controllers in the continuous-time domain helps to understand the general steps used in designing the discrete-time controllers. Therefore, the design of the current controllers of MMC in the continuous-time domain is discussed in this section, and in the later section, the direct discrete-time current controller is proposed.

The sampled three-phase voltages (v_{a123}) are used as input to *Phase Locked Loop* (PLL) for obtaining the three-phase angle (θ_{a}) and three-phase angular speed (ω_{a}) [SAH20, TEO07]. θ_{a} is used for Park and inverse Park transformations. Similarly, a single-phase PLL can be used to obtain the single-phase angle (θ_{b}) and single-phase angular speed (ω_{b}). Referring to Appendix A.2 and Fig. 3.3, Fig. 3.4 represents the mathematical plant model of MMC in the

dq0-frame using complex vector notation. (3.11) and (3.17) are used to obtain the circulating ($i_{\Sigma\text{-dq}} \approx 2i_{\text{b-dq}}$) and the three-phase ($i_{\text{a-dq}}$) currents plant model in the dq-frame. Similarly, (3.8) and (3.13) are used to obtain the plant model of MMC in the 0-frame. The currents in the d-axis and q-axis are coupled due to the Park's (αβ to dq) transformation, which is termed as *Cross-Coupling State Feedback* (CCSFb). Further, another coupling between the arm voltages, *Physical Input Cross-Coupling* (PICC), exists due to the transformation of the arm voltages into the summation and difference systems. The three-phase voltage ($v_{\text{a-dq}}$) acts as a disturbance in the difference plant model in the dq-frame. The circulating current ($i_{\Sigma\text{-dq}} \approx 2i_{\text{b-dq}}$), three-phase current ($i_{\text{a-dq}}$), and single-phase current (i_{b}) can be controlled by varying the summation arm voltage in the dq-frame ($v_{\Sigma\text{-dq}}$), the difference arm voltage ($v_{\Delta\text{-dq}}$) in the dq-frame, and the summation arm voltage in the 0-frame ($v_{\Sigma\text{-dq}}$), respectively.

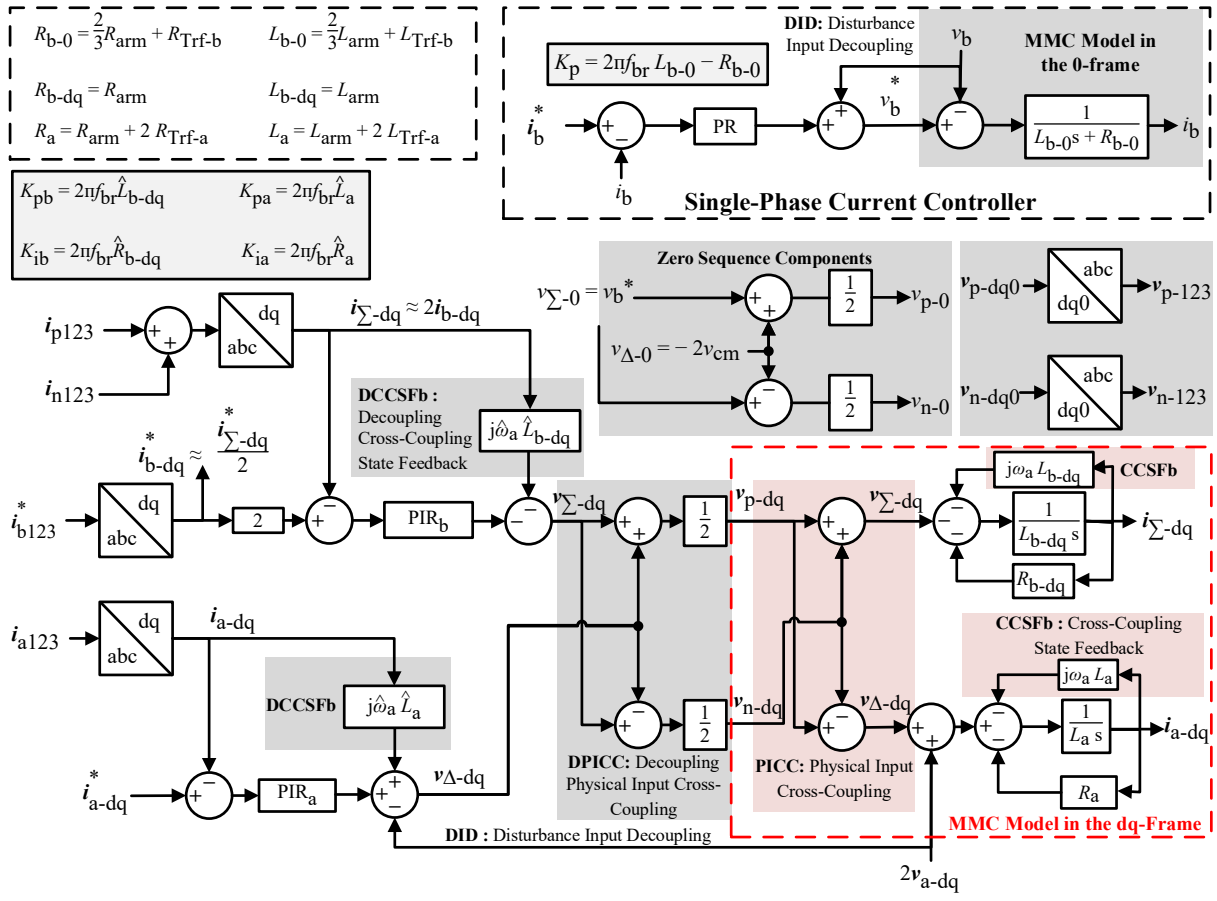

Figure 3.5: Proposed current control loops for MMC in the continuous-time domain.

Fig. 3.5 illustrates the proposed current control loops of MMC in the continuous-time domain. It consists of the circulating ($i_{\Sigma\text{-dq}} \approx 2i_{\text{b-dq}}$) and the three-phase ($i_{\text{a-dq}}$) current controllers in the dq-frame and the single-phase current (i_{b}) controller in the 0-frame. *Proportional Integral Resonant* (PIR) controllers are used for the controllers in the dq-frame. And a *Proportional*

Resonant (PR) or *Proportional Integral* (PI) controller is used for the single-phase current controller. PR controller is selected for the single-phase current controller if the single-phase is AC, and the PI controller is chosen if the single-phase is DC. The *Resonant* (R) controller helps to bring the gain and phase of the closed-loop bode plot close to unity and zero, respectively, at a resonant frequency. In other words, a resonant controller helps to accurately control the signal at the resonant frequency to the reference command. The three-phase current controller can also be realized using only a PI controller based on the selected energy balancing method. For e.g., no harmonics are injected in the three-phase currents when the energy balancing using Method-1 or Method-7 is selected; hence a resonant controller is redundant in the three-phase current controller for these energy balancing methods.

Decoupling Cross-Coupling State Feedback (DCCSFb) and *Decoupling Physical Input Cross-Coupling* (DPICC) are used to decouple the *Cross-Coupling State Feedback* (CCSFb) and *Physical Input Cross-Coupling* (PICC), respectively. These decouplings are essential to control each current component independently. Further, *Disturbance Input Decoupling* (DID) helps decouple the system's disturbance (grid voltage) in the difference system. The zero-sequence component of the difference voltage ($v_{\Delta\text{-}0}$) is used for realizing the common-mode voltage (v_{cm}).

MMC provides two degrees of freedom to realize the single-phase or the three-phase voltage. Three-phase, single-phase, or both sides can be realized in open or closed-loop mode. In the closed-loop mode, the current controllers proposed in Fig. 3.5 can be used for regulating the three-phase and single-phase currents. But in the open-loop mode, *Decoupling Cross-Coupling State Feedback* (DCCSFb), *Disturbance Input Decoupling* (DID) and PIR controller are disabled in the three-phase current controller, and the PR (or PI) controller and DID are disabled in the single-phase current controller. The desired open-loop three-phase voltage ($v^*_{a\text{-}dq}$) is set with the help of the difference voltage in the dq-frame ($v^*_{a\text{-}dq} = -0.5v_{\Delta\text{-}dq}$), and the desired open-loop single-phase voltage (v^*_b) is set with the help of the summation voltage in the 0-frame ($v^*_b = v_{\Sigma\text{-}0}$). For e.g., in the HVDC application, MMC could set the DC-link voltage to a desired open-loop voltage (v^*_b) and control three-phase active power (or currents) to regulate the MMC's total energy. Alternatively, MMC could also set the three-phase voltage to a desired open-loop voltage ($v^*_{a\text{-}dq}$) and regulate MMC's total energy by controlling the single-phase active power (or current).

3.2.1 Selection of Resonant Frequencies

(3.18) shows the transfer function of a resonant controller in the Laplace domain. Here, ω_r, ω_c, and K_{ir} represent resonant frequency, cutoff frequency, and gain, respectively. The resonant

controller parameters (ω_c and K_i) can be tuned using the method mentioned in [TEO06]. At the resonant frequency ($s = j\omega = j\omega_r$, $Y(s) = K_{ir} E(s)$), the phase error between the input signal ($E(s)$) and the output signal ($Y(s)$) of the resonant controller is zero, and the value of K_{ir} decides the gain of the resonant controller.

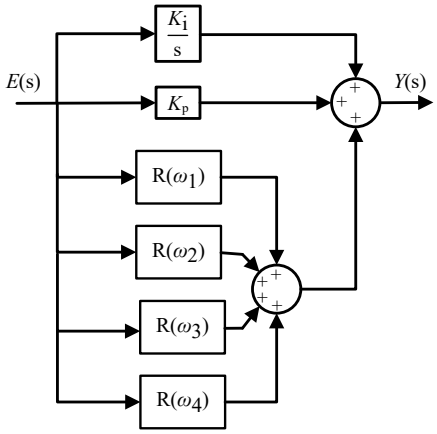

Figure 3.6: A PIR controller.

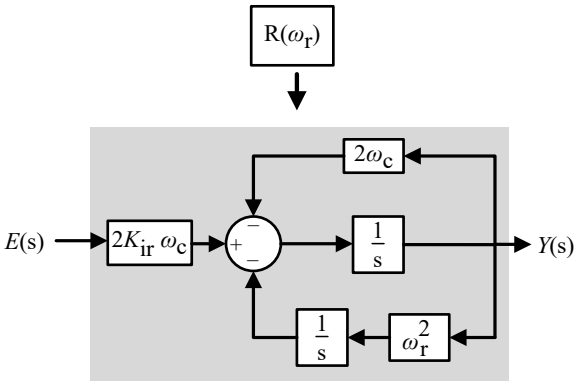

Figure 3.7: A resonant controller.

$$R(s) = \frac{2\,K_{ir}\,\omega_c\,s}{s^2 + 2\,\omega_c\,s + \omega_r^2} \tag{3.18}$$

Fig. 3.7 elaborates on the state block diagram for realizing a resonant controller in a continuous-time domain. A resonant controller enables tracking the AC command at resonant frequencies. Fig. 3.6 shows a PIR controller with multiple resonant controllers connected in parallel with the PI controller. Multiple resonant controllers can help to control the signals accurately at multiple resonant frequencies. Actually, for an MMC controller, a PIR controller with multiple resonant controllers is essential to control the currents to a reference command accurately.

As discussed in Chapter 2, circulating current ($i_{b\alpha\beta}$), three-phase current ($i_{a\alpha\beta}$), or single-phase current (i_b) can have components in phase with the three-phase ($v_{a\alpha\beta}$), the single phase (v_b) and the common-mode (v_{cm}) voltages based on the selected arm energy balancing method. But it is important to note that $i_{b\alpha\beta}$, $i_{a\alpha\beta}$, or i_b doesn't need to have the single-phase frequency (f_b), the three-phase frequency (f_a), and the common-mode frequency (f_{cm}) components at the same time. The need for resonant controllers and their resonant frequencies vary with the selected energy balancing method and the system frequencies.

At most, the single-phase current controller will require three resonant controllers with resonant frequencies f_a, f_b, and f_{cm}. And at most, five resonant frequencies ($2f_a$, $f_b - f_a$, $f_b + f_a$, $f_{cm} - f_a$, and $f_{cm} + f_a$) are possible for the current controllers in the dq-frame. Referring to Appendix A.1, an

unsymmetrical component with frequency f_x in the αβ-frame would have two frequency components ($f_x - f_a$ and $f_x + f_a$) in the dq-frame. Resonant frequency, $2f_a$, would be required because of the negative sequence current components ($i_{b\text{-}dq-}$ or $i_{a\text{-}dq-}$). Resonant frequencies, $f_b - f_a$ and $f_b + f_a$, would be required because of the unsymmetrical current components ($i^{b}_{b\text{-}\alpha\beta}$ or $i^{b}_{a\text{-}\alpha\beta}$) in phase with the single-phase voltage (v_b). And resonant frequencies, $f_{cm} - f_a$ and $f_{cm} + f_a$, would be required because of the unsymmetrical current components ($i^{cm}_{b\text{-}\alpha\beta}$ or $i^{cm}_{a\text{-}\alpha\beta}$) in phase with the common-mode voltage (v_{cm}).

Assuming the energy balancing using Method-7 is selected for the equal frequency operation ($f_b = f_a$), the circulating current in the αβ-frame ($i_{b\text{-}\alpha\beta}$) will have three components: (a) symmetrical component in phase with the three-phase voltage ($i_{b\text{-}d+}$), (b) unsymmetrical component in phase with the single-phase voltage ($i^{b}_{b\text{-}\alpha\beta}$), and (c) unsymmetrical component in phase with the common-mode voltage ($i^{cm}_{b\text{-}\alpha\beta}$). Hence the circulating current controller in the dq-frame requires two resonant controllers with resonant frequencies ($2f_a$ and $4f_a$). Here, $f_{cm} = 3f_a$ is considered. A resonant controller is not required for the zero-frequency ($f_b - f_a$) component. Whereas the three-phase current contains only positive sequence components ($i_{a\text{-}dq+}$) in phase with the three-phase voltage; hence no resonant controller is required for the three-phase current controller in the dq-frame.

Similarly, considering the same energy balancing Method-7 but the single-phase frequency is now 1/3rd of the three-phase frequency ($f_b = f_a/3$). For this case, the circulating current controller would require four resonant controllers with resonant frequencies $|f_b - f_a|$, $f_b + f_a$, $2f_a$, and $4f_a$ in the dq-frame. Again, $f_{cm} = 3f_a$ is considered. Similarly, assuming the same energy balancing Method-7 and the single-phase system is DC ($f_b = 0$), the circulating current controller would require three resonant controllers with resonant frequencies f_a, $2f_a$, and $4f_a$ in the dq-frame. Again, $f_{cm} = 3f_a$ is considered. Therefore, whether a resonant controller is essential and the selection of resonant frequencies depends on the system frequencies and selected energy balancing method.

The suitable value of K_{ir} is obtained using the hit and trial method so that the phase and magnitude error between the reference AC command at the resonant frequency and controlled states are negligible, ideally zero, in steady-state. Cutoff frequency (ω_c) values of 5 to 15 rad/s have been found to provide a good compromise [TEO07].

3.2.2 Tuning of the PI controller Gains of the Current Control Loops

The resonant controller helps only to accurately track the signals corresponding to the resonant frequencies. But the closed-loop bandwidth of the current controllers should also be placed accurately to get desired dynamic performance. The closed-loop bandwidth can be placed at the desired value by correctly selecting the gains of the PI or P controller. A mathematical plant model of direct MMC topology helps to tune the PI or P controller parameters.

Fig. 3.8 represents the simplified state block diagram of Fig. 3.5, which is obtained after ignoring all decouplings and all couplings in the corresponding current control loops. Fig. 3.8a can be used to tune the closed-loop bandwidth of the circulating ($i_{\Sigma\text{-dq}} \approx 2i_{\text{b-dq}}$) and three-phase current ($i_{\text{a-dq}}$) controllers in the dq-frame. (3.19) represents the open-loop transfer function ($G_{\text{dq}}(s)$) of the current controllers in the dq-frame. The necessary condition for the pole-zero cancellation is given in (3.20). (3.21) represents the simplified open-loop transfer function with pole-zero cancellation. The closed-loop transfer function (*Command Tracking* (CT)) of the current control loop with the pole-zero cancellation is given in (3.22).

The closed-loop eigenvalue of the proposed current controller can be placed at break frequency (f_{br}) by comparing the denominator of (3.22) with ($s + 2\pi f_{\text{br}}$) and solving with (3.20). The general expression for the proportional and integral gains (K_{p} and K_{i}) for tuning the closed-loop bandwidth of the current controller at f_{br} is given in (3.23) and (3.24), respectively.

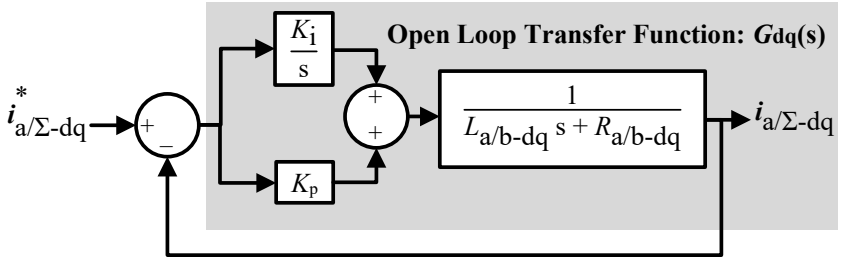

(a) PI Tuning for Current Controllers in the dq-frame

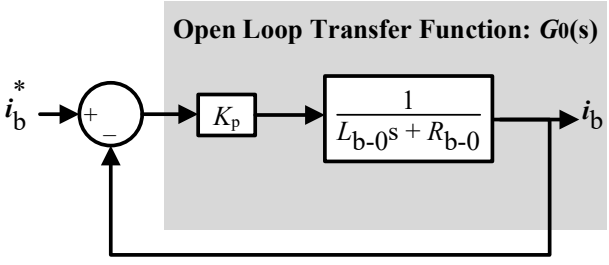

(b) P Tuning for Single-Phase Current Controller

Figure 3.8: State block diagram for tuning PI or P controller gains.

$$G_{dq}(s) = \frac{K_p}{L_{a/b\text{-}dq}\, s}\left(s + \frac{K_i}{K_p}\right)\left(\frac{1}{s + \frac{R_{a/b\text{-}dq}}{L_{a/b\text{-}dq}}}\right) \tag{3.19}$$

$$\frac{K_i}{K_p} = \frac{R_{a/b\text{-}dq}}{L_{a/b\text{-}dq}} \tag{3.20}$$

$$G_{dq}(s) = \frac{K_p}{L_{a/b\text{-}dq}\, s} \tag{3.21}$$

$$CT_{dq}(s) = \frac{\boldsymbol{I}_{a/b\text{-}dq}(s)}{\boldsymbol{I}^*_{a/b\text{-}dq}(s)} = \frac{K_p}{L_{a/b\text{-}dq}\, s + K_p} \tag{3.22}$$

$$K_p = 2\pi f_{br}\, L_{a/b\text{-}dq} \tag{3.23}$$

$$K_i = 2\pi f_{br}\, R_{a/b\text{-}dq} \tag{3.24}$$

Similarly, referring to Fig. 3.8b, (3.25) and (3.26) represent the open-loop and closed-loop transfer functions for tuning the single-phase current controller. The closed-loop eigenvalue of the proposed single-phase current controller can be placed at break frequency (f_{br}) by comparing the denominator of equation (3.26) with ($s + 2\pi f_{br}$). The result of the comparison is given in (3.27). If a PI controller is used for the single-phase current controller, the PI tuning expressions in (3.23) and (3.24) can be used. The general expressions for tuning the PI and P controller gains to place the closed-loop bandwidth of the current control loops at the desired frequency are also given in Fig. 3.5.

$$G_0(s) = \frac{K_p}{L_{b\text{-}0}\, s + R_{b\text{-}0}} \tag{3.25}$$

$$CT_0(s) = \frac{\boldsymbol{I}_b(s)}{\boldsymbol{I}^*_b(s)} = \frac{K_p}{L_{b\text{-}0}\, s + R_{b\text{-}0} + K_p} \tag{3.26}$$

$$K_p = 2\pi f_{br}\, L_{b\text{-}0} - R_{b\text{-}0} \tag{3.27}$$

3.3 Design of the Current Controllers in the Discrete-Time Domain

Almost all power converter controls are implemented using digital controllers like *Digital Signal Processing* (DSP), *Field-Programmable Gate Array* (FPGA), etc. Hence, designing a controller in the discrete-time domain is essential to accurately place its closed-loop bandwidth

at a desired frequency. It is found that the system could become unstable for some system parameters if the continuous-time approach controller is implemented in the digital converter [SAH20]. Generally, Tustin or Forward Euler approximation models are used to obtain the discrete-time plant model from the continuous-time domain plant model [SCH22]. But the accuracy of the discrete-time plant models obtained using these approximations cannot be guaranteed, especially for the lower sampling frequency.

A correct discrete-time plant model plays a vital role in accurately tuning the closed-loop bandwidth of the controller. A direct discrete-time plant model is the most accurate discrete-time plant model; hence, a direct discrete-time plant model can be used to accurately design the discrete-time current controller [SCH18].

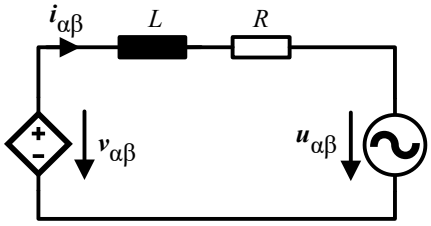

Figure 3.9: *RL* plant model.

Table 3.1: MMC variables in the summation (Σ) and difference (Δ) systems.

System	R	L	$\boldsymbol{v}_{\alpha\beta}$	$\boldsymbol{i}_{\alpha\beta}$	$\boldsymbol{u}_{\alpha\beta}$
Σ–αβ	R_{arm}	L_{arm}	$\boldsymbol{v}_{\Sigma\text{-}\alpha\beta}$	$-\boldsymbol{i}_{\Sigma\text{-}\alpha\beta}$	0
Σ–0	$R_{b\text{-}0}$	$L_{b\text{-}0}$	$v_{\Sigma\text{-}0}$	i_b	v_b
Δ–αβ	R_a	L_a	$\boldsymbol{v}_{\Delta\text{-}\alpha\beta}$	$\boldsymbol{i}_{a\text{-}\alpha\beta}$	$-2\boldsymbol{v}_{a\text{-}\alpha\beta}$

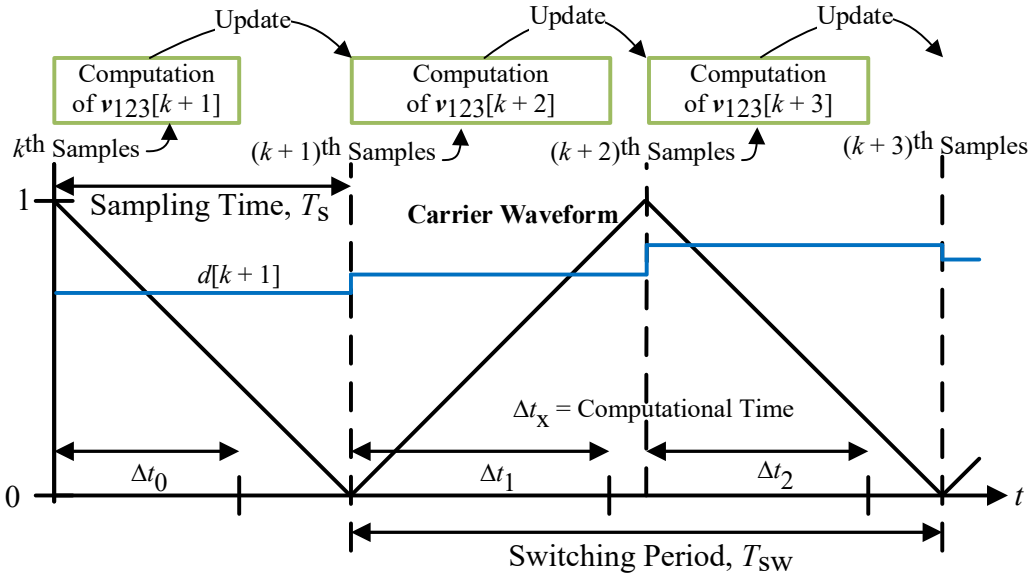

Figure 3.10: Proposed *Sampling Method* (SM).

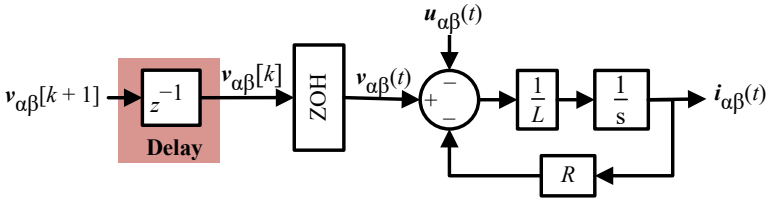

(a) Continuous-time (s) domain plant model in the αβ-frame

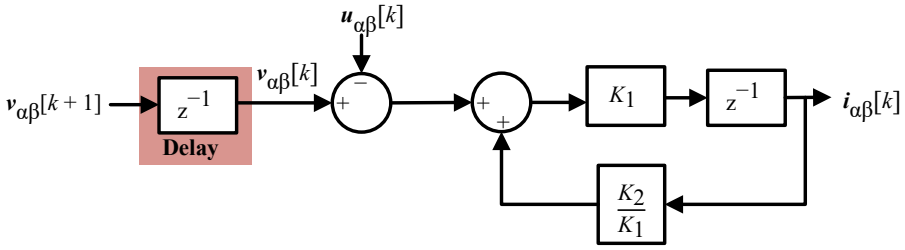

(b) Discrete-time (z) domain plant model in the αβ-frame

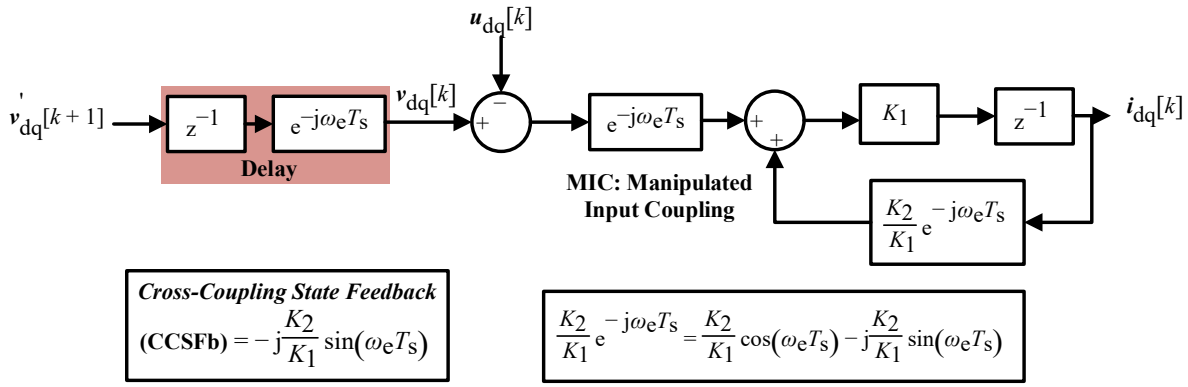

(c) Discrete-time (z) domain plant model in the dq-frame

Figure 3.11: State block diagram of the *RL* plant models in the continuous-time and discrete-time domains.

3.3.1 Direct Discrete-Time RL Plant Model

Fig. 3.9 and Table 3.1 represent the MMC average circuit diagrams shown in Fig. 3.3 using the general average *RL* plant model. Here, $\boldsymbol{v}_{\alpha\beta}$ and $\boldsymbol{u}_{\alpha\beta}$ represent the manipulated input and the disturbance, respectively. A direct discrete-time plant model and the discrete-time current controller obtained from Fig. 3.9 can be used as a basis to design the discrete-time current controllers for MMC. Fig. 3.10 represents the proposed *Sampling Method* (SM) (two sampling events in one switching time). T_s, T_{sw}, and Δt_x are the sampling time, switching time, and controller's computational time. The unavoidable controller's computational time (Δt_x) introduces a unit delay in the abc or αβ-frame. The unit delay can be compensated by computing the future converter voltage ($v_{123}[k+1]$) (or duty cycle ($d_{123}[k+1]$)) at present (k^{th} sample) and updating it in the future ((k + 1)th sample). The current and voltage at *Point of Common*

Coupling (PCC) are sampled at the extremes of the carrier waveform. Also, the duty cycle is updated at the extremes of the carrier waveforms.

(3.28) illustrates the transfer function of the *RL* plant model in the continuous-time domain using Laplace (s) notation. Fig. 3.11a represents the state block diagram of the *RL* plant model in the continuous-time domain using the complex vector notation ($\boldsymbol{F}_{\alpha\beta} = F_\alpha + \mathrm{j}\, F_\beta$). Here, *Zero-Order Hold* (ZOH) is used to sample and hold the signals, representing the analog-to-digital (A/D) interface and the average behavior of the *Pulse Width Modulation* (PWM) [SAH20]. A direct discrete-time transfer function ($G(z)$) can be obtained from the continuous-time transfer function ($G(s)$) using the relation (3.29). The z-transfer of G(s)/s can be obtained using the well-documented table of Laplace and z-transforms. The direct discrete-time *RL* plant model in the αβ-frame is obtained by performing z-transformation of (3.28) using (3.29) and solving it with the help of (3.30). (3.31) represents the simplified direct discrete-time *RL* plant model. τ represent the *RL* time constant. The general expressions of τ, K_1, and K_2 are shown in (3.32). Referring to (3.31), Fig. 3.11b represents the state block diagram of the direct discrete-time *RL* plant model in the αβ-frame.

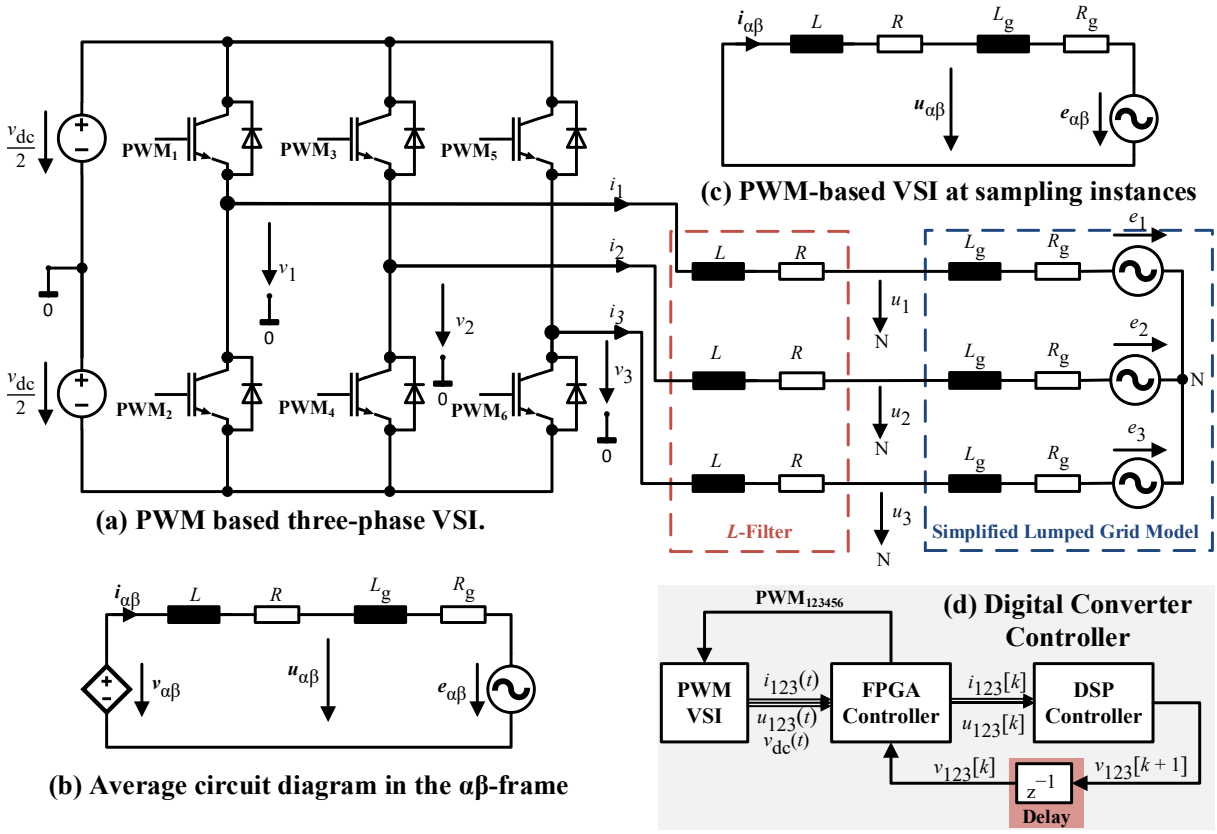

Figure 3.12: PWM-based *Voltage Source Inverter* (VSI) connected to grid via *L*-filter.

Table 3.2: List of parameters for designing current controllers.

S.N.	Variables	Value	S.N.	Variables	Value
1	f_{a}	50 Hz	11	$R_{\text{Trf-b}}(\text{for } f_{\mathrm{b}} \neq 0)$	123.4 mΩ
2	f_{b}	f_{a}, $f_{\mathrm{a}}/3$ and 0	12	$L_{\text{Trf-b}}(\text{for } f_{\mathrm{b}} \neq 0)$	8.9 mH
3	$V_{\text{a-LL}}$	20 kV	13	$R_{\text{Trf-b}}(\text{for } f_{\mathrm{b}} = 0)$	0 mΩ
4	V_{b} for $f_{\mathrm{b}} \neq 0$	25 kV	14	$L_{\text{Trf-b}}(\text{for } f_{\mathrm{b}} = 0)$	0 mH
5	V_{b} for $f_{\mathrm{b}} = 0$	$25\sqrt{2}$ kV	15	f_{br}	200 Hz
6	$S_{\text{load}}^{\text{nom}}$	40 MVA	16	$K_{\text{ir-b0}}$	25
7	R_{arm}	10 mΩ	17	$K_{\text{ir-b-dq}}$ & $K_{\text{ir-a}}$	10
8	L_{arm}	3.2 mH	18	ω_c	2π rad/s
9	$R_{\text{Trf-a}}$	100 mΩ	19	f_{sw}	2.5 kHz
10	$L_{\text{Trf-a}}$	3.8 mH	20	f_{s}	$2f_{\text{sw}}$

$$G_{\alpha\beta}(\mathrm{s}) = \frac{\boldsymbol{I}_{\alpha\beta}(\mathrm{s})}{\boldsymbol{V}_{\alpha\beta}(\mathrm{s}) - \boldsymbol{U}_{\alpha\beta}(\mathrm{s})} = \frac{1}{L\,\mathrm{s} + R} \tag{3.28}$$

$$G(z) = \left(1 - z^{-1}\right) Z\left(\frac{G(\mathrm{s})}{\mathrm{s}}\right) \tag{3.29}$$

$$Z\left(\frac{\mathrm{a}}{\mathrm{s}(\mathrm{s}+\mathrm{a})}\right) = \frac{\left(1 - \mathrm{e}^{-\mathrm{a}\,T_{\mathrm{s}}}\right) z^{-1}}{\left(1 - z^{-1}\right)\left(1 - \mathrm{e}^{-\mathrm{a}T_{\mathrm{s}}}\, z^{-1}\right)} \tag{3.30}$$

$$G_{\alpha\beta}(z) = \frac{\boldsymbol{I}_{\alpha\beta}(z)}{\boldsymbol{V}_{\alpha\beta}(z) - \boldsymbol{U}_{\alpha\beta}(z)} = \frac{z^{-1}\left(1 - \mathrm{e}^{-T_{\mathrm{s}}/\tau}\right)}{R\left(1 - \mathrm{e}^{-T_{\mathrm{s}}/\tau}\, z^{-1}\right)} = \frac{K_1\, z^{-1}}{1 - K_2\, z^{-1}} \tag{3.31}$$

$$\tau = \frac{L}{R};\; K_2 = \mathrm{e}^{-T_{\mathrm{s}}/\tau};\; K_1 = \frac{1 - K_2}{R} \tag{3.32}$$

(3.33) represents the direct discrete-time plant model in the dq-frame, which is obtained by transforming the delays in the direct discrete-time plant model in the αβ-frame (3.31), using $z^{-1}|^{\alpha\beta} \rightarrow \mathrm{e}^{-\mathrm{j}\omega_{\mathrm{e}}T_{\mathrm{s}}}\, z^{-1}|^{\mathrm{dq}}$ [SAH20]. Here, ω_{e} represents the angular speed of the park transformation angle. Similarly, Fig. 3.11c elaborates on the direct discrete-time plant model in the dq-frame.

Cross-Coupling State Feedback (CCSFb) expression in the discrete-time domain differs from the continuous-time domain. Further, the manipulated inputs (v_{dq}) are coupled due to the *Manipulated Input Coupling* (MIC) and the delay in the discrete-time domain. These couplings are only present due to the Park's transformation.

3.3.2 Inaccuracy of the Sampled Voltage at PCC

The direct discrete-time plant model is obtained without approximations and is assumed to represent the system accurately [SCH22]. But, [SAH23] has presented that the direct discrete-time plant model may accurately represent the average plant model in the continuous-time domain, but it fails to represent the actual PWM-based *Voltage Source Inverter* (VSI) for all frequency values. [SAH23] has presented a detailed study on the direct discrete-time plant model's accuracy. Here, only the accuracy of the direct discrete-time plant model with PWM-based VSI is compared. Fig. 3.12a represents the two-level three-phase PWM-based VSI connected to the grid via *L*-filter. Fig. 3.12b represents the average plant model of the PWM-based VSI in the αβ frame. Here, a simplified lumped grid model is considered. Table 3.2 presents the list of parameters of MMC used in this work to simulate and validate the proposed energy balancing and current control loops. The corresponding resistances ($R_{b\text{-}0}$, $R_{b\text{-}dq}$, and R_a) and inductances ($L_{b\text{-}0}$, $L_{b\text{-}dq}$, and L_a) for tuning the current control loops can be computed from Table 3.2 (also see Fig. 3.5).

$$G_{dq}(z) = \frac{\boldsymbol{I}_{dq}(z)}{\boldsymbol{V}_{dq}(z) - \boldsymbol{U}_{dq}(z)} = \frac{K_1\, z^{-1}\, e^{-j\omega_e T_s}}{1 - K_2\, z^{-1}\, e^{-j\omega_e T_s}} \tag{3.33}$$

Fig. 3.13 compares the voltage (u_1) and current (i_1) of one phase of the three-phase system at the *Point of Common Coupling* (PCC) when the actual PWM-based VSI is used. Here, the grid impedance (Z_g) equals the filter impedance (Z). The actual grid voltage at PCC (u_{123}) fluctuates because the voltage at PCC is not a state. Therefore, u_{123} solely depends on the switching conditions of the PWM-based VSI [SAH21]. All upper or lower switches are turned on in the sampling instances (also see Fig. 3.10). In other words, the inverter voltage is zero in the sampling instances. The circuit diagram of the PWM-based VSI at the sampling instances is shown in Fig. 3.12c. Since the inverter voltage is zero at the sampling instants, the grid voltage ($u_{1\text{-}SM}$) sampled using SM in Fig. 3.10 deviates significantly from the average grid voltage at PCC. Therefore, it is recommended to find the average voltage at PCC ($u_{1\text{-}Mean}$) using multiple samples in one sampling time and use it in the controller. The only drawback is that the computed average grid voltage at PCC introduces an additional half sampling time ($0.5T_s$) delay

in the system. The sampled current ($i_{1\text{-SM}}$) using the proposed sampling method matches closely with the actual average inductor current. Therefore, the sampled current can be used in the controller as it is.

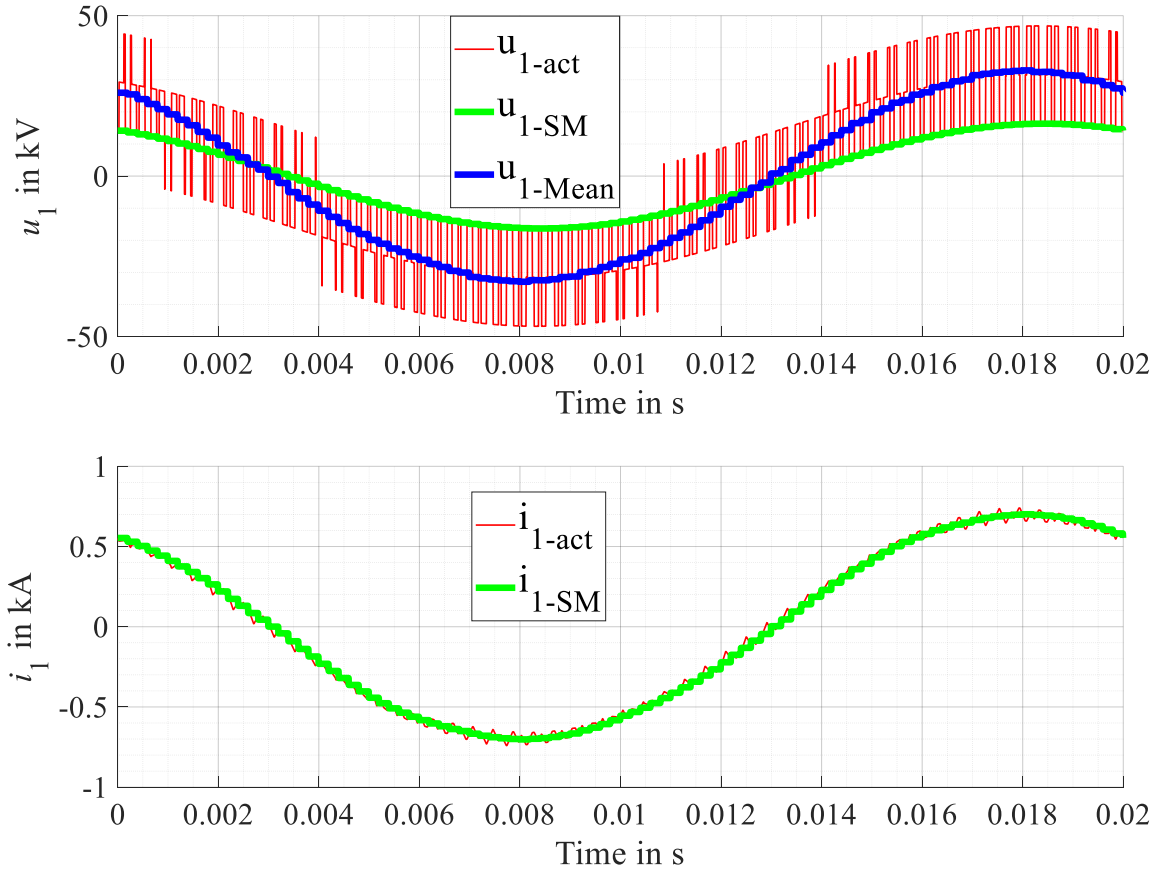

Figure 3.13: Grid voltage and current at PCC. Here, $E_{\text{LL}}^{\text{rms}} = 2V_{\text{a-LL}}$, $V_{\text{dc}} = 2\text{x}1.4\text{x}\sqrt{\frac{2}{3}}E_{\text{LL}}^{\text{rms}}$, $Z = (R_{\text{a}} + \text{j}\omega_{\text{a}}L_{\text{a}})$, and $Z_{\text{g}} = Z$.

3.3.3 Inaccuracy of the Direct Discrete-Time Plant Model and State Observers

As mentioned in Section 3.3.1, the unit delay can be compensated by computing the future converter voltage ($v_{123}[k + 1]$) at present (k^{th} sample) and updating it in the future ($(\text{k} + 1)^{\text{th}}$ sample) (also see Fig. 3.10). This can be realized by controlling the future converter current ($i_{123}[k + 1]$) at present. But it is impossible to sample the current at present; hence, a state observer should estimate the future current. The future current can be estimated in the dq-frame or the αβ-frame. Fig. 3.14 shows the proposed *Discrete Luenberger Style Observer* (DLSO) in the αβ-frame [SAH20]. Here, the observer in the αβ-frame is chosen because the states are not coupled in the αβ-frame. The derived direct discrete-time plant model in the αβ-frame is mathematically implemented in the observer (also see Fig. 3.11). The sampled current acts as a

reference for the observer, and the estimated current is used as a feedback signal. Here, the disturbance voltage ($\overline{\boldsymbol{u}}_{\alpha\beta}[k] \approx \boldsymbol{u}_{\alpha\beta}[k-0.5]$) is rotated by an angle ($\omega_e T_s$) to compensate for the unit delay. Rotation by angle $0.5\omega_e T_s$ compensates for the half-sampling time delay caused due to the mean computation of the voltage at PCC. And the remaining half-sample time advancement (rotation by angle $0.5\omega_e T_s$) helps to decouple the disturbance with minimum error [SAH23]. The controller in the observer can be realized using either PI or deadbeat (DB) controller. The method of tuning the PI and deadbeat controllers is shown in the sections below.

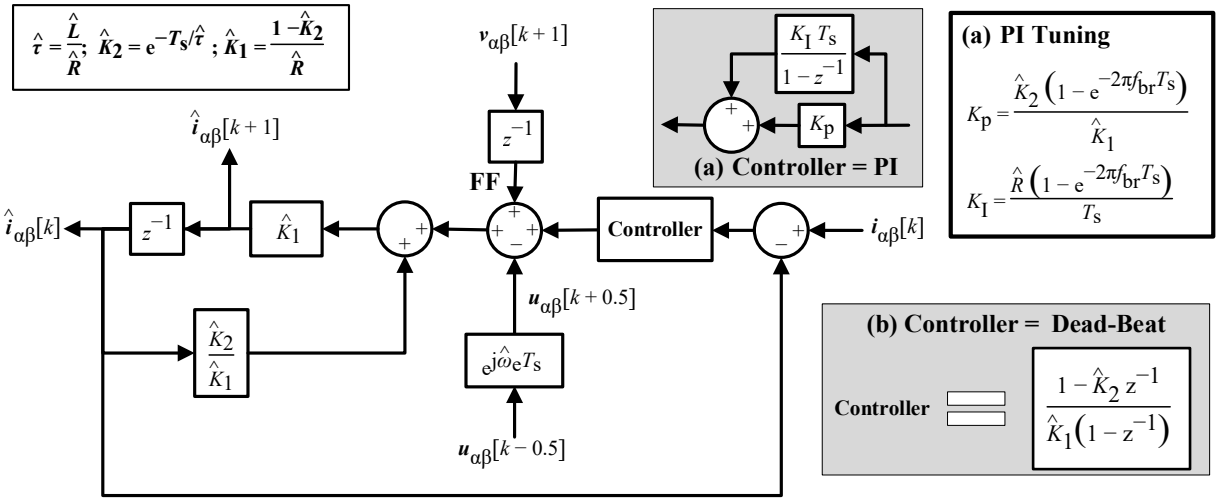

Figure 3.14: *Discrete Luenberger Style Observer* (DLSO) in the αβ-frame.

3.3.3.1 PI-Based Observer Tuning

(3.34) presents the discrete-time transfer function of the proposed PI controller. Ignoring the feedforward (FF) and the disturbance in the observer, (3.35) represents the observer's open-loop transfer function. The condition of the pole-zero cancelation is given in (3.36). (3.37) illustrates the open-loop transfer function after the pole-zero cancellation. (3.38) represents the closed-loop transfer function of the state observer. The closed-loop bandwidth of the observer can be placed at a break frequency (f_{br}) by comparing the denominator of (3.38) with ($z - e^{-2\pi f_{br} T_s}$). The result of the comparison is shown in (3.39). (3.40) elaborates on the general expression for the gains of the PI controllers, which are obtained by solving (3.36) and (3.39). The PI gains are also shown in Fig. 3.14. The observer has low pass filter attributes for the sampled currents. Decreasing its bandwidth can help reduce the effect of the noise of the sampled current signals in the controller. But less bandwidth also lowers the overall system's robustness. Therefore, the bandwidth has to be selected appropriately regarding robustness and noise requirements.

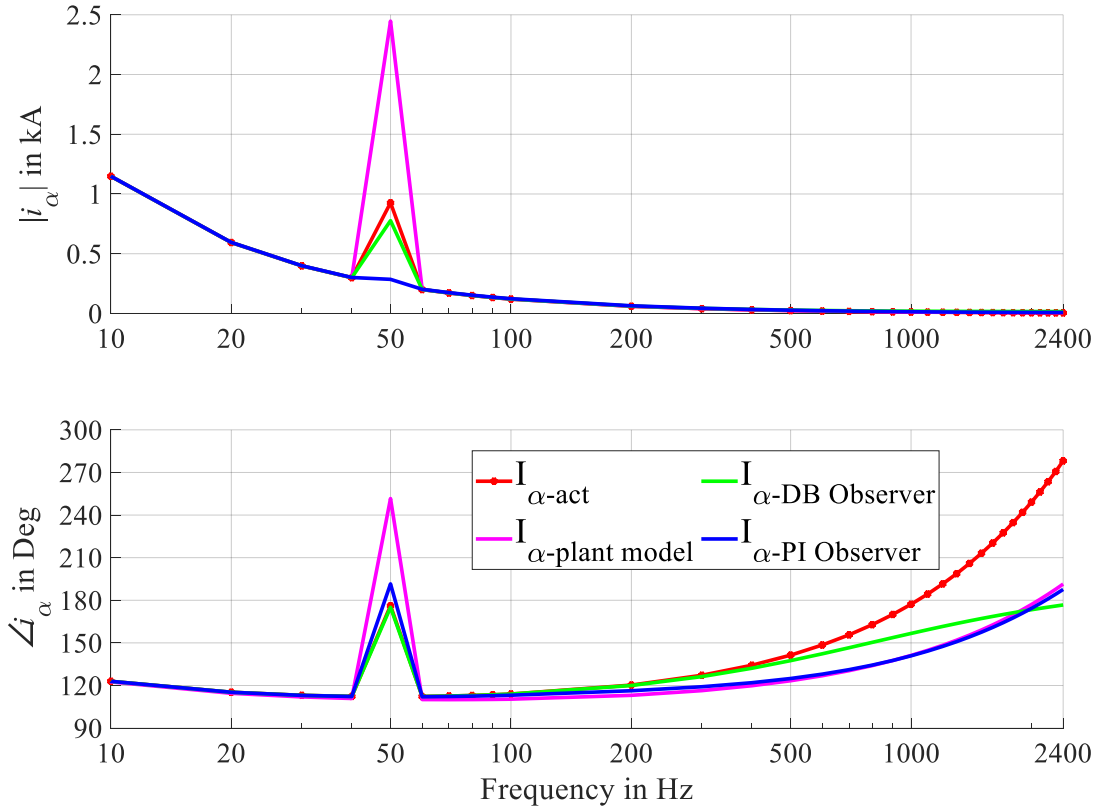

Figure 3.15: Open-loop bode plot of the converter current in the α-frame when the sampled voltage ($\boldsymbol{u}_{\alpha\beta\text{-SM}}$) at PCC is used in the plant model and the observer. Here, $E_{\text{LL}}^{\text{rms}} = 2V_{\text{a-LL}}$, $V_{\text{dc}} = 2\text{x}1.4\text{x}\sqrt{\frac{2}{3}}E_{\text{LL}}^{\text{rms}}$, $Z = (R_{\text{a}} + \text{j}\omega_{\text{a}}L_{\text{a}})$, and $Z_{\text{g}} = Z$.

$$\text{PI}(z) = K_{\text{p}} + \frac{K_{\text{I}}\,T_{\text{s}}}{1 - z^{-1}} = \frac{(K_{\text{p}} + K_{\text{I}}\,T_{\text{s}})\left(z - \dfrac{K_{\text{p}}}{K_{\text{p}} + K_{\text{I}}\,T_{\text{s}}}\right)}{z - 1} \tag{3.34}$$

$$\boldsymbol{G}_{\text{o}}(z) = \text{PI}(z)\frac{K_1}{z - K_2} = \left(\frac{K_1\,(K_{\text{p}} + K_{\text{I}}\,T_{\text{s}})}{(z-1)}\right)\left(\frac{z - \dfrac{K_{\text{p}}}{K_{\text{p}} + K_{\text{I}}\,T_{\text{s}}}}{z - K_2}\right) \tag{3.35}$$

$$\frac{K_{\text{p}}}{K_{\text{p}} + K_{\text{I}}\,T_{\text{s}}} = K_2 \tag{3.36}$$

$$\boldsymbol{G}_{\text{o}}(z) = \left(\frac{K_1\,(K_{\text{p}} + K_{\text{I}}\,T_{\text{s}})}{(z-1)}\right) \tag{3.37}$$

$$\frac{\hat{\boldsymbol{I}}_{\alpha\beta}(z)}{\boldsymbol{I}_{\alpha\beta}(z)} = \frac{K_1\,(K_{\text{p}} + K_{\text{I}}\,T_{\text{s}})}{z - 1 + K_1\,(K_{\text{p}} + K_{\text{I}}\,T_{\text{s}})} \tag{3.38}$$

$$1 - K_1\,(K_{\text{p}} + K_{\text{I}}\,T_{\text{s}}) = \text{e}^{-2\pi f_{\text{br}}T_{\text{s}}} \tag{3.39}$$

$$K_p = \frac{K_2\left(1 - e^{-2\pi f_{br} T_s}\right)}{K_1}, \text{ and } K_I = \frac{R\left(1 - e^{-2\pi f_{br} T_s}\right)}{T_s} \tag{3.40}$$

3.3.3.2 Dead-Beat (DB)-Based Observer Tuning

The dead-beat controller provides the fastest possible response in the discrete-time domain [SCH22]. The closed-loop transfer function of the dead-beat controller-based observer is shown in (3.41). The closed-loop bandwidth of the deadbeat-based observer is placed at infinity. Thus, the deadbeat observer can track the reference command in one sampling time (T_s). The deadbeat-based observer provides no noise filtering. The solution of (3.41) is given in (3.42), which provides the general expression for the dead-beat controller (DB(z)).

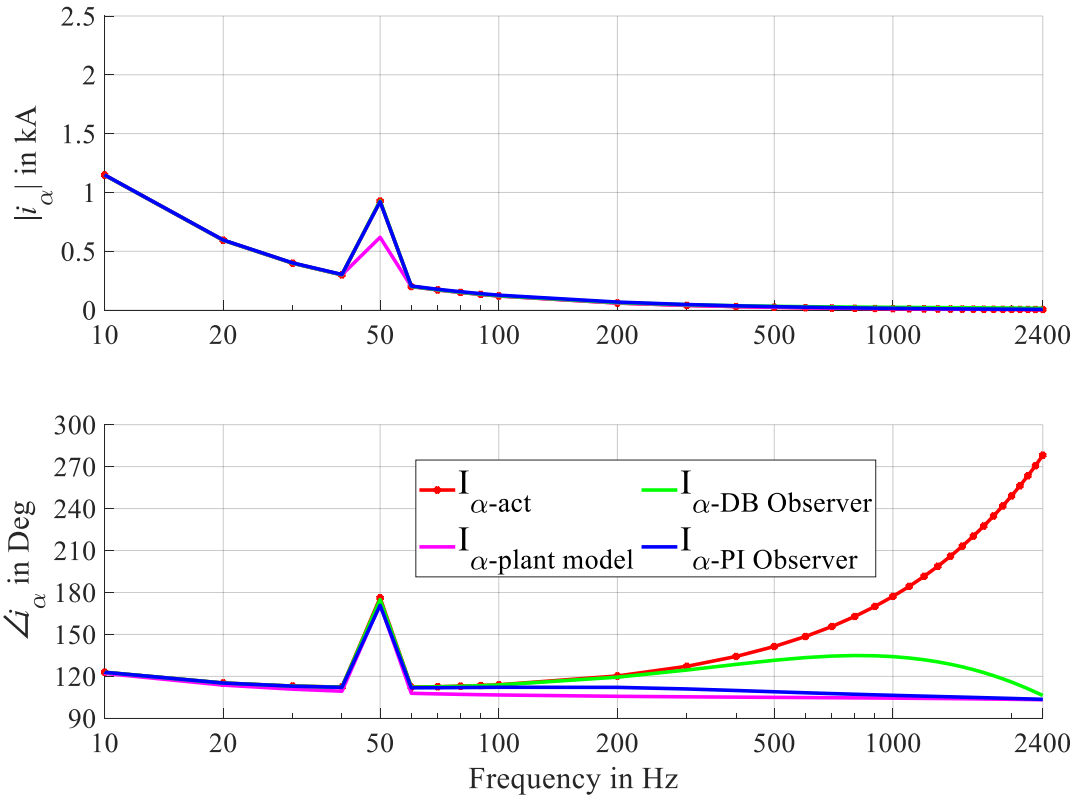

Figure 3.16: Open-loop bode plot of the converter current in the α-frame when the average voltage ($\boldsymbol{u}_{\alpha\beta\text{-Mean}}$) at PCC is used in the plant model and the observer. Here, $E_{LL}^{rms} = 2V_{a\text{-LL}}$, $V_{dc} = 2\text{x}1.4\text{x}\sqrt{\frac{2}{3}}E_{LL}^{rms}$, $Z = (R_a + j\omega_a L_a)$, and $Z_g = Z$.

$$\frac{\hat{\boldsymbol{I}}_{\alpha\beta}(z)}{\boldsymbol{I}_{\alpha\beta}(z)} = z^{-1} = \frac{\text{DB}(z)\dfrac{K_1}{z - K_2}}{1 + \text{DB}(z)\dfrac{K_1}{z - K_2}} \tag{3.41}$$

$$Controller\ (\mathrm{DB}(z)) = \frac{1 - K_2\, z^{-1}}{K_1\left(1 - z^{-1}\right)} \tag{3.42}$$

3.3.3.3 Comparison of the Direct Discrete-Time Model and State Observers with the PWM-based VSI

Fig. 3.15 and Fig. 3.16 represent the comparison of the actual converter current ($I_{\alpha\text{-act}}$), estimated current using the direct discrete-time plant model ($I_{\alpha\text{-plant model}}$), estimated current using the deadbeat-based observer ($I_{\alpha\text{-DB Observer}}$), and estimated current using the PI controller-based observer ($I_{\alpha\text{-DB Observer}}$). The grid impedance ($Z_g$) equals the converter filter impedance (Z). Both figures show the open-loop bode plot of the converter current in the α-frame. The sampled voltage at PCC ($u_{\alpha\beta\text{-SM}}$) (also see Fig. 3.10) is used in Fig. 3.15, and the average computed voltage at PCC ($u_{\alpha\beta\text{-Mean}}$) is used in Fig. 3.16. Here, the three-phase system frequency is 50 Hz. The sampling and switching frequencies are 5 kHz and 2.5 kHz. The closed-loop band-width of the PI controller-based observer is placed at 200 Hz. The direct discrete-time plant model and the observers fail to track the current magnitude at the fundamental frequency (50 Hz) when the sampled voltage ($u_{\alpha\beta\text{-SM}}$) at PCC is used in the plant model and the observers (see Fig. 3.13). Thus, using the sampled voltage at PCC cannot help to estimate the future converter current accurately.

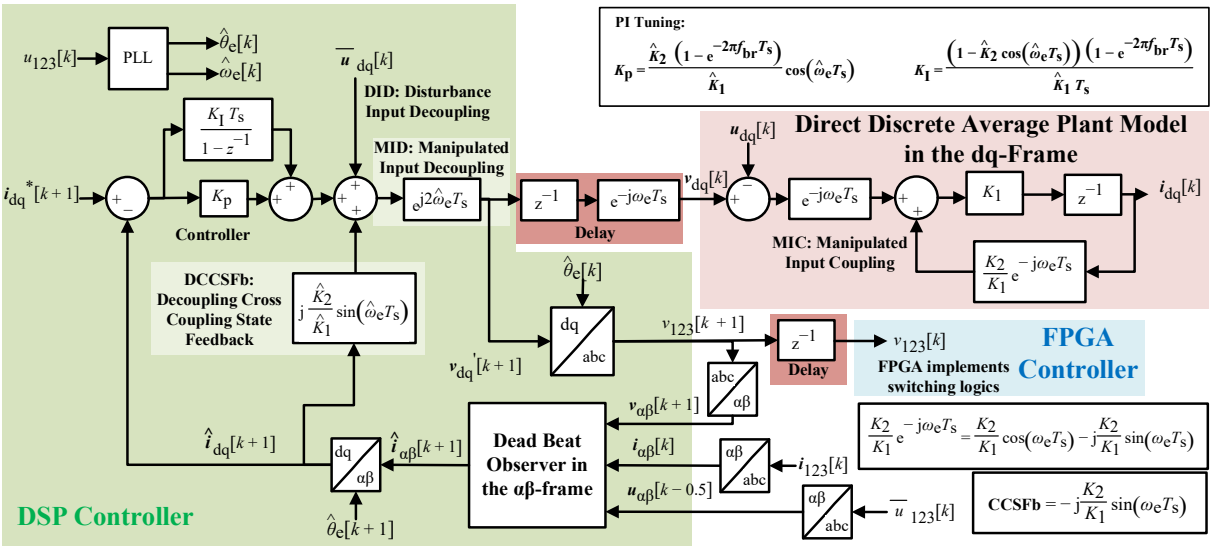

Figure 3.17: Proposed PI controller based synchronous (dq) frame direct discrete-time current controller using the deadbeat-based observer (DLSO) implemented in the αβ-frame.

Further, Fig. 3.16 suggests that the direct discrete-time plant model also fails to represent the system accurately even if the average computed voltage at PCC ($u_{\alpha\beta\text{-Mean}}$) is used. PI-based and deadbeat-based observers represent the system accurately at the fundamental frequency. But

the PI-based observer and deadbeat-based observer were found to accurately represent the actual system for the system frequency until 100 Hz and 300 Hz, respectively. The accuracy range of the PI-based observer can be further increased by increasing its closed-loop bandwidth. But the PI-based observer cannot become faster than the deadbeat-based observer because the closed-loop bandwidth of the deadbeat-based observer is located at infinity. Thus, a deadbeat-based observer accurately represents the system for a high range of frequencies. Therefore, the deadbeat-based observer is proposed in this work to estimate the converter's future current for compensation for the system's unit delay. But it should be remembered that even a deadbeat-based observer fails to represent the system at high frequencies because an additional half-sampled time delay is introduced due to the mean computation of the voltage at PCC.

In conclusion, the direct discrete-time plant model can accurately represent the average plant model. Still, it fails to accurately represent the actual PWM VSI because of the voltage fluctuation at PCC ($u_{123}(t)$). On the other hand, the mean computation of the voltage at PCC only helps to behave the state observers accurately until a specific frequency. Simply put, none of the methods can accurately represent the system for all frequency values. Thus, the proposed state observer cannot help the converter behave passively for high frequencies [SAH23].

3.3.4 Proposed Discrete-Time Current Controllers in the dq0-Frame using the Deadbeat-Based Observer in the αβ0-Frame

This subsection proposes the design of the direct discrete-time current controllers in the dq0-frame. The overall control structure of the PWM VSI is shown in Fig. 3.12d. The main current controller is implemented using a slow (DSP) controller, and the PWM is realized using a fast FPGA controller. Fig. 3.17 represents the proposed PI controller-based direct discrete-time synchronous (dq) frame current controller using the deadbeat-based observer in the αβ-frame. The state block diagram is drawn using the complex vector notation ($\boldsymbol{F}_{\mathrm{dq}} = F_{\mathrm{d}} + \mathrm{j}F_{\mathrm{q}}$ and $\boldsymbol{F}_{\alpha\beta} = F_{\alpha} + \mathrm{j}F_{\beta}$). This controller can be used to design the three-phase and the circulating current controllers for MMC. Mean computed voltage at PCC ($\overline{\boldsymbol{u}}_{\mathrm{dq}}[k] \approx \boldsymbol{u}_{\mathrm{dq}}[k - 0.5]$) is used for *Disturbance Input Decoupling* (DID). Deadbeat-based observer (also see Fig. 3.14) is selected because it closely represents the actual system for a wide range of system frequencies. The deadbeat-based observer estimates the future current ($\hat{i}_{\alpha\beta}[\mathrm{k+1}]$), which is used as a feedback signal to the main current controller in the dq-frame. *Disturbance Input Decoupling* (DID) decouples the disturbance (voltage at PCC), *Decoupling Cross-Coupling State Feedback* (DCCSFb) recouples the *Cross-Coupling State Feedback* (CCSFb), and *Manipulated Input*

Decoupling (MID) decouples the cross-coupling present due to delay (*Manipulated Input Coupling* (MIC)).

Similarly, Fig. 3.18 represents the proposed PR or PIR controller-based direct discrete-time current controller in the 0-frame using the deadbeat observer in the 0-frame. It can be used to design the single-phase current controller for MMC. A PR controller can be used for AC-AC MMC topology, and a PIR (or PI) controller can be used for DC-AC MMC topology. The deadbeat observer estimates the future single-phase current ($\hat{i}_b[k+1]$), a feedback signal to the main current controller. Here, the voltage at PCC (u_b) is not rotated anticlockwise to compensate for the unit delay as it was done in the dq current controller. One may think that the magnitude and phase of u_b can be obtained using a single-phase PLL, and the angle can be rotated. Alternatively, the voltage (u_b) could also be rotated using the *Second-Order Generalized Integrator* SOGI [TEO07]. But both PLL and SOGI will introduce additional delay in the system, further complicating the controller and compromising the controller's dynamic performance.

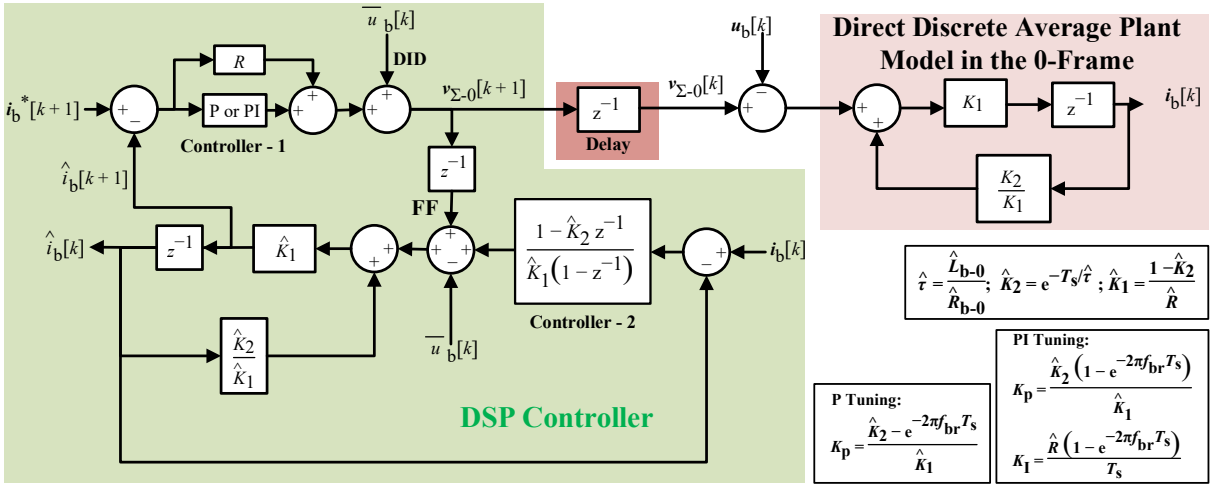

Figure 3.18 Proposed PR or PIR controller based single-phase direct discrete-time current controller using the deadbeat-based observer (DLSO) implemented in the 0-frame.

3.3.4.1 Tuning of the PI Controller-Based Discrete Controller in the dq-Frame

Manipulated Input Decoupling (MID), *Disturbance Input Decoupling* (DID), and *Decoupling Cross-Coupling State Feedback* (DCCSFb) cancel the *Manipulated Input Coupling* (MIC), *Disturbance Input Coupling* (DIC), and *Cross-Coupling State Feedback* (CCSFb), respectively. The delay is compensated by controlling the future current at present. Ignoring all the couplings and the decouplings in Fig. 3.17, (3.43) represents the main controller's open-loop transfer function. The condition of the pole-zero cancelation is shown in (3.44). (3.45) presents the

open-loop transfer function after the pole-zero cancellation. (3.46) illustrates the closed-loop transfer function of the controller. The closed-loop bandwidth of the controller can be placed at break frequency (f_{br}) by comparing the denominator of (3.46) with ($z - e^{-2\pi f_{br} T_s}$). The result of the comparison is shown in (3.47). (3.48) elaborates on the general expression for the gains of the PI controllers, which are obtained by solving (3.44) and (3.47). The PI gains are also given in Fig. 3.17.

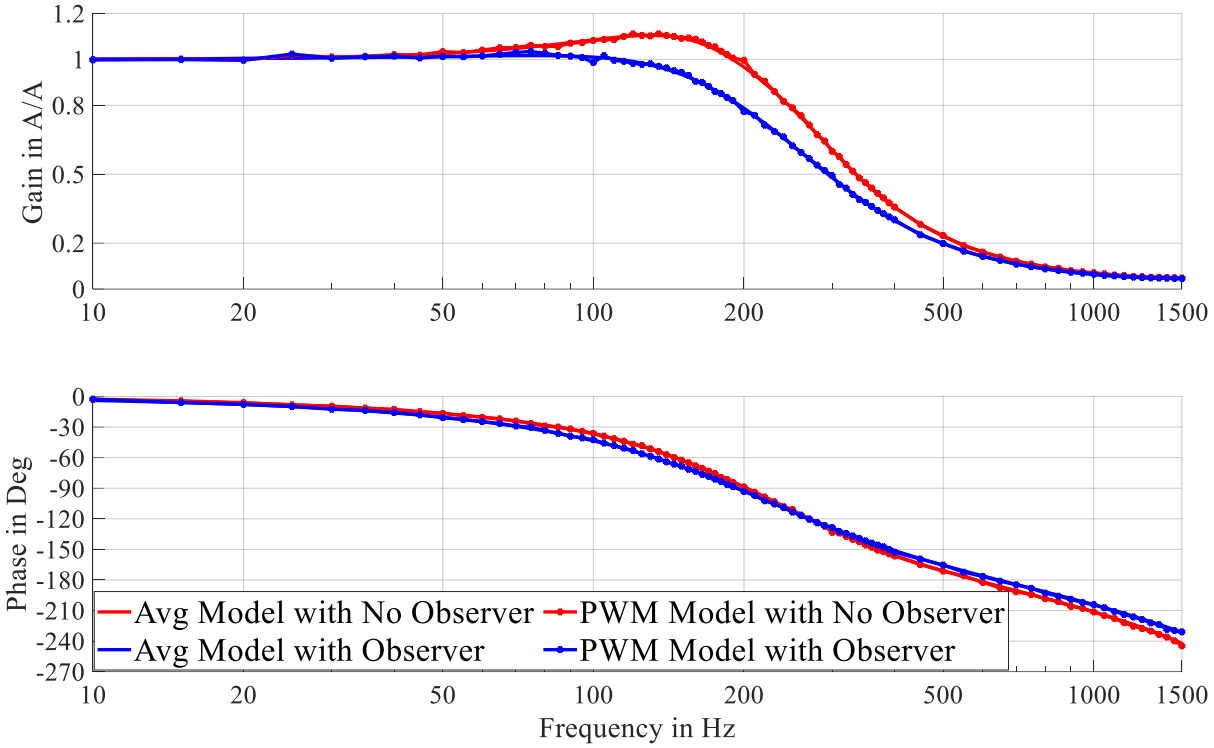

Figure 3.19: *Command.Tracking* (CT) or closed-loop bode plot of the discrete-time current controllers in the dq-frame. Here, f_{br} = 200 Hz, $E_{LL}^{rms} = 2V_{a\text{-}LL}$, $V_{dc} = 2\text{x}1.4\text{x}\sqrt{\frac{2}{3}}E_{LL}^{rms}$, $Z = (R_a + j\omega_a L_a)$, and $Z_g = Z$.

$$\boldsymbol{G}_o(z) = \text{PI}(z)\frac{K_1}{z - K_2\cos(\omega_e T_s)} = \left(\frac{K_1\left(K_p + K_I T_s\right)}{(z-1)}\right)\left(\frac{z - \dfrac{K_p}{K_p + K_I T_s}}{z - K_2\cos(\omega_e T_s)}\right) \tag{3.43}$$

$$\frac{K_p}{K_p + K_I T_s} = K_2\cos(\omega_e T_s) \tag{3.44}$$

$$\boldsymbol{G}_o(z) = \left(\frac{K_1\left(K_p + K_I T_s\right)}{(z-1)}\right) \tag{3.45}$$

$$\frac{\hat{\boldsymbol{I}}_{\mathrm{dq}}(z)}{\boldsymbol{I}^{*}_{\mathrm{dq}}(z)} = \frac{K_1\left(K_\mathrm{p} + K_\mathrm{I}\,T_\mathrm{s}\right)}{z - 1 + K_1\left(K_\mathrm{p} + K_\mathrm{I}\,T_\mathrm{s}\right)} \tag{3.46}$$

$$1 - K_1\left(K_\mathrm{p} + K_\mathrm{I}\,T_\mathrm{s}\right) = \mathrm{e}^{-2\pi f_\mathrm{br} T_\mathrm{s}} \tag{3.47}$$

$$K_\mathrm{p} = \frac{\hat{K}_2\left(1 - \mathrm{e}^{-2\pi f_\mathrm{br} T_\mathrm{s}}\right)}{\hat{K}_1}\cos\left(\omega_\mathrm{e}\,T_\mathrm{s}\right);\;\; K_\mathrm{I} = \frac{\left(1 - \hat{K}_2\cos\left(\hat{\omega}_\mathrm{e} T_\mathrm{s}\right)\right)\left(1 - \mathrm{e}^{-2\pi f_\mathrm{br} T_\mathrm{s}}\right)}{\hat{K}_1\,T_\mathrm{s}} \tag{3.48}$$

3.3.4.2 Tuning of the P or PI Controller-Based Discrete Controller in the 0-Frame

Similarly, ignoring all the couplings and the decouplings in Fig. 3.18, (3.49) represents the main controller's open-loop transfer function. (3.50) illustrates the closed-loop transfer function of the controller. The closed-loop bandwidth of the controller can be placed at break frequency (f_br) by comparing the denominator of (3.50) with ($z - e^{-2\pi f_\mathrm{br} T_\mathrm{s}}$). The result of the comparison is shown in (3.51). The expression for the P controller gain is also shown in Fig. 3.18. In case the current controller in the 0-frame is realized using a PI controller, the PI gains can be solved using the expressions in Section 3.3.3.1.

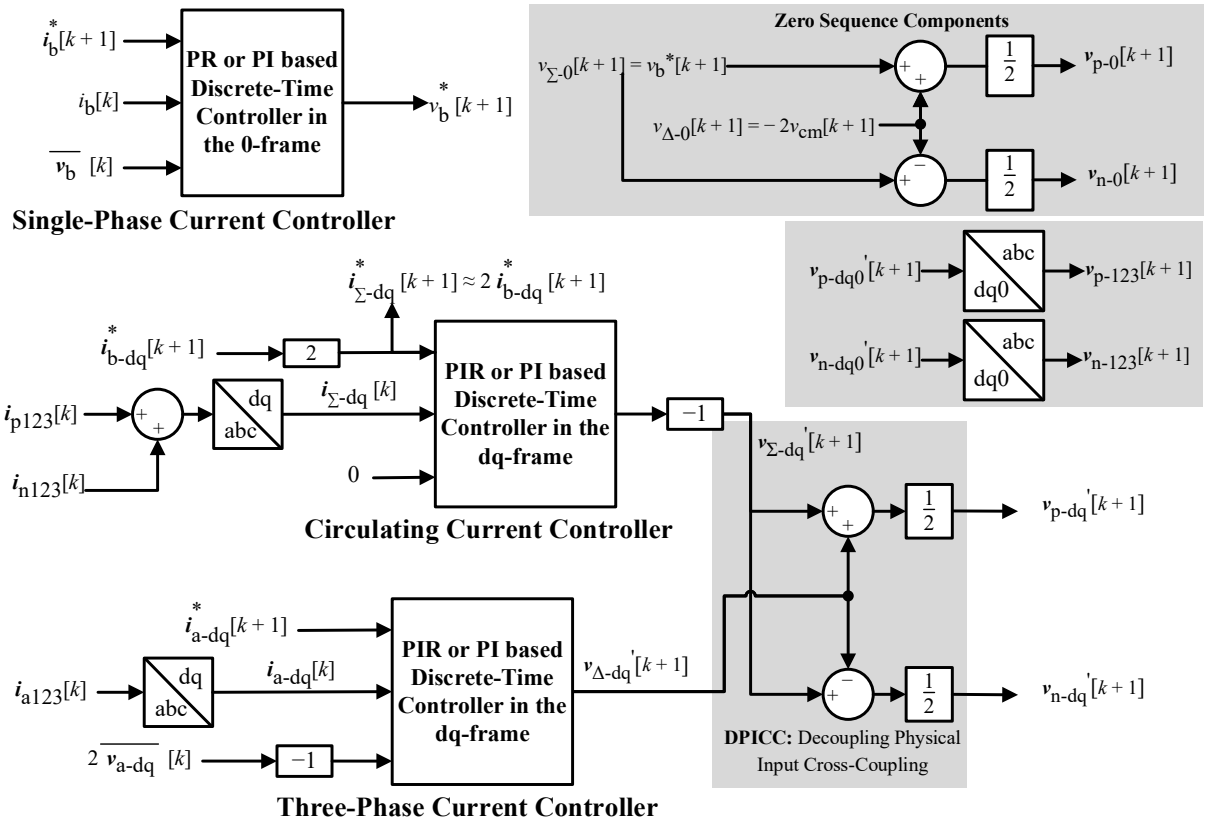

Figure 3.20: Proposed direct discrete-time current controllers of MMC.

$$G_{\mathrm{o}}(z) = \frac{K_{\mathrm{p}}\, K_1}{z - K_2} \tag{3.49}$$

$$\frac{\hat{I}_{\mathrm{b}}(z)}{I_{\mathrm{b}}^{*}(z)} = \frac{K_1\, K_{\mathrm{p}}}{z - K_2 + K_1\, K_{\mathrm{p}}} \tag{3.50}$$

$$K_{\mathrm{p}} = \frac{K_2 - \mathrm{e}^{-2\pi f_{\mathrm{br}} T_{\mathrm{s}}}}{K_1} \tag{3.51}$$

3.3.4.3 Command Tracking Plots

The PWM VSI shown in Fig. 12a is used to validate the accuracy of the tuning of the proposed direct discrete-time current controller in the dq-frame. Fig. 3.19 presents the closed-loop bode (*Command Tracking* (CT)) plots of the discrete-time current controllers for various controller conditions. The PI gains of the controllers are tuned to place the closed-loop bandwidth of the current controller at 200 Hz. The magnitude of the grid impedance (Z_{g}) is considered equal to the converter's impedance (Z). The command tracking plots obtained using the PWM VSI circuit diagram match the command tracking bode plot obtained using the average VSI model circuit diagram. The closed-loop bandwidth of the current controller with the observer is found close to the desired value. Further, the command tracking plot resembles the first-order filter behavior. On the other hand, the closed-loop bandwidth of the direct discrete-time current controller without an observer deviates from the desired value. Also, the gain of the command tracking plot is higher than one at certain frequencies. Hence, the closed-loop bandwidth of the current controller can be tuned close to the desired frequency using the proposed direct discrete-time current controller.

3.3.5 Proposed Discrete-Time Current Controller for MMC

Referring to Fig. 3.9, Table 3.1, and Section 3.3.4, Fig. 3.20 represents the proposed direct discrete-time current controllers of MMC. Circulating currents (i_{b123}) and three-phase currents (i_{a123}) are controlled in the dq-frame, and the single-phase current (i_{b}) is controlled in the 0-frame. The circulating currents (i_{b123}) are controlled using the summation (Σ) plant model in the dq-frame, the three-phase currents (i_{a123}) are controlled using the difference (Δ) plant model in the dq-frame, and the single-phase current (i_{b}) is controlled using the summation (Σ) plant model in the 0-frame. The zero-sequence difference voltage ($v_{\Delta\text{-}0}$) is used to virtually realize the common-mode voltage (v_{cm}). *Decoupling Physical Input Cross-Coupling* (DPICC) helps to decouple the *Physical Input Cross-Coupling* (PICC) (also see Fig. 3.5). Referring to Appendix

A.4, (3.52) and (3.53) represents the direct discrete-time transfer function of the resonant controller. (3.52) is implemented to realize a resonant controller in the PIR or PR-based controllers.

$$R(z) = \left(\frac{\left(1 - z^{-1}\right) z^{-1}}{1 - 2\, e^{-\omega_c T} \cos(\delta\, T)\, z^{-1} + e^{-2\omega_c T} z^{-2}} \right) \frac{2\, K_{ir}\, \omega_c\, e^{-\omega_c T} \sin(\delta\, T)}{\delta} \quad (3.52)$$

$$\delta = \sqrt{\omega_r^2 - \omega_c^2} \quad (3.53)$$

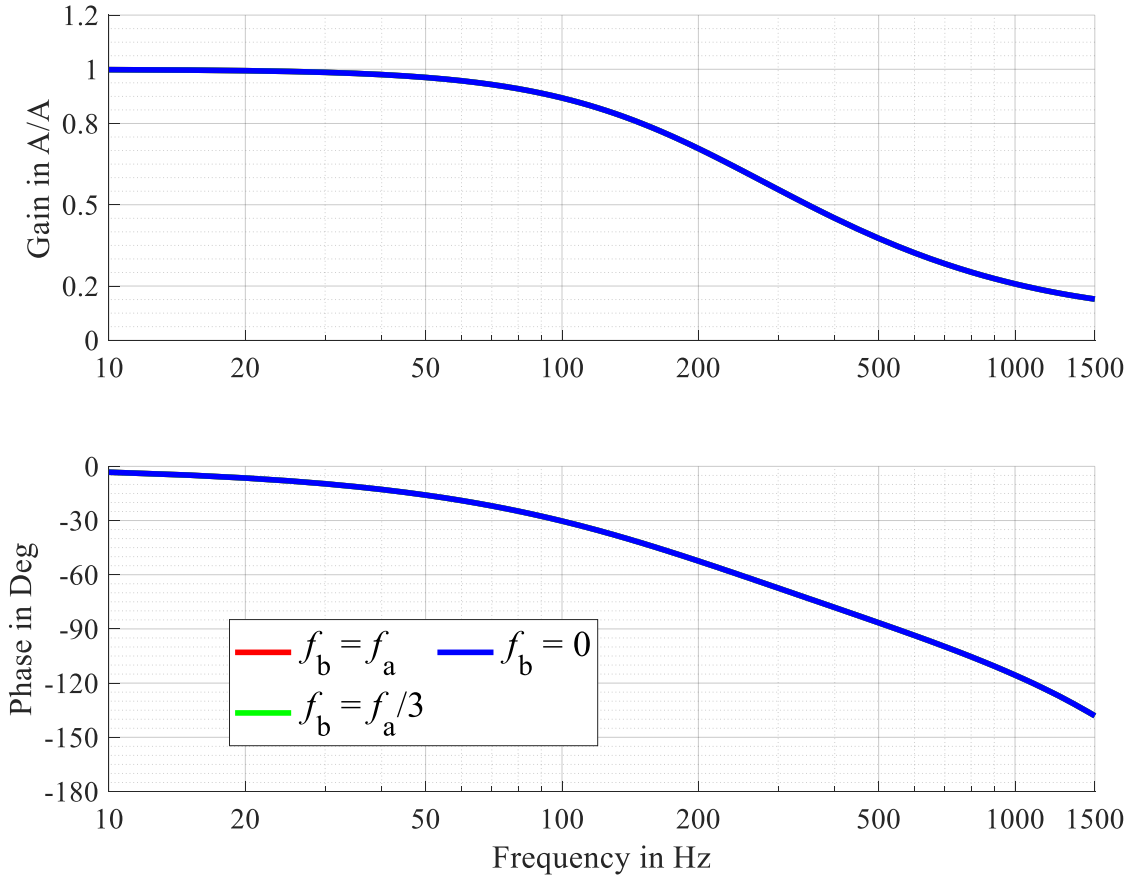

Figure 3.21: Command tracking plot of the proposed direct discrete-time three-phase current controller of MMC in the dq-frame for various single-phase system frequencies for energy balancing Method-7.

3.3.5.1 Command Tracking Plots

The list of parameters used in the simulation and tuning of the controllers is shown in Table 3.2. Fig. 3.21 represents the closed-loop (command tracking) bode plot of the proposed direct discrete-time three-phase current controller in the dq-frame for various single-phase system frequencies when the arm energies are regulated using Method-7. Referring to Section 3.2.1, a three-phase current would only have a DC value in the dq-frame hence only a PI (without

resonant) controller is used. The closed-loop bandwidth of the current controller matches closely with the desired bandwidth (200 Hz). The bode plots of the three-phase current controller overlap because the three-phase controller remains the same for all the single-phase system frequencies ($f_b = f_a$, $f_b = f_a/3$, and $f_b = 0$).

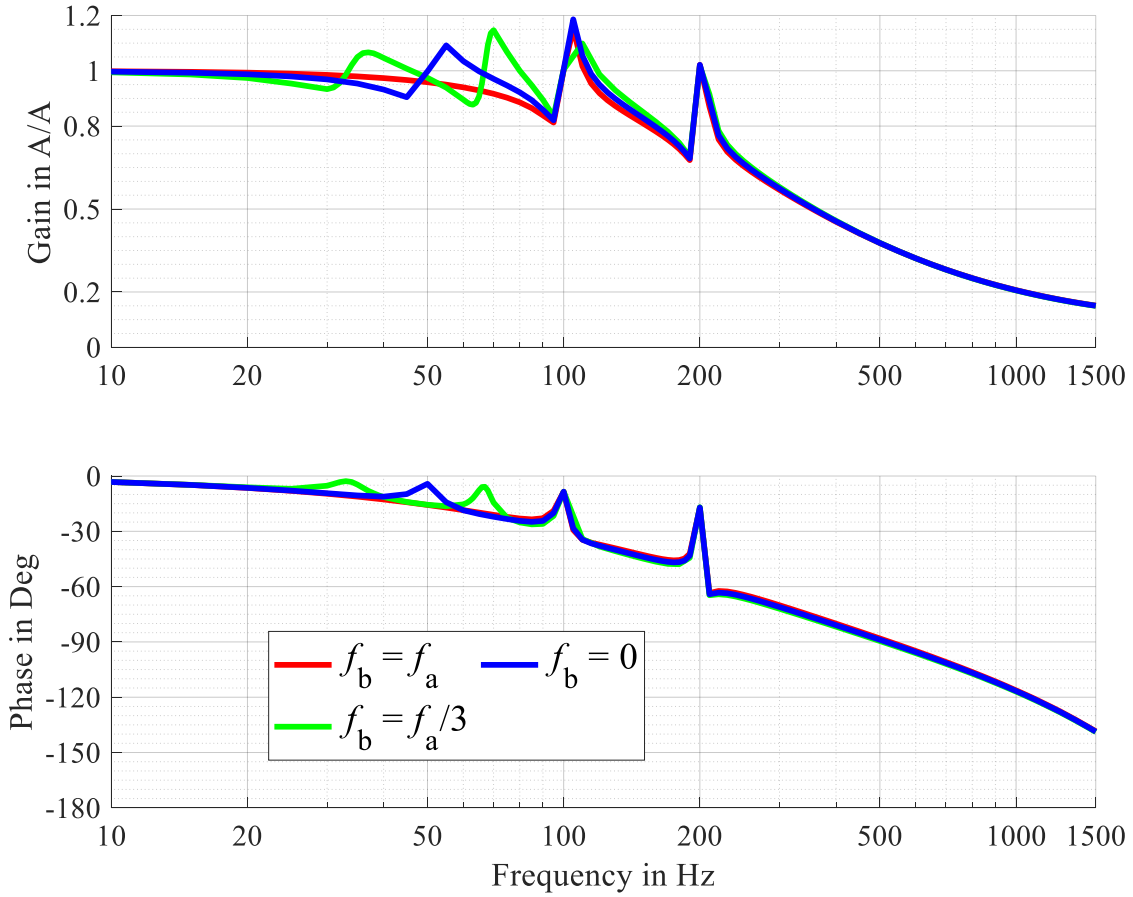

Figure 3.22: Command tracking plot of the proposed direct discrete-time circulating current controller of MMC in the dq-frame for various single-phase system frequencies for energy balancing Method-7.

Fig. 3.22 shows the command tracking plot of the proposed direct discrete-time circulating current controller in the dq-frame for various single-phase system frequencies when the arm energies are regulated using Method-7. Referring to Section 3.2.1, the circulating current controller requires resonant controllers; hence, the PIR controller is used for the current controller. Considering $f_{cm} = 3f_a$, two resonant controllers with resonant frequencies ($2f_a$, and $4f_a$) are required for equal frequency operation ($f_b = f_a$). Four resonant controllers with resonant frequencies ($f_b + f_a$, $|f_b - f_a|$, $2f_a$, and $4f_a$) are required for $1/3^{rd}$ frequency operation ($f_b = f_a/3$). And three resonant controllers with resonant frequencies (f_a, $2f_a$, and $4f_a$) are required for DC-AC MMC application ($f_b = 0$). The resonant controllers are tuned using the hit-and-trial method. The resonant controller tuning parameters are also shown in Table 3.2. With the help

of the resonant controller, the gain of the command tracking plot is close to unity at resonant frequencies. But the phase of the bode plot is not exactly zero. The phase can be further brought close to zero by increasing the gain of the resonant controller (K_{ir}). The gain of the command tracking plot is disturbed around the resonant frequencies. This disturbance rises with the increase in the gain of the resonant controller; hence it is not advisable to increase the gain of the resonant controller to avoid resonance behavior in the system. Therefore, bringing the phase of the command tracking plot exactly to zero is not a practical solution.

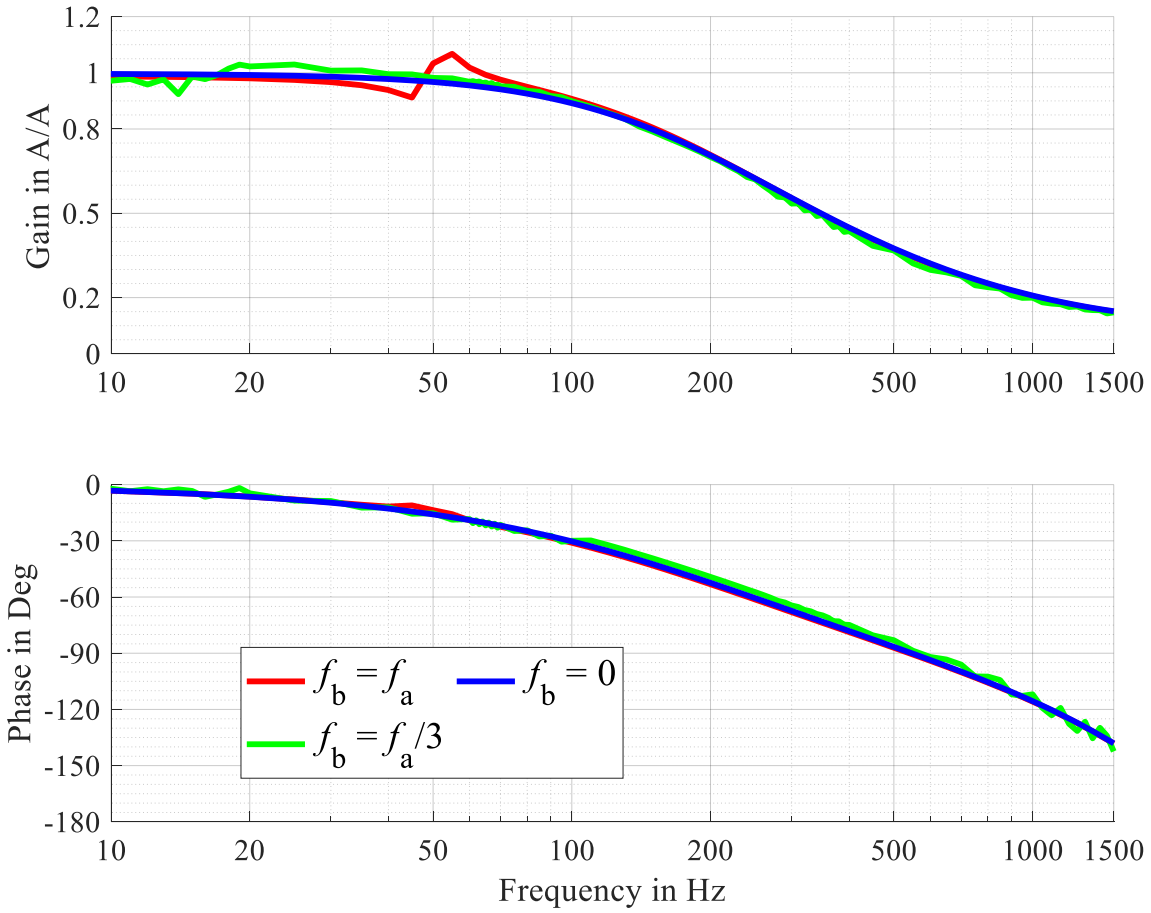

Figure 3.23: Command tracking plot of the proposed direct discrete-time single-phase current controller of MMC in the 0-frame for various single-phase system frequencies for energy balancing Method-12.

Similarly, Fig. 3.23 illustrates the command tracking plot of the proposed direct discrete-time single-phase current controller in the 0-frame for various single-phase system frequencies when the arm energies are regulated using Method-12. A single-phase current controller requires a resonant controller with resonant frequency (f_b) when the arm energies are controlled using Method-12 for AC-AC MMC topology. And it does not require a resonant controller for DC-AC MMC topology. Fig. 3.23 suggests that a resonant controller may be omitted for 1/3rd

frequency operation ($f_b = f_a/3$) because the gain and phase of the command tracking plot are already close to unity and zero, respectively, at resonant frequency($f_a/3$).

4 Design of the Average Arm Energy Control Loops of MMC

The general control structure of MMC is already shown in Fig. 1.2 in Chapter 1. This chapter focuses on designing the six average arm energy controllers using the six average arm power equations in the αβ0-frame. The arm energy controllers are necessary to compensate for the losses and asymmetries in the existing system. The design of the controllers in continuous-time and discrete-time domains is presented, and the physical limitation of tuning the average arm energy controllers will be discussed using the command tracking plots.

4.1 Derivation of the Average Arm Power Equations in the αβ0-Frame for a Selected Arm Energy Balancing Method

In Section 2.1, (2.17) to (2.22) represent the instantaneous arm power expressions in the αβ0-frame using summation (Σ) and difference (Δ) notations. And in Section 2.4, (2.32) to (2.36) show the general expression of the instantaneous three-phase current ($i_{a\alpha\beta}$), circulating current in the αβ-frame ($i_{b\alpha\beta}$), and circulating current in the 0-frame (i_{b0}) or single-phase current ($i_b = -3\, i_{b0}$), including all 18 *Degree of Freedom* (DOF) and reactive current components $\left(i_{aq+} \text{ and } i_{b0}^{\perp b}\right)$. For a selected arm energy balancing method, the general current expressions retain only the reactive current components $\left(i_{aq+} \text{ and } i_{b0}^{\perp b}\right)$, active load power component $\left(i_{ad+} \text{ or } i_{b0}^{b}\right)$, and the selected six degrees of freedom or *Manipulated Inputs* (MI). The remaining degrees of freedom are ignored or set to zero.

Let us consider two energy balancing methods (Method-7 and Method-12) to understand better the steps used in designing the average arm energy controllers of MMC for a selected energy balancing method. The arm energy balancing Method-7 and Method-12 are selected because these are the only two methods that do not inject harmonics into source and load currents and are stable for both equal ($f_b = f_a \neq 0$) and unequal ($f_b \neq f_a$) input and output system frequencies.

Referring to Table 2.2, the selected six degrees of freedom or *Manipulated Inputs* (MI) for Method-7 and Method-12 are (i_{ad+}, i_{bd+}, $\overset{b}{i}_{b\alpha\beta}$, & $\overset{cm}{i}_{b\alpha\beta}$) and ($\overset{b}{i}_{b0}$, i_{bd+}, $\overset{b}{i}_{b\alpha\beta}$, & $\overset{cm}{i}_{b\alpha\beta}$), respectively. Fig. 4.1 shows the phasor diagrams of the manipulated inputs in the abc-frame for the corresponding arm energies regulation using Method-7 and Method-12. Both methods use the same five degrees of freedom (i_{bd+}, $\overset{b}{i}_{b\alpha\beta}$, & $\overset{cm}{i}_{b\alpha\beta}$) for regulation of the total upper and lower arms energies ($\overline{w}_{\Delta 0}$), summation phase energies ($\overline{w}_{\Sigma\alpha\beta}$), and difference phase energies ($\overline{w}_{\Delta\alpha\beta}$). Only the first manipulated input (MI_1) to regulate the total arm energy ($\overline{w}_{\Sigma 0}$) of MMC is different. The three-phase active power helps to balance $\overline{w}_{\Sigma 0}$ by controlling the positive sequence three-phase current in the d-axis (i_{ad+}) for Method-7. The single-phase active power regulates $\overline{w}_{\Sigma 0}$ by controlling the zero-sequence circulating current in phase with v_b ($\overset{b}{i}_{b0}$) for Method-12.

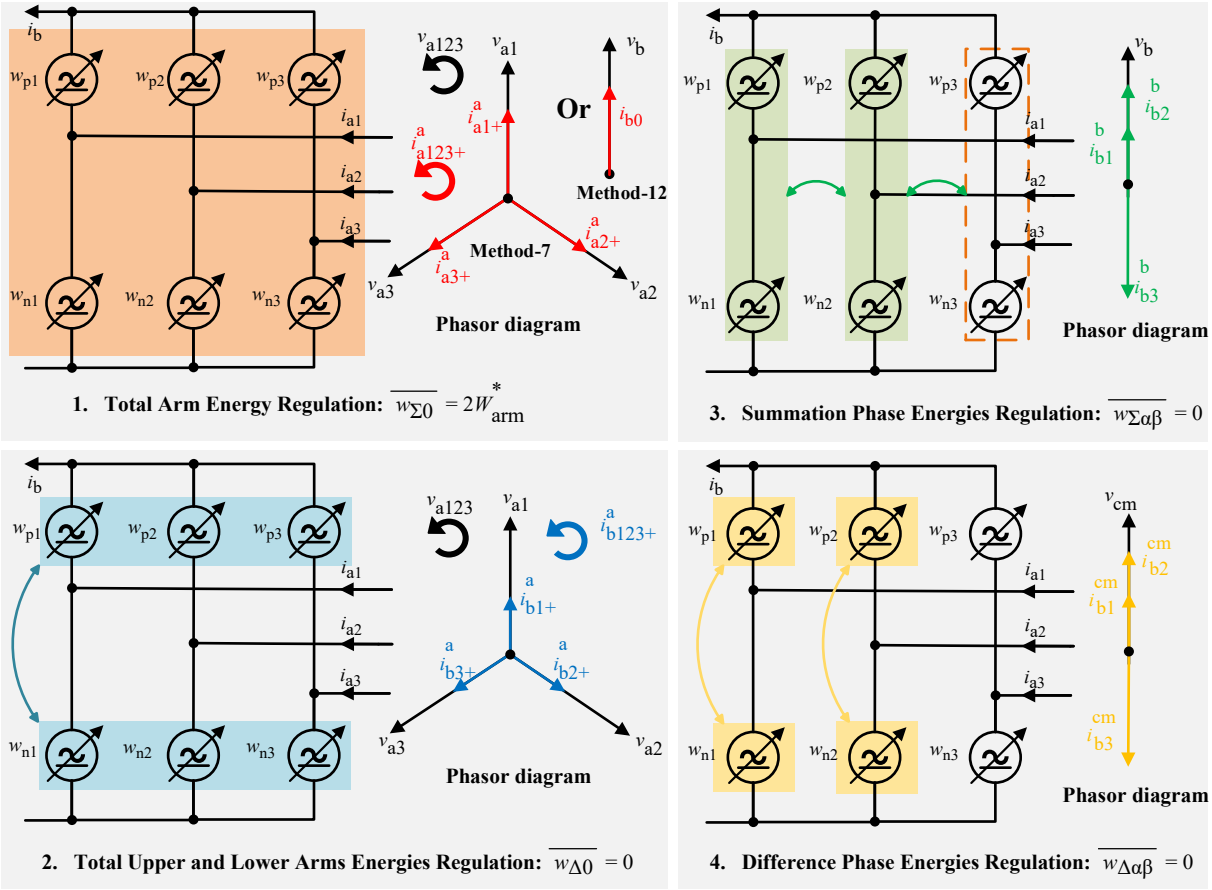

Figure 4.1: Phasor diagrams of the manipulated inputs for arm energy balancing using Method-7 and Method-12.

Manipulated inputs $\overset{b}{i}_{b\alpha\beta}$ and $\overset{cm}{i}_{b\alpha\beta}$ are unsymmetrical components because they are in phase with the zero sequence voltages (v_b and v_{cm}). On the other hand, the arm current components corresponding to i_{bd+} and i_{ad+} are symmetrical in the αβ-frame or abc-frame because these currents are in phase with the balanced three-phase voltage ($v_{a\alpha\beta}$). Having more unsymmetrical

current components makes one arm's current higher and another arm's current lower hence having more symmetrical current components will help to distribute current stress and losses equally among the arms of MMC. But, unlike the unequal frequency operation, the unsymmetrical current component cannot be omitted because the common-mode voltage is a must to regulate arm energies for equal frequency operation. (4.1) to (4.5) represent the general expressions of the instantaneous three-phase ($i_{a\alpha\beta}$), circulating ($i_{b\alpha\beta}$), and single-phase (i_{b0}) currents for Method-7 and Method.12, including the selected six degrees of freedom, the load active power component $\left(i_{ad+} \text{ or } i_{b0}^{b}\right)$, and two reactive current components $\left(i_{aq+} \text{ and } i_{b0}^{\perp b}\right)$, respectively.

$$i_{a\alpha} = i_{ad+}\cos(\theta_a) - i_{aq+}\sin(\theta_a) \tag{4.1}$$

$$i_{a\beta} = i_{aq+}\cos(\theta_a) + i_{ad+}\sin(\theta_a) \tag{4.2}$$

$$i_{b\alpha} = i_{bd+}\cos(\theta_a) + \sqrt{2}I_{b\alpha}^{cm}\cos(\theta_{cm}) + \sqrt{2}I_{b\alpha}^{b}\cos(\theta_b) \tag{4.3}$$

$$i_{b\beta} = i_{bd+}\sin(\theta_a) + \sqrt{2}I_{b\beta}^{cm}\cos(\theta_{cm}) + \sqrt{2}\,I_{b\beta}^{b}\cos(\theta_b) \tag{4.4}$$

$$i_{b0} = \sqrt{2}I_{b0}^{\perp b}\sin(\theta_b) + \sqrt{2}I_{b0}^{b}\cos(\theta_b) \tag{4.5}$$

(4.6) to (4.12) represents the simplified expression of the average arm power equations in the αβ0-frame for equal frequency operation ($f_b = f_a \neq 0$) considering only the selected six degrees of freedom, reactive current components $\left(i_{aq+} \text{ and } i_{b0}^{\perp b}\right)$, and load active power current component $\left(i_{ad+} \text{ or } i_{b0}^{b}\right)$. (4.6) to (4.12) are obtained by substituting (4.1) to (4.5) in the instantaneous arm power equations from (2.17) to (2.22), finding average and simplifying them with the help of the average expressions from (4.13) to (4.17). The frequency for mean calculation is $f_{Mean} = f_a$ for equal frequency operation ($f_b = f_a \neq 0$). The average powers because of the positive sequence d-axis current (i_{xd+}) and the negative sequence currents (i_{xdq-}) are illustrated using (4.13) to (4.15). Here, x = a or b. (4.16) represents the average of the product of v_g and $i_{x\alpha/\beta/0}^{g}$. Here, $i_{x\alpha/\beta/0}^{g}$ represents the component of the current $i_{x\alpha/\beta/0}$ in phase with the voltage v_g.

The common-mode frequency ($f_{cm} = 3f_a$) is selected to not make average power with the three-phase and single-phase frequencies current components (also see (4.17)). Further, $f_{cm} = 3f_a$ helps to realize a higher magnitude of the three-phase fundamental voltage. Here, v_b, $v_{a\alpha\beta}$, $i_{a\alpha\beta}$, $i_{b\alpha\beta}^{b}$, i_{bd+} and i_{b0} represent the instantaneous components, and V_b, V_a, I_{b0}^{b}, $I_{b\alpha\beta}^{b}$ and $I_{b\alpha\beta}^{cm}$ represent

the RMS quantities. (4.6) corresponds to Method-7 and (4.7) corresponds to Method-12. The average power expressions from (4.8) to (4.12) are common for Method-7 and Method-12.

$$\overline{P_{\Sigma 0}} = \frac{V_a}{\sqrt{2}} i_{ad+} + \overline{v_b\, i_{b0}} \text{ for Method-7} \tag{4.6}$$

$$\overline{P_{\Sigma 0}} = V_b\, I^{b}_{b0} + \overline{\frac{v_{a\alpha}\, i_{a\alpha} + v_{a\beta}\, i_{a\beta}}{2}} \text{ for Method-12} \tag{4.7}$$

$$\overline{P_{\Delta 0}} = -\sqrt{2}\, V_a\, i_{bd+} \overline{-\, v_{a\alpha}\, i^{b}_{b\alpha} - v_{a\beta}\, i^{b}_{b\beta}} \tag{4.8}$$

$$\overline{P_{\Sigma \alpha}} = V_b\, I^{b}_{b\alpha} + \overline{v_b\, i_{bd+} \cos(\theta_a)} \tag{4.9}$$

$$\overline{P_{\Sigma \beta}} = V_b\, I^{b}_{b\beta} + \overline{v_b\, i_{bd+} \sin(\theta_a)} \tag{4.10}$$

$$\overline{P_{\Delta \alpha}} = -2\, V_{cm}\, I^{cm}_{b\alpha} \overline{-\frac{v_b\, i_{a\alpha}}{2} - 2\, v_{a\alpha}\, i_{b0} - v_{a\alpha}\, i^{b}_{b\alpha} + v_{a\beta}\, i^{b}_{b\beta}} \tag{4.11}$$

$$\overline{P_{\Delta \beta}} = -2\, V_{cm}\, I^{cm}_{b\beta} \overline{-\frac{v_b\, i_{a\beta}}{2} - 2\, v_{a\beta}\, i_{b0} + v_{a\alpha}\, i^{b}_{b\beta} + v_{a\beta}\, i^{b}_{b\alpha}} \tag{4.12}$$

$$\overline{v_{a\alpha}\, i_{x\alpha} + v_{a\beta}\, i_{x\beta}} = \sqrt{2}\, V_a\, i_{xd+} \tag{4.13}$$

$$\overline{v_{a\alpha}\, i_{x\alpha} - v_{a\beta}\, i_{x\beta}} = \sqrt{2}\, V_a\, i_{xd-} \tag{4.14}$$

$$\overline{v_{a\alpha}\, i_{x\beta} + v_{a\beta}\, i_{x\alpha}} = \sqrt{2}\, V_a\, i_{xq-} \tag{4.15}$$

$$\overline{v_g\, i^{g}_{x\alpha/\beta/0}} = V_g\, I^{g}_{x\alpha/\beta/0}; \text{ Here, } g = \text{a, b, or cm, and } x = \text{a or b.} \tag{4.16}$$

$$\overline{v_{cm}\, i^{a}_{x\alpha\beta 0}} = 0,\ \overline{v_{cm}\, i^{b}_{x\alpha\beta 0}} = 0,\ \overline{v_{cm}\, i^{a}_{xdq+}} = 0 \text{ and } \overline{v_{cm}\, i^{a}_{xdq-}} = 0 \tag{4.17}$$

The average power term ($\overline{(-0.5\, v_b\, i_{a\alpha\beta} - 2\, v_{a\alpha\beta}\, i_{b0})} \neq 0$) in (4.11) and (4.12) is nonzero for equal frequency operation ($f_b = f_a \neq 0$), which has to be compensated using corresponding manipulated inputs $MI_{5\&6}$. But for unequal frequency operation ($f_a = n\, f_b$, $f_b = n\, f_a$, ($f_b = 0$ & $f_a \neq 0$)), the average power term ($\overline{(-0.5\, v_b\, i_{a\alpha\beta} - 2\, v_{a\alpha\beta}\, i_{b0})} = 0$) equals zero; hence the

corresponding manipulated inputs $MI_{5\&6}$ only need to compensate for the losses for the unequal frequency operations. Here, n = integer.

(4.18) to (4.22) represent the simplified average arm power equations for unequal frequency operations ($f_a = n\,f_b$, $f_b = n\,f_a$, ($f_b = 0$ & $f_a \neq 0$)). Here, $f_{cm} = 3f_a$, $f_{Mean} = f_a$ if ($f_b = 0$ & $f_a \neq 0$), and $f_{Mean} = \text{Min}(f_a, f_b)$ if $f_b \neq 0$. (4.18) to (4.22) can be derived from (4.8) to (4.12) with the help of (4.23). (4.23) suggests that the single-phase voltage (v_b) and the three-phase frequency current components ($i^{a}_{x\alpha\beta0}$) do not make average power with each other. Further, the three-phase voltage ($v_{a\alpha\beta}$) and the circulating current components in phase with v_b ($i^{b}_{x\alpha\beta0}$) do not make average power. The average summation arm power in the 0-frame ($\overline{p_{\Sigma 0}}$) is unaffected and remains the same for both equal and unequal frequency operations. Note: if $f_b = 0$, $V_b = V_{dc}$, and all current components in phase with v_b represent DC quantities.

In general, the common-mode frequency ($f_{cm} = \text{Max}(f_o, 3f_a)$ if $f_b \neq 3f_a$, or $f_{cm} = f_x$ if $f_b = 3f_a$) is selected so that it does not make average power with the three-phase and single-phase frequency's current components. **Note**: v_{cm} can also be DC for AC-AC MMC application. The frequency for mean calculation is $f_{Mean} = f_a$ if $f_b = f_a \neq 0$, $f_{Mean} = f_a$ if $f_b = 0$ & $f_a \neq 0$, $f_{Mean} = \text{Min}(f_a, f_b)$ if $f_b \neq 0$, and $f_{Mean} = f_{cm}$ if $f_b = f_a = 0$. The selected f_{Mean} and f_{cm} help to reduce additional coupling in the systems.

$$\overline{P_{\Delta 0}} = -\sqrt{2}\, V_a\, i_{bd+} \tag{4.18}$$

$$\overline{P_{\Sigma\alpha}} = V_b\, I^{b}_{b\alpha} \tag{4.19}$$

$$\overline{P_{\Sigma\beta}} = V_b\, I^{b}_{b\beta} \tag{4.20}$$

$$\overline{P_{\Delta\alpha}} = -2\, V_{cm}\, I^{cm}_{b\alpha} \tag{4.21}$$

$$\overline{P_{\Delta\beta}} = -2\, V_{cm}\, I^{cm}_{b\beta} \tag{4.22}$$

$$\overline{v_b\, i^{a}_{x\alpha\beta0}} = 0, \quad \overline{v_{a\alpha\beta}\, i^{b}_{x\alpha\beta0}} = 0 \tag{4.23}$$

$$\overline{P_{(mn)}} = V_{MI(mn)}\, I_{MI(mn)} + \overline{P_{dis(mn)}} \tag{4.24}$$

All six average arm power expressions for equal and unequal frequency operations can be generalized using (4.24). Here, $m = \Sigma$ or Δ and $n = \alpha$, β or 0. $I_{MI(mn)}$ represents the RMS or DC manipulated input current, $V_{MI(mn)}$ represents the RMS or DC voltage corresponding to $I_{MI(mn)}$. If $v_{MI(mn)}$ is an AC quantity, $V_{MI(mn)}$ and $I_{MI(mn)}$ are RMS quantities. And if $v_{MI(mn)}$ is a DC quantity, $V_{MI(mn)}$ and $I_{MI(mn)}$ are DC quantities. Further, if $f_b = 0$, $V_b = V_{dc}$ and all current components in phase with v_b are DC quantities. $\overline{P_{dis(mn)}}$ represents the average disturbance power that must be compensated using the manipulated inputs ($I_{MI(mn)}$) to regulate the average arm energy.

Table 4.1: Coefficients of the general average arm power equation $\left(\overline{P_{(mn)}}\right)$ for Method-7 and Method-12.

Method	**Average Arm Power**	$I_{MI(mn)}$	$V_{MI(mn)}$	$\overline{P_{dis(mn)}}$	
				$f_a = f_b \neq 0$	$f_a \neq f_b$
7	$\overline{P_{\Sigma 0}}$	i_{ad+}	$\frac{V_a}{\sqrt{2}}$	$\overline{v_b\, i_{b0}}$	$\overline{v_b\, i_{b0}}$
	$\overline{P_{\Delta 0}}$	i_{bd+}	$-\sqrt{2}\, V_a$	$\overline{-v_{a\alpha}\, i^{b}_{b\alpha} - v_{a\beta}\, i^{b}_{b\beta}}$	0
	$\overline{P_{\Sigma \alpha}}$	$I^{b}_{b\alpha}$	V_b	$\overline{v_b\, i_{bd+} \cos(\theta_a)}$	0
	$\overline{P_{\Sigma \beta}}$	$I^{b}_{b\beta}$	V_b	$\overline{v_b\, i_{bd+} \sin(\theta_a)}$	0
	$\overline{P_{\Delta \alpha}}$	$I^{cm}_{b\alpha}$	$-2\, V_{cm}$	$\overline{-\frac{v_b\, i_{a\alpha}}{2} - 2\, v_{a\alpha}\, i_{b0} - v_{a\alpha}\, i^{b}_{b\alpha} + v_{a\beta}\, i^{b}_{b\beta}}$	0
	$\overline{P_{\Delta \beta}}$	$I^{cm}_{b\beta}$	$-2\, V_{cm}$	$\overline{-\frac{v_b\, i_{a\beta}}{2} - 2\, v_{a\beta}\, i_{b0} + v_{a\alpha}\, i^{b}_{b\beta} + v_{a\beta}\, i^{b}_{b\alpha}}$	0
12	$\overline{P_{\Sigma 0}}$	I^{b}_{b0}	V_b	$\frac{V_a\, i_{ad+}}{\sqrt{2}}$	$\frac{V_a\, i_{ad+}}{\sqrt{2}}$
	$\overline{P_{\Delta 0}}$	i_{bd+}	$-\sqrt{2}\, V_a$	$\overline{-v_{a\alpha}\, i^{b}_{b\alpha} - v_{a\beta}\, i^{b}_{b\beta}}$	0
	$\overline{P_{\Sigma \alpha}}$	$I^{b}_{b\alpha}$	V_b	$\overline{v_b\, i_{bd+} \cos(\theta_a)}$	0
	$\overline{P_{\Sigma \beta}}$	$I^{b}_{b\beta}$	V_b	$\overline{v_b\, i_{bd+} \sin(\theta_a)}$	0
	$\overline{P_{\Delta \alpha}}$	$I^{cm}_{b\alpha}$	$-2\, V_{cm}$	$\overline{-\frac{v_b\, i_{a\alpha}}{2} - 2\, v_{a\alpha}\, i_{b0} - v_{a\alpha}\, i^{b}_{b\alpha} + v_{a\beta}\, i^{b}_{b\beta}}$	0
	$\overline{P_{\Delta \beta}}$	$I^{cm}_{b\beta}$	$-2\, V_{cm}$	$\overline{-\frac{v_b\, i_{a\beta}}{2} - 2\, v_{a\beta}\, i_{b0} + v_{a\alpha}\, i^{b}_{b\beta} + v_{a\beta}\, i^{b}_{b\alpha}}$	0

Referring to the above average power expressions, the coefficients of (4.24) for Method-7 and Method-12 for equal and unequal frequency operations are documented in Table 4.1. $I_{\mathrm{MI}(mn)}$ and $V_{\mathrm{MI}(mn)}$ remain the same for equal and unequal frequency operations and only $\overline{P_{\mathrm{dis}(mn)}}$ differs for equal and unequal frequency operations. Following the same steps, the coefficients of (4.24) for all 15 energy balancing methods in Table 2.2 are documented in Appendix A.8 for equal frequency operation. The term ($\overline{P_{\mathrm{dis}(mn)}}$) for unequal frequency operation can easily be derived by further solving the equal frequency term ($\overline{P_{\mathrm{dis}(mn)}}$) from Appendix A.8 with the help of (4.23).

4.2 Design of a General Average Arm Energy Controller

Fig. 4.2 represents a general average arm energy controller derived from the general average arm power expression shown in (4.24). The average arm energy plant model is shown in the continuous-time domain in the top right. The direct discrete-time average arm energy plant model can be obtained by finding the direct discrete-time transfer function of an integral term (1/s) by following the steps mentioned in Chapter 3. The direct discrete-time transfer function of the integrator is shown in the bottom left of Fig. 4.2. *Disturbance Input Decoupling* (DID) helps decouple the system's disturbance ($\overline{P_{\mathrm{dis}(mn)}}$). A PI controller is selected so that the steady-state error ($w^{*}_{(mn)} - \overline{w_{(mn)}} = 0$) equals zero.

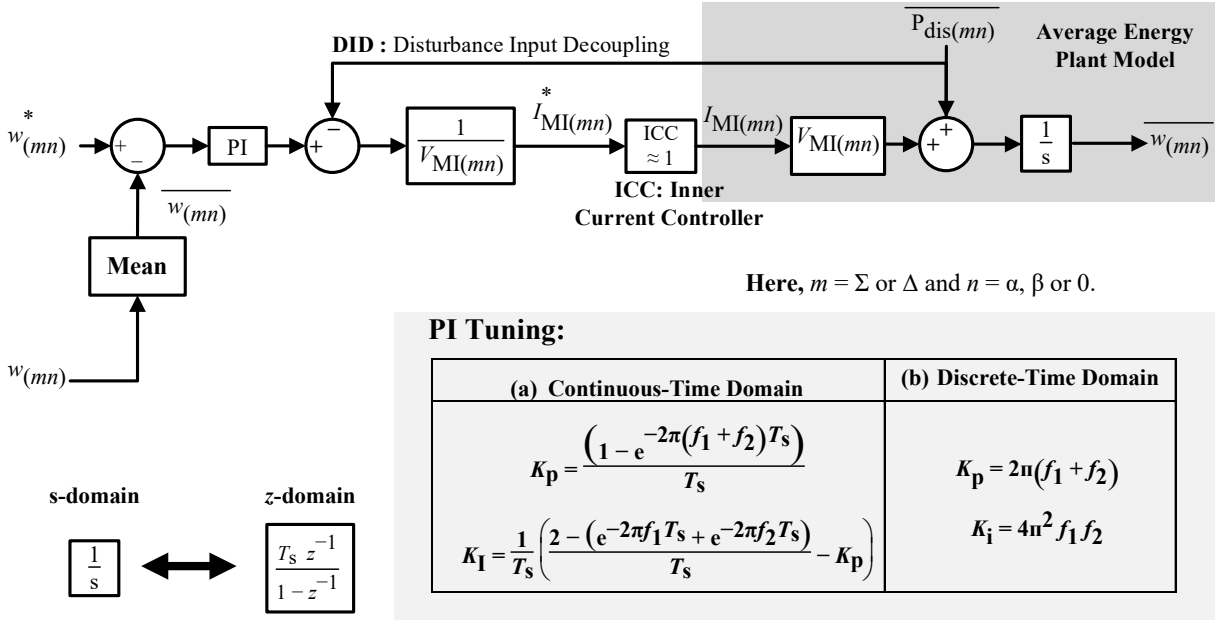

Figure 4.2: Design of a general average outer arm energy control loop for MMC.

Fig. 4.3a shows the state block diagram for computing the instantaneous arm energies in the αβ0-frame ($w_{\Sigma/\Delta 123}$) using the sampled arm voltages ($v_{p/n123}$) and currents ($i_{p/n123}$) in the abc-frame. Further, the instantaneous arm energies in the αβ0-frame ($w_{\Sigma/\Delta 123}$) can be computed using the DC-link *submodule* (SM) voltages using Fig. 4.3b. N and C_{SM} are the numbers of submodules in an arm and submodule capacitance, respectively. Fig. 4.3b is used for the actual MMC system, and Fig. 4.3a is used for the average MMC plant model to calculate the instantaneous arm energies. (4.25) illustrates that the instantaneous arm energies ($w_{p/n123}$) are obtained by integrating the instantaneous arm power ($p_{p/n123}$). The arm powers ($p_{p/n123} = v_{p/n123} \odot i_{p/n123}$) are obtained by multiplying the arm voltages ($v_{p/n123}$) and currents ($i_{p/n123}$). Here, $\odot$ represents the elementwise multiplications.

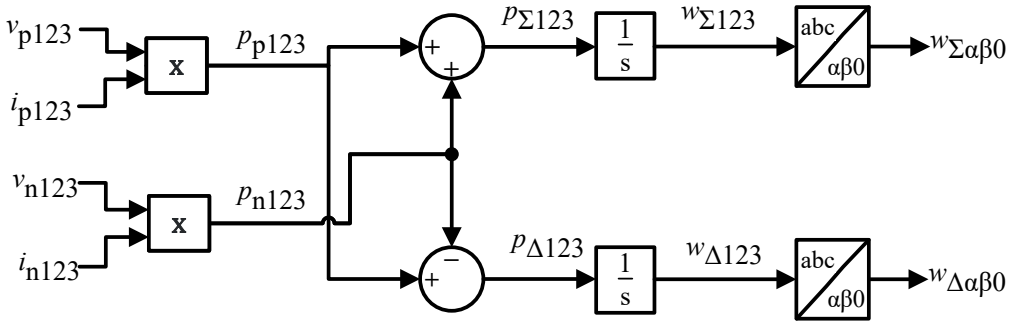

(a) Arm energies computation using the arm currents and voltages

$$w_{xy} = \frac{C_{SM}}{2} \sum_{n=1}^{N} v_{cxyn}^2$$

Here, x = p, or n

y = 1, 2, or 3

v_{cxyn} = DC-link voltage of n^{th} SM for the arm xy

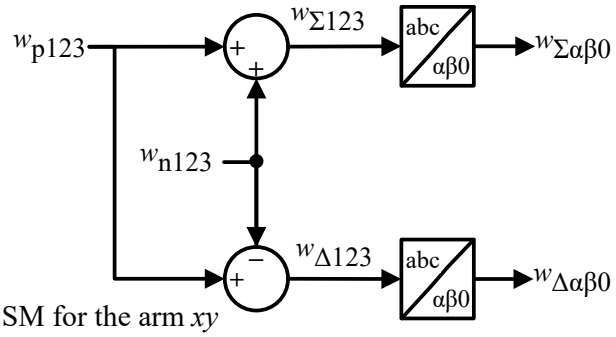

(b) Arm energies computation using the DC-link SM's capacitor voltages

Figure 4.3: Computation of the instantaneous arm energies in the αβ0-frame.

$$w_{p123} = w_{p123}(t=0) + \int_0^T p_{p123}\, dt \;\; ; \;\; w_{n123} = w_{n123}(t=0) + \int_0^T p_{n123}\, dt \qquad (4.25)$$

The arm energies in the abc-frame ($w_{p/n123}$) are transformed first into the summation ($w_{\Sigma 123}$) and difference ($w_{\Delta 123}$) systems and then into the αβ0-frame ($w_{\Sigma/\Delta\alpha\beta 0}$) using Clarke's transformation. The mean of $w_{\Sigma/\Delta 123}$ ($\overline{w_{\Sigma/\Delta 123}}$) is used as a feedback signal to the average arm energy controller

shown in Fig. 4.2. The output of the arm energy controller ($I^{*}_{\mathrm{MI}(mn)}$) acts as the reference to the *Inner Current Controller* (ICC). The closed-loop bandwidth of the inner current controller ($f_{\text{br-ICC}}$) is recommended to be set at least ten times higher than the bandwidth of the outer energy controller ($f_{\text{br-ICC}} \geq 10\, f_{\text{br-OEL}}$) so that the inner current controller's gain approximately equals unity at least until $f_{\text{br-OEL}}$. Thus, the inner current controller can be ignored for tuning the PI parameters of the outer energy control loops.

4.2.1 Tuning of the PI Controllers in the Continuous and Discrete-Time Domains

This section uses the average arm energy plant models in continuous and discrete-time domains to tune the PI controllers' gain. Referring to Fig. 4.2, Fig. 4.4 represents the simplified state block diagram of the proposed average arm energy controllers in the continuous-time and discrete-time domains after ignoring *Inner Current Controller* (ICC) and *Disturbance Input Decoupling* (DID).

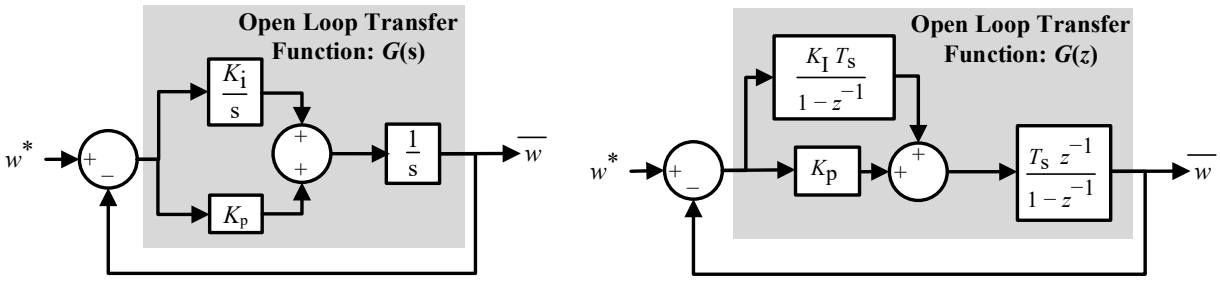

(a) PI tuning in the continuous-time domain **(b) PI tuning in the discrete-time domain**

Figure 4.4: PI tuning of the average outer arm energy controller for MMC.

4.2.1.1 PI Tuning in the Continuous-time Domain

(4.26) shows the open-loop transfer function of the average arm energy controller in the continuous-time domain (also see Fig. 4.4a). The pole-zero cancellation technique cannot be used here because the pole is located at the origin. (4.27) presents the controller's closed-loop or *Command Tracking* (CT) transfer function. The closed-loop transfer function resembles a second-order system; hence its two eigenvalues can be placed at f_1 and f_2 by comparing the denominator of (4.27) with $s^2 + 2\pi (f_1 + f_2) + 4\pi^2 f_1 f_2$). The comparison result is shown in (4.28) and (4.29). The general expression for tuning the PI controller's gain in the continuous-time domain is also shown in Fig 4.2. The closed-loop bandwidth of the controller can be placed around $f_{\text{br-OEL}}$ by substituting ($f_1 = f_{\text{br-OEL}}$ & $f_2 = f_1/10$) in (4.28) and (4.29).

$$G(\mathrm{s}) = \frac{K_\mathrm{p}\,\mathrm{s} + K_\mathrm{i}}{\mathrm{s}^2} \tag{4.26}$$

$$CT(\mathrm{s}) = \frac{G(\mathrm{s})}{1 + G(\mathrm{s})} = \frac{K_\mathrm{p}\,\mathrm{s} + K_\mathrm{i}}{\mathrm{s}^2 + K_\mathrm{p}\,\mathrm{s} + K_\mathrm{i}} \tag{4.27}$$

$$K_\mathrm{p} = 2\pi\left(f_1 + f_2\right) \tag{4.28}$$

$$K_\mathrm{i} = 4\pi^2 f_1 f_2 \tag{4.29}$$

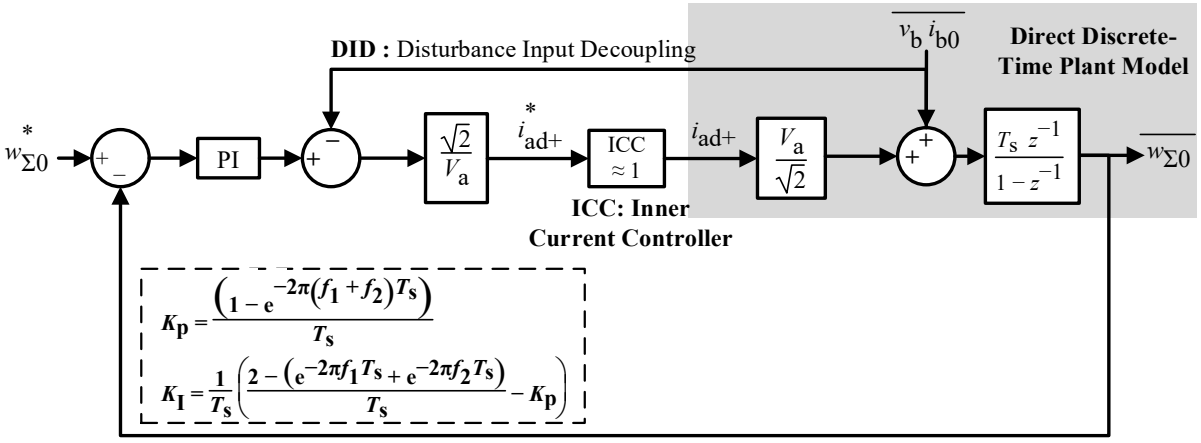

(a) Method -7

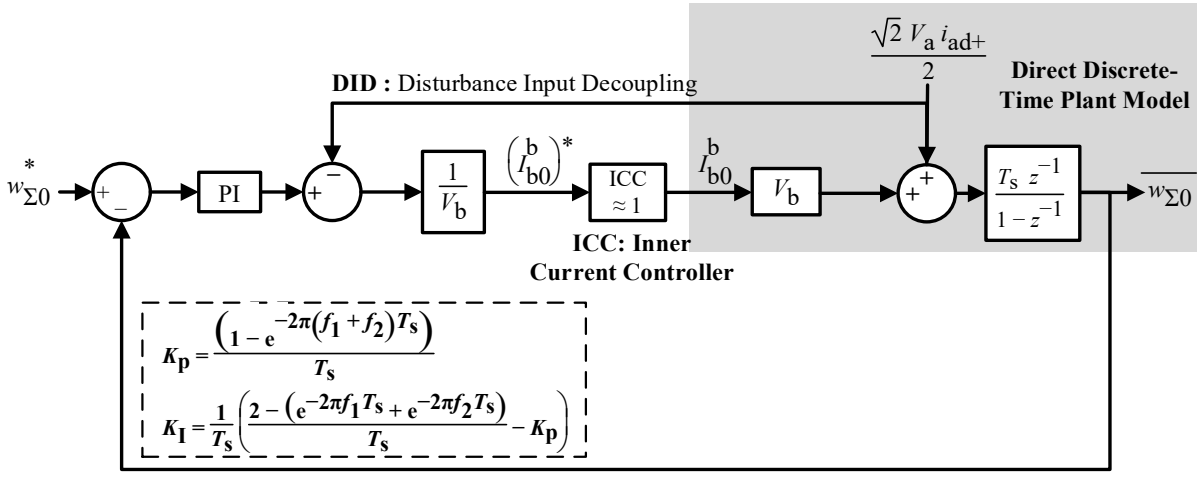

(b) Method -12

Figure 4.5: Design of the total arm energy controller of MMC in the discrete-time domain for Method-7 and Method-12.

4.2.1.2 PI Tuning in the Discrete-time Domain

Referring to Chapter 3, (4.30), and (4.31) give the general expression of a PI controller in the discrete-time domain. (4.32) shows the open-loop transfer function of the average arm energy controller in the discrete-time domain (also see Fig. 4.4b). The closed-loop transfer function is

given in (4.33). The two closed-loop eigenvalues can be placed at f_1 and f_2 by comparing the denominator of (4.33) with $z^2 - (e^{-2\pi f_1} + e^{-2\pi f_2})\, z + e^{-2\pi(f_1+f_2)}$. The comparison result is given in (4.34) and (4.35). Solving (4.31), (4.34), and (4.35) would provide (4.36) and (4.37) (the PI tuning expressions in the discrete-time). The PI tuning expressions in the discrete-time domain are also shown in Fig. 4.2.

$$\mathrm{PI}(z) = \frac{K_{\mathrm{pi}}\,(z-\delta)}{(z-1)} \tag{4.30}$$

$$K_{\mathrm{pi}} = K_{\mathrm{p}} + K_{\mathrm{I}}\,T_{\mathrm{s}} \;\; ; \;\; \delta = \frac{K_{\mathrm{p}}}{K_{\mathrm{pi}}} \tag{4.31}$$

$$\boldsymbol{G}(z) = \mathrm{PI}(z)\left(\frac{T_{\mathrm{s}}}{z-1}\right) = \frac{K_{\mathrm{pi}}\,(z-\delta)}{(z-1)}\left(\frac{T_{\mathrm{s}}}{z-1}\right) \tag{4.32}$$

$$\mathbf{CT}(z) = \frac{\boldsymbol{G}(z)}{1+\boldsymbol{G}(z)} = \frac{K_{\mathrm{pi}}\,T_{\mathrm{s}}\,(z-\delta)}{z^2 - \left(2 - K_{\mathrm{pi}}\,T_{\mathrm{s}}\right) z + 1 - K_{\mathrm{pi}}\,T_{\mathrm{s}}\,\delta} \tag{4.33}$$

$$2 - K_{\mathrm{pi}}\,T_{\mathrm{s}} = \mathrm{e}^{-2\pi f_1 T_{\mathrm{s}}} + \mathrm{e}^{-2\pi f_2 T_{\mathrm{s}}} \tag{4.34}$$

$$1 - K_{\mathrm{pi}}\,T_{\mathrm{s}}\,\delta = \mathrm{e}^{-2\pi f_1 T_{\mathrm{s}}}\,\mathrm{e}^{-2\pi f_2 T_{\mathrm{s}}} \tag{4.35}$$

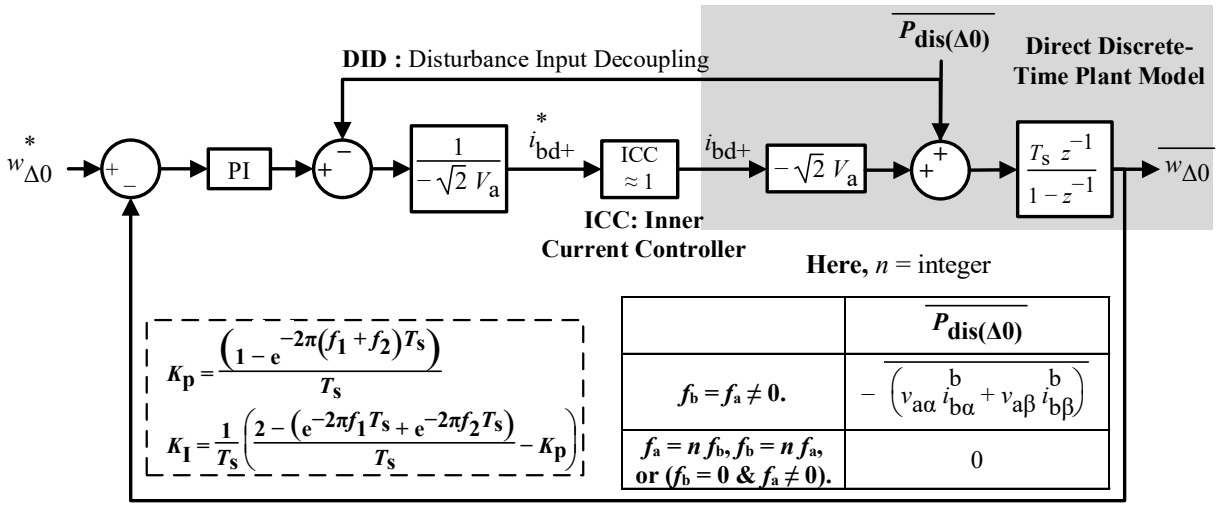

(a) Method -7 or Method-12

Figure 4.6: Design of the total upper and lower arms energies controller of MMC in the discrete-time domain for Method-7 and Method-12.

$$K_{\mathrm{p}} = \frac{\left(1-\mathrm{e}^{-2\pi(f_1+f_2)T_{\mathrm{s}}}\right)}{T_{\mathrm{s}}} \tag{4.36}$$

$$K_{\mathrm{I}} = \frac{1}{T_{\mathrm{s}}}\left(\frac{2 - \left(\mathrm{e}^{-2\pi f_1 T_{\mathrm{s}}} + \mathrm{e}^{-2\pi f_2 T_{\mathrm{s}}}\right)}{T_{\mathrm{s}}} - K_{\mathrm{p}}\right) \tag{4.37}$$

The closed-loop bandwidth of the outer energy controller is further limited by the mean computation frequency (f_{Mean}). For safe operation, it is advisable to place the bandwidth ($f_{\mathrm{br\text{-}OEL}} \leq f_{\mathrm{Mean}}/5$) of the average energy control below 1/5$^{\mathrm{th}}$ of f_{Mean}. The mean computation introduces a significant amount of delay ($T_{\mathrm{delay}} = 1/(2\,f_{\mathrm{Mean}})$) in the system, which obstacles tuning the closed-loop bandwidth of the arm energy controllers accurately using the derived PI's gain expressions.

Estimating the future average arm energies using the observers to compensate for this huge delay is also not a practical solution. The average arm energy plant model is obtained by ignoring the arm and transformer impedances; hence it cannot exactly represent the actual system. Assuming the plant model can accurately describe the existing system, K^{th} ($K = T_{\mathrm{delay}}/T_{\mathrm{s}}$) future value should be estimated at present (k^{th} sample) to compensate for the delay ($T_{\mathrm{delay}} = 1/(2\,f_{\mathrm{Mean}})$). Here, T_{s} is the controller sample time. Assuming $f_{\mathrm{Mean}} = f_{\mathrm{a}}$, and $T_{\mathrm{s}} = 0.2$ ms gives $K = 50$. It suggests that 50 observers should be connected in a cascade to compensate for the delay (T_{delay}), which would require a massive amount computational cycle hence using the observer is also not advisable.

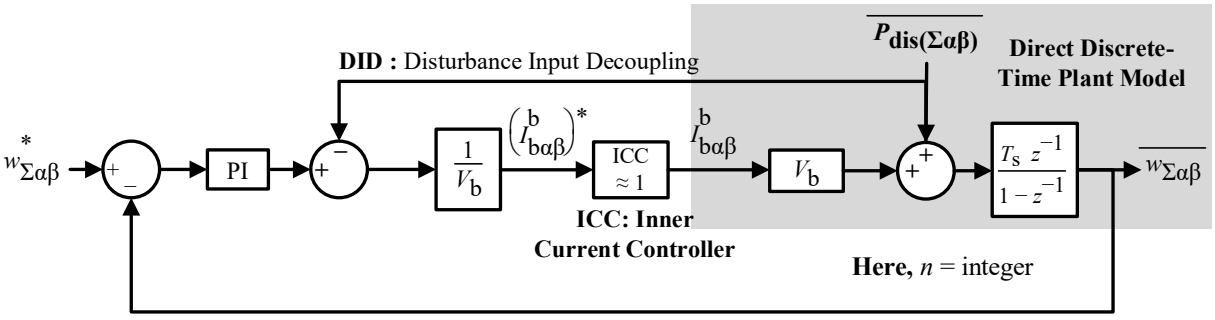

$$K_{\mathrm{p}} = \frac{\left(1 - \mathrm{e}^{-2\pi(f_1 + f_2)T_{\mathrm{s}}}\right)}{T_{\mathrm{s}}}$$

$$K_{\mathrm{I}} = \frac{1}{T_{\mathrm{s}}}\left(\frac{2 - \left(\mathrm{e}^{-2\pi f_1 T_{\mathrm{s}}} + \mathrm{e}^{-2\pi f_2 T_{\mathrm{s}}}\right)}{T_{\mathrm{s}}} - K_{\mathrm{p}}\right)$$

	$\overline{P_{\mathrm{dis}(\Sigma\alpha)}}$	$\overline{P_{\mathrm{dis}(\Sigma\beta)}}$
$f_{\mathrm{b}} = f_{\mathrm{a}} \neq 0$	$\overline{v_{\mathrm{b}}\, i_{\mathrm{bd+}} \cos(\theta_{\mathrm{a}})}$	$\overline{v_{\mathrm{b}}\, i_{\mathrm{bd+}} \sin(\theta_{\mathrm{a}})}$
$f_{\mathrm{a}} = n\, f_{\mathrm{b}}, f_{\mathrm{b}} = n\, f_{\mathrm{a}}$, or ($f_{\mathrm{b}} = 0$ & $f_{\mathrm{a}} \neq 0$).	0	0

(a) Method -7 or Method-12

Figure 4.7: Design of the summation phase energy controllers of MMC in the discrete-time domain for Method-7 and Method-12.

Therefore, the dynamic behavior of the arm energy controller could not be guaranteed using the above tuning expressions. The error in tuning the closed-loop bandwidth of the average arm

energy controller will be seen in the command tracking plots shown in Section 4.4. But it should be remembered that the steady-state error can be guaranteed to reach zero using a PI controller.

4.3 Design of the Six Average Arm Energy Controllers for MMC

Referring to (4.24), Fig 4.2 and Table 4.1, Fig 4.5 to Fig 4.8 represent the six average arm energies controllers of MMC using Method-7 and Method-12 for equal ($f_b = f_a$) and unequal ($f_a = n f_b, f_b = n f_a$, ($f_b = 0$ & $f_a \neq 0$)) frequency operations. Here, n = integer. Fig. 4.5 regulates the total arm energy, Fig. 4.6 balances the total upper and lower arms energies, Fig. 4.7 controls the summation phase energies, and Fig. 4.8 regulates the difference phase energies. In Chapter 3, it is mentioned that the average sampled voltage is used in the current controllers and PLL; hence the controller only knows the three-phase ($\theta_a[k - 0.5]$), single-phase ($\theta_b[k - 0.5]$) and common-mode ($\theta_{cm}[k - 0.5]$) voltage angles at present (k^{th}) sample. The half sampling delay ($0.5T_s$) is because of finding the average voltage over a controller sample time (T_s). Further, the reference ($I^*[k + 1]$) of the current controller should be the future value at present (k^{th} sample) to compensate for the unit delay in the system (also see Fig 3.20). Thus, the computed angle ($\theta_x[k - 0.5]$) from PLL should be rotated by $1.5\omega_x T_s$ to compensate for delays in the system. (4.38) to (4.40) illustrate the rotation of three-phase, single-phase, and common-mode voltage angles, respectively, to compensate for the delays in the system.

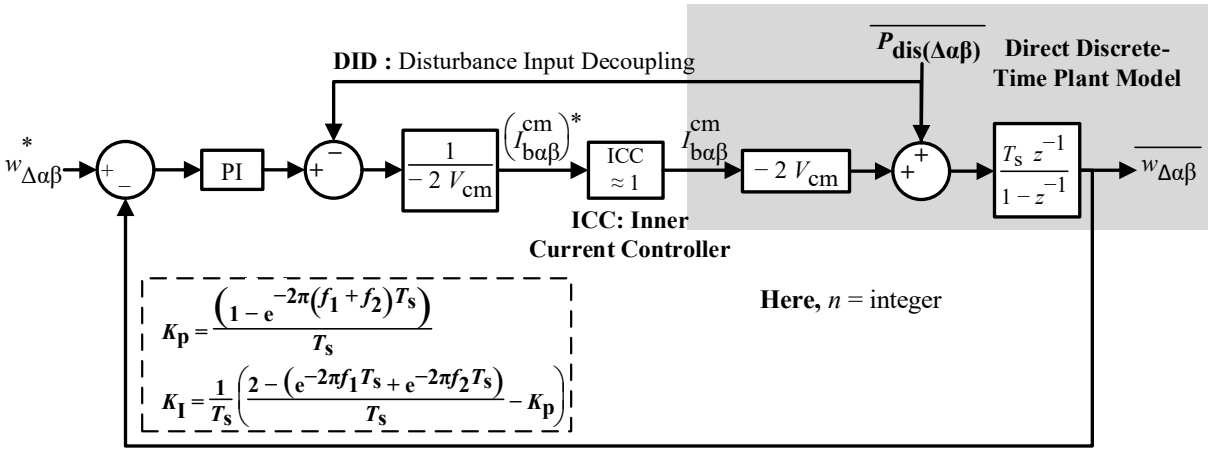

	$\overline{P_{dis(\Delta\alpha)}}$	$\overline{P_{dis(\Delta\beta)}}$
$f_b = f_a \neq 0$	$-\frac{v_b i_{a\alpha}}{2} - 2 v_{a\alpha} i_{b0} - v_{a\alpha} i^b_{b\alpha} + v_{a\beta} i^b_{b\beta}$	$-\frac{v_b i_{a\beta}}{2} - 2 v_{a\beta} i_{b0} + v_{a\alpha} i^b_{b\beta} + v_{a\beta} i^b_{b\alpha}$
$f_a = n f_b, f_b = n f_a$, or ($f_b = 0$ & $f_a \neq 0$).	0	0

(a) Method -7 or Method-12

Figure 4.8: Design of the difference phase energy controllers of MMC in the discrete-time domain for Method-7 and Method-12.

$$\theta_{\mathrm{a}}[k+1] = \theta_{\mathrm{a}}[k-0.5] + 1.5\ \omega_{\mathrm{a}}\ T_{\mathrm{s}} \tag{4.38}$$

$$\theta_{\mathrm{b}}[k+1] = \theta_{\mathrm{b}}[k-0.5] + 1.5\ \omega_{\mathrm{b}}\ T_{\mathrm{s}} \tag{4.39}$$

$$\theta_{\mathrm{cm}}[k+1] = \theta_{\mathrm{cm}}[k-0.5] + 1.5\ \omega_{\mathrm{cm}}\ T_{\mathrm{s}} \tag{4.40}$$

Referring from Fig. 4.5 to Fig. 4.8, (4.41) to (4.44) shows the reference future three-phase ($i^{*}_{\mathrm{a}\alpha\beta}[k+1]$) and circulating ($i^{*}_{\mathrm{b}\alpha\beta}[k+1]$) current commands in the αβ-frame for the average arm energy balancing Method-7. The three-phase and circulating reference signals in the dq-frame can be obtained by performing Park's transformation of $i^{*}_{\mathrm{a}\alpha\beta}[k+1]$ and $i^{*}_{\mathrm{b}\alpha\beta}[k+1]$ using the park transformation angle $\theta_{\mathrm{a}}[k+1]$. The load connected to MMC decides single-phase current ($i_{\mathrm{b}} = -3\ i_{\mathrm{b0}}$). The three-phase reactive current component ($i^{*}_{\mathrm{aq+}}$) can either be set to zero or computed with the help of (4.46) for equal frequency operation of MMC.

If $i^{*}_{\mathrm{aq+}} = 0$, no reactive power flows in the source (three-phase). The arm currents will increase significantly if the load (single-phase) reactive power increases because the manipulated input ($i^{\mathrm{cm}*}_{\mathrm{b}\alpha\beta}$) alone has to compensate for additional average power, caused due to the load reactive power current component (also see Table 2.6). This extra average power due to the reactive load power can be compensated by injecting reactive power into the source, reducing the stress on $i^{\mathrm{cm}*}_{\mathrm{b}\alpha\beta}$. Reducing $i^{\mathrm{cm}*}_{\mathrm{b}\alpha\beta}$ helps to reduce unsymmetrical components in the arm current, and increasing $i^{*}_{\mathrm{aq+}}$ introduces symmetrical components; thus, the overall arm current magnitude is reduced by compensating the extra average power terms due to the load reactive power current component with the source reactive power current component.

$$i^{*}_{\mathrm{a}\alpha}[k+1] = i^{*}_{\mathrm{ad+}}\cos\big(\theta_{\mathrm{a}}[k+1]\big) - i^{*}_{\mathrm{aq+}}\sin\big(\theta_{\mathrm{a}}[k+1]\big) \tag{4.41}$$

$$i^{*}_{\mathrm{a}\beta}[k+1] = i^{*}_{\mathrm{aq+}}\cos\big(\theta_{\mathrm{a}}[k+1]\big) + i^{*}_{\mathrm{ad+}}\sin\big(\theta_{\mathrm{a}}[k+1]\big) \tag{4.42}$$

$$i^{*}_{\mathrm{b}\alpha}[k+1] = i^{*}_{\mathrm{bd+}}\cos\big(\theta_{\mathrm{a}}[k+1]\big) + \sqrt{2}\left(I^{\mathrm{cm}}_{\mathrm{b}\alpha}\right)^{*}\cos\big(\theta_{\mathrm{cm}}[k+1]\big) + \sqrt{2}\left(I^{\mathrm{b}}_{\mathrm{b}\alpha}\right)^{*}\cos\big(\theta_{\mathrm{b}}[k+1]\big) \tag{4.43}$$

$$i^{*}_{\mathrm{b}\beta}[k+1] = i^{*}_{\mathrm{bd+}}\sin\big(\theta_{\mathrm{a}}[k+1]\big) + \sqrt{2}\left(I^{\mathrm{cm}}_{\mathrm{b}\beta}\right)^{*}\cos\big(\theta_{\mathrm{cm}}[k+1]\big) + \sqrt{2}\left(I^{\mathrm{b}}_{\mathrm{b}\beta}\right)^{*}\cos\big(\theta_{\mathrm{b}}[k+1]\big) \tag{4.44}$$

$$i^{*}_{\mathrm{b0}}[k+1] = \sqrt{2}\left(I^{\perp\mathrm{b}}_{\mathrm{b0}}\right)^{*}\sin\big(\theta_{\mathrm{b}}[k+1]\big) + \sqrt{2}\left(I^{\mathrm{b}}_{\mathrm{b0}}\right)^{*}\cos\big(\theta_{\mathrm{b}}[k+1]\big) \tag{4.45}$$

$$i^{*}_{\mathrm{aq+}} = -\frac{4\sqrt{2}\ V_{\mathrm{a}}\ I^{\perp\mathrm{b}}_{\mathrm{b0}}}{V_{\mathrm{b}}} = \frac{4\sqrt{2}\ V_{\mathrm{a}}\ I^{\perp\mathrm{b}}_{\mathrm{b}}}{3\ V_{\mathrm{b}}} \text{ if } MI_1 = i_{\mathrm{ad+}} \text{ (Method-7)} \tag{4.46}$$

$$\left(I_{\mathrm{b0}}^{\perp \mathrm{b}}\right)^{*} = -\frac{V_{\mathrm{b}}\, i_{\mathrm{aq+}}}{4\sqrt{2}\, V_{\mathrm{a}}} \text{ if } MI_1 = I_{\mathrm{b0}}^{\mathrm{b}} \text{ (Method-12)} \tag{4.47}$$

$$v_{\mathrm{b}} = V_{\mathrm{b}} = V_{\mathrm{dc}} \text{ if } f_{\mathrm{b}} = 0 \tag{4.48}$$

$$i_{\mathrm{b}\alpha}^{*}[k+1] = i_{\mathrm{bd+}}^{*} \cos\left(\theta_{\mathrm{a}}[k+1]\right) + \sqrt{2}\left(I_{\mathrm{b}\alpha}^{\mathrm{cm}}\right)^{*} \cos\left(\theta_{\mathrm{cm}}[k+1]\right) + \left(I_{\mathrm{b}\alpha}^{\mathrm{b}}\right)^{*} \text{ if } f_{\mathrm{b}} = 0 \tag{4.49}$$

$$i_{\mathrm{b}\beta}^{*}[k+1] = i_{\mathrm{bd+}}^{*} \sin\left(\theta_{\mathrm{a}}[k+1]\right) + \sqrt{2}\left(I_{\mathrm{b}\beta}^{\mathrm{cm}}\right)^{*} \cos\left(\theta_{\mathrm{cm}}[k+1]\right) + \left(I_{\mathrm{b}\beta}^{\mathrm{b}}\right)^{*} \text{ if } f_{\mathrm{b}} = 0 \tag{4.50}$$

$$i_{\mathrm{b0}}^{*} = \left(I_{\mathrm{b0}}^{\mathrm{b}}\right)^{*} \text{ if } f_{\mathrm{b}} = 0 \tag{4.51}$$

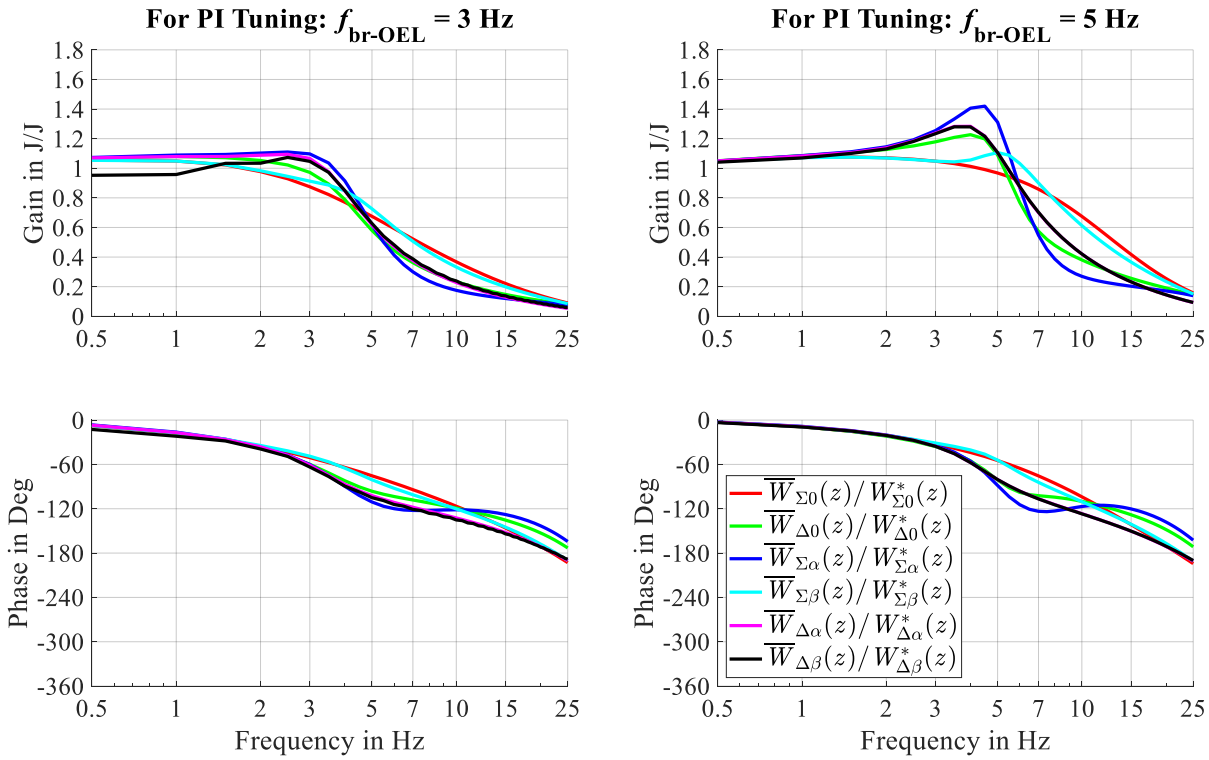

Figure 4.9: Closed-loop bode or *Command Tracking* (CT) plot of the proposed average arm energy controllers using Method-7 for equal frequency operation ($f_{\mathrm{b}} = f_{\mathrm{a}} = 50$ Hz). Here, $f_{\mathrm{Mean}} = f_{\mathrm{a}}, f_{\mathrm{cm}} = 3\, f_{\mathrm{a}}$.

Similarly, (4.43) to (4.45) represent the reference current signals for the arm energy balancing Method-12. The three-phase currents ($i_{\mathrm{a}\alpha\beta}$) depend on the load connected to MMC. Again, the source reactive power component ($I_{\mathrm{b0}}^{\mathrm{b}*}$) can also be set to zero or realized using (4.47) to compensate for the average power term caused due to the load reactive power component ($i_{\mathrm{aq+}}^{*}$) for equal frequency operation of MMC.

Further, (4.48) to (4.51) illustrates the modified expressions of single-phase voltage (v_b) and reference currents ($I^{b*}_{b\alpha\beta0}$) in phase with v_b for Method-7 and Method-12 for DC-AC application of MMC.

4.4 Command Tracking

Here, the accuracy of tuning the proposed average arm energies controllers is investigated using their corresponding closed-loop bode or *Command Tracking* (CT) plot. The bode plots are obtained by simulating the actual MMC topology, the proposed average arm energies, and the current controllers in Matlab/Simulink. The parameters used for the simulation are listed in Table 5.1. The bandwidth of the inner current controller ($f_{br\text{-}ICC}$) is placed at 200 Hz. The controller's sampling frequency (f_s) is 5 kHz.

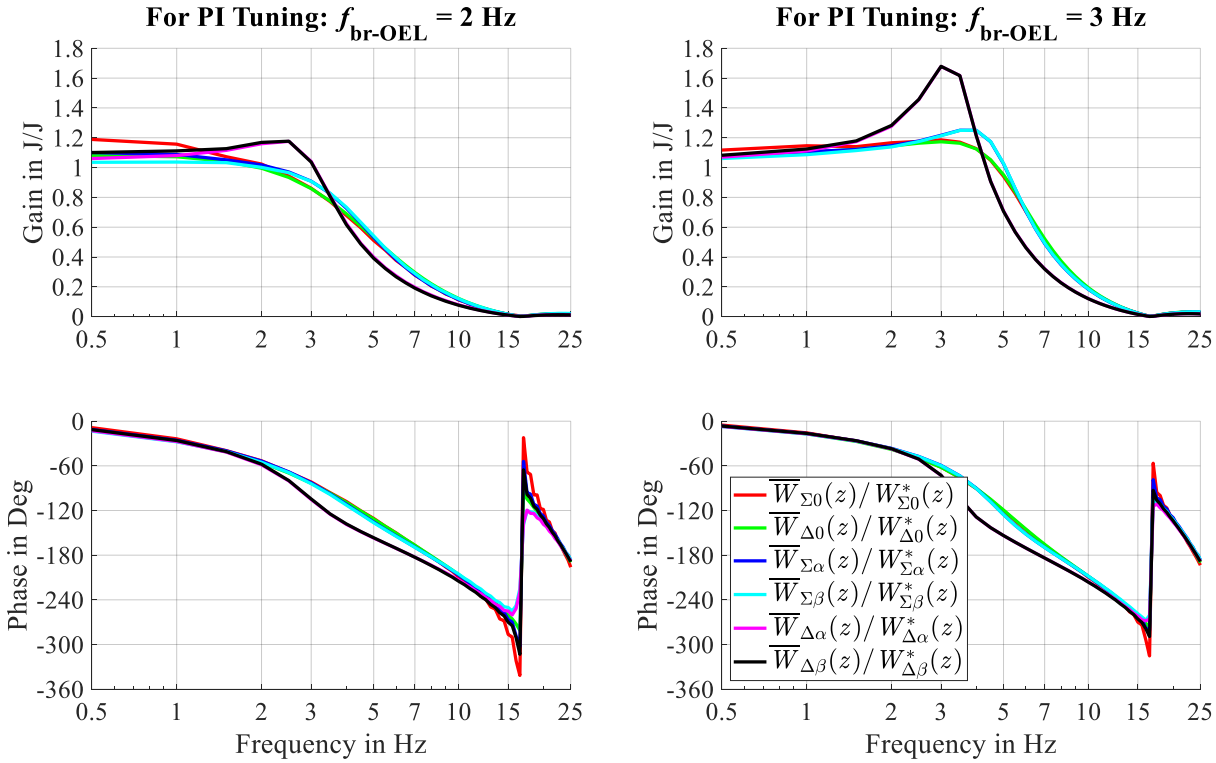

Figure 4.10: Closed-loop bode or *Command Tracking* (CT) plot of the proposed average arm energy controllers using Method-7 for unequal frequency operation ($f_b = f_a/3 = 50/3$ Hz). Here, $f_{Mean} = f_b$, $f_{cm} = 3f_a$.

Fig. 4.9 shows the proposed six-arm energy controller's closed-loop bode plot for the average arm energy controllers using Method-7 for equal frequency operation ($f_b = f_a = 50$ Hz). Here, $f_{Mean} = f_a$ and $f_{cm} = 3f_a$. The right side of Fig. 4.9 shows the bode plots when the closed-loop eigenvalues ($f_1 = f_{br\text{-}OEL}$ & $f_2 = f_1/10$) are selected so that the desired bandwidth ($f_{br\text{-}OEL}$ = 5 Hz) would be around 5 Hz. And the left side of Fig. 4.9 shows the bode plots when $f_{br\text{-}OEL}$ = 3 Hz.

For both cases, the controllers' desired and actual bandwidth are different. As mentioned in Section 4.2.1, an additional delay ($T_{delay} = 1/(2f_{Mean})$) is introduced in the feedback signals due to the mean computation block. Further, compensating for this delay is complicated and not economical; hence, an actual and desired bandwidth error is expected. The bode-plot of each average arm energy controller also differs because of different couplings into the different arm power equations. It should also be remembered that the average arm power equations only help estimate values in the steady state and lack in providing the system's exact dynamic behavior.

Assuming the desired controller's bandwidth is around 5 Hz, the simple and economical solution is to tune the PI controller's gain using derived equations but with a less bandwidth value, say $f_{br\text{-}OEL} = 3$ Hz. The left side of Fig. 4.9 shows the command tracking plot when $f_{br\text{-}OEL} = 3$ Hz is used for PI tuning. The actual controller's bandwidth lies around 5 Hz, and the high gains are reduced to lower values. Simply put, the derived PI tuning expressions can still help place the average energy controller's closed-loop bandwidth to a desired value by adjusting $f_{br\text{-}OEL}$ using hit & trial.

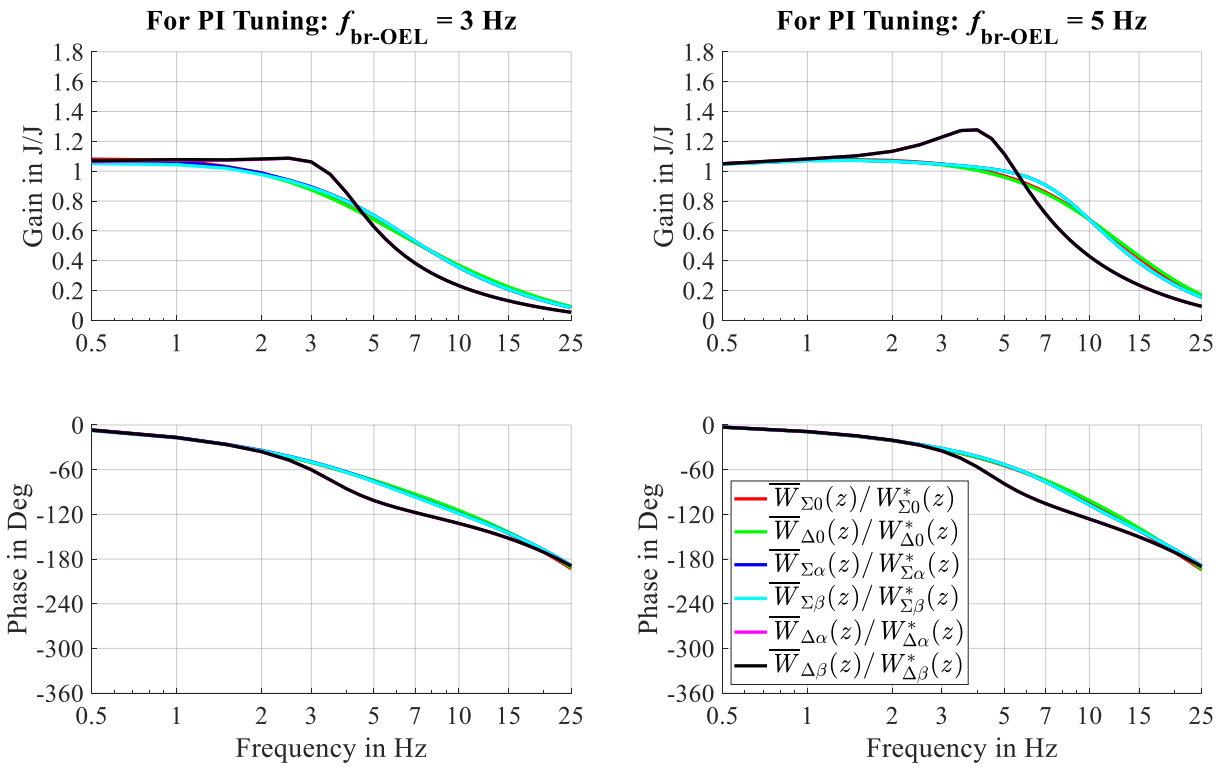

Figure 4.11: Closed-loop bode or *Command Tracking* (CT) plot of the proposed average arm energy controllers using Method-7 for unequal frequency operation ($f_b = 0, f_a = 50$ Hz). Here, $f_{Mean} = f_a, f_{cm} = 3f_a$.

Fig. 4.10 shows the closed-loop bode plot of the proposed average arm energies controllers using Method-7 for 1/3rd single-phase frequency operation ($f_b = f_a/3 = 50/3$ Hz). Here, $f_{Mean} = f_b$, $f_{cm} = 3 f_a$. Fig. 4.10 also suggests that the desired closed-loop bandwidth of the average arm energy controllers can be placed around 3.5 Hz by tuning the PI gains using $f_{br\text{-}OEL} = 2$ Hz. Similarly, Fig. 4.11 represents the command tracking plot of the proposed average arm energy controllers using Method-7 for the DC-AC application ($f_b = 0$) of MMC. Here, $f_{Mean} = f_a$, $f_{cm} = 3 f_a$. Once again, it suggests that the closed-loop bandwidth of the proposed average arm energies controllers can be placed around 5 Hz by tuning the PI gains with $f_{br\text{-}OEL} = 3$ Hz (the same way it was done for equal frequency operation because the mean frequency is identical for both conditions).

5 Simulation and Analytical Results

This work mainly focuses on identifying, designing, and validating all stable possible arm energy balancing methods for various three-phase and single-phase frequency operations of MMC. This chapter presents, analyzes, validates, and compares the performance of MMC using simulation and analytical results for different arm energy balancing methods in normal operations. The simulation results are obtained using MATLAB/SIMULINK.

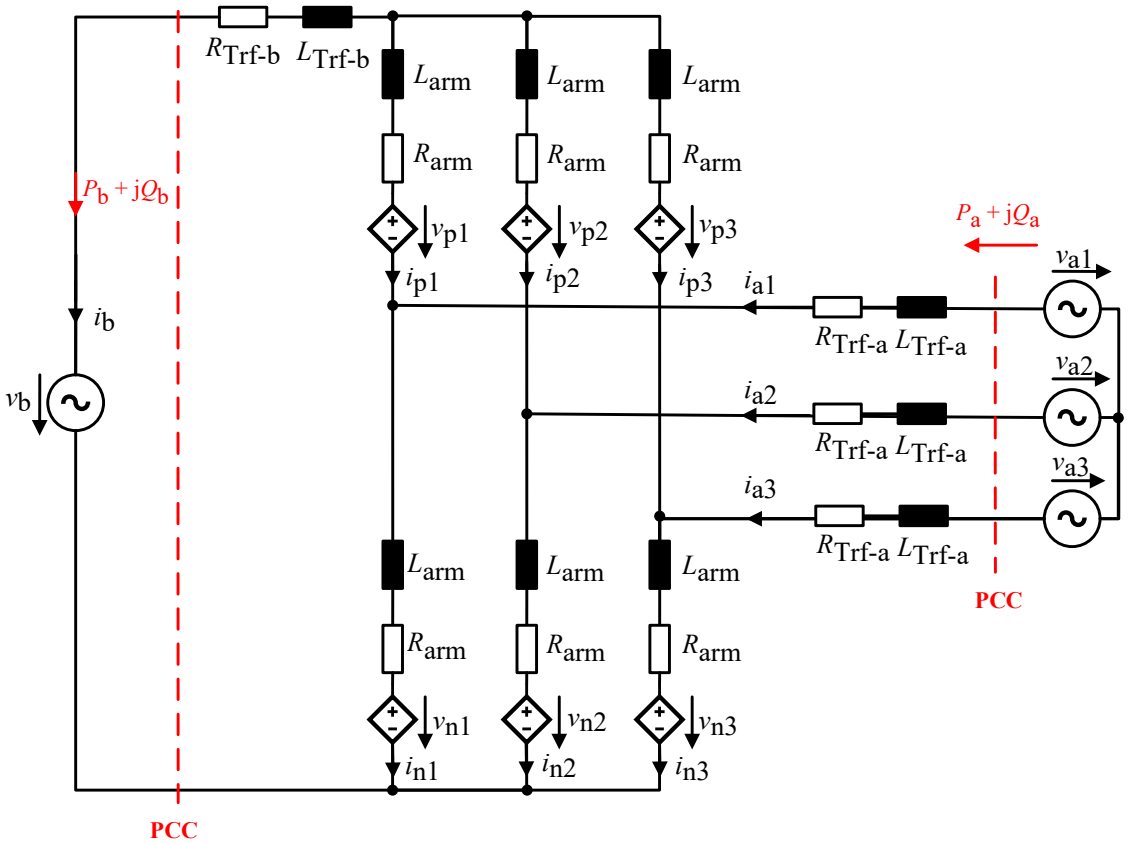

Figure 5.1: Average circuit diagram of MMC used in simulation to validate the proposed controls.

5.1 System Definitions

Fig. 5.1 represents the average circuit diagram of MMC used in the simulation to analyze the performance of the proposed arm energy controllers for various load and system frequency

conditions. The three-phase neutral point is considered floating. The three-phase ($S_a = P_a + j\,Q_a$) and single-phase ($S_b = P_b + j\,Q_b$) powers are defined at the *Point of Common Coupling* (PCC).

Table 5.1: List of parameters for simulations.

S.N.	Variables	Value	S.N.	Variables	Value
1	f_a	50 Hz	17	N	21
2	f_b	f_a, $f_a/3$, or 0	18	C_{SM}	7.5 mF
3	f_{cm}	$3f_a$	19	V^*_{SM}	2 kV
4	$V^{nom}_{a\text{-}LL}$	20 kV	20	W^*_{arm}	315 kJ
5	V_{cm}	$\frac{0.45}{\sqrt{3}}V^{nom}_{a\text{-}LL}$	21	f_{sw}	2.5 kHz
6	V^{nom}_b for $f_b \neq 0$	25 kV	22	f_s	$2f_{sw}$
7	$V^{nom}_b = V_{dc}$ if $f_b = 0$	$25\sqrt{2}$ kV	23	$f_{br\text{-}ICC}$	200 Hz
8	S^{nom}_{load}	40 MVA	24	$K_{ir\text{-}b0}$	25
9	R_{arm}	10 mΩ	25	$K_{ir\text{-}b\text{-}dq}$ & $K_{ir\text{-}a}$	10
10	L_{arm}	3.2 mH	26	ω_c	2π rad/s
11	$R_{Trf\text{-}a}$	100 mΩ	27	$f_{br\text{-}OEL}$ for $f_b = f_a$	3 Hz
12	$L_{Trf\text{-}a}$	3.8 mH	28	$f_{br\text{-}OEL}$ for $f_b = f_a/3$	2 Hz
13	$R_{Trf\text{-}b}$(for $f_b \neq 0$)	123.4 mΩ	29	$f_{br\text{-}OEL}$ for $f_b = 0$	3 Hz
14	$L_{Trf\text{-}b}$(for $f_b \neq 0$)	8.9 mH	30	f_{Mean} for $f_b = f_a$	f_a
15	$R_{Trf\text{-}b}$(for $f_b = 0$)	0 mΩ	31	f_{Mean} for $f_b = f_a/3$	f_b
16	$L_{Trf\text{-}b}$(for $f_b = 0$)	0 mH	32	f_{Mean} for $f_b = 0$	f_a

The MMC's topology parameters and the controller's design parameters to validate the proposed average arm energy control methods are listed in Table 5.1. Here, the three-phase

frequency (f_a) is fixed to 50 Hz , and a different single-phase frequency (f_b) is considered to realize DC-AC MMC ($f_b = 0$), AC-AC MMC with equal frequency ($f_b = f_a$), or AC-AC MMC with unequal (1/3rd) frequency ($f_b = f_a/3$) operation. The common-mode voltage frequency (f_{cm}) equals $3f_a$. The RMS of the common-mode voltage is considered 45% of the three-phase line to neutral voltage ($V_{cm} = 0.45\ V_{a\text{-}LL}^{nom}/\sqrt{3}$). The controller's sampling frequency is 5 kHz. If $f_b \neq 0$, the single-phase voltage is defined as $v_b = \sqrt{2}\ V_b^{nom} \cos(\theta_b)$ and if $f_b = 0$, $v_b = V_b^{nom}$. The value of V_b^{nom} are different for $f_b \neq 0$ and $f_b = 0$ (also see Table 5.1). Further, if $f_b = 0$, all manipulated inputs in phase with v_b are DC signals.

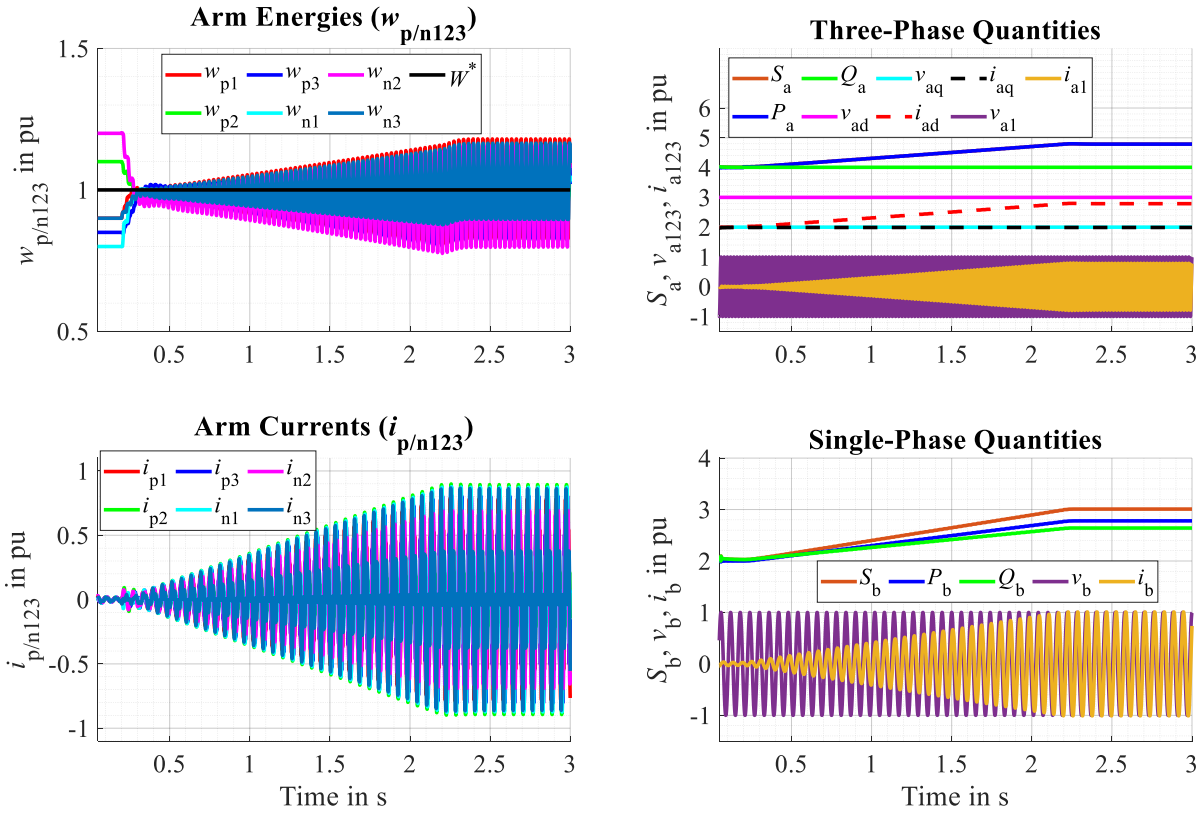

Figure 5.2: Simulation results of AC-AC MMC with unequal (1/3rd) frequency ($f_b = f_a/3$) operation when the arm energy balancing Method-1 is used to regulate the average arm energies of MMC. Load condition: $S_b = 1$ pu, $PF_b = 0.8$.

The closed-loop bandwidths of the *Inner Current Controllers* (ICC) are tuned around 200 Hz. The closed-loop bandwidths of the *Outer Energy Controllers* (OEL) are placed around 5 Hz by tuning the controllers by substituting $f_{br\text{-}OEL} = 3$ Hz in the derived PI tuning equations for DC-AC MMC ($f_b = 0$) and AC-AC MMC with equal frequency ($f_b = f_a$) operations (also see Section 4.4). Similarly, the bandwidths of the outer energy controllers are placed around 3.5 Hz by tuning the controllers with $f_{br\text{-}OEL} = 2$ Hz for AC-AC MMC with unequal frequency ($f_b = f_a/3$)

operation. The mean calculation frequency (f_{Mean}) for DC-AC MMC and AC-AC MMC with equal frequency ($f_b = f_a$) operations is f_a. And $f_{Mean} = f_b$ for $f_b = f_a/3$ operation.

The simulation and analytical results for only the first fifteen arm energy balancing methods (listed in Table 2.2) are presented to validate the performance and stability of the controllers. The remaining arm energy balancing methods (given in Table 2.3) can also be easily realized by following the steps in Chapter 4.

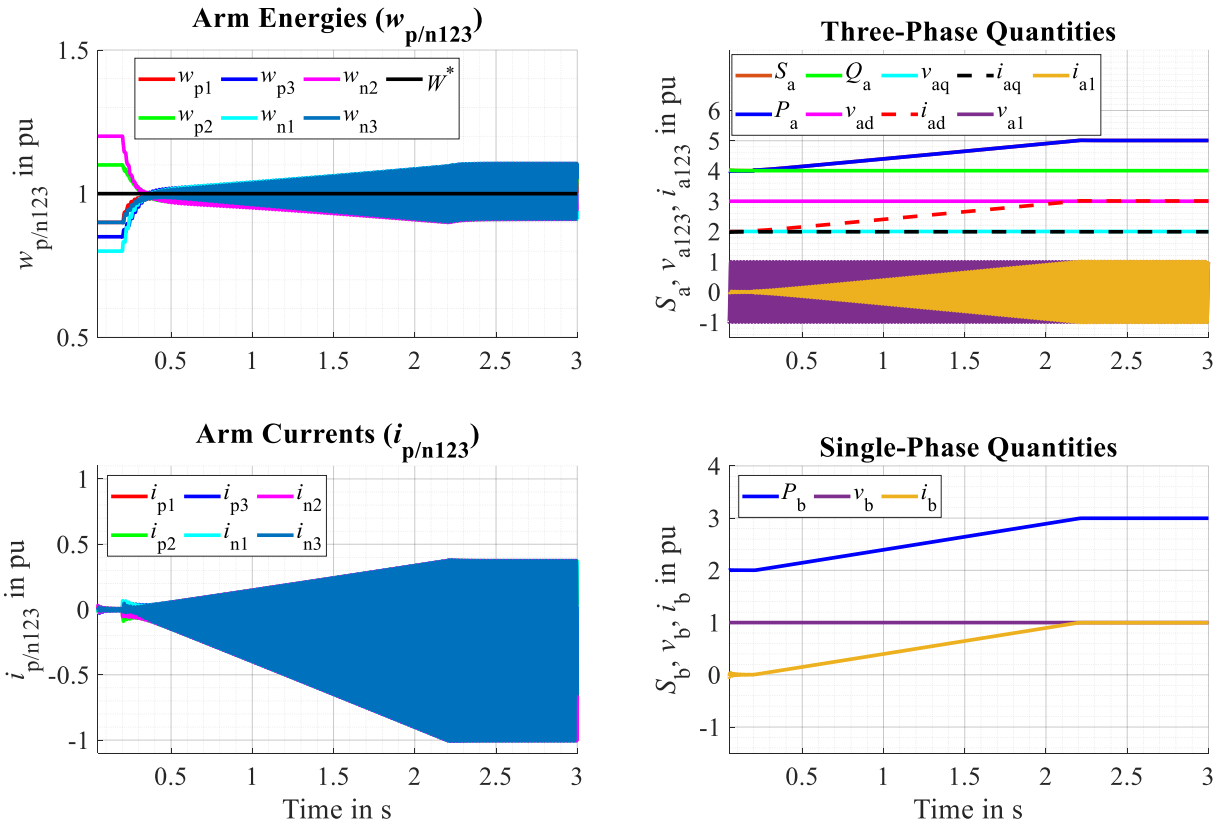

Figure 5.3: Simulation results of DC-AC MMC topology when the arm energy balancing Method-1 is used to regulate the average arm energies of MMC. Load condition: S_b = 1 pu.

5.2 The Arm Energy Balancing using Kolb's Method

As discussed in Chapter 2, only four energy balancing methods (Method-1, 5, 7, and 12) are possible to regulate the six arm energies of MMC, which do not inject harmonics to both source and load currents. Referring to Section 2.6, Method-5 is used by Mr. Kolb to regulate the arm energies of DC-AC MMC for variable speed drive application in the high speed or frequency (hf) mode. Here, the total arm energy of MMC is regulated using the single-phase active power, or the single-phase acts like a source. The arm energy balancing Method-1 can also be linked to Kolb's method. The only difference between Method-1 and Method-5 is that the three-phase system is the source for Method-1 and the single-phase is the source for Method-5 (see

Table 2.2). Method-1 and Method-5 use the same remaining five manipulated inputs or degrees of freedom. Table 2.2 suggests that these two methods are only stable for unequal frequency operations and are unstable for equal frequency operations.

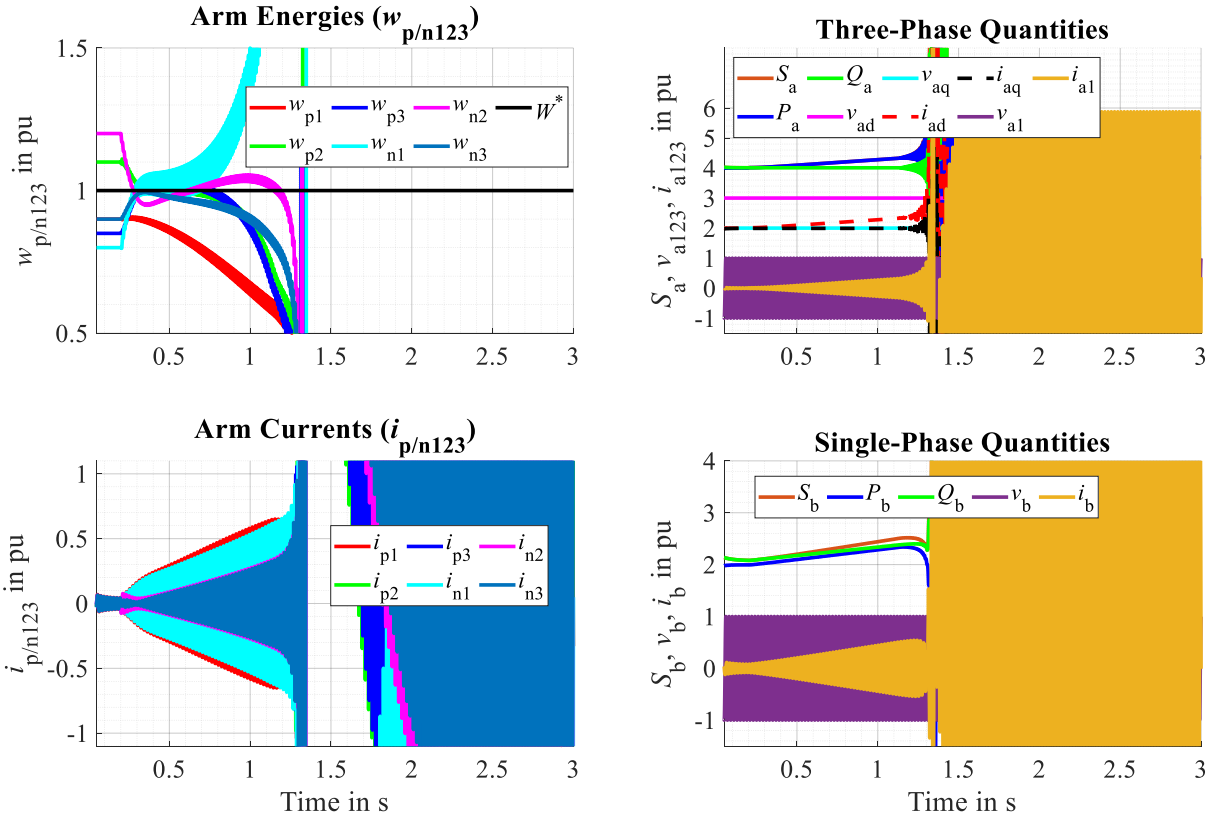

Figure 5.4: Simulation results of AC-AC MMC with equal frequency ($f_b = f_a$) operation when the arm energy balancing Method-1 is used to regulate the average arm energies of MMC. Load condition: S_b = 1 pu, PF_b = 0.8.

Fig. 5.2, Fig. 5.3, and Fig. 5.4 represent the simulation results of MMC for AC-AC with unequal frequency ($f_b = f_a/3$), DC-AC and AC-AC equal frequency ($f_b = f_a$) operations, respectively, for the arm energy balancing Method-1. All physical quantities are presented in the *per unit* (pu) system. The nominal RMS voltages ($V_{a\text{-}LL}^{nom}$, and (V_b^{nom} or V_{dc}^{nom})) are the base voltages, and the nominal load power (S_{load}^{nom}) is the base power. (5.1) to (5.3) are used to compute the base three-phase (I_a^{base}), single-phase (I_b^{base}), and arm (I_{arm}^{base}) currents. (5.4) illustrates how the instantaneous arm currents ($i_{p/n123}^{pu}$) are computed the in the pu system. The base arm energy ($W_{arm}^{base} = W_{arm}^{*}$) equals the reference arm energy (W_{arm}^{*}) in the abc-frame.

The single-phase system acts like a load for Method-1. For the AC-AC MMC topology, the load is operating at nominal power ($S_b = S_b^{nom}$) with 0.8 *Power Factor* (PF_b). And the load is operating at full load ($S_b = P_b = S_b^{nom}$) for DC-AC MMC topology. The load power is ramped

up from no load to full load in two seconds. A few signals (S_a, P_a, Q_a, $\boldsymbol{v}_{adq}$, $\boldsymbol{i}_{adq}$, S_b, P_b, and Q_b) are vertically shifted and plotted in one graph. Signals ($\boldsymbol{v}_{adq}$, $\boldsymbol{i}_{adq}$, S_b, P_b, and Q_b) are vertically shifted by 2 pu, and the signals (S_a, P_a, Q_a) are vertically shifted by 4 pu.

No reactive power is flowing into the source (three-phase). The arm energy ripple is higher for 1/3rd frequency operation ($f_b = f_a/3$) than DC-AC ($f_b = 0$) operation because reactive load power (Q_b) flows into MMC, further increasing arm energy oscillation [KOL15a].

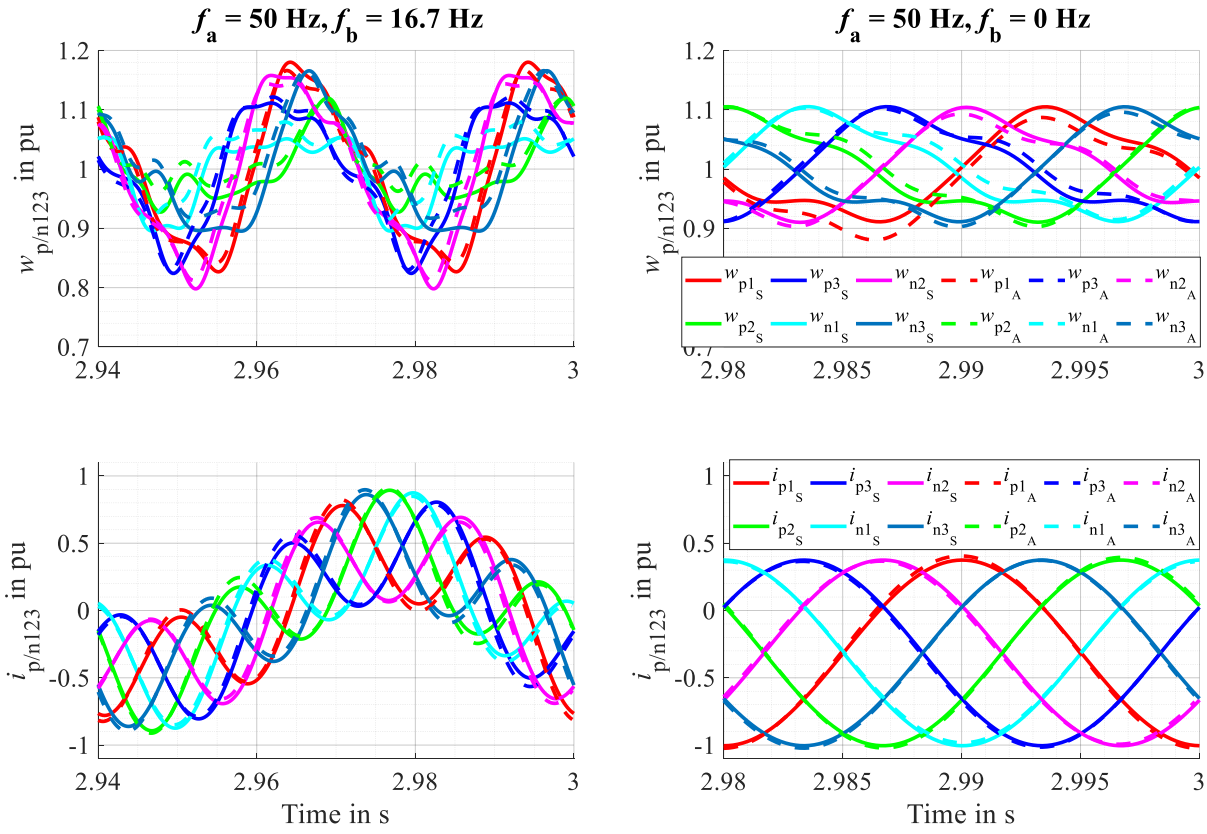

Figure 5.5: Simulation and analytical results of MMC when the arm energy balancing Method-1 is used to regulate the average arm energies of MMC.

$$I_a^{base} = \frac{S_{load}^{nom}}{\sqrt{3} V_{a\text{-}LL}^{base}} \tag{5.1}$$

$$I_b^{base} = \frac{S_{load}^{nom}}{V_b^{nom}} \text{ if } f_b \neq 0 \text{ and } I_b^{base} = \frac{S_{load}^{nom}}{V_{dc}^{nom}} \text{ if } f_b = 0 \tag{5.2}$$

$$I_{arm}^{base} = \frac{I_a^{base}}{2} + \frac{I_b^{base}}{3} \text{ if } f_b \neq 0 \text{ and } I_{arm}^{base} = \frac{I_a^{base}}{2} + \frac{I_b^{base}}{3\sqrt{2}} \text{ if } f_b = 0 \tag{5.3}$$

$$i_{\mathrm{p/n123}}^{\mathrm{pu}} = \frac{i_{\mathrm{p/n123}}}{\sqrt{2}\, I_{\mathrm{arm}}^{\mathrm{base}}} \tag{5.4}$$

As proved in Section 2.4, the arm energy balancing Method-1 is unstable ($|A| = 0$) for equal frequency ($f_b = f_a$) operation (also see Fig. 5.4) and is stable ($|A| \neq 0$) for unequal frequency ($f_b = 0$ or $f_b = f_a/3$) operation (also see Fig. 5.2 and Fig. 5.3). Method-1 or Method-5 is unstable for the equal frequency operation because of the couplings between the manipulated inputs ($|A| = 0$). On the other hand, the manipulated inputs are naturally decoupled (A_{6x6} = diagonal matrix) for unequal frequency operations ($f_a = n f_b$, $f_b = n f_a$, ($f_b = 0$ & $f_a \neq 0$)); hence all arm energy balancing methods are stables. Here, n = integer.

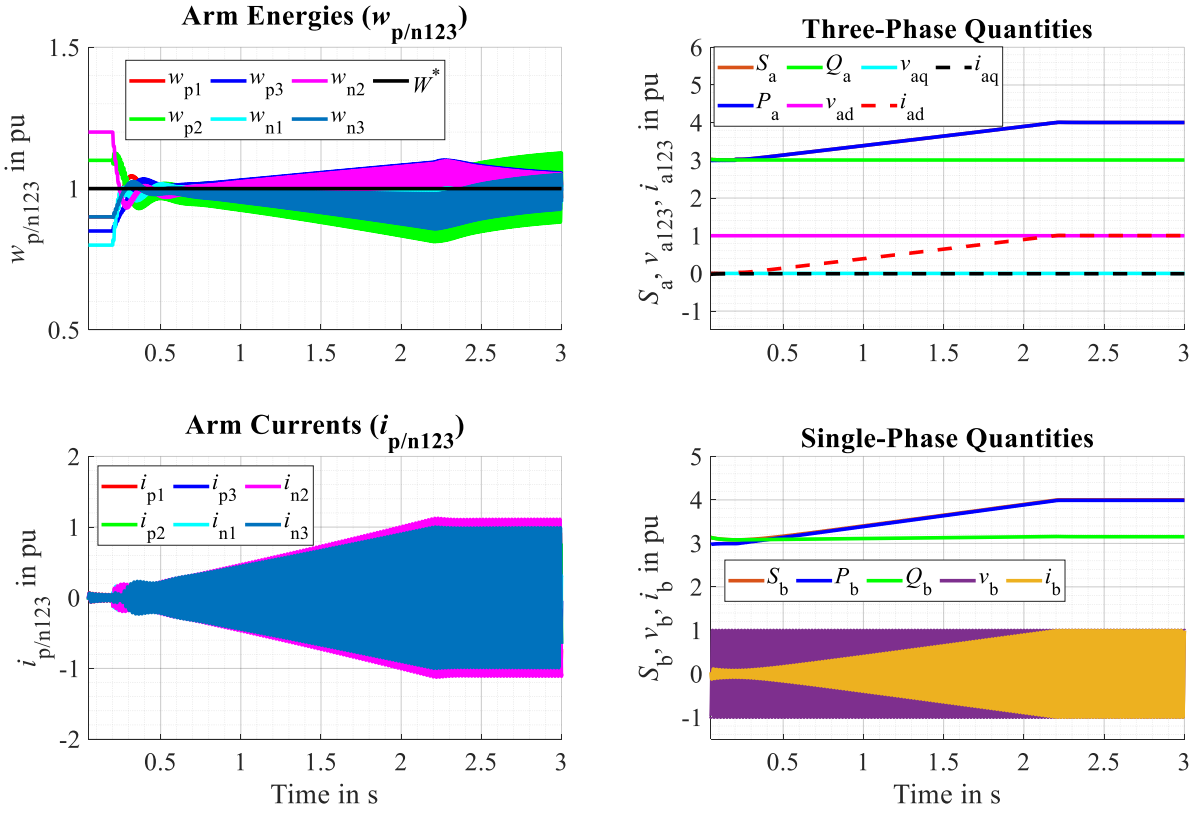

Figure 5.6: Simulation results of AC-AC MMC with equal frequency ($f_b = f_a$) operation when the arm energy balancing Method-7 is used to regulate the average arm energies of MMC. Load condition: S_b = 1 pu, PF_b = 1.

Fig. 5.5 shows the zoomed instantaneous arm energies ($w_{p/n123}$) and currents ($i_{p/n123}$) in the steady state for $f_b = f_a/3$ and $f_b = 0$ operations obtained using the simulation and the proposed analytical toolchain. The solid line signals correspond to the simulation results, and the dotted line signals belong to the analytical solutions. The arm currents have zero offsets for $f_b = f_a/3$ operation and a definite offset ($-I_b/3$) for $f_b = 0$ operation. But the arm currents are symmetrical

for both conditions. The mismatch between the proposed analytical and simulation results is expected because the analytical toolchain ignores the arm and transformer impedances. But the simulation and analytical results resemble similar behavior. Therefore, analytical results can also be used as a first-hand toolchain to quickly predict and compare the behavior of MMC in a steady state for various normal and abnormal operating conditions, saving time and money. The proposed toolchain can also help to compare the performance of MMC for different arm energy balancing methods, which will be discussed later in Section 5.4.

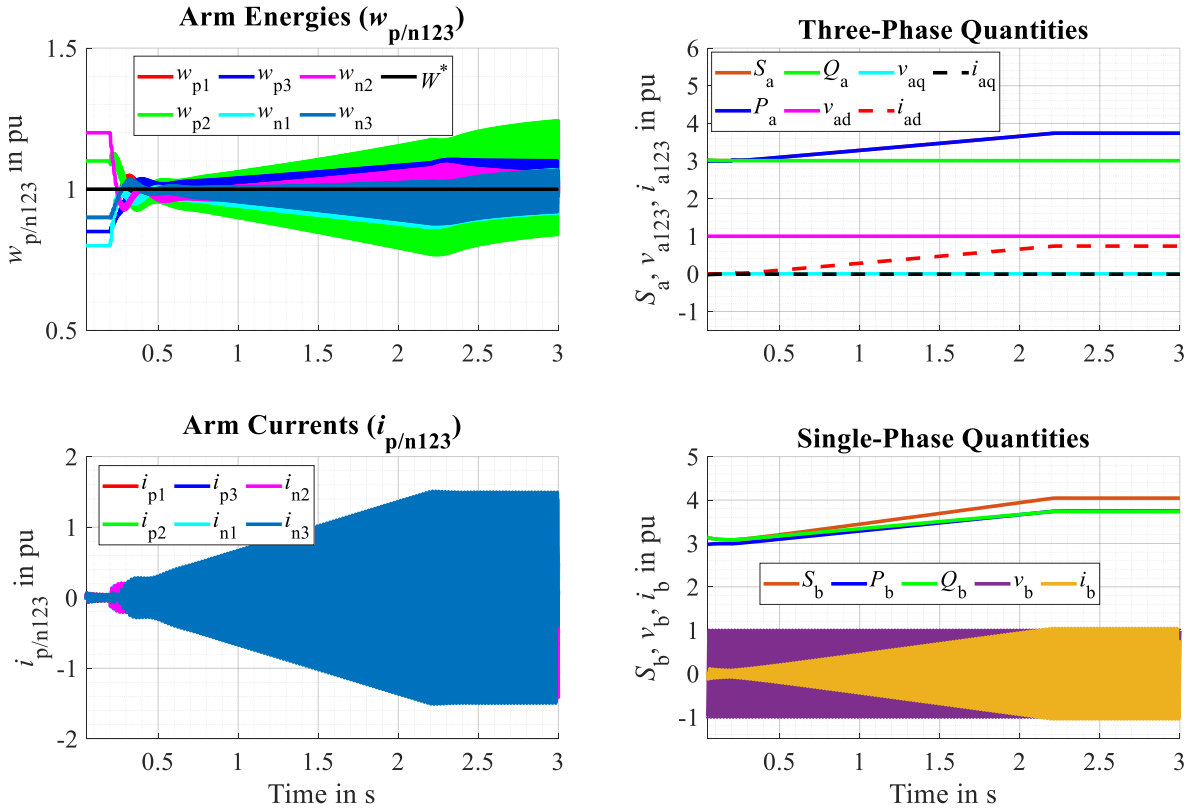

Figure 5.7: Simulation results of AC-AC MMC with equal frequency ($f_b = f_a$) operation when the arm energy balancing Method-7 is used and the load reactive power compensation is not implemented ($i^*_{aq+} = 0$). Load condition: $S_b = 1$ pu, $PF_b = 0.8$.

5.3 The Arm Energy Balancing using Method-7 and Method-12

Method-7 and Method-12 are another two possible arm energy balancing methods that do not inject harmonics into the source and load currents. Table 2.2 suggests that both Method-7 and Method-12 are stable ($|A| \neq 0$) for equal and unequal frequency operations. The three-phase and single-phase are sources for Method-7 and Method-12, respectively. Fig. 5.6 represents the direct AC-AC MMC simulation result for equal frequency ($f_b = f_a$) operation when the arm

energy balancing Method-7 is used. Now, the physical quantities (S_a, P_a, Q_a, S_b, P_b, and Q_b) are vertically shifted by 3 pu. The load is operating at nominal power with a unity power factor.

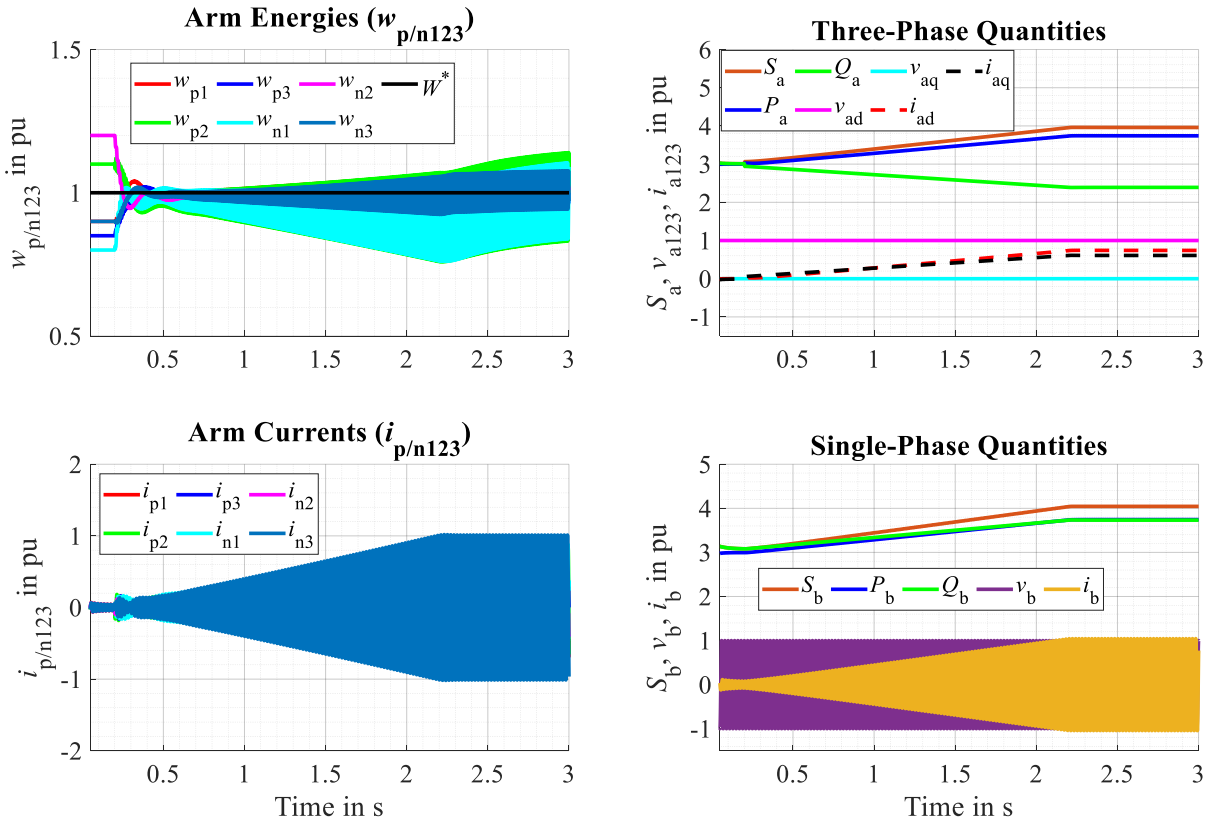

Figure 5.8: Simulation results of AC-AC MMC with equal frequency ($f_b = f_a$) operation when the arm energy balancing Method-7 is used and the load reactive power is compensated using (4.46) (i^*_{aq+} = eq.). Load condition: S_b = 1 pu, PF_b = 0.8.

Fig. 5.6 validates that Method-7 is stable for equal frequency operation. Similarly, Fig. 5.7 shows the simulation result for equal frequency operation using Method-7 when the load (S_b) operates at the nominal power with 0.8 power factor. Here, no reactive flows in the three-phase system ($i^*_{aq+} = 0$). The overall arm current and energy ripple has increased significantly for the poor power factor load compared to the unity power factor load. In other words, the arm current and energy ripple magnitudes increase with the load reactive power. It is because the load reactive current component ($I^{\perp b}_{b0}$) makes an additional average power with the source voltage ($v_{a\alpha\beta}$) in $\bar{p}_{\Delta\alpha\beta}$, which needs to be compensated using the manipulated inputs ($MI_{5\&6} = i^{cm}_{b\alpha\beta}$) (also see Table 2.6). The current component $i^{cm}_{b\alpha\beta}$ is unsymmetrical. Ideally, $\bar{p}_{\Delta 0} \approx \bar{p}_{\Sigma\alpha\beta} \approx 0$, therefore, the manipulated inputs (i_{bd+}, $i^{b}_{b\alpha\beta}$) responsible for regulating $\bar{w}_{\Delta 0}$, and $\bar{w}_{\Sigma\alpha\beta}$ only need to compensate for the losses in the arms, i.e. $i_{bd+} \approx i^{b}_{b\alpha\beta} \approx 0$. Thus, $i^{cm}_{b\alpha\beta}$ majorly accountable for the unsymmetrical arm's current behavior during equal-frequency operation. The unsymmetric

component increases the magnitude of a few arm currents and reduces the magnitude of other arm currents resulting in overall higher arm current magnitude and higher dimensioning of the converter (also see Fig. 5.9).

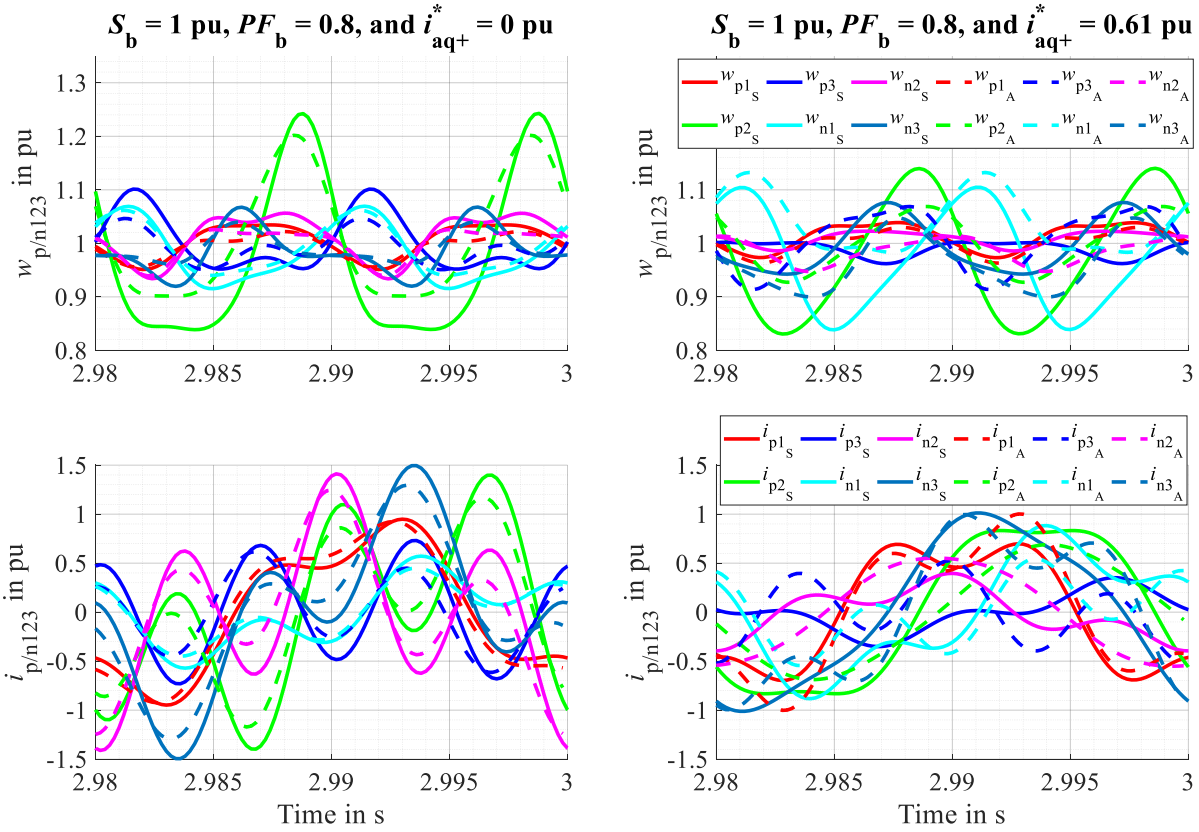

(a) Without load reactive power compensation (b) With load reactive power compensation

Figure 5.9: Simulation and analytical results of MMC when the arm energy balancing Method-7 is used to regulate the average arm energies of MMC. Load condition: S_b = 1 pu, PF_b = 0.8.

The magnitude of the unsymmetrical arm current component ($i^{cm}_{b\alpha\beta}$) can be reduced by compensating the additional average arm power caused due to the reactive load power current component ($I^{\perp b}_{b0}$) using the source reactive power current component (i^*_{aq+}) (also see (4.46)). Fig. 5.8 presents the simulation result for equal frequency operation using Method-7 when the additional average arm power due to the reactive load power is compensated using the source reactive power with the help of (4.46). A significant reduction (about 0.5 pu) in the overall arm current magnitude is observed by realizing the proposed load reactive power compensation strategy. i_{aq+} increases the symmetrical (i_{aq+}) and reduces the unsymmetrical ($i^{cm}_{b\alpha\beta}$) arm current components, resulting in overall less arm current magnitude.

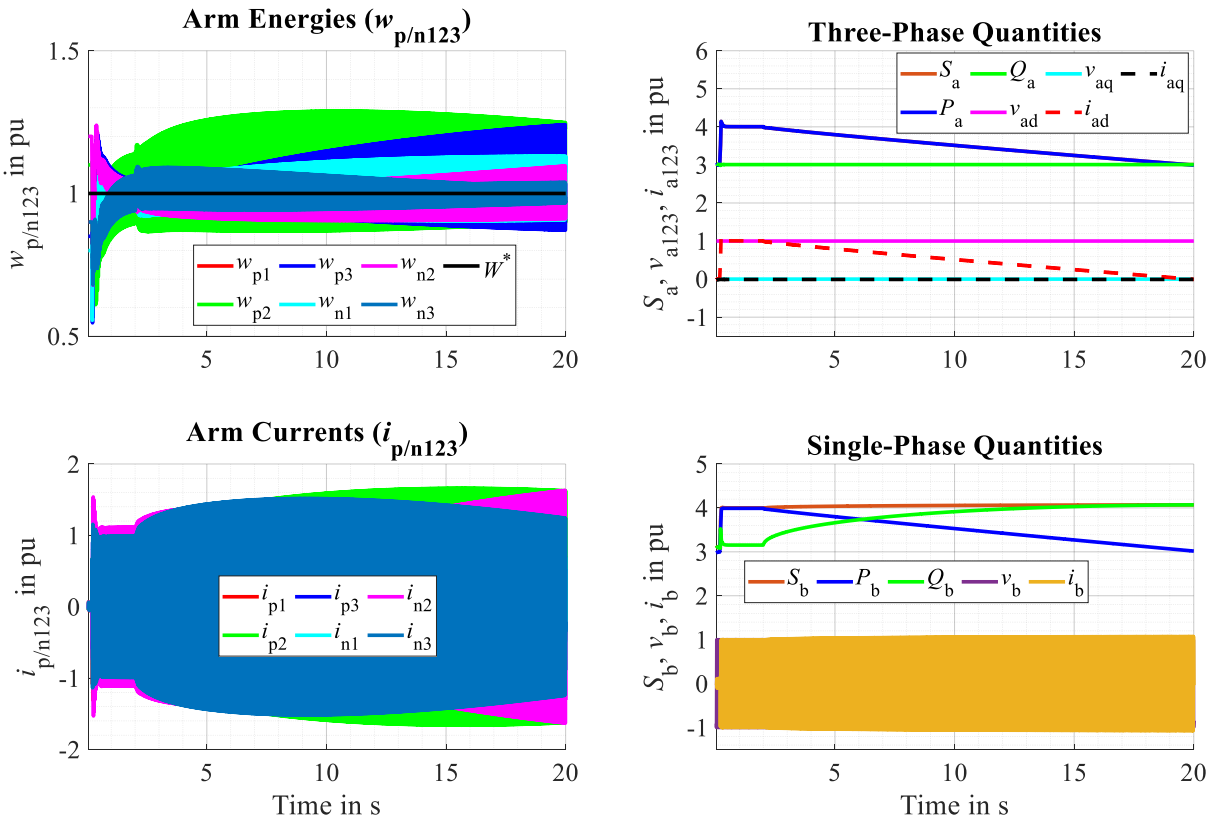

Figure 5.10: Simulation results of AC-AC MMC with equal frequency ($f_b = f_a$) operation when the arm energy balancing Method-7 is used and the load reactive power compensation is not implemented ($i^*_{aq+} = 0$). Load condition: $S_b = 1$ pu, PF_b = varying from 1 to 0.

Fig. 5.9 shows the zoomed steady-state instantaneous arm energies and currents when the load is operating at full load with 0.8 power factor. The left-side plots correspond to Fig. 5.7, where the reactive load power is not compensated, and the right-side plots belong to Fig. 5.8, where the reactive load power is compensated using the proposed strategy. Again, the solid line plots represent the simulation results, and the dotted line plots are obtained using the proposed analytical toolchain. As discussed, the arm currents are highly unsymmetrical when the reactive load power is not compensated. The three arm currents (i_{p2}, i_{n2}, i_{n3}) have a higher magnitude, and the other three arm currents (i_{p1}, i_{n1}, i_{p3}) have less magnitude. Also, the arm energies are highly unsymmetrical. The arm energy w_{p2} has a significantly high ripple.

As mentioned in Chapter 2, this unsymmetrical nature cannot be omitted because the current components in the phase with the common-mode voltage (v_{cm}) are a must for stable operation during equal frequency operation. And the current component in phase with v_{cm} is always unsymmetrical in the abc-frame. But the unsymmetrical part can be reduced significantly by compensating the load reactive power component ($I^{\perp b}_{b0}$) using the source reactive power component (i_{aq+}) shown on the right side of Fig. 5.9. Also, the overall arm energy ripple is

reduced using the proposed load reactive power compensation. Although the analytical results do not match with the simulation results (which is expected), the analytical and simulation results show similar behavior. The analytical results also show that the overall arm energy ripple and current magnitudes are reduced by compensating the additional average arm power term due to the load reactive power using the source reactive power.

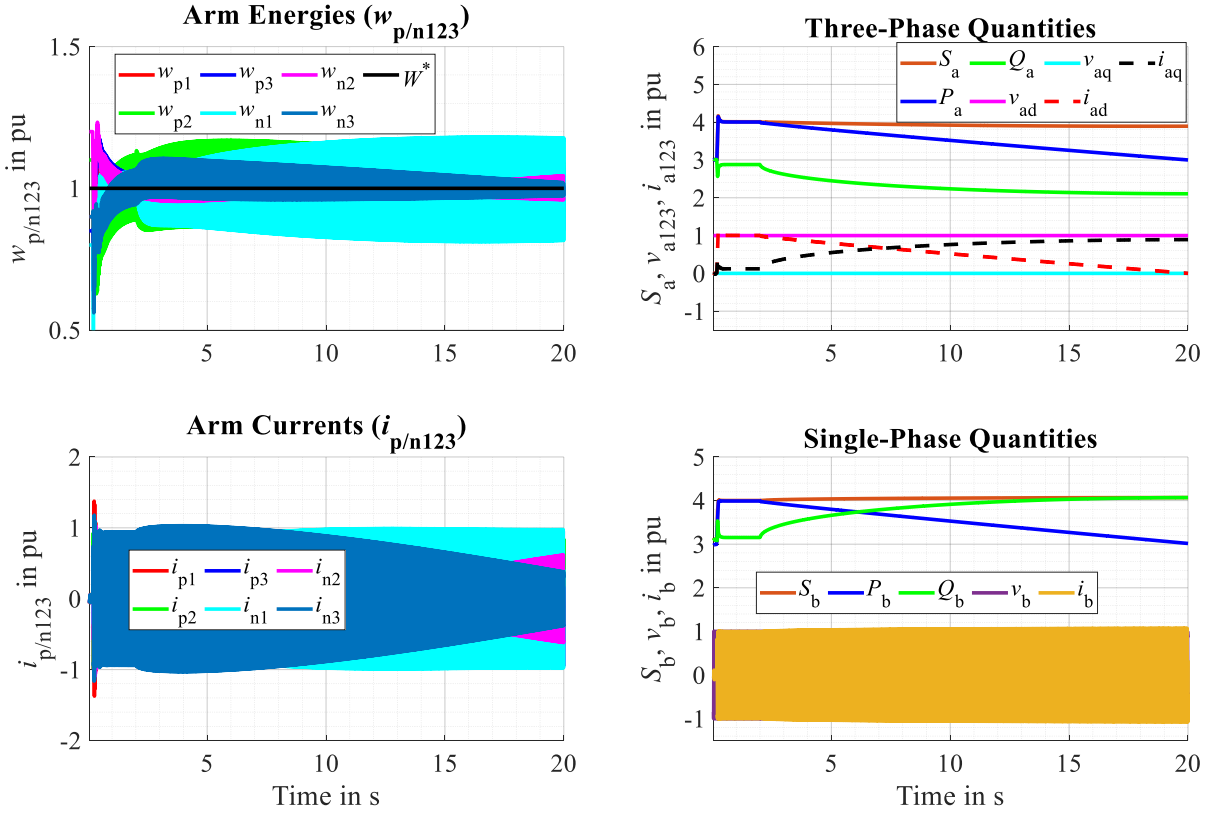

Figure 5.11: Simulation results of AC-AC MMC with equal frequency ($f_b = f_a$) operation when the arm energy balancing Method-7 is used and the load reactive power is compensated using (4.46) (i^*_{aq+} = eq.). Load condition: S_b = 1 pu, PF_b = varying from 1 to 0.

Fig. 5.10 shows the simulation result using Method-7 for equal frequency operation without the load reactive power compensation when the load operates at nominal power and the power factor is slowing ramping down from 1 to 0. The arm currents increase with the increase in the load reactive power when $i_{aq+} = 0$. Similarly, Fig. 5.11 shows the same graph but with the proposed load reactive power compensation being enabled. A significant reduction in the arm current magnitude (about 0.5 pu) is observed for the whole power factor range, suggesting that the converter's power density can be increased with the proposed load-reactive power compensation strategy.

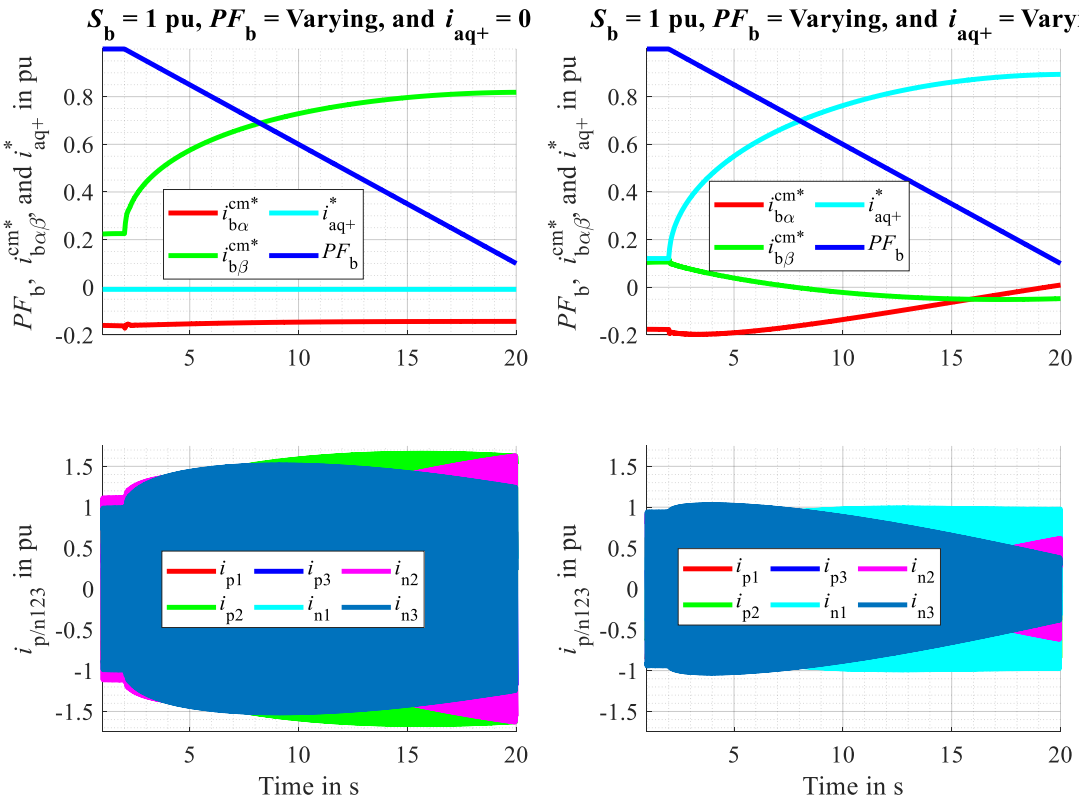

(a) Without load reactive power compensation (b) With load reactive power compensation

Figure 5.12: Simulation results of AC-AC MMC for equal frequency ($f_b = f_a$) operation when the arm energy balancing Method-7 is used. Load condition: S_b = 1 pu, PF_b = varying from 1 to 0.

Fig. 5.12 represents the variation of the manipulated inputs ($MI_{5\&6} = i^{cm}_{b\alpha\beta}$) with the variation in the load reactive power factor from 1 to 0. As discussed before, when the source reactive power ($i_{aq+} = 0$) is zero, the magnitude of $i^{cm}_{b\alpha\beta}$ is higher (see the left side of Fig. 5.12). When the additional average power term due to load reactive power is compensated using the source reactive power, the variation in the magnitude of $i^{cm}_{b\alpha\beta}$ is comparatively smaller (see the right side of Fig. 5.12).

$$i^{pu}_{aq+} = 0.85\left(\frac{V^{pu}_a}{V^{pu}_b}\right)^2\left(I^{\perp b}_b\right)^{pu}, \text{ or } \left(I^{\perp b}_b\right)^{pu} = 1.18\left(\frac{V^{pu}_b}{V^{pu}_b}\right)^2 i^{pu}_{aq+} \tag{5.5}$$

Fig. 5.13 and Fig. 5.14 represent the simulation results for the arm energy balancing Method-12 for equal frequency operation when the load power factor is varying linearly from 1 to 0 at a nominal load. The effect due to the load reactive power component is not compensated in Fig. 5.13, and the load reactive power is compensated using the source reactive power in Fig. 5.14 with the help of (4.47). Again, the arm current magnitude is significantly reduced by

compensating the effect of the load reactive power current component (i_{aq+}) using the proposed strategy. But the single-phase current magnitude and the overall arm energy ripple are found to increase considerably using the proposed load reactive power compensation strategy for Method-12, which is undesirable. Writing (4.46) or (4.47) in the pu system and solving it with the parameters in Table 5.1 gives (5.5). At nominal conditions ($V_b^{pu} = V_a^{pu} = 1$), it suggests that less three-phase reactive current component ($i_{aq+} = 0.85$ pu) is required to compensate for the nominal single-phase load reactive current component ($I_b^{Lb} = 1$ pu) for Method-7. But the more single-phase reactive current ($I_b^{Lb} = 1.18$ pu) is needed to compensate $i_{aq+} = 1$ pu for Method-12. It is because i_{aq+} makes average power with V_b (which is 2.17 times V_a) and I_b^{Lb} makes average power with V_a. (also see Table 2.6). Therefore, it is recommended to saturate I_b^{Lb} to safely operate between the boundary conditions for Method-12 for the parameter values in Table 5.1.

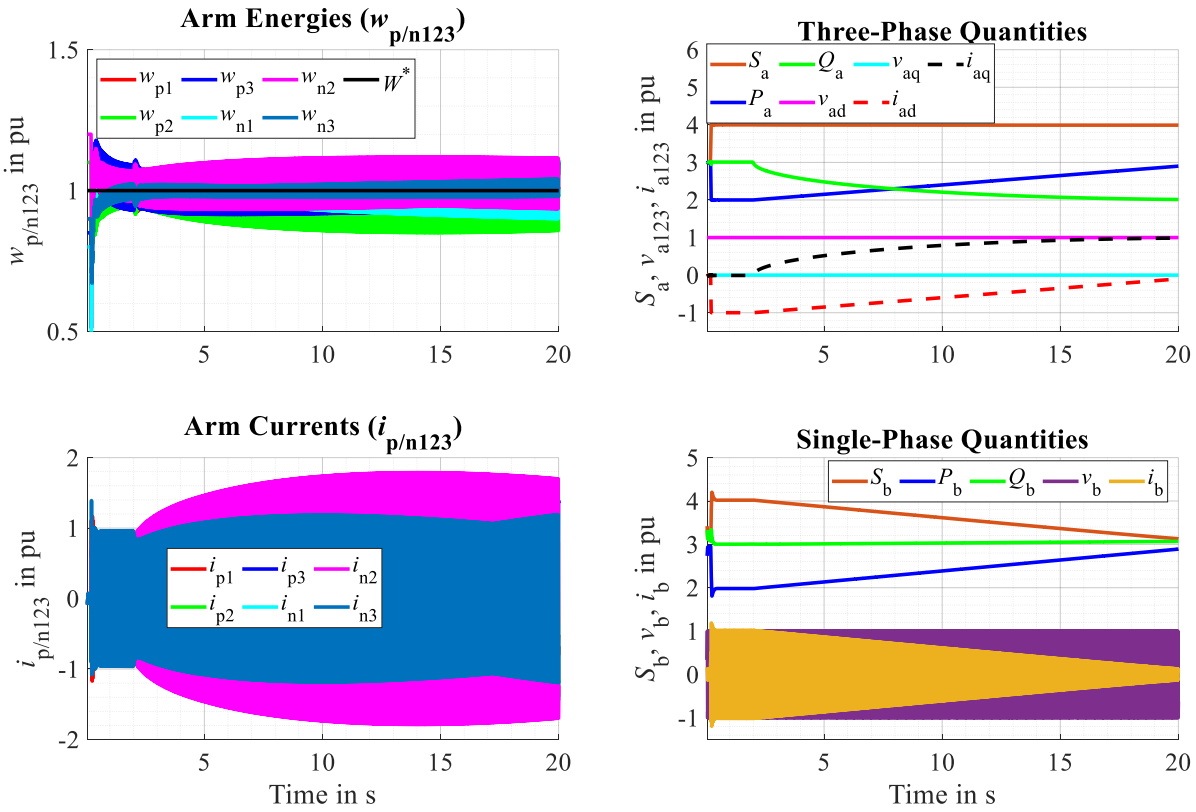

Figure 5.13: Simulation results of AC-AC MMC with equal frequency ($f_b = f_a$) operation when the arm energy balancing Method-12 is used and the load reactive power compensation is not implemented ($I_{b0}^{Lb*} = 0$). Load condition: $S_a = 1$ pu, PF_a = varying from 1 to 0.

Fig. 5.15 represents the simulation results for equal frequency operation using Method-12 when the load reactive is compensated using the source reactive power and I_b^{Lb} is saturated to 0.8 pu.

Limiting I_{b}^{Lb} to 0.8 pu has helped to reduce the single-phase current and the overall arm energy ripple significantly compared to when I_{b}^{Lb} is not saturated (also see Fig. 5.14).

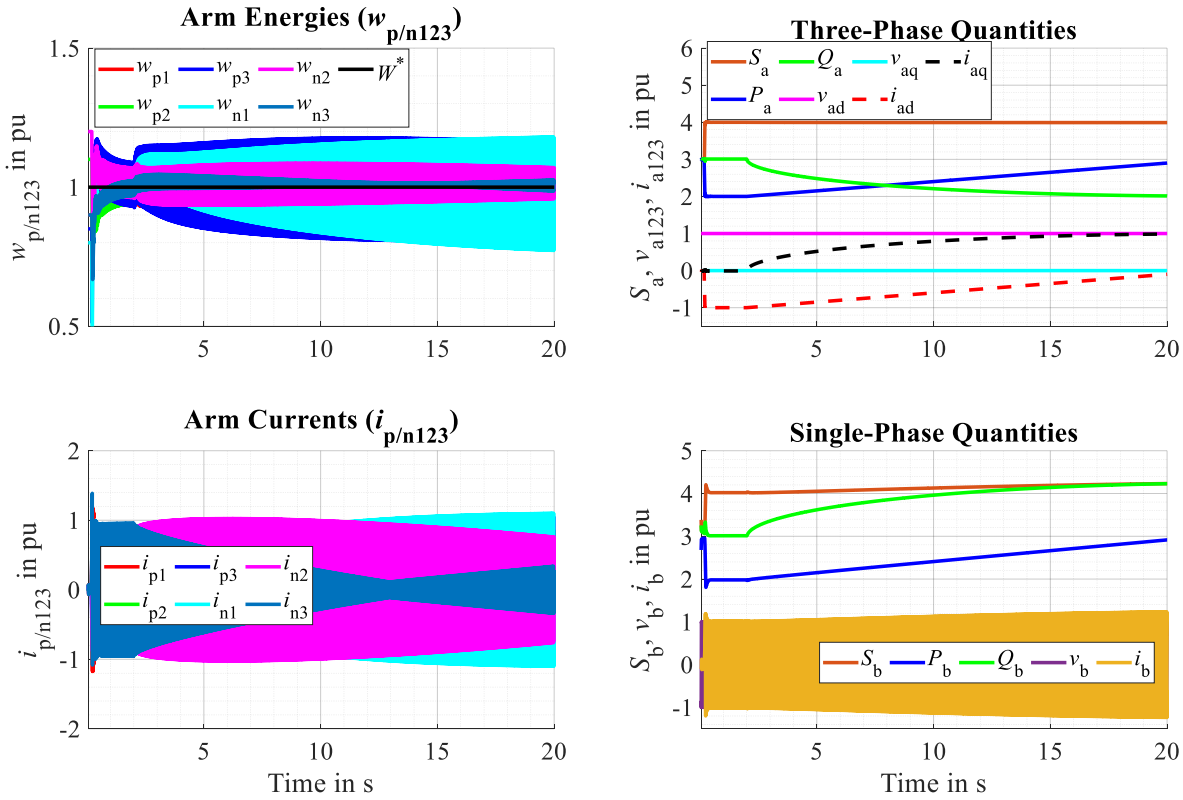

Figure 5.14: Simulation results of AC-AC MMC with equal frequency ($f_{\text{b}} = f_{\text{a}}$) operation when the arm energy balancing Method-12 is used and the load reactive power is compensated using equation (4.47) ($I_{\text{b0}}^{\text{Lb}*}$ = eq). Load condition: S_{a} = 1 pu, PF_{a} = varying from 1 to 0.

5.4 Comparison of Various Arm Energy Balancing Methods

In the previous sections, only the performance of the arm energy balancing Method-1, 5, 7, and 12 are demonstrated and analyzed for various three-phase and single-phase system frequencies at different load conditions. This section will compare the performance of all stable arm energy balancing methods listed in Table 2.2. Referring to Appendix A.8 and Chapter 4, the six average arm energy controllers for all energy balancing methods given in Table 2.2 can be designed easily. The general definition of three-phase (θ_{a}) and single-phase (θ_{b}) voltage angle for AC-AC MMC topology is given in (5.6). The single-phase voltage angle is leading three-phase voltage angle by ϕ_{b}. The maximum arm current magnitude for equal frequency ($f_{\text{b}} = f_{\text{a}}$) operation would differ for different ϕ_{b}. Hence, it is essential to analyze the performance of direct AC-AC MMC for all possible values of ϕ_{b} ($0^{\text{o}} \le \phi_{\text{b}} \le 360^{\text{o}}$).

$$\theta_{\text{a}} = \omega_{\text{a}} t \;\; ; \;\; \theta_{\text{b}} = \omega_{\text{b}} t + \phi_{\text{b}} \tag{5.6}$$

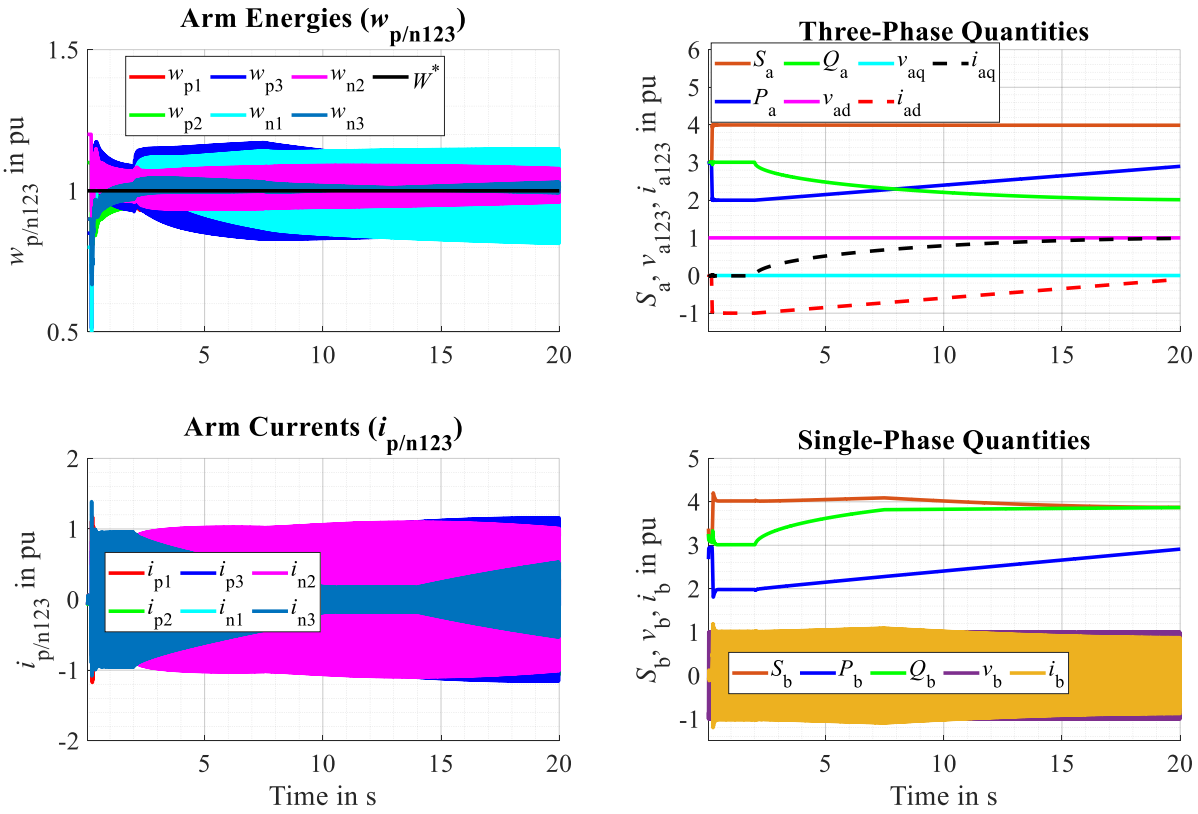

Figure 5.15: Simulation results of AC-AC MMC with equal frequency ($f_b = f_a$) operation when the arm energy balancing Method-12 is used and the load reactive power is compensated using equation (4.47) ($I_{b0}^{\perp b*}$ = eq) and $I_{b0}^{\perp b*}$ is saturated to 0.8 pu. Load condition: S_a = 1 pu, PF_a = varying from 1 to 0.

Fig. 5.16 and Fig. 5.17 represent the analytical and simulation results of direct AC-AC MMC for equal frequency operation for all stable arm energy balancing methods at various load conditions for all possible values of ϕ_b. Here, the proposed compensation of the effect of the load reactive power using source reactive power is disabled. The maximum of the single-phase current ($|i_b^{pu}|^{max}$), three-phase current ($|i_{a123}^{pu}|^{max}$), arm current ($|i_{arm}^{pu}|^{max}$), and arm ripple energy ($|w_{arm}^{pu}|^{max}$) are plotted for all possible values of ϕ_b to analyze and compare the performance of all stable arm energy regulation methods. Fig. 5.18 illustrates the definition of $|i_{arm}^{pu}|^{max}$ and $|w_{arm}^{pu}|^{max}$ using an arbitrary example. Three-phase is the source for energy balancing Method-7, 8, 9, 10, and 11. Whereas the single-phase is the source for the arm energy balancing Method-12, 14, and 15.

As discussed, the performance of MMC obtained using both analytical and simulation results for all stable arm energy balancing methods is similar. However, analytical results do not match precisely with the simulation results because it ignores the arm and transformer impedances. The controller's performance for various conditions can be estimated using the proposed

analytical toolchain very quickly (in about a few seconds) compared to simulation (which takes several hours), saving time and money.

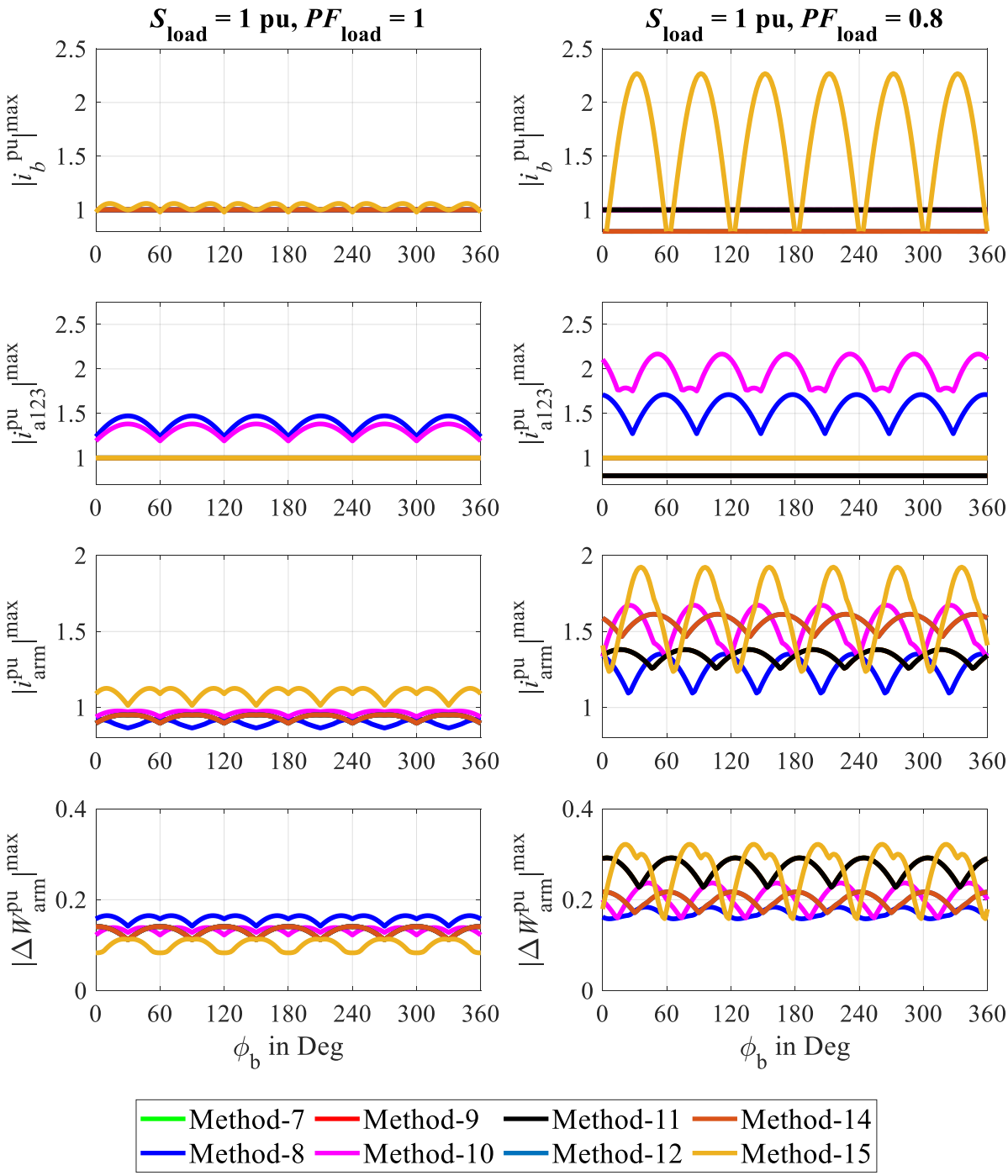

Figure 5.16: Analytical result of direct AC-AC MMC for all stable arm energy regulation techniques for equal frequency ($f_b = f_a$) application during normal operations at various load power factors at nominal load (S_{load} = 1 pu). Here, the proposed load reactive power compensation using the source reactive power is disabled. **Note**: Method-7, 9, and 11 are overlapped together and Method-12, and 14 are overlapped together.

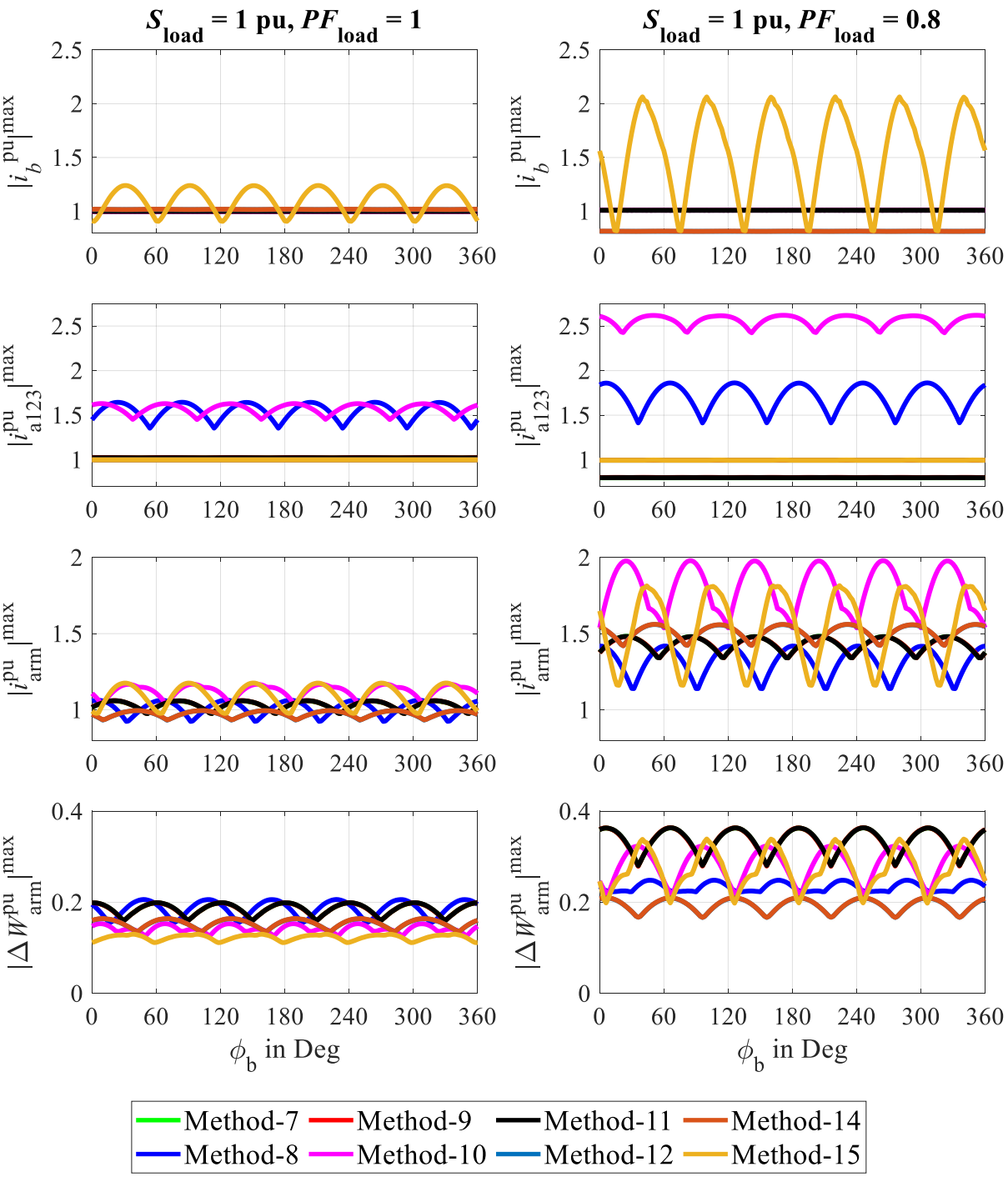

Figure 5.17: Simulation result of direct AC-AC MMC for all stable arm energy regulation techniques for equal frequency ($f_b = f_a$) application during normal operations at various load power factors at nominal load (S_{load} = 1 pu). Here, the proposed load reactive power compensation using the source reactive power is disabled. **Note**: Method-7, 9, and 11 are overlapped together and Method-12, and 14 are overlapped together.

Both analytical and simulation results indicate that the arm energy balancing Method-8, 10, and 15 are not good because they require huge currents to regulate the average arm energies. These methods need more currents to compensate for the strong coupling between the manipulated

inputs. Therefore, only Method-7, 9, and 11 are suitable arm energy balancing methods if three-phase is the source, and only Method-12 and Method-14 are suitable energy balancing methods if single-phase is the source.

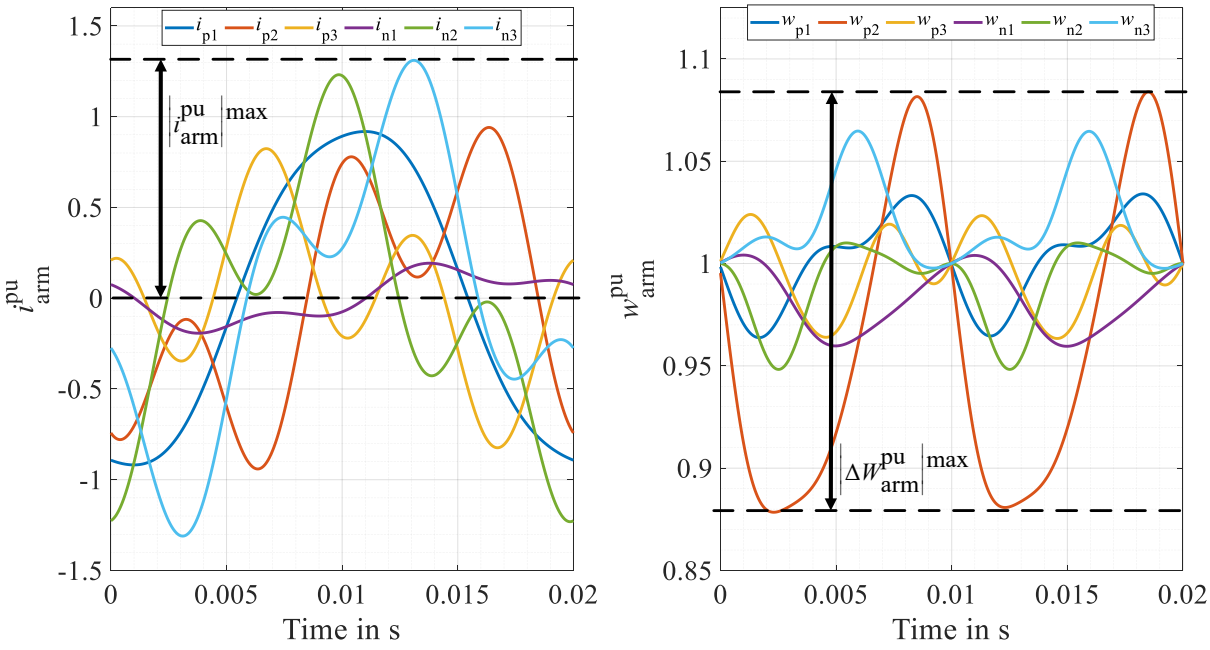

Figure 5.18: Definition of the *Maximum Arm Current* (left image) and the *Arm Energy Ripple* (right image) using an example test case ($f_b = f_a$).

Further, the arm current magnitude increases significantly when the power factor load is poor, which is also observed using the time domain plots in Section 5.3. It can be further observed that the arm current and energy ripple magnitudes vary with ϕ_b, which must be considered while dimensioning the converter. And the maximum peak repeats after every 60° intervals. Further, the overall arm energy ripple increases with the load reactive power increase [KOL15a].

Similarly, Fig. 5.19 and Fig. 5.20 represent the analytical and simulation results of direct AC-AC MMC for equal frequency operation for all well-behaved arm energy balancing methods when the proposed load reactive power compensation is enabled. As shown before, analytical and simulation results prove that the overall arm current magnitude is significantly reduced when the proposed load reactive power compensation is implemented. But the magnitude of the single-phase current for Method-12, and Method-14 is higher than 0.8 pu for $PF_{load} = 0.8$ because it consists of both active ($I_{b0}^{b} = 0.8$ pu) and reactive ($I_{b0}^{\perp b} = 0.708$ pu) power current components. Similarly, the three-phase current magnitude is higher than 0.8 pu at $PF_{load} = 0.8$ for Method-7, 9, and 11 because it consists of active ($i_{ad+} = 0.8$ pu) and reactive ($i_{aq+} = 0.51$ pu) current components (also see (5.5)).

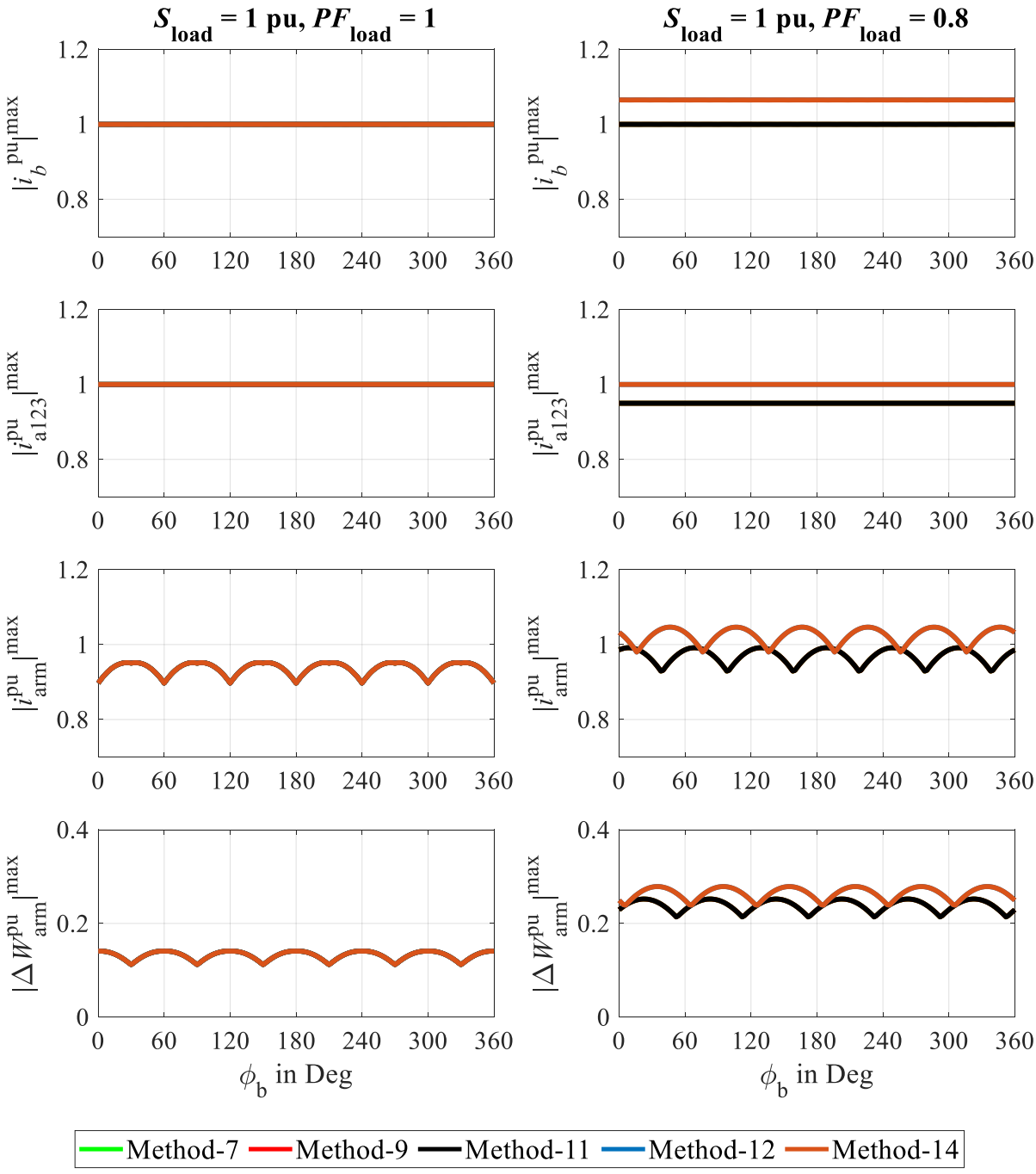

Figure 5.19: Analytical result of direct AC-AC MMC for the well-behaved stable arm energy regulation techniques for equal frequency ($f_b = f_a$) application during normal operations at various load power factors at nominal load (S_{load} = 1 pu). Here, the proposed load reactive power compensation using the source reactive power is enabled. **Note**: Method-7, 9, and 11 are overlapped together and Method-12, and 14 are overlapped together.

Further, the overall arm energy ripple is increased for Method-12 and Method-14 when the reactive load power is compensated using the source reactive power (see Fig. 5.17 and Fig. 5.20). Single-phase is the source, and the three-phase is the load for Method-12 and Method-14.

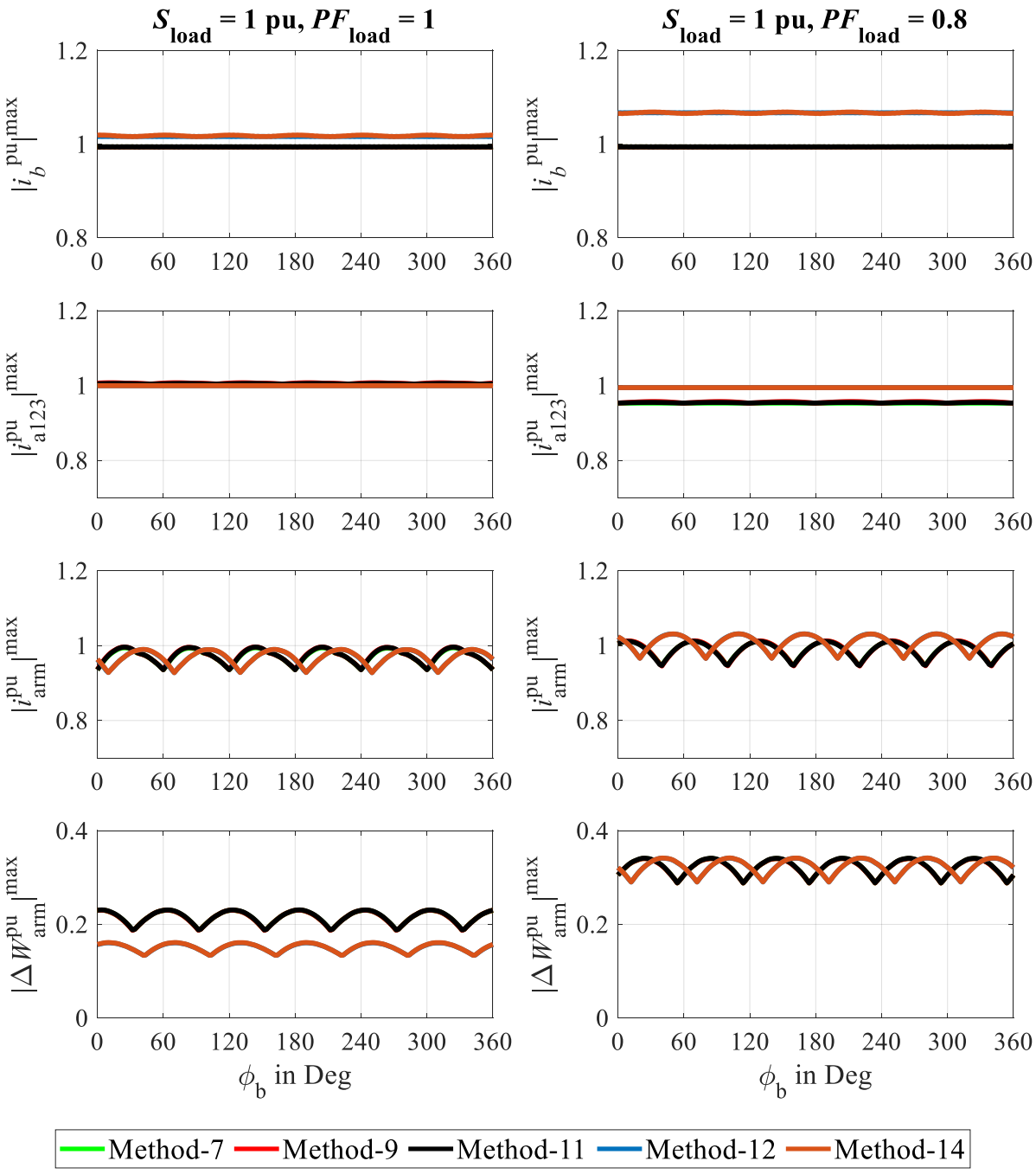

Figure 5.20: Simulation result of direct AC-AC MMC for the well-behaved stable arm energy regulation techniques for equal frequency ($f_b = f_a$) application during normal operations at various load power factors at nominal load (S_{load} = 1 pu). Here, the proposed load reactive power compensation using the source reactive power is enabled. **Note**: Method-7, 9, and 11 are overlapped together and Method-12, and 14 are overlapped together.

More arm energy ripple for poor power factor operation is because more single-phase reactive power current component (I_{b0}^{1b} = 0.708 pu) is required to compensate for the given three-phase reactive power component (i_{aq+} = 0.6 pu) (also see (5.5)). Therefore, comparatively more reactive power (Q_b = 0.708 pu, and Q_a = 0.8 pu) flows in MMC for Method-12 and Method-14,

resulting in more arm energy oscillation [KOL15a]. Further, the resulting magnitude of the single-phase current is considerably high ($I_b \approx 1.07$ pu).

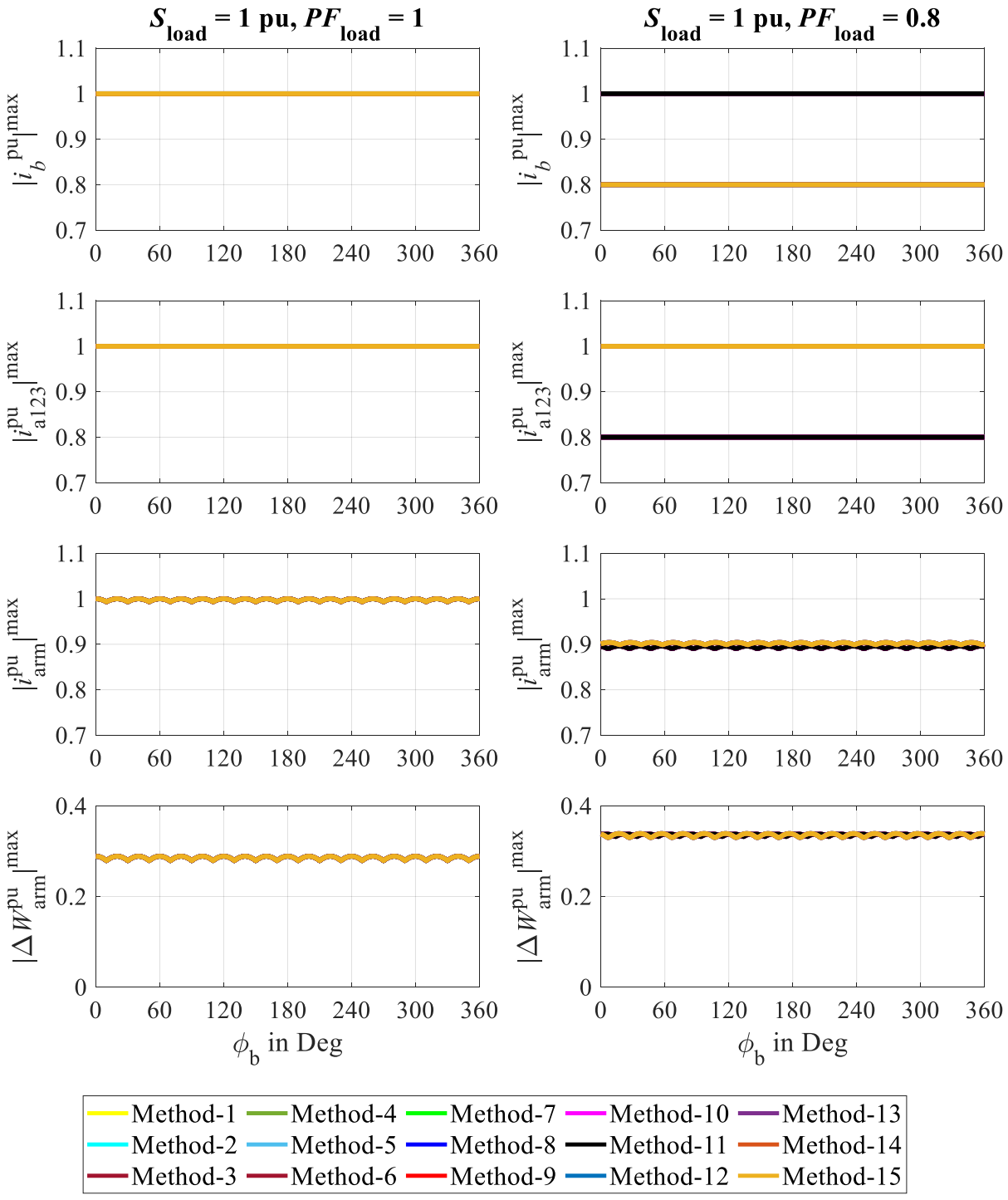

Figure 5.21: Analytical result of direct AC-AC MMC for all stable arm energy regulation techniques for unequal frequency ($f_b = f_a/3$) application during normal operations at various load power factors at nominal load (S_{load} = 1 pu).

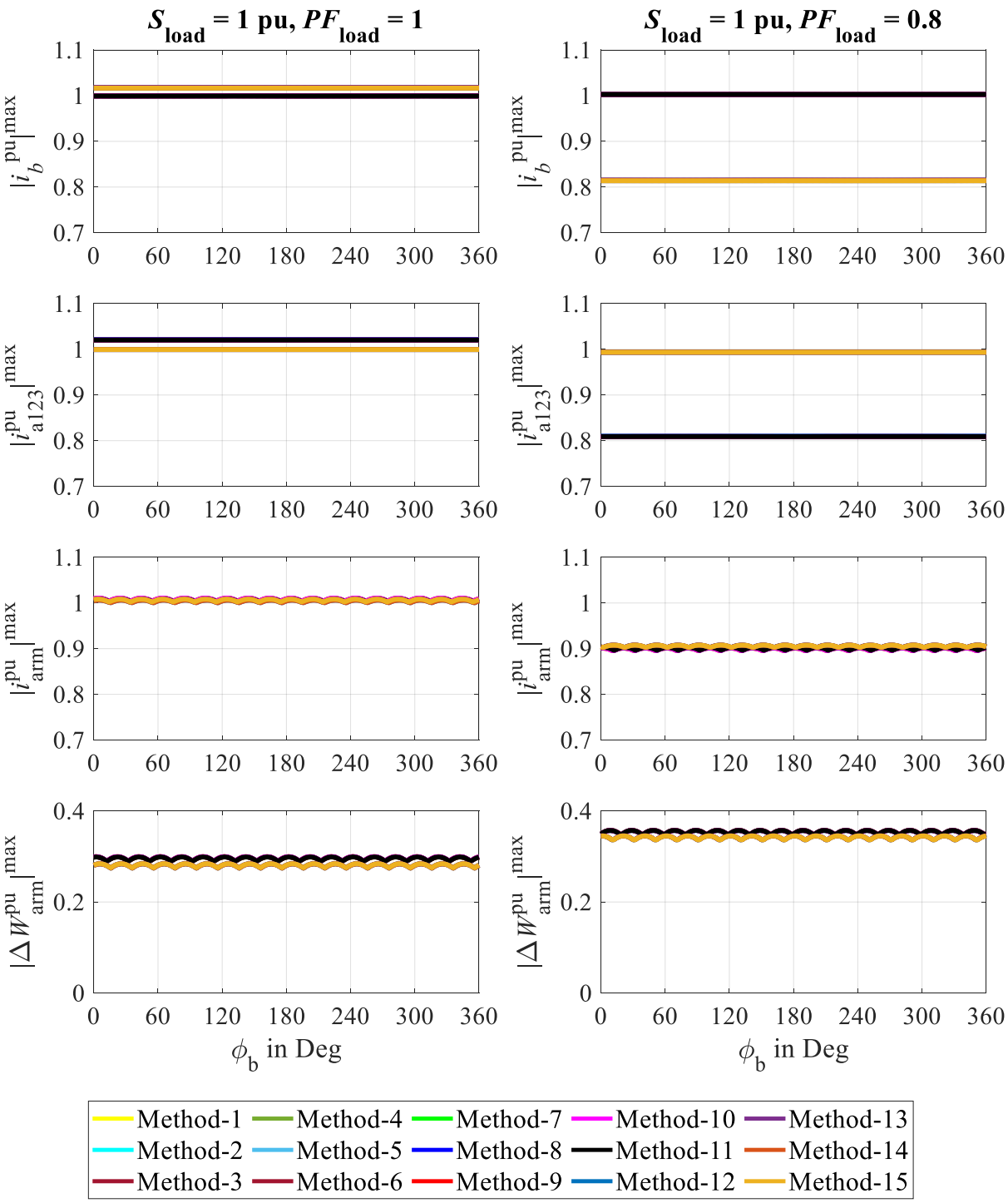

Figure 5.22: Simulation result of direct AC-AC MMC for all stable arm energy regulation techniques for unequal frequency ($f_b = f_a/3$) application during normal operations at various load power factors at nominal load (S_{load} = 1 pu).

But the arm energy ripple is improved with the proposed reactive power compensation for Method-7, 9, and 11 because the three-phase is the source for these methods. Thus, less three-phase reactive power (i_{aq+} = 0.51 pu) is required to compensate for the given single-phase load reactive power ($I_{b0}^{\perp b}$ = 0.6 pu). Thus, comparatively less reactive power (Q_b = 0. 8 pu, and

Q_a = 0.51 pu) flows in MMC for Method-7, Method-9, and Method-11, resulting in less arm energy oscillation. Also, the resulting three-phase current magnitude is comparably low ($I_a \approx 0.95$ pu).

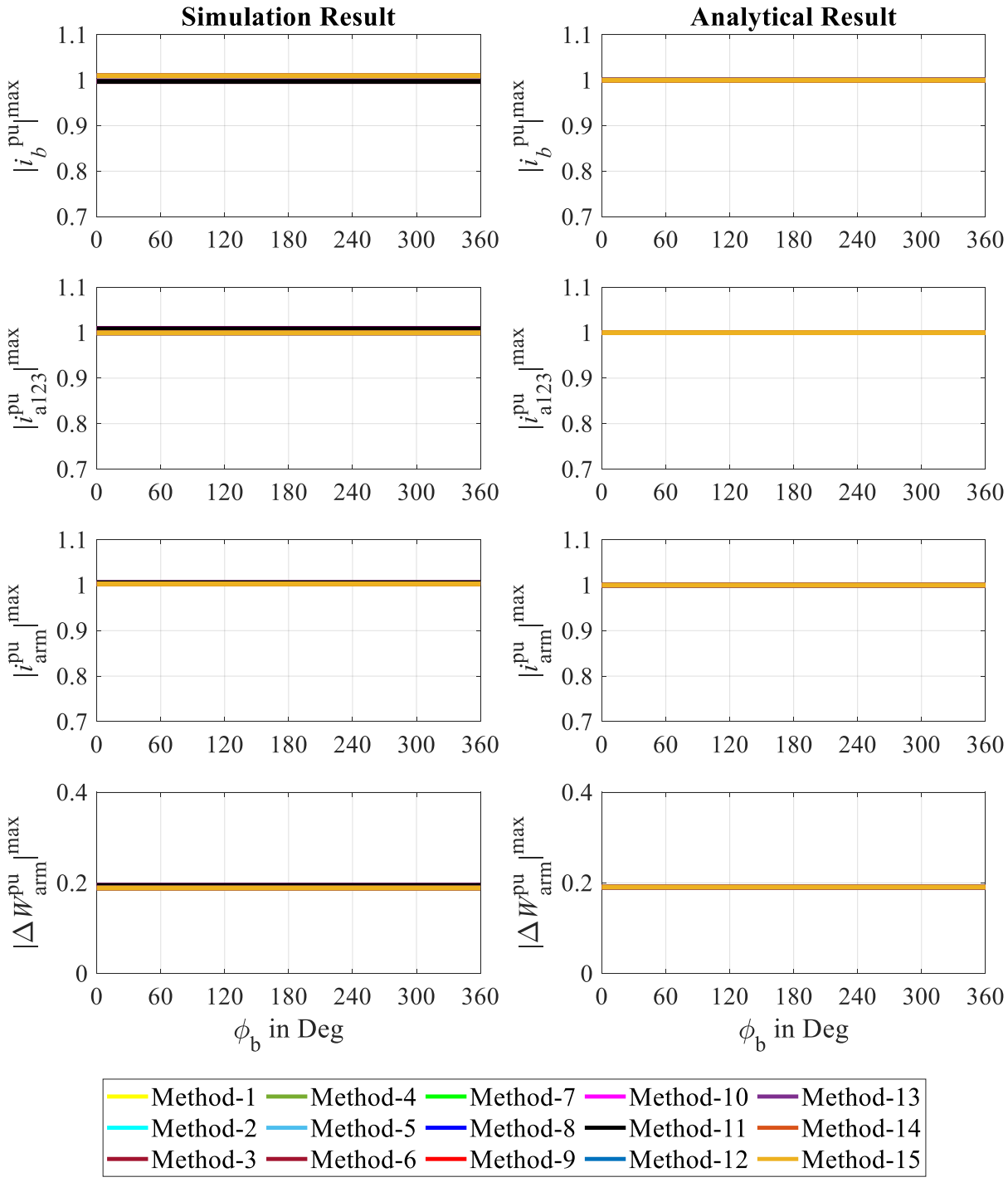

Figure 5.23: Analytical and simulation results of DC-AC MMC for all stable arm energy regulation techniques during normal operations at the nominal load (S_{load} = 1 pu).

Fig. 5.21 and Fig. 5.22 show the analytical and simulation results of direct AC-AC MMC for $1/3^{rd}$ ($f_b = f_a/3$) frequency operation for all stable arm energy regulation methods at full load with various power factors. Unlike equal frequency operation, all energy balancing methods are stable. The arm current reduces with power factor because the manipulated inputs only compensate for the losses because the manipulated inputs are naturally decoupled (A_{6x6} = diagonal). Unlike the equal frequency operation, the variation of the current magnitudes and the overall arm energy ripple with ϕ_b is minimal.

Fig. 5.23 shows the analytical and simulation results of DC-AC MMC for all stable arm energy regulation methods at full load. Like $1/3^{rd}$ frequency operation ($f_b = f_a/3$) frequency operation, all energy balancing methods are stable, and the manipulated inputs only compensate for the losses because the manipulated inputs are naturally decoupled (A_{6x6} = diagonal).

6 Seven-Arm Direct AC-AC MMC for Equal Frequency Operation

Several results in Chapter 5 have shown that the arm currents magnitude increases with the reactive power flowing into MMC when the three-phase and single-phase system frequencies are the same ($f_b = f_a \neq 0$). An effective solution to compensate for the effect of the load reactive power using the source reactive power is proposed in Chapter 2 to reduce the arm current magnitude. But this solution is only feasible if the source allows the reactive power to flow through it. This chapter proposes a small change in the hardware to reduce the arm current magnitude when the load reactive power is present, and the source does not allow reactive power to flow across it.

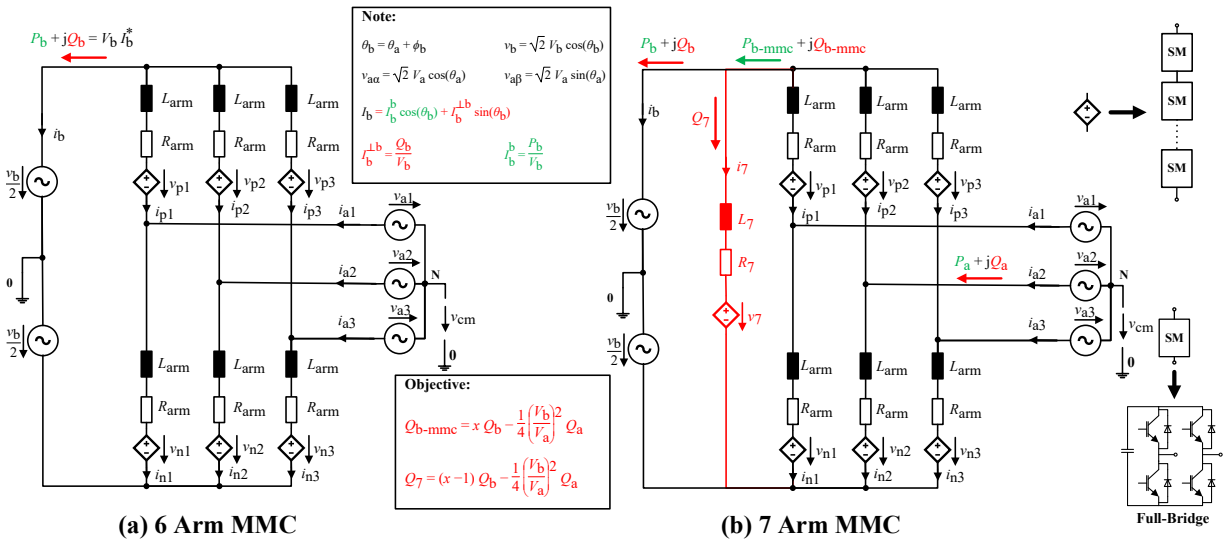

Figure 6.1: Electrical circuit diagram of direct AC-AC MMC using (a) the six-arm (or three-phase) topology and (b) the proposed seven-arm (or four-phase) topology.

Fig. 6.1b presents the proposed seven-arm direct AC-AC MMC topology, which can help to increase the power density or reduce the overall dimensioning of the direct AC-AC *Modular Multilevel Converter* (MMC) for equal three-phase and single-phase frequency operation ($f_b = f_a$) by introducing an additional 7th arm (or 4th phase) in the conventional six-arm (or three-

phase) MMC (also see Fig. 6.1a). The proposed 7th arm topology can play a significant role in the equal frequency operation of MMC and could be omitted for unequal frequency operations.

6.1 Performance Analysis of the Conventional Six-Arm Direct AC-AC MMC

As proved in Section 2.4, only arm energy balancing Method-7 and Method-12 are found stable, which does not inject harmonics into both source and load currents (also see Fig. 4.1). Thus, these methods are the only practical solutions to be selected in the normal condition for equal frequency operations. Referring to Appendix A.6 and Appendix A.8, (6.1) to (6.6) present the average of the instantaneous arm power equations of the six-arm MMC (also see from (2.17) to (2.22)) for the arm energy balancing Method-7 or Method-12. In the steady state, all average arm powers should equal zero for the average of all arm energies to be regulated. Solving (6.2) to (6.4) tells that the manipulated inputs i_{bd+}, and $I^{b}_{b\alpha\beta}$ are zero. In other words, i_{bd+} and $I^{b}_{b\alpha\beta}$ only need to compensate for the system losses in the steady state. (6.5) and (6.6) do not contain the average power terms due to i_{bd+}, and $I^{b}_{b\alpha\beta}$ because they are zero in the steady state.

$$\overline{p_{\Sigma 0}} = -\frac{V_b I^{b}_{b}}{3} + \frac{\sqrt{2}\, V_a\, i_{ad+}}{2} = 0 \tag{6.1}$$

$$\overline{P_{\Delta 0}} = -\sqrt{2}\, V_a\, i_{bd+} \overline{-v_{a\alpha}\, i^{b}_{b\alpha} - v_{a\beta}\, i^{b}_{b\beta}} = 0 \tag{6.2}$$

$$\overline{P_{\Sigma \alpha}} = V_b\, I^{b}_{b\alpha} + \overline{v_b\, i_{bd+} \cos(\theta_a)} = 0 \tag{6.3}$$

$$\overline{P_{\Sigma \beta}} = V_b\, I^{b}_{b\beta} + \overline{v_b\, i_{bd+} \sin(\theta_a)} = 0 \tag{6.4}$$

$$\overline{P_{\Delta \alpha}} = -\left(\frac{V_b\, i_{aq+}}{2\sqrt{2}} - \frac{2}{3} V_a\, I^{\perp b}_{b}\right) \sin(\phi_b) - \left(\frac{V_b}{2\sqrt{2}}\, i_{ad+} - \frac{2}{3} V_a\, I^{b}_{b}\right) \cos(\phi_b) - 2\, V_{cm}\, I^{cm}_{b\alpha} = 0 \tag{6.5}$$

$$\overline{P_{\Delta \beta}} = -\left(\frac{V_b\, i_{aq+}}{2\sqrt{2}} - \frac{2}{3} V_a\, I^{\perp b}_{b}\right) \cos(\phi_b) + \left(\frac{V_b}{2\sqrt{2}}\, i_{ad+} - \frac{2}{3} V_a\, I^{b}_{b}\right) \sin(\phi_b) - 2\, V_{cm}\, I^{cm}_{b\beta} = 0 \tag{6.6}$$

On the other hand, the manipulated input $I^{cm}_{b\alpha\beta}$ has to compensate for the additional average power terms due to the three-phase and single-phase active (P_a, P_b) and reactive (Q_a, Q_b) power components (also see (6.5) and (6.6)) along with the system losses. The additional average power terms in (6.5) and (6.6) only exist because the three-phase and single-phase frequencies are the same ($f_b = f_a$). (6.7) and (6.8) represent (6.5) and (6.6) using variables: P_a, P_b, Q_a, and Q_b.

The average power term due to P_a and P_b can be canceled out if the single-phase voltage magnitude is twice the three-phase line to neutral voltage magnitude ($V_b = 2V_a$) because $P_a = P_b$ in the steady state.

$$\overline{P_{\Delta\alpha}} = \frac{2}{3}\frac{V_a}{V_b}\left(\frac{1}{4}\left(\frac{V_b}{V_a}\right)^2 Q_a + Q_b\right)\sin(\phi_b) - \frac{2}{3}\frac{V_a}{V_b}\left(\frac{1}{4}\left(\frac{V_b}{V_a}\right)^2 P_a - P_b\right)\cos(\phi_b) - 2\,V_{cm}\,I_{b\alpha}^{cm} = 0 \quad (6.7)$$

$$\overline{P_{\Delta\beta}} = \frac{2}{3}\frac{V_a}{V_b}\left(\frac{1}{4}\left(\frac{V_b}{V_a}\right)^2 Q_a + Q_b\right)\cos(\phi_b) + \frac{2}{3}\frac{V_a}{V_b}\left(\frac{1}{4}\left(\frac{V_b}{V_a}\right)^2 P_a - P_b\right)\sin(\phi_b) - 2\,V_{cm}\,I_{b\beta}^{cm} = 0 \quad (6.8)$$

$$\frac{1}{4}\left(\frac{V_b}{V_a}\right)^2 Q_a + Q_b = 0 \quad (6.9)$$

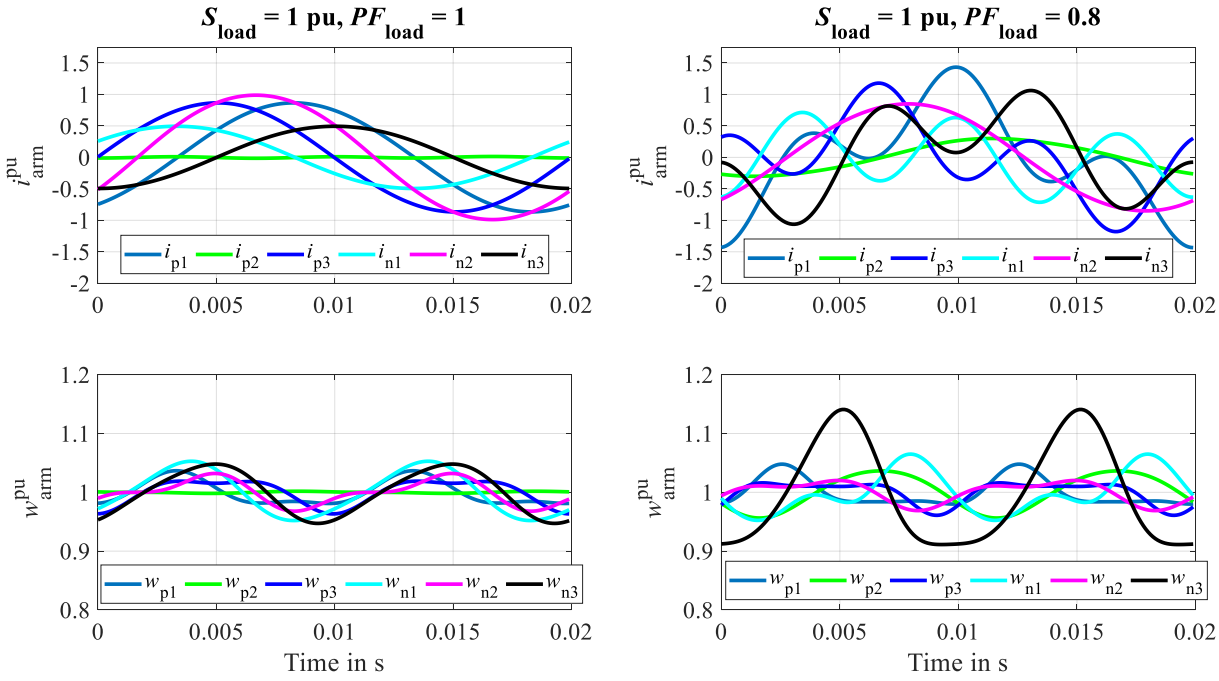

Figure 6.2: Performance analysis of the six arm MMC using the instantaneous arm currents (i_{arm}^{pu}) and energies (w_{arm}^{pu}) for unity load power factor (left) and 0.8 load power factor (right) at nominal load ($S_{load} = 1$) when the arm energies are regulated using Method-7 (Source = 3Ph and Load = 1Ph). Here, $f_a = f_b = 50$ Hz, $\phi_b = 60^o$.

Further, assuming $V_b = 2V_a$, the average power term due to Q_a and Q_b can be canceled out if $Q_a = -Q_b$. Suppose the grid code allows feeding the reactive power to the source; then the effect of the load reactive power can also be cancelled with the help of (6.9) and $I_{b\alpha\beta}^{cm}$ only need to compensate for the losses. But, if the grid code does not allow to supply of the reactive power to the source, then $I_{b\alpha\beta}^{cm}$ also needs to compensate for the additional average power term due to the load reactive power even if $V_b = 2V_a$. In this chapter, it is assumed that the grid code

demands the source reactive power equal to zero, which means $I^{cm}_{b\alpha\beta}$ will increase with the load reactive power for the equal frequency operation of direct AC-AC MMC.

The single-phase current (i_b), three-phase current (i_{a123}), and the circulating current in phase with v_{cm} (I^{cm}_{b123}) majorly decide the arm current magnitudes because $i_{bd+} \approx I^{b}_{b\alpha\beta} \approx 0$ (also see (4.1) to (4.5)) for the arm energy balancing Method-7 and Method-12. All figures below are obtained using the proposed analytical toolchain for the parameters in Table 5.1, expect ($V_b = 23$ kV) so that $V_b = 2V_a$. Fig. 6.2 shows the analytical results of the direct AC-AC MMC topology for equal frequency operation ($f_a = f_b = 50$ Hz) at nominal load ($S_{load} = 1$) for various load power factors when the arm energy balancing Method-7 (Source = 3Ph and Load = 1Ph) is used. Here, $V_b = 2V_a$, and the three-phase reactive power equals zero ($Q_a = 0$). The arm currents and energies are shown in the per-unit (pu) system. The arm currents in the pu system are obtained using (5.4). The base arm energy is kept equal to its reference command (W^{*}_{arm}).

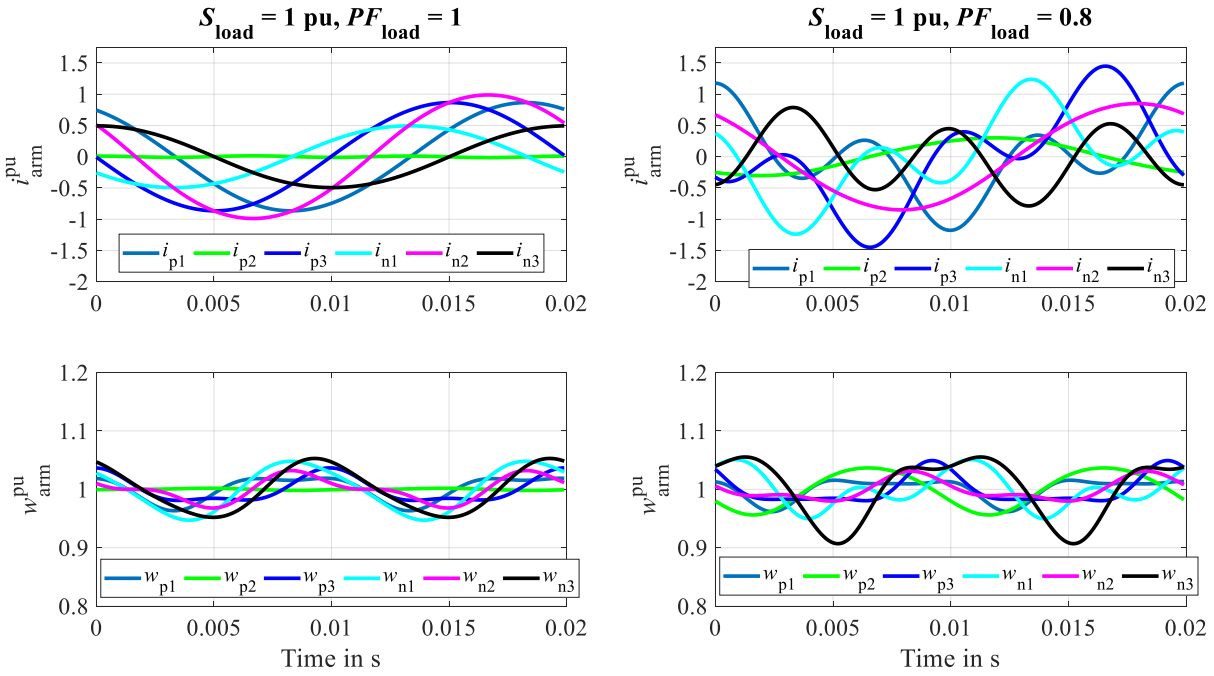

Figure 6.3: Performance analysis of the six arm MMC using the instantaneous arm currents (i^{pu}_{arm}) and energies (w^{pu}_{arm}) for unity load power factor (left) and 0.8 load power factor (right) at nominal load ($S_{load} = 1$) when the arm energies are regulated using Method-12 (Source = 1Ph and Load = 3Ph). Here, $V_b = 2V_a, f_a = f_b = 50$ Hz, $\phi_b = 60^{o}$.

As expected, the overall arm current magnitude is about 1 pu for the unity load power factor ($PF_{load} = 1$) because $I^{cm}_{b\alpha\beta} \approx 0$ if $Q_b = 0$, $Q_a = 0$, and $V_b = 2V_a$. But the overall arm current magnitude has increased significantly for the poor load power factor ($PF_{load} = 0.8$) because $I^{cm}_{b\alpha\beta}$

has to compensate for the additional average power term due to the single-phase reactive power (Q_b = 0.6 pu). The common-mode voltage magnitude is considered 0.45 pu with respect to the three-phase line to neutral voltage magnitude (V_{cm} = 0.45 V_a). The magnitude of v_{cm} can be further increased by increasing the number of submodules in an arm, but this would increase the converter dimensioning. As V_{cm} is significantly less than V_a, the magnitude of $I^{cm}_{b\alpha\beta}$ should be higher to compensate for the additional average power term due to Q_b. Thus, the overall arm current magnitude increases significantly for the poor load power factor condition. Further, the overall arm energy ripple also increased for the poor load power factor operation.

Similarly, Fig. 6.3 shows the direct AC-AC MMC analytical performance analysis ($f_a = f_b$ = 50 Hz) when the arm energies are regulated using Method-12 (Source = 1Ph and Load = 3Ph). Here, $V_b = 2V_a$, and $Q_b = 0$. The overall arm current magnitude and energy ripple have increased with the load reactive power (Q_a).

In conclusion, circulating currents in phase with v_{cm} ($I^{cm}_{b\alpha\beta}$) is a must for equal frequency operation ($f_a = f_b$) of direct AC-AC MMC. The magnitude of $I^{cm}_{b\alpha\beta}$ increases with the load reactive power, resulting in overall more arm current and energy ripple magnitudes. Thus, the dimensioning of the direct AC-AC MMC should be increased to guarantee safe operation during poor load power factor operations if the reactive power cannot be supplied to the source.

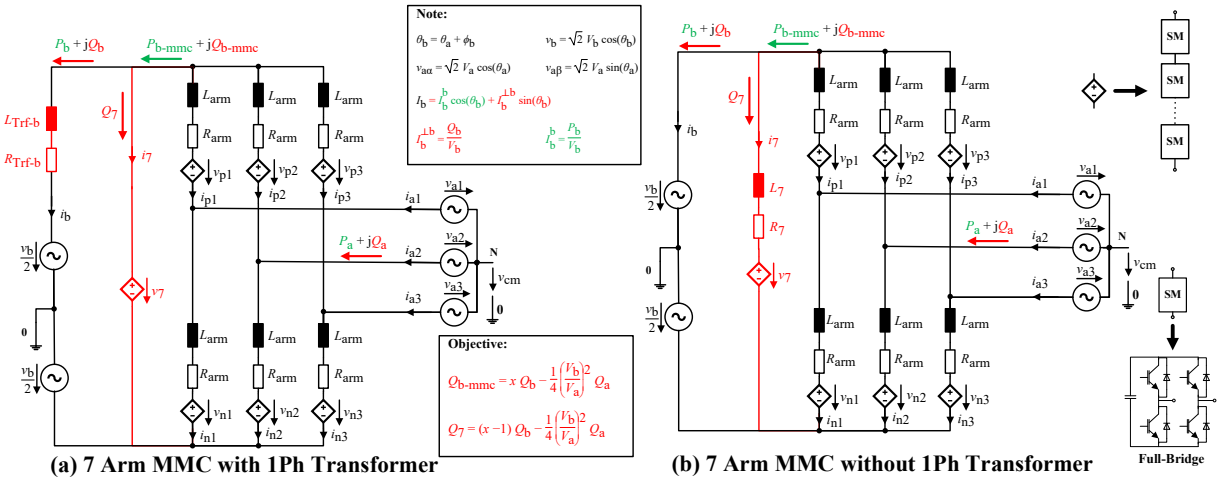

Figure 6.4: Proposed seven-arm (or four-phase) direct AC-AC MMC topology for equal frequency operation.

6.2 Performance Analysis of the Proposed Seven-Arm Direct AC-AC MMC

Fig. 6.4 shows the proposed seven-arm (or four-phase) direct AC-AC MMC topology that can also help realize (6.9) and increase the converter's power density. The 7th arm may not require an additional L-filter (also see Fig. 6.4a). The 7th arm energy can be regulated by controlling the six-arm MMC's output single-phase active power ($P_{\text{b-mmc}}$). The single-phase reactive power flowing through the six-arm MMC ($Q_{\text{b-mmc}}$) can be reduced with the help of an additional 7th arm or 4th phase. Reducing the single-phase reactive power flowing through the six-arm MMC can help to reduce the magnitude of $I^{\text{cm}}_{\text{b}\alpha\beta}$, and hence the power density of the six-arm MMC can be increased significantly. x defines the fraction of the single-phase reactive power (Q_{b}) that flows into the six-arm MMC ($Q_{\text{b-mmc}} = xQ_{\text{b}}$). The rest single-phase reactive power flows into the 7th arm or 4th phase ($Q_7 = (x - 1)\ Q_{\text{b}}$). Additionally, $Q_{\text{b-mmc}}$ consists of an additional term to compensate for the average power term due to the three-phase reactive power (Q_{a}), according to (6.9). The general expression of $Q_{\text{b-mmc}}$ and Q_7 are also shown in Fig. 6.4. (6.10) and (6.11) represent the modified average arm power expressions (6.7) and (6.8) of the six-arm direct AC-AC MMC for equal frequency operation.

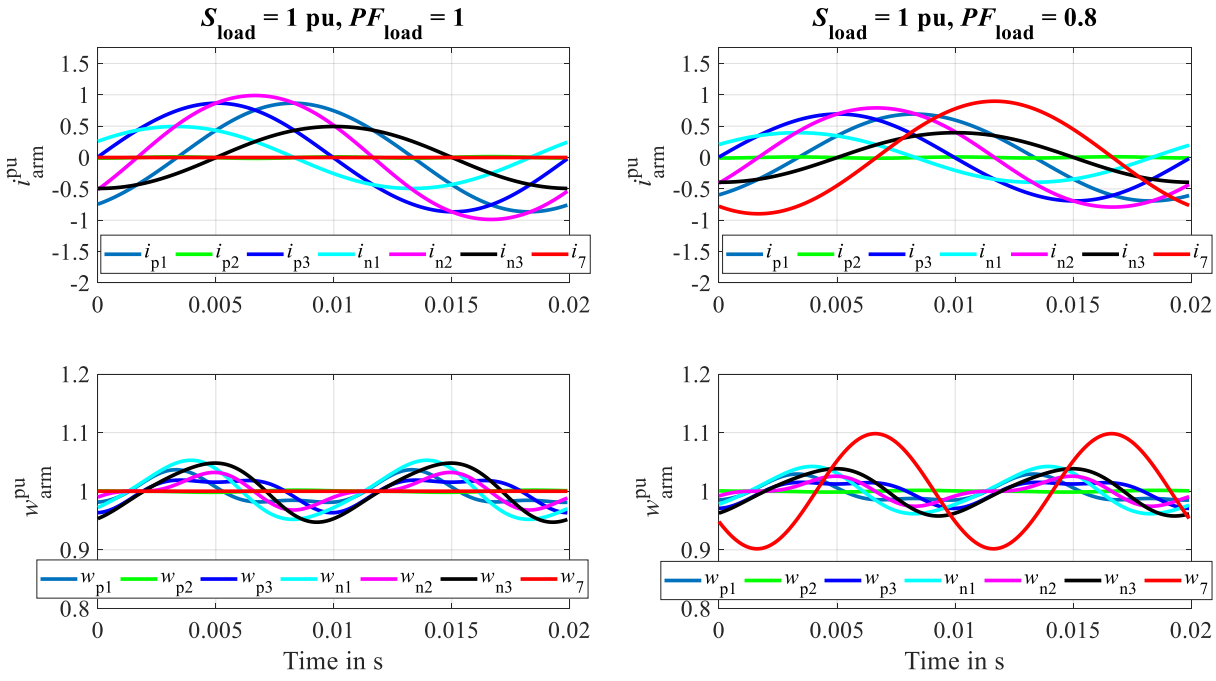

Figure 6.5: Performance analysis of the seven-arm MMC using the instantaneous arm currents ($i^{\text{pu}}_{\text{arm}}$) and energies ($w^{\text{pu}}_{\text{arm}}$) for unity load power factor (left) and 0.8 load power factor (right) at nominal load ($S_{\text{load}} = 1$) when the arm energies are regulated using Method-7 (Source = 3Ph and Load = 1Ph). Here, $x = 0$, $V_{\text{b}} = 2V_{\text{a}}$, $f_{\text{a}} = f_{\text{b}} = 50$ Hz, $\phi_{\text{b}} = 60^{\text{o}}$.

$$\overline{P_{\Delta\alpha}} = \frac{2\,V_{\text{a}}}{3\,V_{\text{b}}}\left(\frac{1}{4}\left(\frac{V_{\text{b}}}{V_{\text{a}}}\right)^2 Q_{\text{a}} + Q_{\text{b-mmc}}\right)\sin(\phi_{\text{b}}) - \frac{2\,V_{\text{a}}}{3\,V_{\text{b}}}\left(\frac{1}{4}\left(\frac{V_{\text{b}}}{V_{\text{a}}}\right)^2 P_{\text{a}} - P_{\text{b}}\right)\cos(\phi_{\text{b}}) - 2\,V_{\text{cm}}\,I^{\text{cm}}_{\text{b}\alpha} \quad (6.10)$$

$$\overline{P_{\Delta\beta}} = \frac{2\,V_a}{3\,V_b}\left(\frac{1}{4}\left(\frac{V_b}{V_a}\right)^2 Q_a + Q_{b\text{-}mmc}\right)\cos(\phi_b) + \frac{2\,V_a}{3\,V_b}\left(\frac{1}{4}\left(\frac{V_b}{V_a}\right)^2 P_a - P_b\right)\sin(\phi_b) - 2\,V_{cm}\,I_{b\beta}^{cm} \quad (6.11)$$

Fig. 6.5 shows the analytical results of the seven-arm direct AC-AC MMC topology for equal frequency operation ($f_a = f_b = 50$ Hz) at nominal load for various load power factors when the arm energy balancing Method-7 (Source = 3Ph and Load = 1Ph) is used. Here, $V_b = 2V_a$, the source reactive power equals zero ($Q_a = 0$), and the 7th arm supplies full load reactive power ($x = 0$). In contrast to the six-arm MMC topology (also see Fig. 6.2), the overall arm current and energy ripple magnitude is reduced for the six-arm MMC when the 7th arm supplies the full single-phase load reactive power ($x = 0$). The 7th arm energy ripple is high because the total load reactive power ($Q_b = -Q7 = 0.6$ pu) flows into the 7th arm. The 7th arm energy ripple can be further reduced by increasing its submodule's DC-link capacitance value.

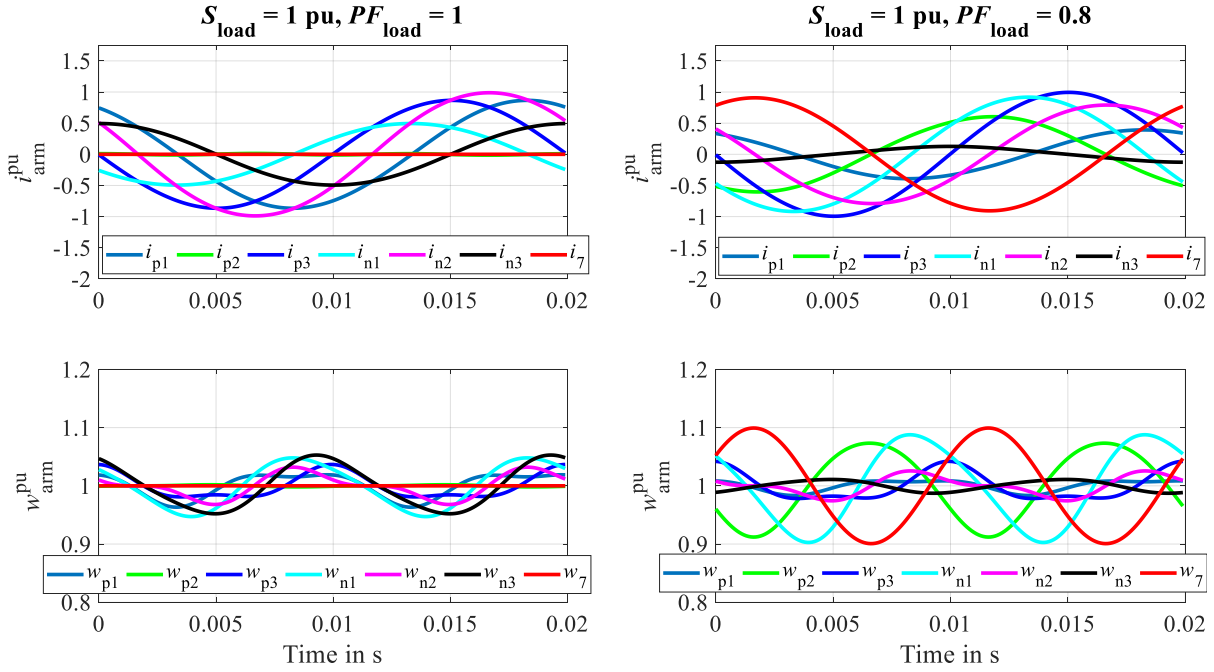

Figure 6.6: Performance analysis of the seven-arm MMC using the instantaneous arm currents (i_{arm}^{pu}) and energies (w_{arm}^{pu}) for unity load power factor (left) and 0.8 load power factor (right) at nominal load ($S_{load} = 1$) when the arm energies are regulated using Method-12 (Source = 1Ph and Load = 3Ph). Here, $x = 0$, $V_b = 2V_a$, $f_a = f_b = 50$ Hz, $\phi_b = 60^o$.

Similarly, Fig. 6.6 presents the analytical results of the seven-arm direct AC-AC MMC topology for equal frequency operation ($f_a = f_b = 50$ Hz) at nominal load for various load power factors when the arm energy balancing Method-12 (Source = 1Ph and Load = 3Ph) is used. As expected, the overall six-arm MMC current magnitude is reduced using the proposed seven-arm MMC topology. But the overall six-arm MMC energy ripple is increased because

additional single-phase reactive power ($Q_{\text{b-mmc}}$) flows through the six-arm MMC (also see (6.9)) to cancel the additional average power term in (6.10) and (6.11) due to Q_{a}. Generally, the arm energy ripple increases if more reactive (Q_{a} and $Q_{\text{b-mmc}}$) flows within the six-arm MMC [KOL15a]. As the single-phase load reactive power equals zero ($Q_{\text{b}} = 0$), reactive power flowing to the 7th arm (Q_7) equals $Q_{\text{b-mmc}}$ ($Q_7 = Q_{\text{b-mmc}}$).

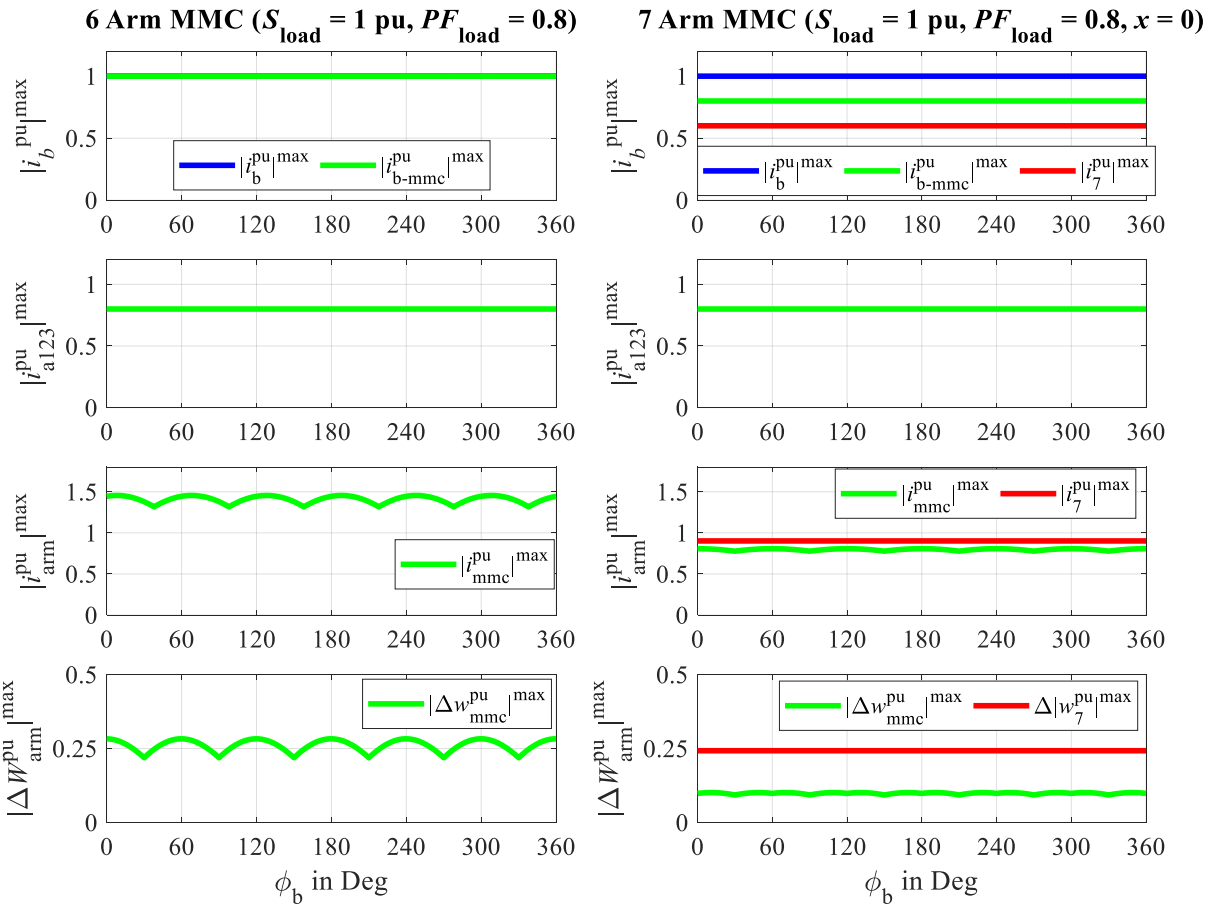

Figure 6.7: Performance analysis of the six-arm (left) and seven-arm (right) MMC topologies using various current magnitudes and energy ripples for 0.8 load power factor at nominal load ($S_{\text{load}} = 1$) when the arm energies are regulated using Method-7 (Source = 3Ph and Load = 1Ph). Here, $x = 0$, $V_{\text{b}} = 2V_{\text{a}}$, $f_{\text{a}} = f_{\text{b}} = 50$ Hz, ϕ_{b} = Varying.

6.3 Performance Comparison of the Conventional Six-Arm and Proposed Seven-Arm Direct AC-AC MMC

Fig. 6.7 shows the performance analysis for the six-arm and seven-arm direct AC-AC MMC for all possible values of ϕ_{b} ($= \theta_{\text{b}} - \theta_{\text{a}}$) when the arm energy balancing Method-7 (Source 3Ph and Load = 1Ph) is used. Here, $Q_7 = -Q_{\text{b}}$ ($x = 0$), $f_{\text{a}} = f_{\text{b}} = 50$ Hz, $V_{\text{b}} = 2V_{\text{a}}$, $S_{\text{load}} = 1$, $PF_{\text{load}} = 0.8$, and $Q_{\text{a}} = 0$. Fig. 6.8 illustrates the definition of the six-arm MMC's maximum arm current magnitude ($|i_{\text{mmc}}^{\text{pu}}|^{\text{max}}$), the 7th arm current magnitude ($|i_7^{\text{pu}}|^{\text{max}}$), the six-arm MMC's

maximum arm energy ripple ($|w_{mmc}^{pu}|^{max}$), and the 7th arm energy ripple ($|w_7^{pu}|^{max}$). Fig. 6.7 suggests that the six-arm MMC's maximum arm current magnitude ($|i_{mmc}^{pu}|^{max}$) and energy ripple ($|w_{mmc}^{pu}|^{max}$) has reduced significantly using the proposed seven-arm MMC topology. Further, $|i_{mmc}^{pu}|^{max}$ is found to vary with ϕ_b for the six-arm MMC topology because of the non-zero value of $I_{b\alpha\beta}^{cm}$. In contrast, variation of $|i_{mmc}^{pu}|^{max}$ with ϕ_b is negligible for the proposed seven-arm MMC topology.

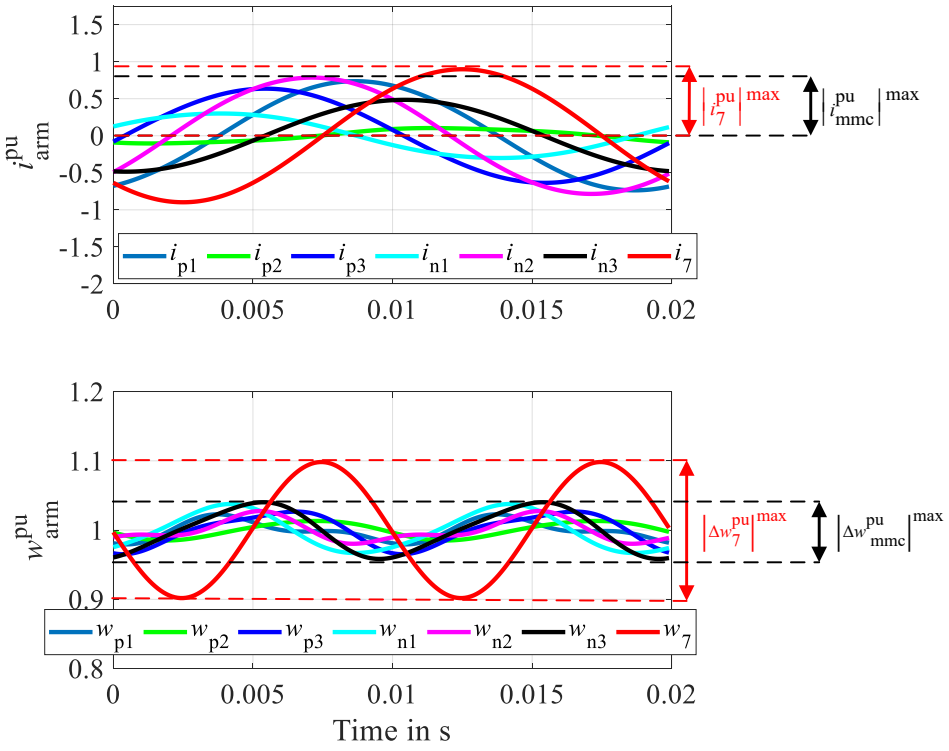

Figure 6.8: Arm currents and energy ripples magnitude definitions.

Similarly, Fig. 6.9 shows the analytical results of the proposed seven-arm MMC when the full (x = 0) and half (x = 0.5) single-phase reactive power (Q_b) is supplied by the 7th arm using the arm energy balancing Method-7. Here, $V_b = 2V_a$, $S_{load} = 1$, $PF_{load} = 0.8$, and $Q_a = 0$. Sharing the load reactive power by the 7th arm and six-arm MMC can help to reduce the current and energy ripple magnitudes of the 7th arm. But the magnitude of $|i_{mmc}^{pu}|^{max}$ and $|w_{mmc}^{pu}|^{max}$ has increased slightly when a fraction (50%) of Q_b flows into the six-arm MMC.

Fig. 6.10 presents the performance analysis for the six-arm and seven-arm direct AC-AC MMC for all possible values of ϕ_b (= $\theta_b - \theta_a$) when the arm energy balancing Method-12 (Source 1Ph and Load = 3Ph) is used. Here, $x = 0$, $f_a = f_b = 50$ Hz, $V_b = 2V_a$, $S_{load} = 1$, $PF_{load} = 0.8$, and $Q_b = 0$. The magnitude of $|i_{mmc}^{pu}|^{max}$ is reduced significantly using the proposed seven-arm direct

AC-AC MMC topology. But the magnitude of $|w_{\text{mmc}}^{\text{pu}}|^{\text{max}}$ has increased because more reactive power ($Q_{\text{b-mmc}}$ and Q_{a}) flows into the six-arm MMC.

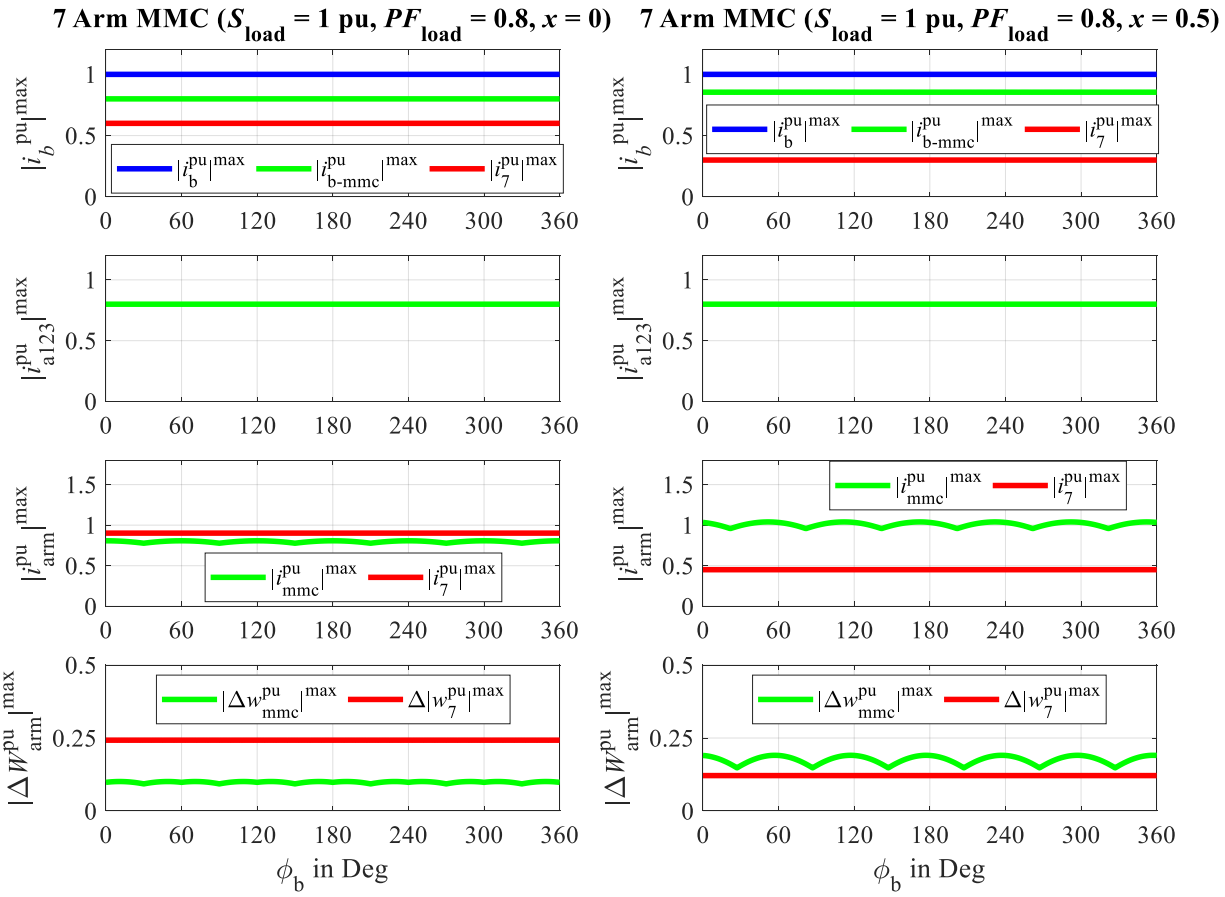

Figure 6.9: Performance analysis of the proposed seven-arm MMC topology when the full (left: $x = 0$) and half (right: $x = 0.5$) single-phase load reactive power (Q_{b}) is supplied by the 7$^{\text{th}}$ arm for $PF_{\text{load}} = 0.8$ using the arm energy regulation Method-7 (Source = 3Ph and Load = 1Ph). Here, $V_{\text{b}} = 2V_{\text{a}}$, $f_{\text{a}} = f_{\text{b}} = 50$ Hz, ϕ_{b} = Varying.

Fig. 6.11 shows the performance analysis for the six-arm and seven-arm direct AC-AC MMC for varying load power factor (PF_{load} = varying) at nominal load ($S_{\text{load}} = 1$) when the arm energy balancing Method-7 (Source 3Ph and Load = 1Ph) is used. Here, $x = 0$, $f_{\text{a}} = f_{\text{b}} = 50$ Hz, $\phi_{\text{b}} = 60^{\text{o}}$, $V_{\text{b}} = 2V_{\text{a}}$, and $Q_{\text{a}} = 0$. The values of $|i_{\text{mmc}}^{\text{pu}}|^{\text{max}}$ and $|w_{\text{mmc}}^{\text{pu}}|^{\text{max}}$ reduces linearly with PF_{load} when the load reactive power is supplied entirely from the 7$^{\text{th}}$ arm ($x = 0$). As the 7$^{\text{th}}$ arm supplies the full single-phase load reactive power, the 7$^{\text{th}}$ arm current magnitude is high (1 pu with respect to $I_{\text{b}}^{\text{base}}$ and 1.5 pu with respect to $I_{\text{arm}}^{\text{base}}$) at $PF_{\text{load}} = 0$. The results suggest that the dimensioning of the six-arm MMC can be reduced significantly with the proposed 7$^{\text{th}}$ arm topology, but the 7$^{\text{th}}$ arm should be dimensioned so that full single-phase current magnitude can flow through it.

In case one wishes to use the same submodules for the 7th arm and six-arm MMC, then Q_b can be shared by both the 7th arm and six-arm MMC (as shown in Fig. 6.12) so that the stress on the 7th arm is reduced. The 7th arm current and energy ripple magnitudes are reduced to half, and the values of $|i_{mmc}^{pu}|^{max}$ and $|w_{mmc}^{pu}|^{max}$ are increased. Further, sharing reactive power by the 7th arm and six-arm MMC helps to utilize the submodules to the fullest for all load conditions. Therefore, the proposed seven-arm direct AC-AC MMC provides various degrees of freedom to design and control the converter. And it can help reduce the overall system cost and dimensioning with additional degrees of freedom.

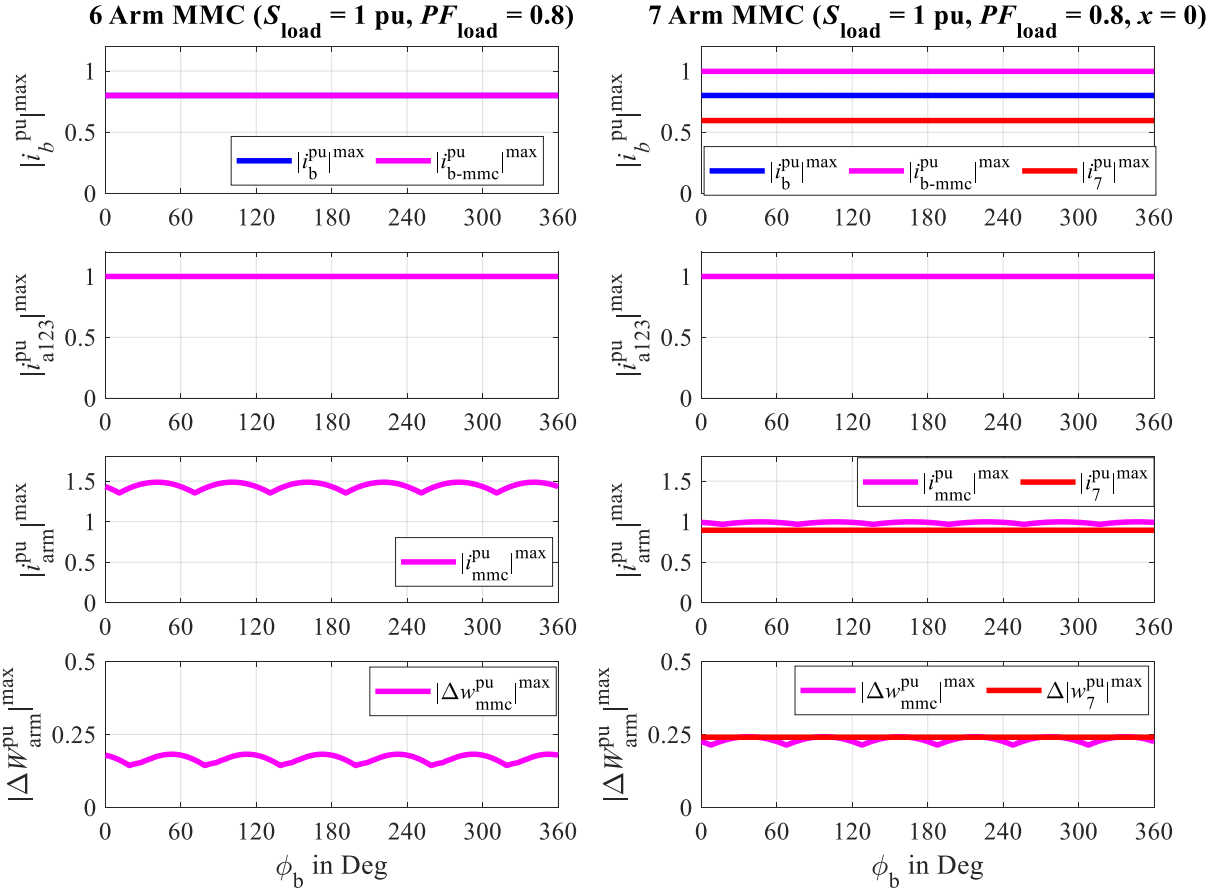

Figure 6.10: Performance analysis of the six-arm (left) and seven-arm (right) MMC topologies using various current magnitudes and energy ripples for 0.8 load power factor at nominal load (S_{load} = 1) when the arm energies are regulated using Method-12 (Source = 1Ph and Load = 3Ph). Here, x = 0, $V_b = 2V_a$, $f_a = f_b$ = 50 Hz, ϕ_b = Varying.

Fig. 6.11 and Fig. 6.12 suggest that the current stress of each submodule of the six-arm MMC is reduced by about (1.59 − 1) = 0.59 pu (in total 0.59x6xN = 3.54N pu for the six-arm MMC) using an additional 7th arm. The 7th arm can be realized using (a) 1.5N pu (if x = 0) or (b) 0.75N pu (if x = 0.5) out of the saved 3.54N pu current, resulting in total (a)

(3.54 − 1.5)/(6x1.59) = 21.38 % (if x = 0) or (b) (3.54 − 0.75)/(6x1.59) = 29.25 % (if x = 0.5) current requirement reduction for the entire proposed seven-arm MMC topology if Method-7 is used.

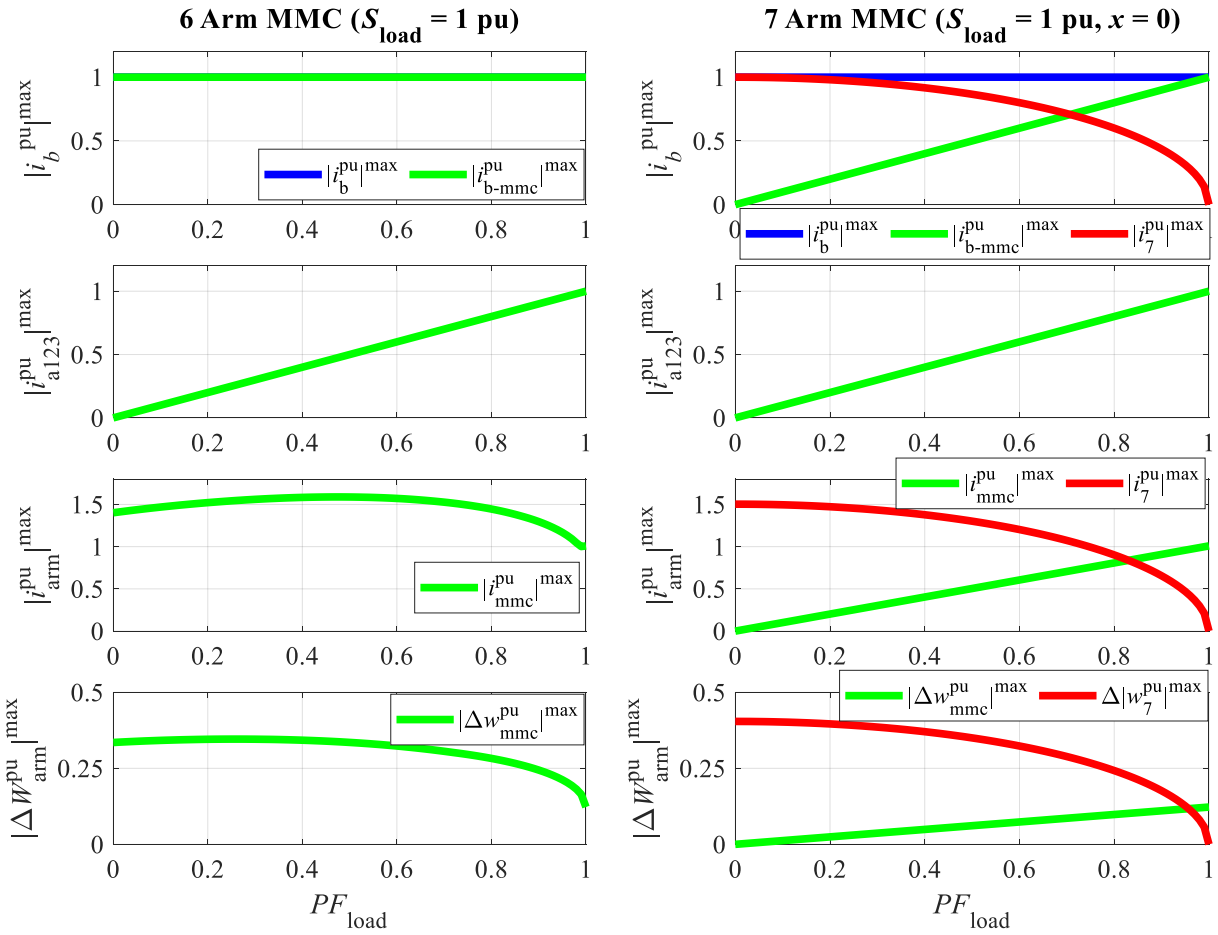

Figure 6.11: Performance analysis of the six-arm (left) and seven-arm (right) MMC topologies using various current magnitudes and energy ripple for varying load power factor at nominal load (S_{load} = 1) when the arm energies are regulated using Method-7 (Source = 3Ph and Load = 1Ph). Here, $V_b = 2V_a$, $f_a = f_b$ = 50 Hz, ϕ_b = 60°.

Fig. 6.13 shows the performance analysis for the six-arm and seven-arm direct AC-AC MMC for varying load power factor (PF_{load} = varying) at nominal load (S_{load} = 1) when the arm energy balancing Method-12 (Source 1Ph and Load = 3Ph) is used. Here, x = 0, $f_a = f_b$ = 50 Hz, ϕ_b = 60°, $V_b = 2V_a$, and Q_a = 0. The magnitude of $|i_{mmc}^{pu}|^{max}$ is reduced significantly, but the magnitude of $|w_{mmc}^{pu}|^{max}$ is increased because $Q_{b\text{-}mmc}$ is used to cancel the average power term in (6.10) and (6.11) due to Q_a. Thus, more reactive power flows into the six-arm MMC, resulting in higher energy ripple. Additionally, the current rating of the 7th arm should be more so that the full single-phase current magnitude can flow through it. Similarly, the proposed seven-arm

MMC topology reduces about 20.63% of current requirement for the entire system if Method-12 is used.

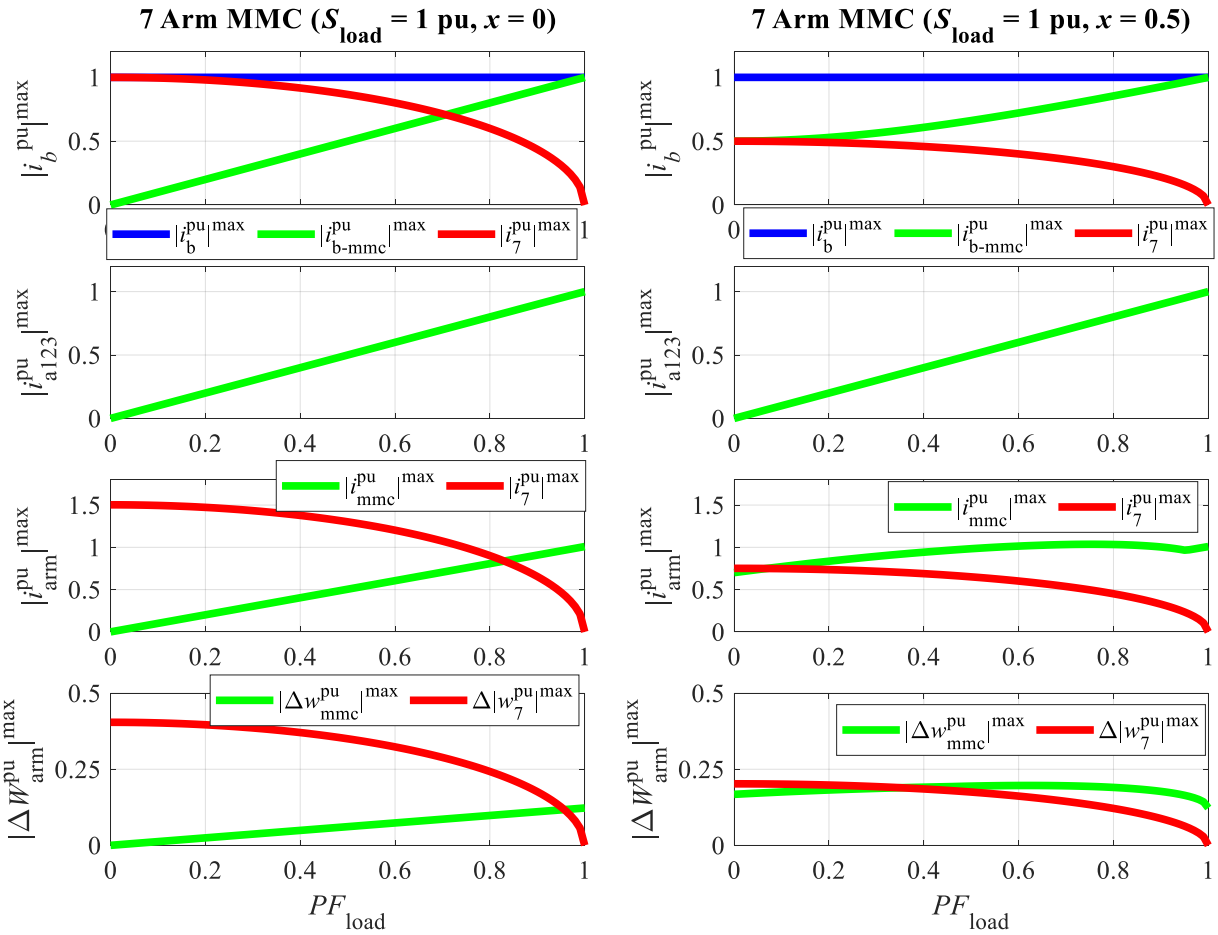

Figure 6.12: Performance analysis of the proposed seven-arm MMC topology when the full (left: $x = 0$) and half (right: $x = 0.5$) single-phase load reactive power (Q_b) is supplied by the 7th arm for varying load power factor at nominal load ($S_{load} = 1$) using the arm energy regulation Method-7 (Source = 3Ph and Load = 1Ph). Here, $V_b = 2V_a$, $f_a = f_b = 50$ Hz, $\phi_b = 60^o$.

In conclusion, the proposed seven-arm direct AC-AC MMC provides an additional degree of freedom (i_7 or Q_7) which can help to reduce the current stress on the six-arm MMC by sharing the single-phase reactive power (Q_b) and compensating the average power term in (6.10) and (6.11) due to the three-phase reactive power (Q_a) according to (6.9). Further, the 7th arm enables the six-arm MMC to balance its energy by injecting harmonics into the zero-sequence circulating current without injecting harmonics into the actual single-phase system. In other words, along with the two energy balancing methods (Method-7 and 12), an additional four methods (Method-14, 15, 21, and 22) are stable for equal frequency operation, which does not inject harmonics into both source and load. Also, the overall cost can be reduced, or the converter's power density can be increased using the seven-arm direct AC-AC MMC topology.

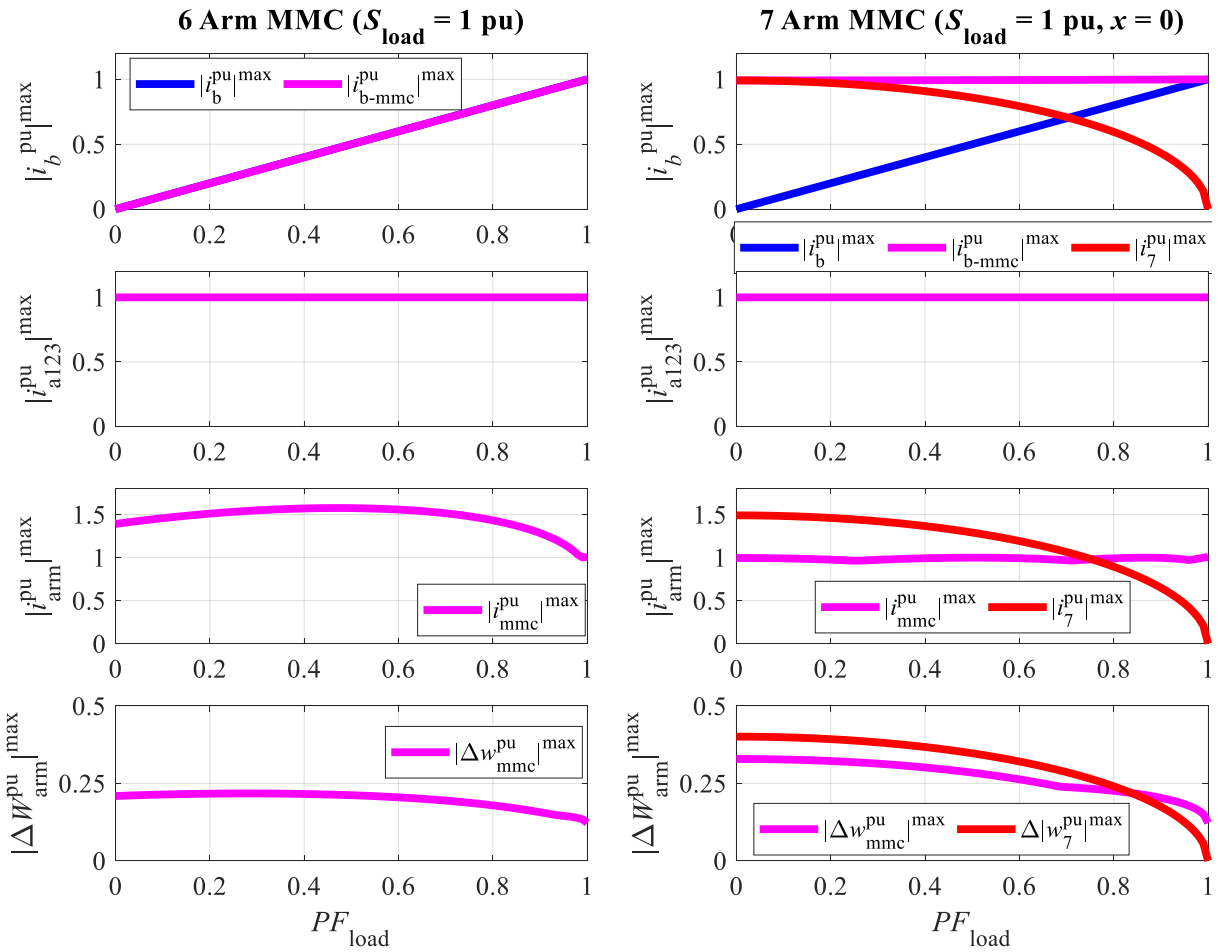

Figure 6.13: Performance analysis of the six-arm (left) and seven-arm (right) MMC topologies using various current magnitudes and energy ripple for varying load power factor at nominal load ($S_{load} = 1$) when the arm energies are regulated using Method-12 (Source = 1Ph and Load = 3Ph). Here, $V_b = 2V_a$, $f_a = f_b = 50$ Hz, $\phi_b = 60^o$.

7 Conclusion

Modular Multilevel converter (MMC) finds applications in medium and high voltage industries due to its modular structure. One side of MMC is connected to a three-phase system, and another side is connected to a single-phase system. The MMC can be used for single-phase DC to three-phase AC (DC-AC) and single-phase AC to three-phase AC (AC-AC) applications. The AC-AC MMC converter can operate with equal single-phase (f_b) and three-phase (f_a) frequencies ($f_b = f_a$) or unequal single-phase and three-phase frequencies ($f_b \neq f_a$).

MMC provides numerous *Degrees of Freedom* (DOF) to regulate six arm energies of MMC. The general arm power equations are derived in the αβ0-frame. This work has identified all possible degrees of freedom which can help to regulate the arm energies of MMC. Further, all possible arm energy regulation methods are derived by finding all suitable combinations of six degrees of freedom to balance the six arm energies of MMC. The stability of all these methods for different single-phase and three-phase system frequencies is presented mathematically. An analytical toolchain is proposed to mathematically analyze the performance of a stable arm energy regulation method during various normal and abnormal conditions. The proposed toolchain also facilitates quickly analyzing and comparing the performance of MMC for various stable arm energy balancing techniques, saving time and money.

It is found that the arm energies of MMC can be regulated in 48 ways. Here, the neutral point of the three-phase voltage is considered floating. Only four out of 48 energy balancing methods are possible, which do not inject harmonics into both source and load currents. Rest all methods injects harmonics to the source or both source and load currents. All energy balancing methods without current components in phase with the common-mode voltage are unstable because of the coupling between the manipulated inputs. Therefore, the common-mode voltage is vital for the stable operation of MMC for equal frequency operation. Among these four energy balancing methods, only two arm energy balancing methods (one when three-phase is source and one when single-phase is source) are stable for equal frequency operation. In contrast, all methods are stable for unequal frequency operation, and the manipulated inputs are naturally decoupled.

The arm voltages and currents are transformed into the summation (Σ) and difference (Δ) systems to design the current controllers of MMC. The summation and difference systems decouple the circulating and three-phase current controllers. The summation system only affects the circulating and single-phase currents, and the difference system only affects the three-phase currents. The current controllers of MMC are designed into both continuous-time and discrete-time domains. The direct discrete-time plant model is assumed to be the most accurate discrete-time model. But it is shown here that even a direct discrete-time plant model cannot represent the actual system because of the limitation to accurately sampling the average voltage at *Point of Common Coupling* (PCC) from the existing PWM-based converters. A deadbeat-based observer is proposed to minimize the direct discrete-time plant model error, which can help tune the current controller's closed-loop bandwidth accurately to a desired bandwidth. The accuracy of the proposed current controllers is validated using the closed-loop bode or command tracking plot.

A generalized step is proposed to design six average arm energy controllers of MMC for a selected arm energy-regulated method for various single-phase and three-phase system frequencies. The average energy controllers introduce a significant delay in the system due to mean computation. This huge delay does not allow to accurately tune the closed-loop bandwidth of the proposed average arm energy controllers using derived PI tuning expressions. But the proposed hit-and-trial method can adjust the closed-loop bandwidth of the proposed average arm energy controllers to a desired value. Command tracking plots for various single-phase and three-phase system frequencies are presented in this work.

The performance analysis of the discussed arm energy regulation techniques for various single-phase and three-phase system frequencies at different load conditions are presented, analyzed, and compared using simulation and analytical results. For equal frequency operation, the arm current magnitude increases with the reactive load power because the reactive load power current component makes an additional average power ($\overline{p_{\Delta\alpha\beta}}$) that must be compensated using corresponding manipulated inputs ($MI_{5\&6}$). A strategy to compensate for this additional average arm power using the source reactive power current component is proposed. The proposed load reactive power compensation significantly reduces the arm current magnitude by slightly increasing the source current magnitude.

Reducing the arm current stress by compensating the load reactive power using the source reactive power is only feasible if the source allows reactive power through it. If the source does not allow reactive power to flow through it, the proposed seven-arm direct AC-AC MMC

topology can help significantly reduce the current stress of the six-arm MMC. The additional 7^{th} arm can share the single-phase reactive power and help compensate for the three-phase reactive power to reduce the arm's current magnitude. Further, the overall dimensioning of the system can be reduced, or the power rating of the converter can be increased using the proposed seven-arm topology for equal frequency operation. The proposed seven-arm MMC could be redundant for unequal frequency operations.

Unlike equal frequency operation, the arm current magnitude is unaffected by the load reactive power change for unequal frequency operation because the manipulated inputs and systems are naturally decoupled. Hence the arm current magnitude is majorly decided by the active load power because manipulated inputs only need to compensate for the losses in the system. But the arm energy ripple increases with the load reactive power increase for equal or unequal frequency operations.

Bibliography

[AKA10] H. Akagi, "Classification, terminology, and application of the modular multilevel cascade converter (MMCC)," The 2010 International Power Electronics Conference - ECCE ASIA -, Sapporo, Japan, 2010, pp. 508-515, doi: 10.1109/IPEC.2010.5543243.

[AKA17] H. Akagi, "Multilevel Converters: Fundamental Circuits and Systems," in Proceedings of the IEEE, vol. 105, no. 11, pp. 2048-2065, Nov. 2017, doi: 10.1109/JPROC.2017.2682105.

[ALL08] S. Allebrod, R. Hamerski and R. Marquardt, "New transformerless, scalable Modular Multilevel Converters for HVDC-transmission," 2008 IEEE Power Electronics Specialists Conference, Rhodes, Greece, 2008, pp. 174-179, doi: 10.1109/PESC.2008.4591920.

[ANT09] A. Antonopoulos, L. Angquist and H. -P. Nee, "On dynamics and voltage control of the Modular Multilevel Converter," 2009 13th European Conference on Power Electronics and Applications, Barcelona, Spain, 2009, pp. 1-10.

[ÄNG11a] L. Angquist, A. Antonopoulos, D. Siemaszko, K. Ilves, M. Vasiladiotis and H. -P. Nee, "Open-Loop Control of Modular Multilevel Converters Using Estimation of Stored Energy," in IEEE Transactions on Industry Applications, vol. 47, no. 6, pp. 2516-2524, Nov.-Dec. 2011, doi: 10.1109/TIA.2011.2168593.

[ÄNG10] L. Ängquist, A. Antonopoulos, D. Siemaszko, K. Ilves, M. Vasiladiotis and H. -P. Nee, "Inner control of Modular Multilevel Converters - An approach using open-loop estimation of stored energy," The 2010 International Power Electronics Conference - ECCE ASIA -, Sapporo, Japan, 2010, pp. 1579-1585, doi: 10.1109/IPEC.2010.5544607.

[ÄNG11b] L. Ängquist, A. Haider, H. -P. Nee and H. Jiang, "Open-loop approach to control a Modular Multilevel Frequency Converter," Proceedings of the 2011 14th European Conference on Power Electronics and Applications, Birmingham, UK, 2011, pp. 1-10.

[BAR11a] L. Baruschka and A. Mertens, "Comparison of Cascaded H-Bridge and Modular Multilevel Converters for BESS application," 2011 IEEE Energy Conversion Congress and Exposition, Phoenix, AZ, USA, 2011, pp. 909-916, doi: 10.1109/ECCE.2011.6063868.

[BAR11b] L. Baruschka and A. Mertens, "A new 3-phase AC/AC modular multilevel converter with six branches in hexagonal configuration," 2011 IEEE Energy Conversion Congress and Exposition, Phoenix, AZ, USA, 2011, pp. 4005-4012, doi: 10.1109/ECCE.2011.6064314.

[BAR11c] L. Baruschka and A. Mertens, "A new 3-phase direct modular multilevel converter," Proceedings of the 2011 14th European Conference on Power Electronics and Applications, Birmingham, UK, 2011, pp. 1-10.

[BAR13] L. Baruschka and A. Mertens, "A New Three-Phase AC/AC Modular Multilevel Converter With Six Branches in Hexagonal Configuration," in IEEE Transactions on Industry Applications, vol. 49, no. 3, pp. 1400-1410, May-June 2013, doi: 10.1109/TIA.2013.2252593.

[BAR14] L. Baruschka, D. Karwatzki, M. von Hofen and A. Mertens, "Low-speed drive operation of the modular multilevel converter Hexverter down to zero frequency," 2014 IEEE Energy Conversion Congress and Exposition (ECCE), Pittsburgh, PA, USA, 2014, pp. 5407-5414, doi: 10.1109/ECCE.2014.6954142.

[BÄR12] H. Bärnklau, A. Gensior and S. Bernet, "Derivation of an equivalent submodule per arm for modular multilevel converters," 2012 15th International Power Electronics and Motion Control Conference (EPE/PEMC), Novi Sad, Serbia, 2012, pp. LS2a.2-1-LS2a.2-5, doi: 10.1109/EPEPEMC.2012.6397407.

[BEC21] Sofia Becker, Thilo Becker,…, "EUROPEAN MOBILITY ATLAS: Facts and Figures about Transport and Mobility in Europe Facts and figures about transport," Heinrich-Böll-Stiftung European Union, Brussels, Belgium, February 2021

[BER12] G. Bergna et al., "Modular Multilevel Converter leg-energy controller in rotating reference frame for voltage oscillations reduction," 2012 3rd IEEE International Symposium on Power Electronics for Distributed Generation Systems (PEDG), Aalborg, Denmark, 2012, pp. 698-703, doi: 10.1109/PEDG.2012.6254078.

[BES16] L. Bessegato, L. Harnefors, K. Ilves, S. Norrga and S. Östlund, "Control of direct AC/AC modular multilevel converters using capacitor voltage estimation," 2016 18th European Conference on Power Electronics and Applications (EPE'16 ECCE Europe), Karlsruhe, Germany, 2016, pp. 1-9, doi: 10.1109/EPE.2016.7695319.

[BRI20] F. Briz, M. W. Degner and R. D. Lorenz, "Analysis and design of current regulators using complex vectors," in IEEE Transactions on Industry Applications, vol. 36, no. 3, pp. 817-825, May-June 2000, doi: 10.1109/28.845057.

[CEB11] S. Ceballos, J. Pou, Sanghun Choi, M. Saeedifard and V. Agelidis, "Analysis of voltage balancing limits in modular multilevel converters," IECON 2011 - 37th Annual Conference of the IEEE Industrial Electronics Society, Melbourne, VIC, Australia, 2011, pp. 4397-4402, doi: 10.1109/IECON.2011.6120032.

[DEB15] S. Debnath, J. Qin, B. Bahrani, M. Saeedifard and P. Barbosa, "Operation, Control, and Applications of the Modular Multilevel Converter: A Review," in IEEE Transactions on Power Electronics, vol. 30, no. 1, pp. 37-53, Jan. 2015, doi: 10.1109/TPEL.2014.2309937.

[DIE20] R. Dierks, J. Kucka and A. Mertens, "Using Both the Circulating Currents and the Common-Mode Voltage for the Branch Energy Control of Modular Multilevel Converters," 2020 22nd European Conference on Power Electronics and Applications (EPE'20 ECCE Europe), Lyon, France, 2020, pp. P.1-P.10, doi: 10.23919/EPE20ECCEEurope43536.2020.9215845.

[DIE21] R. Dierks and A. Mertens, "Validation of an Extended Loss-Optimised Branch Energy Control for Modular Multilevel Converters under Unbalanced Grid Conditions," IECON 2021 – 47th Annual Conference of the IEEE Industrial Electronics Society, Toronto, ON, Canada, 2021, pp. 1-6, doi: 10.1109/IECON48115.2021.9589690.

[DIN22a] Daniel Dinkel, "Direkte Multivariablenregelung von Modularen MultilevelUmrichtern," Ph.D. Thesis, Universität der Bundeswehr München, 2022.

[DIN22b] D. Dinkel, C. Hillermeier and R. Marquardt, "Direct Multivariable Control for Modular Multilevel Converters," in IEEE Transactions on Power Electronics, vol. 37, no. 7, pp. 7819-7833, July 2022, doi: 10.1109/TPEL.2022.3148578.

[ECK12] H.-G. ECKEL, D. WIGGER, "Modular Multilevel Converters with Reverse-Conducting IGBT," PCIM Europe 2012, 8-10 May 2012, Nuremberg, Germany (2012)

[GUA11] M. Guan, Z. Xu and Hairong Chen, "Control and modulation strategies for modular multilevel converter based HVDC system," IECON 2011 - 37th Annual Conference of the IEEE Industrial Electronics Society, Melbourne, VIC, Australia, 2011, pp. 849-854, doi: 10.1109/IECON.2011.6119421.

[GUA12] M. Guan and Z. Xu, "Modeling and Control of a Modular Multilevel Converter-Based HVDC System Under Unbalanced Grid Conditions," in IEEE Transactions on Power Electronics, vol. 27, no. 12, pp. 4858-4867, Dec. 2012, doi: 10.1109/TPEL.2012.2192752.

[GLI03a] M. Glinka & R. Marquardt (2004) A New Single Phase AC/AC-Multilevel Converter for Traction Vehicles Operating On Ac Line Voltage, EPE Journal, 14:4, 7-12, DOI: 10.1080/09398368.2004.11463567

[GLI03b] M. Glinka and R. Marquardt, "A new AC/AC-multilevel converter family applied to a single-phase converter," The Fifth International Conference on Power Electronics and Drive Systems, 2003. PEDS 2003., Singapore, 2003, pp. 16-23 Vol.1, doi: 10.1109/PEDS.2003.1282669.

[GLI05] M. Glinka and R. Marquardt, "A new AC/AC multilevel converter family," in IEEE Transactions on Industrial Electronics, vol. 52, no. 3, pp. 662-669, June 2005, doi: 10.1109/TIE.2005.843973.

[HAG09] M. Hagiwara and H. Akagi, "Control and Experiment of Pulsewidth-Modulated Modular Multilevel Converters," in IEEE Transactions on Power Electronics, vol. 24, no. 7, pp. 1737-1746, July 2009, doi: 10.1109/TPEL.2009.2014236.

[HAG10] M. Hagiwara, K. Nishimura and H. Akagi, "A Medium-Voltage Motor Drive With a Modular Multilevel PWM Inverter," in IEEE Transactions on Power Electronics, vol. 25, no. 7, pp. 1786-1799, July 2010, doi: 10.1109/TPEL.2010.2042303.

[HAG11] M. Hagiwara, R. Maeda and H. Akagi, "Control and Analysis of the Modular Multilevel Cascade Converter Based on Double-Star Chopper-Cells (MMCC-DSCC)," in IEEE Transactions on Power Electronics, vol. 26, no. 6, pp. 1649-1658, June 2011, doi: 10.1109/TPEL.2010.2089065.

[HAG08] M. Hagiwara and H. Akagi, "PWM control and experiment of modular multilevel converters," 2008 IEEE Power Electronics Specialists Conference, Rhodes, Greece, 2008, pp. 154-161, doi: 10.1109/PESC.2008.4591917.

[HAR11] L. Harnefors, S. Norrga, A. Antonopoulos and H. -P. Nee, "Dynamic modeling of modular multilevel converters," Proceedings of the 2011 14th European Conference on Power Electronics and Applications, Birmingham, UK, 2011, pp. 1-10.

[HAR13] L. Harnefors, A. Antonopoulos, S. Norrga, L. Angquist and H. -P. Nee, "Dynamic Analysis of Modular Multilevel Converters," in IEEE Transactions on Industrial Electronics, vol. 60, no. 7, pp. 2526-2537, July 2013, doi: 10.1109/TIE.2012.2194974.

[HAR16] K. Haridas, S. Khandelwal and A. Das, "Three phase to single phase modular multilevel converter using full bridge cells," 2016 IEEE International Conference on Power Electronics, Drives and Energy Systems (PEDES), Trivandrum, India, 2016, pp. 1-5, doi: 10.1109/PEDES.2016.7914555.

[HIL09a] M. Hiller, D. Krug, R. Sommer and S. Rohner, "A new highly modular medium voltage converter topology for industrial drive applications," 2009 13th European Conference on Power Electronics and Applications, Barcelona, Spain, 2009, pp. 1-10.

[HAG9b] M. Hagiwara, K. Nishimura and H. Akagi, "A modular multilevel PWM inverter for medium-voltage motor drives," 2009 IEEE Energy Conversion Congress and Exposition, San Jose, CA, USA, 2009, pp. 2557-2564, doi: 10.1109/ECCE.2009.5316479.

[HIL15] A. Hillers, M. Stojadinovic and J. Biela, "Systematic comparison of modular multilevel converter topologies for battery energy storage systems based on split batteries," 2015 17th European Conference on Power Electronics and Applications

(EPE'15 ECCE-Europe), Geneva, Switzerland, 2015, pp. 1-9, doi: 10.1109/EPE.2015.7309385.

[HIM17] P. Himmelmann and M. Hiller, "A Generalized Approach to the Analysis and Control of Modular Multilevel Converters," PCIM Europe 2017; International Exhibition and Conference for Power Electronics, Intelligent Motion, Renewable Energy and Energy Management, Nuremberg, Germany, 2017, pp. 1-8.

[ILV12a] K. Ilves, A. Antonopoulos, S. Norrga and H. -P. Nee, "Steady-State Analysis of Interaction Between Harmonic Components of Arm and Line Quantities of Modular Multilevel Converters," in IEEE Transactions on Power Electronics, vol. 27, no. 1, pp. 57-68, Jan. 2012, doi: 10.1109/TPEL.2011.2159809.

[ILV12b] K. Ilves, S. Norrga, L. Harnefors and H. -P. Nee, "Analysis of arm current harmonics in modular multilevel converters with main-circuit filters," International Multi-Conference on Systems, Signals & Devices, Chemnitz, Germany, 2012, pp. 1-6, doi: 10.1109/SSD.2012.6197915.

[ILV12c] K. Ilves, A. Antonopoulos, L. Harnefors, S. Norrga and H. -P. Nee, "Circulating current control in modular multilevel converters with fundamental switching frequency," Proceedings of The 7th International Power Electronics and Motion Control Conference, Harbin, China, 2012, pp. 249-256, doi: 10.1109/IPEMC.2012.6258844.

[ILV14] K. Ilves, L. Bessegato and S. Norrga, "Comparison of cascaded multilevel converter topologies for AC/AC conversion," 2014 International Power Electronics Conference (IPEC-Hiroshima 2014 - ECCE ASIA), Hiroshima, Japan, 2014, pp. 1087-1094, doi: 10.1109/IPEC.2014.6869722.

[KOL11] J. Kolb, F. Kammerer and M. Braun, "Straight forward vector control of the Modular Multilevel Converter for feeding three-phase machines over their complete frequency range," IECON 2011 - 37th Annual Conference of the IEEE Industrial Electronics Society, Melbourne, VIC, Australia, 2011, pp. 1596-1601, doi: 10.1109/IECON.2011.6119545.

[KOL15a] J. Kolb, F. Kammerer, M. Gommeringer and M. Braun, "Cascaded Control System of the Modular Multilevel Converter for Feeding Variable-Speed Drives," in IEEE Transactions on Power Electronics, vol. 30, no. 1, pp. 349-357, Jan. 2015, doi: 10.1109/TPEL.2014.2299894.

[KOL15b] M. Schnarrenberger, F. Kammerer, M. Gommeringer, J. Kolb and M. Braun, "Current control and energy balancing of a square-wave powered 1AC-3AC modular multilevel converter," 2015 IEEE Energy Conversion Congress and Exposition (ECCE), Montreal, QC, Canada, 2015, pp. 3607-3614, doi: 10.1109/ECCE.2015.7310170.

[KOL12a] F. Kammerer, J. Kolb and M. Braun, "Fully decoupled current control and energy balancing of the Modular Multilevel Matrix Converter," 2012 15th International Power Electronics and Motion Control Conference (EPE/PEMC), Novi Sad, Serbia, 2012, pp. LS2a.3-1-LS2a.3-8, doi: 10.1109/EPEPEMC.2012.6397408.

[KOL12b] J. Kolb, F. Kammerer and M. Braun, "Dimensioning and design of a Modular Multilevel Converter for drive applications," 2012 15th International Power Electronics and Motion Control Conference (EPE/PEMC), Novi Sad, Serbia, 2012, pp. LS1a-1.1-1-LS1a-1.1-8, doi: 10.1109/EPEPEMC.2012.6397380.

[KOL14] J. Kolb, "Optimale Betriebsführung des modularen Multilevel-Umrichters als Antriebsumrichter für Drehstrommaschinen," Ph.D. Thesis, Karlsruhe: KIT Scientific Publ, 2014.

[KAR15] D. Karwatzki, L. Baruschka, J. Kucka and A. Mertens, "Current control and branch energy balancing of the Modular Multilevel Matrix Converter," 2015 IEEE Energy Conversion Congress and Exposition (ECCE), Montreal, QC, Canada, 2015, pp. 6360-6367, doi: 10.1109/ECCE.2015.7310551.

[KAR16] D. Karwatzki, L. Baruschka, M. Dokus, J. Kucka and A. Mertens, "Branch energy balancing with a generalised control concept for modular multilevel topologies — Using the example of the modular multilevel converter," 2016 18th European Conference on Power Electronics and Applications (EPE'16 ECCE Europe), Karlsruhe, Germany, 2016, pp. 1-10, doi: 10.1109/EPE.2016.7695619.

[KAR17] D. Karwatzki, “Analyse und Regelung einer Klasse von modularen Multilevelumrichter-Topologien,” Ph.D. dissertation, 2017.

[KAR18] D. Karwatzki and A. Mertens, "Generalized Control Approach for a Class of Modular Multilevel Converter Topologies," in IEEE Transactions on Power Electronics, vol. 33, no. 4, pp. 2888-2900, April 2018, doi: 10.1109/TPEL.2017.2703917.

[KAM14] F. Kammerer, M. Gommeringer, J. Kolb and M. Braun, "Energy balancing of the Modular Multilevel Matrix Converter based on a new transformed arm power analysis," 2014 16th European Conference on Power Electronics and Applications, Lappeenranta, Finland, 2014, pp. 1-10, doi: 10.1109/EPE.2014.6910939.

[KOR10] A. J. Korn, M. Winkelnkemper and P. Steimer, "Low output frequency operation of the Modular Multilevel Converter," 2010 IEEE Energy Conversion Congress and Exposition, Atlanta, GA, USA, 2010, pp. 3993-3997, doi: 10.1109/ECCE.2010.5617802.

[KEN11] S. Kenzelmann, A. Rufer, M. Vasiladiotis, D. Dujic, F. Canales and Y. R. de Novaes, "A versatile DC-DC converter for energy collection and distribution using the Modular Multilevel Converter," Proceedings of the 2011 14th European

Conference on Power Electronics and Applications, Birmingham, UK, 2011, pp. 1-10.

[KNA11] H. -J. Knaak, "Modular multilevel converters and HVDC/FACTS: A success story," Proceedings of the 2011 14th European Conference on Power Electronics and Applications, Birmingham, UK, 2011, pp. 1-6.

[LAC11] A. Lachichi and L. Harnefors, "Comparative analysis of control strategies for modular multilevel converters," 2011 IEEE Ninth International Conference on Power Electronics and Drive Systems, Singapore, 2011, pp. 538-542, doi: 10.1109/PEDS.2011.6147301.

[LES03a] A. Lesnicar and R. Marquardt, "An innovative modular multilevel converter topology suitable for a wide power range," 2003 IEEE Bologna Power Tech Conference Proceedings, Bologna, Italy, 2003, pp. 6 pp. Vol.3-, doi: 10.1109/PTC.2003.1304403.

[LES03b] A. Lesnicar and R. Marquardt, "A new modular voltage source inverter topology, " In: EPE 2003, Toulouse (2003)

[LI10] K. Li and C. Zhao, "New Technologies of Modular Multilevel Converter for VSC-HVDC Application," 2010 Asia-Pacific Power and Energy Engineering Conference, Chengdu, China, 2010, pp. 1-4, doi: 10.1109/APPEEC.2010.5449237.

[LI22] G. Li and J. Liang, "Modular Multilevel Converters: Recent Applications [History]," in IEEE Electrification Magazine, vol. 10, no. 3, pp. 85-92, Sept. 2022, doi: 10.1109/MELE.2022.3187886.

[LEI17] M. Lei, Y. Li, Z. Li, F. Xu, P. Wang and C. Zhao, "A sept-branch modular multilevel converter for three-phase to single-phase direct AC/AC equal frequency conversion," IECON 2017 - 43rd Annual Conference of the IEEE Industrial Electronics Society, Beijing, China, 2017, pp. 2239-2244, doi: 10.1109/IECON.2017.8216377.

[LEI18a] M. Lei, Y. Li, Z. Li, C. Zhao and P. Wang, "Branch Energy Control of the Three-Phase to Single-Phase Direct AC-AC Modular Multilevel Converter Under Equal Frequency Operation Condition," IECON 2018 - 44th Annual Conference of the IEEE Industrial Electronics Society, Washington, DC, USA, 2018, pp. 2001-2006, doi: 10.1109/IECON.2018.8591624.

[LEI18b] M. Lei, Y. Li, Z. Li, F. Xu, C. Zhao and P. Wang, "A Single-Phase Direct AC-AC Modular Multilevel Converter for Railway Power Conditioning," 2018 20th European Conference on Power Electronics and Applications (EPE'18 ECCE Europe), Riga, Latvia, 2018, pp. P.1-P.10.

[LEI18c] M. Lei, Y. Li, Z. Li, C. Zhao, B. Xia and P. Wang, "Exploration of a Modular Multilevel Converter for Direct AC-AC Conversion," 2018 IEEE International

Power Electronics and Application Conference and Exposition (PEAC), Shenzhen, China, 2018, pp. 1-6, doi: 10.1109/PEAC.2018.8590353.

[LEI20] M. Lei et al., "A Single-Phase Five-Branch Direct AC–AC Modular Multilevel Converter for Railway Power Conditioning," in IEEE Transactions on Industrial Electronics, vol. 67, no. 6, pp. 4292-4304, June 2020, doi: 10.1109/TIE.2019.2926045.

[LIZ15] R. Lizana, M. A. Perez, D. Arancibia, J. R. Espinoza and J. Rodriguez, "Decoupled Current Model and Control of Modular Multilevel Converters," in IEEE Transactions on Industrial Electronics, vol. 62, no. 9, pp. 5382-5392, Sept. 2015, doi: 10.1109/TIE.2015.2405900.

[LIZ16a] R. Lizana, M. A. Perez, D. Arancibia, J. R. Espinoza and J. Rodriguez, "Decoupled Current Model and Control of Modular Multilevel Converters," in IEEE Transactions on Industrial Electronics, vol. 62, no. 9, pp. 5382-5392, Sept. 2015, doi: 10.1109/TIE.2015.2405900.

[LIZ16b] R. Lizana, M. A. Perez, S. Bernet, J. R. Espinoza and J. Rodriguez, "Control of Arm Capacitor Voltages in Modular Multilevel Converters," in IEEE Transactions on Power Electronics, vol. 31, no. 2, pp. 1774-1784, Feb. 2016, doi: 10.1109/TPEL.2015.2426183.

[MAR01] R. Marquardt, "Stromrichterschaltung mit verteilten Energiespeichern und Verfahren, zur Steuerung einer derartigen Stromrichterschaltung", Patent DE10103031 B4, Jan. 2001.

[MAR04] R. Marquardt; A. Lesnicar, "New Concept for High Voltage -Modular Multilevel Converter". In: PESC 2004 Conference in Aachen, Germany (2004)

[MAR18] R. Marquardt, "Modular Multilevel Converters: State of the Art and Future Progress," in IEEE Power Electronics Magazine, vol. 5, no. 4, pp. 24-31, Dec. 2018, doi: 10.1109/MPEL.2018.2873496.

[MAR10] R. Marquardt, "Modular Multilevel Converter: An universal concept for HVDC-Networks and extended DC-Bus-applications," The 2010 International Power Electronics Conference - ECCE ASIA -, Sapporo, Japan, 2010, pp. 502-507, doi: 10.1109/IPEC.2010.5544594.

[MEI19] S. Meinecke, A. Klettke, D. Sarajlic, …, " general planning and operational principles in german distribution systems used for simbench," 25th international conference on electricity distribution, Madrid, 3-6 june 2019.

[MON16] G. Mondal and S. Nielebock, "Control of M2C direct converter for AC to AC conversion with wide frequency range," 2016 18th European Conference on Power Electronics and Applications (EPE'16 ECCE Europe), Karlsruhe, Germany, 2016, pp. 1-10, doi: 10.1109/EPE.2016.7695262.

[Mün10a] P. Münch, D. Görges, M. Izák and S. Liu, "Integrated current control, energy control and energy balancing of Modular Multilevel Converters," IECON 2010 - 36th Annual Conference on IEEE Industrial Electronics Society, Glendale, AZ, USA, 2010, pp. 150-155, doi: 10.1109/IECON.2010.5675185.

[Mün10b] P. Münch, S. Liu and G. Ebner, "Multivariable current control of Modular Multilevel Converters with disturbance rejection and harmonics compensation," 2010 IEEE International Conference on Control Applications, Yokohama, Japan, 2010, pp. 196-201, doi: 10.1109/CCA.2010.5611205.

[NOV17] B. Novakovic and A. Nasiri, "Modular Multilevel Converter for Wind Energy Storage Applications," in IEEE Transactions on Industrial Electronics, vol. 64, no. 11, pp. 8867-8876, Nov. 2017, doi: 10.1109/TIE.2017.2677314.

[OGA95] Katsuhiko Ogata, "Discrete-Time Control Systems," 2nd Edition, Prentice Hall, 1995.

[OGA10] Katsuhiko Ogata, "Modern Control Engineering," 5th Edition, Prentice Hall, 2010.

[PER12] M. A. Pérez, R. Lizana F. and J. Rodríguez, "Decoupled current control of modular multilevel converter for HVDC applications," 2012 IEEE International Symposium on Industrial Electronics, Hangzhou, China, 2012, pp. 1979-1984, doi: 10.1109/ISIE.2012.6237396.

[PER13] M. A. Perez, D. Arancibia, S. Kouro and J. Rodriguez, "Modular multilevel converter with integrated storage for solar photovoltaic applications," IECON 2013 - 39th Annual Conference of the IEEE Industrial Electronics Society, Vienna, Austria, 2013, pp. 6993-6998, doi: 10.1109/IECON.2013.6700292.

[PER14] M. A. Perez, J. Rodriguez and S. Bernet, "Decoupled capacitor voltage control of modular multilevel converters," 2014 IEEE Energy Conversion Congress and Exposition (ECCE), Pittsburgh, PA, USA, 2014, pp. 4947-4953, doi: 10.1109/ECCE.2014.6954079.

[PER15] M. A. Perez, S. Bernet, J. Rodriguez, S. Kouro and R. Lizana, "Circuit Topologies, Modeling, Control Schemes, and Applications of Modular Multilevel Converters," in IEEE Transactions on Power Electronics, vol. 30, no. 1, pp. 4-17, Jan. 2015, doi: 10.1109/TPEL.2014.2310127.

[QIN19] F. Qin, T. Hao and F. Gao, "A Railway Power Conditioner Using Direct AC-AC Modular Multilevel Converter," 2019 2nd International Conference on Smart Grid and Renewable Energy (SGRE), Doha, Qatar, 2019, pp. 1-5, doi: 10.1109/SGRE46976.2019.9020681.

[RIA13] B. S. Riar, T. Geyer and U. K. Madawala, "Model Predictive Direct Current Control of Modular Multilevel Converters," 2013 IEEE International Conference on

Industrial Technology (ICIT), Cape Town, South Africa, 2013, pp. 582-587, doi: 10.1109/ICIT.2013.6505736.

[ROD07] J. Rodriguez, S. Bernet, B. Wu, J. O. Pontt and S. Kouro, "Multilevel Voltage-Source-Converter Topologies for Industrial Medium-Voltage Drives," in IEEE Transactions on Industrial Electronics, vol. 54, no. 6, pp. 2930-2945, Dec. 2007, doi: 10.1109/TIE.2007.907044.

[ROD09] J. Rodriguez et al., "Multilevel Converters: An Enabling Technology for High-Power Applications," in Proceedings of the IEEE, vol. 97, no. 11, pp. 1786-1817, Nov. 2009, doi: 10.1109/JPROC.2009.2030235.

[ROH10] S. Rohner, S. Bernet, M. Hiller and R. Sommer, "Modelling, simulation and analysis of a Modular Multilevel Converter for medium voltage applications," 2010 IEEE International Conference on Industrial Technology, Via del Mar, Chile, 2010, pp. 775-782, doi: 10.1109/ICIT.2010.5472634.

[SCH15] M. Schnarrenberger, F. Kammerer, M. Gommeringer, J. Kolb and M. Braun, "Current control and energy balancing of a square-wave powered 1AC-3AC modular multilevel converter," 2015 IEEE Energy Conversion Congress and Exposition (ECCE), Montreal, QC, Canada, 2015, pp. 3607-3614, doi: 10.1109/ECCE.2015.7310170.

[SCH17] M. Schütt and H. Eckel, "Design and analysis of complex vector current regulators for modular multilevel converters," 2017 19th European Conference on Power Electronics and Applications (EPE'17 ECCE Europe), 2017, pp. P.1-P.10, doi: 10.23919/EPE17ECCEEurope.2017.8099183.

[SCH18] M. Schütt and H. -G. Eckel, "Design and Analysis of Discrete Current Regulators for VSIs," 2018 20th European Conference on Power Electronics and Applications (EPE'18 ECCE Europe), Riga, Latvia, 2018, pp. P.1-P.10.

[SCH22] M. Schütt, "Physics-based Discrete Modelling and Digital Control Design for Grid-Side Inverters for Renewable Energy," Ph.D. Thesis, Universität Rostock, 2022.

[SAH20] G. K. Sah, M. Schütt and H. -G. Eckel, "Comparison of Decoupling Techniques via Discrete Luenberger Style Observer for Voltage Oriented Control," 2020 22nd European Conference on Power Electronics and Applications (EPE'20 ECCE Europe), Lyon, France, 2020, pp. 1-10, doi: 10.23919/EPE20ECCEEurope43536.2020.9215745.

[SAH21] G. K. Sah, M. Schütt and H. -G. Eckel, "A Simplified Technique for Estimating the Filter- and Grid-Impedances for VSIs Connected to the Grid via L-Filter," 2021 23rd European Conference on Power Electronics and Applications (EPE'21 ECCE Europe), Ghent, Belgium, 2021, pp. 1-10, doi: 10.23919/EPE21ECCEEurope50061.2021.9570567.

[SAH22] Gyanendra Kumar Sah, M. Schütt and H. Eckel, "Overview and Evaluation of Energy Balancing Techniques For MMCs with Various Input and Output Frequencies," 2022 24th European Conference on Power Electronics and Applications (EPE'22 ECCE Europe), 2022, pp. P.1-P.10.

[SAH23] Gyanendra Kumar Sah, M. Schütt and H. Eckel, " Passivity Improvement of the Grid Connected VSI using Active Damping and Investigation of Inaccuracy of the Direct Discrete Plant Model," 2023 25th European Conference on Power Electronics and Applications (EPE'23 ECCE Europe), 2023, pp. P.1-P.10.

[SAN11] D. Soto-Sanchez and T. C. Green, "Control of a modular multilevel converter-based HVDC transmission system," Proceedings of the 2011 14th European Conference on Power Electronics and Applications, Birmingham, UK, 2011, pp. 1-10.

[SOL10] E. Solas, G. Abad, J. A. Barrena, A. Cárear and S. Aurtenetxea, "Modelling, simulation and control of Modular Multilevel Converter," Proceedings of 14th International Power Electronics and Motion Control Conference EPE-PEMC 2010, Ohrid, Macedonia, 2010, pp. T2-90-T2-96, doi: 10.1109/EPEPEMC.2010.5606881.

[SOL13a] E. Solas, G. Abad, J. A. Barrena, S. Aurtenetxea, A. Cárcar and L. Zając, "Modular Multilevel Converter With Different Submodule Concepts—Part I: Capacitor Voltage Balancing Method," in IEEE Transactions on Industrial Electronics, vol. 60, no. 10, pp. 4525-4535, Oct. 2013, doi: 10.1109/TIE.2012.2210378.

[SOL13b] E. Solas, G. Abad, J. A. Barrena, S. Aurtenetxea, A. Cárcar and L. Zając, "Modular Multilevel Converter With Different Submodule Concepts—Part II: Experimental Validation and Comparison for HVDC Application," in IEEE Transactions on Industrial Electronics, vol. 60, no. 10, pp. 4536-4545, Oct. 2013, doi: 10.1109/TIE.2012.2211431.

[SON18] S. SONG, J. LIU, S. OUYANG, X. CHEN and B. LIU, "Control of Direct AC/AC Modular Multilevel Converter in Railway Power Supply System," 2018 International Power Electronics Conference (IPEC-Niigata 2018 -ECCE Asia), Niigata, Japan, 2018, pp. 1051-1055, doi: 10.23919/IPEC.2018.8508001.

[SOT04] D. Soto, R. Pena, F. Gutierrez and T. C. Green, "A new power flow controller based on a bridge converter topology," 2004 IEEE 35th Annual Power Electronics Specialists Conference (IEEE Cat. No.04CH37551), Aachen, Germany, 2004, pp. 2540-2545 Vol.4, doi: 10.1109/PESC.2004.1355229.

[SIE10] D. Siemaszko, A. Antonopoulos, K. Ilves, M. Vasiladiotis, L. Ängquist and H. -P. Nee, "Evaluation of control and modulation methods for modular multilevel converters," The 2010 International Power Electronics Conference - ECCE ASIA -, Sapporo, Japan, 2010, pp. 746-753, doi: 10.1109/IPEC.2010.5544609.

[SHI17] X. Shi, Z. Wang, B. Liu, Y. Li, L. M. Tolbert and F. Wang, "Steady-State Modeling of Modular Multilevel Converter Under Unbalanced Grid Conditions," in IEEE Transactions on Power Electronics, vol. 32, no. 9, pp. 7306-7324, Sept. 2017, doi: 10.1109/TPEL.2016.2629472.

[TEE09] S. P. Teeuwsen, "Simplified dynamic model of a voltage-sourced converter with modular multilevel converter design," 2009 IEEE/PES Power Systems Conference and Exposition, Seattle, WA, USA, 2009, pp. 1-6, doi: 10.1109/PSCE.2009.4839922.

[TEO07] Remus Teodorescu, Marco Liserre, Pedro Rodriguez, "Grid converters for photovoltaic and wind power systems," Wiley-IEEE Press, 2007

[TEO06] R. Teodorescu, F. Blaabjerg, M. Liserre and P. C. Loh, "Proportional-resonant controllers and filters for grid-connected voltage-source converters," in IEE Proceedings - Electric Power Applications, vol. 153, no. 5, pp. 750-762, September 2006, doi: 10.1049/ip-epa:20060008.

[THI13] N. Thitichaiworakorn, M. Hagiwara and H. Akagi, "A single-phase to three-phase direct AC/AC modular multilevel cascade converter based on double-star bridge-cells (MMCC-DSBC)," 2013 1st International Future Energy Electronics Conference (IFEEC), Tainan, Taiwan, 2013, pp. 476-481, doi: 10.1109/IFEEC.2013.6687553.

[TU10] Q. Tu, Z. Xu and J. Zhang, "Circulating current suppressing controller in modular multilevel converter," IECON 2010 - 36th Annual Conference on IEEE Industrial Electronics Society, Glendale, AZ, USA, 2010, pp. 3198-3202, doi: 10.1109/IECON.2010.5675048.

[UTV20] M. Utvić and D. Dujić, "Generalized theory on direct arm energy control in modular multilevel converters," in CPSS Transactions on Power Electronics and Applications, vol. 5, no. 4, pp. 388-399, Dec. 2020, doi: 10.24295/CPSSTPEA.2020.00032.

[VAS12] M. Vasiladiotis, N. Cherix and A. Rufer, "Accurate voltage ripple estimation and decoupled current control for Modular Multilevel Converters," 2012 15th International Power Electronics and Motion Control Conference (EPE/PEMC), Novi Sad, Serbia, 2012, pp. LS1a-1.2-1-LS1a-1.2-8, doi: 10.1109/EPEPEMC.2012.6397381.

[VAS15] M. Vasiladiotis, N. Cherix and A. Rufer, "Operation and control of single-to-three-phase direct AC/AC Modular Multilevel Converters under asymmetric grid conditions," 2015 9th International Conference on Power Electronics and ECCE Asia (ICPE-ECCE Asia), Seoul, Korea (South), 2015, pp. 1061-1066, doi: 10.1109/ICPE.2015.7167912.

[WIN10] M. Winkelnkemper, A. Korn and P. Steimer, "A modular direct converter for transformerless rail interties," 2010 IEEE International Symposium on Industrial Electronics, Bari, Italy, 2010, pp. 562-567, doi: 10.1109/ISIE.2010.5637826.

[YAN11] X. Yang, J. Li, X. Wang, W. Fan and T. Q. Zheng, "Circulating Current Model of Modular Multilevel Converter," 2011 Asia-Pacific Power and Energy Engineering Conference, Wuhan, China, 2011, pp. 1-6, doi: 10.1109/APPEEC.2011.5749067.

[YAN10] Z. Yan, H. Xue-hao, T. Guang-fu and H. Zhi-yuan, "A study on MMC model and its current control strategies," The 2nd International Symposium on Power Electronics for Distributed Generation Systems, Hefei, China, 2010, pp. 259-264, doi: 10.1109/PEDG.2010.5545924.

Appendix

A.1 Clarke and Park Transformations of the Three-Phase Quantities using Complex Vector Notation

The general expression of three-phase unbalanced quantities using positive, negative, and zero sequence components is given in (A1.1). (A1.2) represents the general expressions for Clarke (abc to αβ0) transformation using matrix notation. Substitution of (A1.1) in (A1.2) and simplifying (A1.2) gives in (A1.3). It can be inferred that the zero-sequence component of the three-phase components in the abc-frame are absent in the α- and β-axes.

$$\begin{pmatrix} F_{\mathrm{a}} \\ F_{\mathrm{b}} \\ F_{\mathrm{c}} \end{pmatrix} = \begin{pmatrix} \hat{F}^{+}\cos\left(\omega t + \phi^{+}\right) + \hat{F}^{-}\cos\left(-\omega t + \phi^{-}\right) + F_0 \\ \hat{F}^{+}\cos\left(\omega t + \phi^{+} - \frac{2\pi}{3}\right) + \hat{F}^{-}\cos\left(-\omega t + \phi^{-} - \frac{2\pi}{3}\right) + F_0 \\ \hat{F}^{+}\cos\left(\omega t + \phi^{+} + \frac{2\pi}{3}\right) + \hat{F}^{-}\cos\left(-\omega t + \phi^{-} + \frac{2\pi}{3}\right) + F_0 \end{pmatrix} \tag{A1.1}$$

Where,

$\hat{F}^{+}$ = Positive sequence amplitude

$\hat{F}^{-}$ = Negative sequence amplitude

F_0 = Zero sequence component (can be either DC, AC, or combination of both DC and AC)

ω = Angular speed (rad/s)

t = Time (s)

ϕ^{-} = Phase angle of negative sequence component (rad)

ϕ^{+} = Phase angle of positive sequence component (rad)

$$\begin{pmatrix} F_{\alpha} \\ F_{\beta} \\ F_0 \end{pmatrix} = \frac{2}{3}\begin{pmatrix} 1 & -\frac{1}{2} & -\frac{1}{2} \\ 0 & \frac{\sqrt{3}}{2} & -\frac{\sqrt{3}}{2} \\ \frac{1}{2} & \frac{1}{2} & \frac{1}{2} \end{pmatrix}\begin{pmatrix} F_{\mathrm{a}} \\ F_{\mathrm{b}} \\ F_{\mathrm{c}} \end{pmatrix} \tag{A1.2}$$

$$\begin{pmatrix} F_\alpha \\ F_\beta \\ F_0 \end{pmatrix} = \begin{pmatrix} \hat{F}^+ \cos\left(\omega t + \phi^+\right) + \hat{F}^- \cos\left(-\omega t + \phi^-\right) \\ \hat{F}^+ \sin\left(\omega t + \phi^+\right) + \hat{F}^- \sin\left(-\omega t + \phi^-\right) \\ F_0 \end{pmatrix} \tag{A1.3}$$

(A1.4) represents Euler's formula on a complex number. (A1.5) illustrates the complex vector notation of the three-phase quantities in the αβ-frame. Substituting (A1.3) in (A1.5) gives (A1.6). (A1.7) represents the Euler's complex vector notation of (A1.6) (also see (A1.4)). The positive and negative sequence components rotate in opposite directions with the same speed in the αβ-frame.

$$\hat{F}\, e^{j\varphi} = \hat{F}\cos(\varphi) + j\, \hat{F}\sin(\varphi) \tag{A1.4}$$

$$\boldsymbol{F}_{\alpha\beta} = F_\alpha + j\, F_\beta \tag{A1.5}$$

$$\boldsymbol{F}_{\alpha\beta} = \left(\hat{F}^+ \cos\left(\omega t + \phi^+\right) + j\hat{F}^+ \sin\left(\omega t + \phi^+\right)\right) + \left(\hat{F}^- \cos\left(-\omega t + \phi^-\right) + j\hat{F}^- \sin\left(-\omega t + \phi^-\right)\right) \tag{A1.6}$$

$$\boldsymbol{F}_{\alpha\beta} = \hat{F}^+ e^{j\left(\omega t + \phi^+\right)} + \hat{F}^- e^{j\left(-\omega t + \phi^-\right)} \tag{A1.7}$$

(A1.8) represents the general Park (αβ0 to dq0) transformation expression using matrix notation. Here, φ (= $\omega_1 t + \varphi_o$), and ω_1 representing the transformation angle and its angular speed. The zero-sequence component in both the dq- and the αβ-frames are the same. (A1.9) illustrates the complex vector notation of the three-phase quantities in the dq-frame. Substitution of (A1.8) in (A1.9) gives (A1.10). Refereeing to (A1.4) and (A1.5), (A1.11) represents the Euler's complex vector notation of (A1.10).

$$\begin{pmatrix} F_d \\ F_q \\ F_0 \end{pmatrix} = \begin{pmatrix} \cos(\varphi) & \sin(\varphi) & 0 \\ -\sin(\varphi) & \cos(\varphi) & 0 \\ 0 & 0 & 1 \end{pmatrix} \begin{pmatrix} F_\alpha \\ F_\beta \\ F_0 \end{pmatrix} \tag{A1.8}$$

$$\boldsymbol{F}_{dq} = F_d + j\, F_q \tag{A1.9}$$

$$\boldsymbol{F}_{dq} = \left(\cos(\varphi)F_\alpha + \sin(\varphi)F_\beta\right) + j\left(-\sin(\varphi)F_\alpha + \cos(\varphi)F_\beta\right) = \left(\cos(\varphi) - j\sin(\varphi)\right)\left(F_\alpha + j\, F_\beta\right) \tag{A1.10}$$

$$\boldsymbol{F}_{dq} = e^{-j\varphi}\boldsymbol{F}_{\alpha\beta} \tag{A1.11}$$

Substituting (A1.7) in (A1.11) gives (A1.12). Substituting $\varphi = \omega_1 t + \varphi_o$ in (A1.12) gives (A1.13). The angular speed of the Park transformation angle is subtracted and added with the positive and negative sequence angular speeds in the dq-frame, respectively. (A1.14) represents the particular case of (A1.13) when Park transformation angle ($\varphi = \omega_1 t + \varphi_o = \omega t + \phi^+$) is synchronized with the

positive sequence angle of the three-phase quantity. With $\varphi = \omega_1 t + \varphi_o = \omega t + \phi^+$, the positive sequence component only has DC component in the dq-frame, whereas the negative sequence component has second-order harmonics (2ω) in the dq-frame. Further, if the negative sequence component is absent in the three-phase quantities, there will only be DC components in the dq-frame with $\varphi = \omega_1 t + \varphi_o = \omega t + \phi^+$. Referring to (A1.11), (A1.15) can be used for inverse Park (dq to αβ) transformation in the complex vector form.

$$\boldsymbol{F}_{dq} = \hat{F}^+ e^{j(\omega t + \phi^+ - \varphi)} + \hat{F}^- e^{j(-\omega t + \phi^- - \varphi)} \tag{A1.12}$$

$$\boldsymbol{F}_{dq} = \hat{F}^+ e^{j\left((\omega - \omega_1)t + (\phi^+ - \varphi_o)\right)} + \hat{F}^- e^{j\left((-\omega - \omega_1)t + (\phi^- - \varphi_o)\right)} \tag{A1.13}$$

$$\boldsymbol{F}_{dq} = \hat{F}^+ + \hat{F}^- e^{j\left(-2\omega t + (\phi^- - \phi^+)\right)} \tag{A1.14}$$

$$\boldsymbol{F}_{\alpha\beta} = e^{j\varphi}\boldsymbol{F}_{dq} \tag{A1.15}$$

Note: (A1.13) represents the general expression for transforming three-phase quantities in the dq-frame and can be used to find the frequency components in the dq-frame when ω and ω_1 are the same or different. For example, if $\hat{F}^- = 0$, and $\omega = 3\omega_1$, the three-phase quantity in the dq-frame will have $2\omega_1$ frequency component. Further, if $\hat{F}^- \neq 0$, and $\omega = 3\omega_1$, then three-phase quantity in the dq-frame will have $2\omega_1$, and $4\omega_1$ frequency components.

A.2 Average Plant Model of VSI Connected to the Grid via *L*-Filter in the dq-Frame using the Complex Vector Notation.

Fig. A2.1 and Fig. A2.2 represent the average equivalent electrical circuit diagram of VSI connected to the grid with *L*-filter (RL-load) in the abc- and αβ-frame, respectively. The governing voltage equation of Fig. A2.2 using complex vector notation is given in (A2.1). (A2.2) represents (A2.1) after replacing voltages and current variables using (A1.15). (A2.3) illustrates the simplified expression of (A2.2).

$$\boldsymbol{v}_{\alpha\beta} - \boldsymbol{e}_{\alpha\beta} = L\frac{\mathrm{d}\boldsymbol{i}_{\alpha\beta}}{\mathrm{d}t} + R\,\boldsymbol{i}_{\alpha\beta} \tag{A2.1}$$

$$\boldsymbol{v}_{\mathrm{dq}}\,\mathrm{e}^{\mathrm{j}\varphi} - \boldsymbol{e}_{\mathrm{dq}}\,\mathrm{e}^{\mathrm{j}\varphi} = L\frac{\mathrm{d}\left(\boldsymbol{i}_{\mathrm{dq}}\,\mathrm{e}^{\mathrm{j}\varphi}\right)}{\mathrm{d}t} + R\,\boldsymbol{i}_{\mathrm{dq}}\,\mathrm{e}^{\mathrm{j}\varphi} \tag{A2.2}$$

$$\boldsymbol{v}_{\mathrm{dq}} - \boldsymbol{e}_{\mathrm{dq}} = L\frac{\mathrm{d}\boldsymbol{i}_{\mathrm{dq}}}{\mathrm{d}t} + \mathrm{j}L\omega_1\boldsymbol{i}_{\mathrm{dq}} + R\,\boldsymbol{i}_{\mathrm{dq}} \tag{A2.3}$$

Laplace transformation of (A2.3) is given in (A2.4).

$$\boldsymbol{V}_{\mathrm{dq}}(\mathrm{s}) - \boldsymbol{E}_{\mathrm{dq}}(\mathrm{s}) = Ls\,I_{\mathrm{dq}}(\mathrm{s}) + \mathrm{j}L\omega_1\boldsymbol{I}_{\mathrm{dq}}(\mathrm{s}) + R\,\boldsymbol{I}_{\mathrm{dq}}(\mathrm{s}) = \left(Ls + \mathrm{j}L\omega_1 + R\right)\boldsymbol{I}_{\mathrm{dq}}(\mathrm{s}) \tag{A2.4}$$

Note: Laplace transformation of (A2.1) is shown in (A2.5). The Laplace domain *RL* plant model in the dq-frame can be obtained simply by replacing s with (s + jω_1) in the *RL* plant model in the αβ-frame.

$$\boldsymbol{V}_{\alpha\beta}(\mathrm{s}) - \boldsymbol{E}_{\alpha\beta}(\mathrm{s}) = \left(Ls + R\right)\boldsymbol{I}_{\alpha\beta}(\mathrm{s}) \tag{A2.5}$$

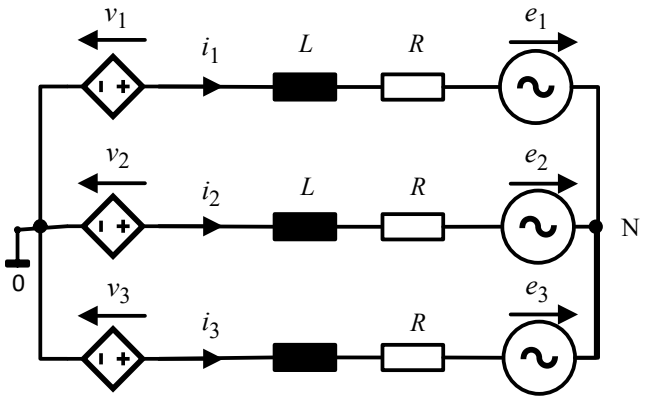

Figure A2.1: Plant model in the abc-frame

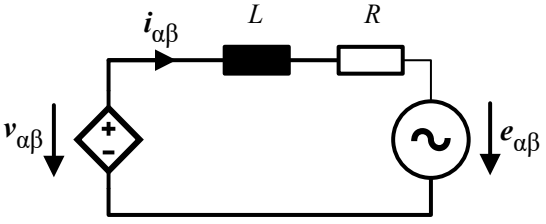

Figure A2.2: Plant model in the αβ-frame

A.3 Derivation of Difference Voltage Equation for Phase *y* of MMC

Referring to Fig. 2.1a, (A3.1) represents the voltage equation in the Laplace domain through a loop consisting of the upper arm-1, the three-phase phase-1, the three-phase-2, and the upper arm-2. Similarly, (A3.2) represents the voltage equation in the Laplace domain through a loop consisting of the lower arm-1, three-phase phase-1, three-phase-2, and lower arm-2. (A3.3) represents the summation of (A3.1) and (A3.2). Here, $V_{\Delta y}(s) = V_{py}(s) - V_{ny}(s)$ represents the difference voltage. Substituting $I_{\Delta y}(s) = I_{py}(s) - I_{ny}(s) = -I_{ay}$ in (A3.3) gives (A3.4).

$$\left(R_{\text{arm}} + sL_{\text{arm}}\right)\left(I_{\text{p1}}(s) - I_{\text{p2}}(s)\right) + V_{\text{p1}}(s) - V_{\text{p2}}(s) - \left(R_{\text{Trf-a}} + sL_{\text{Trf-a}}\right)\left(I_{\text{a1}}(s) - I_{\text{a2}}(s)\right) + V_{\text{a1}}(s) - V_{\text{a2}}(s) = 0 \quad \text{(A3.1)}$$

$$-\left(R_{\text{arm}} + sL_{\text{arm}}\right)\left(I_{\text{n1}}(s) - I_{\text{n2}}(s)\right) - V_{\text{n1}}(s) + V_{\text{n2}}(s) - \left(R_{\text{Trf-a}} + sL_{\text{Trf-a}}\right)\left(I_{\text{a1}}(s) - I_{\text{a2}}(s)\right) + V_{\text{a1}}(s) - V_{\text{a2}}(s) = 0 \quad \text{(A3.2)}$$

$$\left(R_{\text{arm}} + sL_{\text{arm}}\right)\left(I_{\Delta 1}(s) - I_{\Delta 2}(s)\right) + V_{\Delta 1}(s) - V_{\Delta 2}(s) - 2\left(R_{\text{Trf-a}} + sL_{\text{Trf-a}}\right)\left(I_{\text{a1}}(s) - I_{\text{a2}}(s)\right) + 2V_{\text{a1}}(s) - 2V_{\text{a2}}(s) = 0 \quad \text{(A3.3)}$$

$$-\left(\left(R_{\text{arm}} + 2R_{\text{Trf-a}}\right) + \left(L_{\text{arm}} + 2L_{\text{Trf-a}}\right)s\right)\left(I_{\text{a1}}(s) - I_{\text{a2}}(s)\right) + V_{\Delta 1}(s) - V_{\Delta 2}(s) + 2V_{\text{a1}}(s) - 2V_{\text{a2}}(s) = 0 \quad \text{(A3.4)}$$

Substituting $R_{\text{a}} = R_{\text{arm}} + 2R_{\text{Trf-a}}$ and $L_{\text{a}} = L_{\text{arm}} + 2L_{\text{Trf-a}}$ in (A3.4) and rearranging gives (A3.5). Following similar steps from (A3.1) to (A3.5) gives (A3.6) and (A3.7). (A3.5) to (A3.10) gives (A3.11). Zero sequence component of (A3.8) to (A3.10) gives (A3.12). Since the neutral point (N) is floating, three-phase zero-sequence current equals zero ($I_{\text{a0}}(s) = 0$) and $V_{\text{a0}}(s) = V_{\text{cm}}(s)$ represents the zero-sequence component of the three-phase grid voltage (v_{a123}). Hence, (A3.13) is obtained by substituting $I_{\text{a0}}(s) = 0$ and $V_{\text{a0}}(s) = V_{\text{cm}}(s)$ in (A3.12). Therefore, (A3.14) represents the generalized difference voltage equation for phase *y* of MMC.

$$-\left(R_{\text{a}} + L_{\text{a}}s\right) I_{\text{a1}}(s) + V_{\Delta 1}(s) + 2V_{\text{a1}}(s) = -\left(R_{\text{a}} + L_{\text{a}}s\right) I_{\text{a2}}(s) + V_{\Delta 2}(s) + 2V_{\text{a2}}(s) \quad \text{(A3.5)}$$

$$-\left(R_{\text{a}} + L_{\text{a}}s\right) I_{\text{a2}}(s) + V_{\Delta 2}(s) + 2V_{\text{a2}}(s) = -\left(R_{\text{a}} + L_{\text{a}}s\right) I_{\text{a3}}(s) + V_{\Delta 3}(s) + 2V_{\text{a3}}(s) \quad \text{(A3.6)}$$

$$-\left(R_{\text{a}} + L_{\text{a}}s\right) I_{\text{a3}}(s) + V_{\Delta 3}(s) + 2V_{\text{a3}}(s) = -\left(R_{\text{a}} + L_{\text{a}}s\right) I_{\text{a1}}(s) + V_{\Delta 1}(s) + 2V_{\text{a1}}(s) \quad \text{(A3.7)}$$

$$X_1(s) = -\left(R_{\text{a}} + L_{\text{a}}s\right) I_{\text{a1}}(s) + V_{\Delta 1}(s) + 2V_{\text{a1}}(s) \quad \text{(A3.8)}$$

$$X_2(s) = -\left(R_{\text{a}} + L_{\text{a}}s\right) I_{\text{a2}}(s) + V_{\Delta 2}(s) + 2V_{\text{a2}}(s) \quad \text{(A3.9)}$$

$$X_3(s) = -\left(R_{\text{a}} + L_{\text{a}}s\right) I_{\text{a3}}(s) + V_{\Delta 3}(s) + 2V_{\text{a3}}(s) \quad \text{(A3.10)}$$

$$X_1(s) = X_2(s) = X_3(s) \quad \text{(A3.11)}$$

$$X_0(s) = \frac{X_1(s) + X_2(s) + X_3(s)}{3} = -\left(R_{\text{a}} + L_{\text{a}}s\right) I_{\text{a0}}(s) + V_{\Delta\text{-}0}(s) + 2V_{\text{a0}}(s) \quad \text{(A3.12)}$$

$$X_0(s) = X_1(s) = X_2(s) = X_3(s) = V_{\Delta\text{-}0}(s) + 2V_{cm}(s) \tag{A3.13}$$

$$-\left(R_a + L_a s\right) I_{ay}(s) + V_{\Delta y}(s) + 2V_{ay}(s) = V_{\Delta\text{-}0}(s) + 2V_{cm}(s) \tag{A3.14}$$

A.3.1 Derivation of the Upper and Lower Arm Voltages Ignoring Arm and Transformer Impedances

Fig. 2.1b represents the MMC circuit diagram without arm, single-phase transformer, and three-phase transformer impedances. Referring to Fig. 2.1b, (A3.15) is obtained by substituting $R_a = L_a = 0$ in (A3.14).

$$V_{\Delta y}(s) = V_{\Delta\text{-}0}(s) + 2V_{cm}(s) - 2V_{ay}(s) \tag{A3.15}$$

Assuming the zero-sequence difference arm voltage ($V_{\Delta\text{-}0}(s) = -2\,V_{cm}(s)$) is used to realize the three-phase zero-sequence component ($V_{cm}(s)$), (A3.15) can be modified to (A3.16). Referring to Fig. 2.1b, (A3.17) represents the summation arm voltage expressions ignoring the arm and single-phase transformer impedances. The expressions of the upper ($V_{py}(s)$) and lower arm ($V_{ny}(s)$) voltages are given in (A3.18), which is obtained by solving (A3.16) and (A3.17).

$$V_{\Delta y}(s) = V_{py}(s) - V_{ny}(s) = -2V_{ay}(s) \tag{A3.16}$$

$$V_{\Sigma y}(s) = V_{py}(s) + V_{ny}(s) = V_b(s) \tag{A3.17}$$

$$V_{py}(s) = \frac{V_b(s)}{2} - V_{ay}(s), \text{ and } V_{ny}(s) = \frac{V_b(s)}{2} + V_{ay}(s) \tag{A3.17}$$

A.4 Direct Discrete-Time Transfer Function of Resonant Controller

The transfer function of the resonant controller in the s-domain is shown in (A4.1) [TEO06]. (A4.1) is rearranged into (A4.2). The pulse transfer function of a continuous-time plant, $G(\mathrm{s})$, is obtained using (A4.4) [OGA95]. Referring to the s-domain to the z-domain transformation table (Table 2-1 (TABLE OF z TRANSFORMS) in [OGA95]), (A4.5) represents the z transformation of the second ordered Laplace transfer function. Similarly, (A4.6) illustrates the z transfer function of (A4.2). Substituting (A4.3) in (A4.6) and simplifications gives (A4.7), which represents the direct discrete plant model of the resonant controller in (A4.1).

$$R(\mathrm{s}) = \frac{2\,K_{\mathrm{ir}}\,\omega_{\mathrm{c}}\,\mathrm{s}}{\mathrm{s}^2 + 2\,\omega_{\mathrm{c}}\,\mathrm{s} + \omega_{\mathrm{r}}^2} \tag{A4.1}$$

$$R(\mathrm{s}) = \frac{2\,K_{\mathrm{ir}}\,\omega_{\mathrm{c}}\,\mathrm{s}}{\left(\mathrm{s} + \omega_1\right)\left(\mathrm{s} + \omega_2\right)} \tag{A4.2}$$

$$\omega_1 = \omega_{\mathrm{c}} + \mathrm{j}\sqrt{\omega_{\mathrm{r}}^2 - \omega_{\mathrm{c}}^2} \text{ and } \omega_2 = \omega_{\mathrm{c}} - \mathrm{j}\sqrt{\omega_{\mathrm{r}}^2 - \omega_{\mathrm{c}}^2} \tag{A4.3}$$

$$G(z) = Z\left\{\frac{1 - e^{-\mathrm{s}T}}{\mathrm{s}}\,G(\mathrm{s})\right\} = \left(1 - z^{-1}\right) Z\left\{\frac{G(\mathrm{s})}{\mathrm{s}}\right\} \tag{A4.4}$$

$$G(z) = Z\left\{\frac{\omega_1 - \omega_2}{\left(\mathrm{s} + \omega_1\right)\left(\mathrm{s} + \omega_2\right)}\right\} = \frac{\left(e^{-\omega_1 T} - e^{-\omega_2 T}\right) z^{-1}}{\left(1 - e^{-\omega_1 T} z^{-1}\right)\left(1 - e^{-\omega_2 T} z^{-1}\right)} \tag{A4.5}$$

$$R(z) = \left(1 - z^{-1}\right) Z\left\{\frac{2\,K_{\mathrm{ir}}\,\omega_{\mathrm{c}}\,\mathrm{s}}{\left(\mathrm{s} + \omega_1\right)\left(\mathrm{s} + \omega_2\right)\mathrm{s}}\right\} = \frac{2\,K_{\mathrm{ir}}\,\omega_{\mathrm{c}}\left(e^{-\omega_1 T} - e^{-\omega_2 T}\right)\left(1 - z^{-1}\right) z^{-1}}{\left(\omega_1 - \omega_2\right)\left(1 - e^{-\omega_1 T} z^{-1}\right)\left(1 - e^{-\omega_2 T} z^{-1}\right)} \tag{A4.6}$$

$$R(z) = \left(\frac{\left(1 - z^{-1}\right) z^{-1}}{1 - 2\,e^{-\omega_{\mathrm{c}} T}\cos(\delta\,T)\,z^{-1} + e^{-2\omega_{\mathrm{c}} T} z^{-2}}\right)\frac{2\,K_{\mathrm{ir}}\,\omega_{\mathrm{c}}\,e^{-\omega_{\mathrm{c}} T}\sin(\delta\,T)}{\delta} \tag{A4.7}$$

$$\delta = \sqrt{\omega_{\mathrm{r}}^2 - \omega_{\mathrm{c}}^2} \tag{A4.8}$$

A.5 Derivation of the Arm Powers in the αβ0-Frame

A.5.1 Derivation of the Summation and Difference Arm Powers Expressions in the abc-Frame using the Currents and Voltages in the abc-frame.

$$i_{py} = i_{by} - \frac{i_{ay}}{2} \;;\; i_{ny} = i_{by} + \frac{i_{ay}}{2} \tag{A5.1}$$

$$v_{py} = \frac{v_b}{2} - v_{ay} \;;\; v_{ny} = \frac{v_b}{2} + v_{ay} \tag{A5.2}$$

$$i_{\Sigma y} = i_{py} + i_{ny} = 2\, i_{by} \;;\; i_{\Delta y} = i_{py} - i_{ny} = -\, i_{ay} \tag{A5.3}$$

$$v_{\Sigma y} = v_{py} + v_{ny} = v_b \;;\; v_{\Delta y} = v_{py} - v_{ny} = -\, 2\, v_{ay} \tag{A5.4}$$

$$p_{\Sigma y} = p_{py} + p_{ny} \;;\; p_{\Delta y} = p_{py} - p_{ny} \tag{A5.5}$$

$$p_{py} = v_{py}\, i_{py} \;;\; p_{ny} = v_{ny}\, i_{ny} \tag{A5.6}$$

$$p_{\Sigma y} = v_{py}\, i_{py} + v_{ny}\, i_{ny} = v_{py}\left(i_{by} - \frac{i_{ay}}{2}\right) + v_{ny}\left(i_{by} + \frac{i_{ay}}{2}\right)$$

$$p_{\Sigma y} = \left(v_{py} + v_{ny}\right) i_{by} - \frac{i_{ay}}{2}\left(v_{py} - v_{ny}\right) = v_{\Sigma y}\, i_{by} - \frac{i_{ay}}{2}\, v_{\Delta y} = v_b\, i_{by} - \left(-\, 2\, v_{ay}\right)\frac{i_{ay}}{2}$$

$$p_{\Sigma y} = v_b\, i_{by} + v_{ay}\, i_{ay} \tag{A5.7}$$

$$p_{\Delta y} = v_{py}\, i_{py} - v_{ny}\, i_{ny} = v_{py}\left(i_{by} - \frac{i_{ay}}{2}\right) - v_{ny}\left(i_{by} + \frac{i_{ay}}{2}\right) = \left(v_{py} - v_{ny}\right) i_{by} - \frac{i_{ay}}{2}\left(v_{py} + v_{ny}\right)$$

$$p_{\Delta y} = -\, 2\, v_{ay}\, i_{by} - \frac{i_{ay}}{2}\, v_b \tag{A5.8}$$

A.5.2 Derivation of the Summation and Difference Arm Powers Expressions in the abc-Frame using the Currents and Voltages in the αβ0-frame.

$$\mathrm{F}_{\alpha\beta 0} = C\, \mathrm{F}_{abc} \;;\; \mathrm{F}_{abc} = C^{-1}\, \mathrm{F}_{\alpha\beta 0} \tag{A5.9}$$

$$C = \frac{2}{3}\begin{pmatrix} 1 & -\frac{1}{2} & -\frac{1}{2} \\ 0 & \frac{\sqrt{3}}{2} & -\frac{\sqrt{3}}{2} \\ \frac{1}{2} & \frac{1}{2} & \frac{1}{2} \end{pmatrix} \;;\; C^{-1} = \begin{pmatrix} 1 & 0 & 1 \\ -\frac{1}{2} & \frac{\sqrt{3}}{2} & 1 \\ -\frac{1}{2} & -\frac{\sqrt{3}}{2} & 1 \end{pmatrix} \tag{A5.10}$$

Note: $i_{a0} = 0$ and $v_{a0} = v_{cm}$.

(1)
$$p_{\Sigma 1} = v_b\, i_{b1} + v_{a1}\, i_{a1} = v_b\left(i_{b\alpha} + i_{b0}\right) + \left(v_{a\alpha} + v_{cm}\right) i_{a\alpha} \tag{A5.11}$$

(2)
$$p_{\Sigma 2} = v_b\, i_{b2} + v_{a2}\, i_{a2}$$

$$p_{\Sigma 2} = v_b \left(-\frac{1}{2} i_{b\alpha} + \frac{\sqrt{3}}{2} i_{b\beta} + i_{b0} \right) + \left(-\frac{1}{2} v_{a\alpha} + \frac{\sqrt{3}}{2} v_{a\beta} + v_{cm} \right) \left(-\frac{1}{2} i_{a\alpha} + \frac{\sqrt{3}}{2} i_{a\beta} \right) \quad \text{(A5.12)}$$

(3)
$$p_{\Sigma 3} = v_b \, i_{b3} + v_{a3} \, i_{a3}$$

$$p_{\Sigma 3} = v_b \left(-\frac{1}{2} i_{b\alpha} - \frac{\sqrt{3}}{2} i_{b\beta} + i_{b0} \right) + \left(-\frac{1}{2} v_{a\alpha} - \frac{\sqrt{3}}{2} v_{a\beta} + v_{cm} \right) \left(-\frac{1}{2} i_{a\alpha} - \frac{\sqrt{3}}{2} i_{a\beta} \right) \quad \text{(A5.13)}$$

(4)
$$p_{\Delta 1} = -2 \, v_{a1} \, i_{b1} - \frac{v_b \, i_{a1}}{2} = -2 \left(v_{a\alpha} + v_{cm} \right) \left(i_{b\alpha} + i_{b0} \right) - \frac{v_b \, i_{a\alpha}}{2} \quad \text{(A5.14)}$$

(5)
$$p_{\Delta 2} = -2 \, v_{a2} \, i_{b2} - \frac{v_b \, i_{a2}}{2}$$

$$p_{\Delta 2} = -2 \left(-\frac{1}{2} v_{a\alpha} + \frac{\sqrt{3}}{2} v_{a\beta} + v_{cm} \right) \left(-\frac{1}{2} i_{b\alpha} + \frac{\sqrt{3}}{2} i_{b\beta} + i_{b0} \right) - \frac{v_b}{2} \left(-\frac{1}{2} i_{a\alpha} + \frac{\sqrt{3}}{2} i_{a\beta} \right) \quad \text{(A5.15)}$$

(6)
$$p_{\Delta 3} = -2 \, v_{a3} \, i_{b3} - \frac{v_b \, i_{a3}}{2}$$

$$p_{\Delta 3} = -2 \left(-\frac{1}{2} v_{a\alpha} - \frac{\sqrt{3}}{2} v_{a\beta} + v_{cm} \right) \left(-\frac{1}{2} i_{b\alpha} - \frac{\sqrt{3}}{2} i_{b\beta} + i_{b0} \right) - \frac{v_b}{2} \left(-\frac{1}{2} i_{a\alpha} - \frac{\sqrt{3}}{2} i_{a\beta} \right) \quad \text{(A5.16)}$$

A.5.3 Derivation of the Summation and Difference Arm Powers Expressions in the αβ0-Frame using the Currents and Voltages in the αβ0-frame.

(1)
$$p_{\Sigma 0} = \frac{p_{\Sigma 1} + p_{\Sigma 2} + p_{\Sigma 3}}{3} = v_b \, i_{b0} + \frac{1}{3} \left(i_{a\alpha} \left(v_{a\alpha} + \frac{v_{a\alpha}}{2} + v_{cm} - v_{cm} \right) + \frac{\sqrt{3}}{2} i_{a\beta} \left(\sqrt{3} \, v_{a\beta} \right) \right)$$

$$p_{\Sigma 0} = v_b \, i_{b0} + \frac{v_{a\alpha} \, i_{a\alpha} + v_{a\beta} \, i_{a\beta}}{2} \quad \text{(A5.17)}$$

(2)
$$p_{\Delta 0} = \frac{p_{\Delta 1} + p_{\Delta 2} + p_{\Delta 3}}{3}$$

$$= \frac{1}{3} \left(\left(-2 \, v_{a\alpha} - \frac{1}{2} v_{a\alpha} - \frac{1}{2} v_{a\alpha} \right) i_{b\alpha} + \left(-\frac{3}{2} v_{a\beta} - \frac{3}{2} v_{a\beta} \right) i_{b\beta} + \left(-2 \, v_{cm} - 2 \, v_{cm} - 2 \, v_{cm} \right) i_{b0} \right)$$

$$p_{\Delta 0} = -2 \, v_{cm} \, i_{b0} - v_{a\alpha} \, i_{b\alpha} - v_{a\beta} \, i_{b\beta} \quad \text{(A5.18)}$$

(3)
$$p_{\Sigma \alpha} = \frac{2}{3} \left(p_{\Sigma 1} - \frac{1}{2} \left(p_{\Sigma 2} + p_{\Sigma 3} \right) \right)$$

$$= \frac{2}{3} \left(v_b \, i_{b\alpha} + v_b \, i_{b0} + \left(v_{a\alpha} + v_{cm} \right) i_{a\alpha} - \frac{1}{2} \left(v_b \left(-i_{b\alpha} + 2 \, i_{b0} \right) + \left(\frac{-i_{a\alpha}}{2} \right) \left(-v_{a\alpha} + 2 \, v_{cm} \right) + \frac{3}{2} v_{a\beta} \, i_{a\beta} \right) \right)$$

$$= \frac{2}{3} \left(\frac{3}{2} v_b \, i_{b\alpha} + i_{a\alpha} \left(v_{a\alpha} + v_{cm} + \frac{\left(-v_{a\alpha} + 2 \, v_{cm} \right)}{4} \right) - \frac{3}{4} v_{a\beta} \, i_{a\beta} \right)$$

$$= \frac{2}{3} \left(\frac{3}{2} v_b \, i_{b\alpha} + \frac{3}{4} v_{a\alpha} \, i_{a\alpha} + \frac{3}{2} v_{cm} \, i_{a\alpha} - \frac{3}{4} v_{a\beta} \, i_{a\beta} \right)$$

$$p_{\Sigma \alpha} = v_b \, i_{b\alpha} + v_{cm} \, i_{a\alpha} + \frac{v_{a\alpha} \, i_{a\alpha} - v_{a\beta} \, i_{a\beta}}{2} \quad \text{(A5.19)}$$

(4)

$$p_{\Sigma\beta} = \frac{2}{3}\frac{\sqrt{3}}{2}\left(p_{\Sigma 2} - p_{\Sigma 3}\right)$$

$$= \frac{v_b}{\sqrt{3}}\left(\sqrt{3}\, i_{b\beta}\right) + \left(-\frac{i_{a\alpha}}{2\sqrt{3}}\right)\left(\sqrt{3}\, v_{a\beta}\right) + \frac{\sqrt{3}}{2\sqrt{3}}\, i_{a\beta}\left(-v_{a\alpha} + 2\, v_{cm}\right)$$

$$p_{\Sigma\beta} = v_b\, i_{b\beta} + v_{cm}\, i_{a\beta} - \frac{v_{a\alpha}\, i_{a\beta} + v_{a\beta}\, i_{a\alpha}}{2} \qquad \text{(A5.20)}$$

(5)

$$p_{\Delta\alpha} = \frac{2}{3}\left(p_{\Delta 1} - \frac{1}{2}\left(p_{\Delta 2} + p_{\Delta 3}\right)\right) \qquad \text{(A5.21)}$$

$$= \frac{2}{3}\left(\frac{v_b}{2}\left(-i_{a1} - \frac{1}{2}\left(-i_{a2} - i_{a3}\right)\right) - 2\left(v_{a\alpha} + v_{cm}\right)\left(i_{b\alpha} + i_{b0}\right) - \frac{1}{2}\left(i_{b\alpha}\left(-v_{a\alpha} + 2\, v_{cm}\right)\right) + \frac{3}{2} v_{a\beta}\, i_{b\beta} + i_{b0}\left(-v_{a\alpha} + 2\, v_{cm}\right)\right)$$

$$= \frac{2}{3}\left(-\frac{v_b}{2}\frac{3}{2}\, i_{a\alpha} - \frac{3}{2}\, v_{a\alpha}\, i_{b\alpha} - 3\, v_{cm}\, i_{b\alpha} - 3\, v_{a\alpha}\, i_{b0} + \frac{3}{2}\, v_{a\beta}\, i_{b\beta}\right)$$

$$p_{\Delta\alpha} = -\frac{v_b\, i_{a\alpha}}{2} - 2\, v_{a\alpha}\, i_{b0} - 2\, v_{cm}\, i_{b\alpha} - v_{a\alpha}\, i_{b\alpha} + v_{a\beta}\, i_{b\beta} \qquad \text{(A5.22)}$$

(6)

$$p_{\Delta\beta} = \frac{2}{3}\frac{\sqrt{3}}{2}\left(p_{\Delta 2} - p_{\Delta 3}\right) = \frac{p_{\Delta 2} - p_{\Delta 3}}{\sqrt{3}}$$

$$= \frac{1}{\sqrt{3}}\left(\sqrt{3}\, v_{a\beta}\, i_{b\alpha} + \sqrt{3}\left(v_{a\alpha} - 2\, v_{cm}\right) i_{b\beta} - 2\sqrt{3}\, v_{a\beta}\, i_{b0} - \frac{\sqrt{3}}{2}\, v_b\, i_{a\beta}\right)$$

$$p_{\Delta\beta} = -\frac{v_b\, i_{a\beta}}{2} - 2\, v_{a\beta}\, i_{b0} - 2\, v_{cm}\, i_{b\beta} + v_{a\alpha}\, i_{b\beta} + v_{a\beta}\, i_{b\alpha} \qquad \text{(A5.23)}$$

A.5.4 Summation and difference arm powers in the αβ0-frame.

(1)

$$p_{\Sigma 0} = v_b\, i_{b0} + \frac{v_{a\alpha}\, i_{a\alpha} + v_{a\beta}\, i_{a\beta}}{2} \qquad \text{(A5.24)}$$

(2)

$$p_{\Delta 0} = -2\, v_{cm}\, i_{b0} - v_{a\alpha}\, i_{b\alpha} - v_{a\beta}\, i_{b\beta} \qquad \text{(A5.25)}$$

(3)

$$p_{\Sigma\alpha} = v_b\, i_{b\alpha} + v_{cm}\, i_{a\alpha} + \frac{v_{a\alpha}\, i_{a\alpha} - v_{a\beta}\, i_{a\beta}}{2} \qquad \text{(A5.26)}$$

(4)

$$p_{\Sigma\beta} = v_b\, i_{b\beta} + v_{cm}\, i_{a\beta} - \frac{v_{a\alpha}\, i_{a\beta} + v_{a\beta}\, i_{a\alpha}}{2} \qquad \text{(A5.27)}$$

(5)

$$p_{\Delta\alpha} = -\frac{v_b\, i_{a\alpha}}{2} - 2\, v_{a\alpha}\, i_{b0} - 2\, v_{cm}\, i_{b\alpha} - v_{a\alpha}\, i_{b\alpha} + v_{a\beta}\, i_{b\beta} \qquad \text{(A5.28)}$$

(6)

$$p_{\Delta\beta} = -\frac{v_b\, i_{a\beta}}{2} - 2\, v_{a\beta}\, i_{b0} - 2\, v_{cm}\, i_{b\beta} + v_{a\alpha}\, i_{b\beta} + v_{a\beta}\, i_{b\alpha} \qquad \text{(A5.29)}$$

Note: $i_{b0} = \frac{i_{b1} + i_{b2} + i_{b3}}{3} = -\frac{i_b}{3}$

A.6 Average Arm Powers in the αβ0-Frame

A.6.1 Three-Phase, Circulating, and Single-Phase Currents in the αβ0-Frame including all *Degrees of Freedom* (DOF).

$$D(\theta_a) = \begin{pmatrix} \cos(\theta_a) & -\sin(\theta_a) \\ \sin(\theta_a) & \cos(\theta_a) \end{pmatrix} \; ; \; D^{-1}(\theta_a) = \begin{pmatrix} \cos(\theta_a) & \sin(\theta_a) \\ -\sin(\theta_a) & \cos(\theta_a) \end{pmatrix} \tag{A6.1}$$

$$i_{\alpha\beta} = D(\theta_a)\, i_{dq+} + D^{-1}(\theta_a)\, i_{dq-} \rightarrow \begin{pmatrix} i_\alpha \\ i_\beta \end{pmatrix} = \begin{pmatrix} \cos(\theta_a)\left(i_{d+} + i_{d-}\right) + \sin(\theta_a)\left(i_{q-} - i_{q+}\right) \\ \cos(\theta_a)\left(i_{q+} + i_{q-}\right) + \sin(\theta_a)\left(i_{d+} - i_{d-}\right) \end{pmatrix} \tag{A6.2}$$

$$\theta_a = \omega_a t \; ; \; \theta_b = \omega_b t + \phi_b \; ; \; \theta_{cm} = \omega_{cm} t + \phi_{cm} \tag{A6.3}$$

$$v_{a\alpha} = \sqrt{2} V_a \cos\left(\theta_a\right),\; v_{a\beta} = \sqrt{2} V_a \sin\left(\theta_a\right),\; v_{cm} = \sqrt{2} V_{cm} \cos\left(\theta_{cm}\right),\text{ and } v_b = \sqrt{2} V_b \cos\left(\theta_b\right) \tag{A6.4}$$

$$i_{a\alpha} = \cos\left(\theta_a\right)\left(i_{ad+} + i_{ad-}\right) + \sin\left(\theta_a\right)\left(i_{aq-} - i_{aq+}\right) + \sqrt{2} I_{a\alpha}^{cm} \cos\left(\theta_{cm}\right) + \sqrt{2} I_{a\alpha}^{b} \cos\left(\theta_b\right) \tag{A6.5}$$

$$i_{a\beta} = \cos\left(\theta_a\right)\left(i_{aq+} + i_{aq-}\right) + \sin\left(\theta_a\right)\left(i_{ad+} - i_{ad-}\right) + \sqrt{2} I_{a\beta}^{cm} \cos\left(\theta_{cm}\right) + \sqrt{2}\, I_{a\beta}^{b} \cos\left(\theta_b\right) \tag{A6.6}$$

$$i_{b\alpha} = \cos\left(\theta_a\right)\left(i_{bd+} + i_{bd-}\right) + \sin\left(\theta_a\right) i_{bq-} + \sqrt{2} I_{b\alpha}^{cm} \cos\left(\theta_{cm}\right) + \sqrt{2} I_{b\alpha}^{b} \cos\left(\theta_b\right) \tag{A6.7}$$

$$i_{b\beta} = \cos\left(\theta_a\right) i_{bq-} + \sin\left(\theta_a\right)\left(i_{bd+} - i_{bd-}\right) + \sqrt{2} I_{b\beta}^{cm} \cos\left(\theta_{cm}\right) + \sqrt{2}\, I_{b\beta}^{b} \cos\left(\theta_b\right) \tag{A6.8}$$

$$i_{b0} = \sqrt{2} I_{b0}^{\perp b} \sin\left(\theta_b\right) + \sqrt{2} I_{b0}^{b} \cos\left(\theta_b\right) + \sqrt{2} I_{b0}^{cm} \cos\left(\theta_{cm}\right) + \sqrt{2} I_{b0}^{a\text{-}\alpha} \cos\left(\theta_a\right) + \sqrt{2} I_{b0}^{a\text{-}\beta} \sin\left(\theta_a\right) \tag{A6.9}$$

A.6.2 Average Arm Powers in the αβ0-Frame using Matrix Notation.

$$\left(\overline{P_{\Sigma/\Delta\alpha\beta0}}\right)_{6x1} = a_{6x18}\, DOF_{18x1} + \overline{P_{6x1}} \tag{A6.10}$$

$$\left(\overline{P_{\Sigma/\Delta\alpha\beta0}}\right)_{6x1} = \left(\overline{P_{\Sigma0}} \quad \overline{P_{\Delta0}} \quad \overline{P_{\Sigma\alpha}} \quad \overline{P_{\Sigma\beta}} \quad \overline{P_{\Delta\alpha}} \quad \overline{P_{\Delta\beta}}\right)^T \tag{A6.11}$$

(1st Row)

$$p_{\Sigma0} = v_b\, i_{b0} + \frac{v_{a\alpha}\, i_{a\alpha} + v_{a\beta}\, i_{a\beta}}{2}$$

$$= v_b \left(\sqrt{2} I_{b0}^{\perp b} \sin\left(\theta_b\right) + \sqrt{2} I_{b0}^{b} \cos\left(\theta_b\right) + \sqrt{2} I_{b0}^{cm} \cos\left(\theta_{cm}\right) + \sqrt{2} I_{b0}^{a\text{-}\alpha} \cos\left(\theta_a\right) + \sqrt{2} I_{b0}^{a\text{-}\beta} \sin\left(\theta_a\right)\right)$$

$$+ \frac{v_{a\alpha}}{2} \left(\cos\left(\theta_a\right)\left(i_{ad+} + i_{ad-}\right) + \sin\left(\theta_a\right)\left(i_{aq-} - i_{aq+}\right) + \sqrt{2} I_{a\alpha}^{cm} \cos\left(\theta_{cm}\right) + \sqrt{2} I_{a\alpha}^{b} \cos\left(\theta_b\right)\right)$$

$$+ \frac{v_{a\beta}}{2} \left(\cos\left(\theta_a\right)\left(i_{aq+} + i_{aq-}\right) + \sin\left(\theta_a\right)\left(i_{ad+} - i_{ad-}\right) + \sqrt{2} I_{a\beta}^{cm} \cos\left(\theta_{cm}\right) + \sqrt{2}\, I_{a\beta}^{b} \cos\left(\theta_b\right)\right)$$

Now,

$$\overline{P_{\Sigma 0}} = a_{(1,1)}\, i_{ad+} + a_{(1,2)}\, I_{b0}^{b} + a_{(1,3)}\, i_{bd+} + a_{(1,4)}\, I_{b0}^{cm} + a_{(1,5)}\, I_{b\alpha}^{b} + a_{(1,6)}\, I_{b\beta}^{b}$$

$$+ a_{(1,7)}\, I_{a\alpha}^{cm} + a_{(1,8)}\, I_{a\beta}^{cm} + a_{(1,9)}\, i_{ad-} + a_{(1,10)}\, i_{aq-} + a_{(1,11)}\, I_{a\alpha}^{b} + a_{(1,12)}\, I_{a\beta}^{b}$$

$$+ a_{(1,13)}\, I_{b0}^{a\text{-}\alpha} + a_{(1,14)}\, I_{b0}^{a\text{-}\beta} + a_{(1,15)}\, I_{b\alpha}^{cm} + a_{(1,16)}\, I_{b\beta}^{cm} + a_{(1,17)}\, i_{bd-} + a_{(1,18)}\, i_{bq-} + P_1$$

(2nd Row) $p_{\Delta 0} = -2\, v_{a0}\, i_{b0} - v_{a\alpha}\, i_{b\alpha} - v_{a\beta}\, i_{b\beta}$

$$= -2\, v_{a0}\left(\sqrt{2} I_{b0}^{\perp b} \sin(\theta_b) + \sqrt{2} I_{b0}^{b} \cos(\theta_b) + \sqrt{2} I_{b0}^{cm} \cos(\theta_{cm}) + \sqrt{2} I_{b0}^{a\text{-}\alpha} \cos(\theta_a) + \sqrt{2} I_{b0}^{a\text{-}\beta} \sin(\theta_a)\right)$$

$$- v_{a\alpha}\left(\cos(\theta_a)\left(i_{bd+} + i_{bd-}\right) + \sin(\theta_a)\, i_{bq-} + \sqrt{2} I_{b\alpha}^{cm} \cos(\theta_{cm}) + \sqrt{2} I_{b\alpha}^{b} \cos(\theta_b)\right)$$

$$- v_{a\beta}\left(\cos(\theta_a) i_{bq-} + \sin(\theta_a)\left(i_{bd+} - i_{bd-}\right) + \sqrt{2} I_{b\beta}^{cm} \cos(\theta_{cm}) + \sqrt{2}\, I_{b\beta}^{b} \cos(\theta_b)\right)$$

Now,

$$\overline{P_{\Delta 0}} = a_{(2,1)}\, i_{ad+} + a_{(2,2)}\, I_{b0}^{b} + a_{(2,3)}\, i_{bd+} + a_{(2,4)}\, I_{b0}^{cm} + a_{(2,5)}\, I_{b\alpha}^{b} + a_{(2,6)}\, I_{b\beta}^{b}$$

$$+ a_{(2,7)}\, I_{a\alpha}^{cm} + a_{(2,8)}\, I_{a\beta}^{cm} + a_{(2,9)}\, i_{ad-} + a_{(2,10)}\, i_{aq-} + a_{(2,11)}\, I_{a\alpha}^{b} + a_{(2,12)}\, I_{a\beta}^{b}$$

$$+ a_{(2,13)}\, I_{b0}^{a\text{-}\alpha} + a_{(2,14)}\, I_{b0}^{a\text{-}\beta} + a_{(2,15)}\, I_{b\alpha}^{cm} + a_{(2,16)}\, I_{b\beta}^{cm} + a_{(2,17)}\, i_{bd-} + a_{(2,18)}\, i_{bq-} + P_2$$

(3rd Row) $p_{\Sigma\alpha} = v_b\, i_{b\alpha} + v_{cm}\, i_{a\alpha} + \dfrac{v_{a\alpha}\, i_{a\alpha} - v_{a\beta}\, i_{a\beta}}{2} = v_b\, i_{b\alpha} + \dfrac{\left(2\, v_{cm} + v_{a\alpha}\right) i_{a\alpha} - v_{a\beta}\, i_{a\beta}}{2}$

$$= v_b\left(\cos(\theta_a)\left(i_{bd+} + i_{bd-}\right) + \sin(\theta_a)\, i_{bq-} + \sqrt{2} I_{b\alpha}^{cm} \cos(\theta_{cm}) + \sqrt{2} I_{b\alpha}^{b} \cos(\theta_b)\right)$$

$$+ \frac{\left(2\, v_{cm} + v_{a\alpha}\right)}{2}\left(\cos(\theta_a)\left(i_{ad+} + i_{ad-}\right) + \sin(\theta_a)\left(i_{aq-} - i_{aq+}\right) + \sqrt{2} I_{a\alpha}^{cm} \cos(\theta_{cm}) + \sqrt{2} I_{a\alpha}^{b} \cos(\theta_b)\right)$$

$$- \frac{v_{a\beta}}{2}\left(\cos(\theta_a)\left(i_{aq+} + i_{aq-}\right) + \sin(\theta_a)\left(i_{ad+} - i_{ad-}\right) + \sqrt{2} I_{a\beta}^{cm} \cos(\theta_{cm}) + \sqrt{2}\, I_{a\beta}^{b} \cos(\theta_b)\right)$$

Now,

$$\overline{P_{\Sigma\alpha}} = a_{(3,1)}\, i_{ad+} + a_{(3,2)}\, I_{b0}^{b} + a_{(3,3)}\, i_{bd+} + a_{(3,4)}\, I_{b0}^{cm} + a_{(3,5)}\, I_{b\alpha}^{b} + a_{(3,6)}\, I_{b\beta}^{b}$$

$$+ a_{(3,7)}\, I_{a\alpha}^{cm} + a_{(3,8)}\, I_{a\beta}^{cm} + a_{(3,9)}\, i_{ad-} + a_{(3,10)}\, i_{aq-} + a_{(3,11)}\, I_{a\alpha}^{b} + a_{(3,12)}\, I_{a\beta}^{b}$$

$$+ a_{(3,13)}\, I_{b0}^{a\text{-}\alpha} + a_{(3,14)}\, I_{b0}^{a\text{-}\beta} + a_{(3,15)}\, I_{b\alpha}^{cm} + a_{(3,16)}\, I_{b\beta}^{cm} + a_{(3,17)}\, i_{bd-} + a_{(3,18)}\, i_{bq-} + P_3$$

(4th Row) $p_{\Sigma\beta} = v_b\, i_{b\beta} + v_{a0}\, i_{a\beta} - \dfrac{v_{a\alpha}\, i_{a\beta} + v_{a\beta}\, i_{a\alpha}}{2} = v_b\, i_{b\beta} + \dfrac{\left(2\, v_{cm} - v_{a\alpha}\right) i_{a\beta} - v_{a\beta}\, i_{a\alpha}}{2}$

$$= v_b \left(\cos(\theta_a) i_{bq-} + \sin(\theta_a)\left(i_{bd+} - i_{bd-}\right) + \sqrt{2} I_{b\beta}^{cm} \cos(\theta_{cm}) + \sqrt{2}\, I_{b\beta}^{b} \cos(\theta_b)\right)$$

$$+ \frac{\left(2\, v_{cm} - v_{a\alpha}\right)}{2}\left(\cos(\theta_a)\left(i_{aq+} + i_{aq-}\right) + \sin(\theta_a)\left(i_{ad+} - i_{ad-}\right) + \sqrt{2} I_{a\beta}^{cm} \cos(\theta_{cm}) + \sqrt{2}\, I_{a\beta}^{b} \cos(\theta_b)\right)$$

$$- \frac{v_{a\beta}}{2}\left(\cos(\theta_a)\left(i_{ad+} + i_{ad-}\right) + \sin(\theta_a)\left(i_{aq-} - i_{aq+}\right) + \sqrt{2} I_{a\alpha}^{cm} \cos(\theta_{cm}) + \sqrt{2} I_{a\alpha}^{b} \cos(\theta_b)\right)$$

Now,

$$\overline{P_{\Sigma\beta}} = a_{(4,1)}\, i_{ad+} + a_{(4,2)}\, I_{b0}^{b} + a_{(4,3)}\, i_{bd+} + a_{(4,4)}\, I_{b0}^{cm} + a_{(4,5)}\, I_{b\alpha}^{b} + a_{(4,6)}\, I_{b\beta}^{b}$$

$$+ a_{(4,7)}\, I_{a\alpha}^{cm} + a_{(4,8)}\, I_{a\beta}^{cm} + a_{(4,9)}\, i_{ad-} + a_{(4,10)}\, i_{aq-} + a_{(4,11)}\, I_{a\alpha}^{b} + a_{(4,12)}\, I_{a\beta}^{b}$$

$$+ a_{(4,13)}\, I_{b0}^{a\text{-}\alpha} + a_{(4,14)}\, I_{b0}^{a\text{-}\beta} + a_{(4,15)}\, I_{b\alpha}^{cm} + a_{(4,16)}\, I_{b\beta}^{cm} + a_{(4,17)}\, i_{bd-} + a_{(4,18)}\, i_{bq-} + P_4$$

(5th Row) $p_{\Delta\alpha} = -\dfrac{v_b\, i_{a\alpha}}{2} - 2\, v_{a\alpha}\, i_{b0} - 2\, v_{a0}\, i_{b\alpha} - v_{a\alpha}\, i_{b\alpha} + v_{a\beta}\, i_{b\beta}$

$$= -\frac{v_b\, i_{a\alpha}}{2} - 2\, v_{a\alpha}\, i_{b0} - \left(2\, v_{cm} + v_{a\alpha}\right) i_{b\alpha} + v_{a\beta}\, i_{b\beta}$$

$$= -\frac{v_b}{2}\left(\cos(\theta_a)\left(i_{ad+} + i_{ad-}\right) + \sin(\theta_a)\left(i_{aq-} - i_{aq+}\right) + \sqrt{2} I_{a\alpha}^{cm} \cos(\theta_{cm}) + \sqrt{2} I_{a\alpha}^{b} \cos(\theta_b)\right)$$

$$- 2\, v_{a\alpha}\left(\sqrt{2} I_{b0}^{\perp b} \sin(\theta_b) + \sqrt{2} I_{b0}^{b} \cos(\theta_b) + \sqrt{2} I_{b0}^{cm} \cos(\theta_{cm}) + \sqrt{2} I_{b0}^{a\text{-}\alpha} \cos(\theta_a) + \sqrt{2} I_{b0}^{a\text{-}\beta} \sin(\theta_a)\right)$$

$$- \left(2\, v_{cm} + v_{a\alpha}\right)\left(\cos(\theta_a)\left(i_{bd+} + i_{bd-}\right) + \sin(\theta_a)\, i_{bq-} + \sqrt{2} I_{b\alpha}^{cm} \cos(\theta_{cm}) + \sqrt{2} I_{b\alpha}^{b} \cos(\theta_b)\right)$$

$$+ v_{a\beta}\left(\cos(\theta_a) i_{bq-} + \sin(\theta_a)\left(i_{bd+} - i_{bd-}\right) + \sqrt{2} I_{b\beta}^{cm} \cos(\theta_{cm}) + \sqrt{2}\, I_{b\beta}^{b} \cos(\theta_b)\right)$$

Now,

$$\overline{P_{\Delta\alpha}} = a_{(5,1)}\, i_{ad+} + a_{(5,2)}\, I_{b0}^{b} + a_{(5,3)}\, i_{bd+} + a_{(5,4)}\, I_{b0}^{cm} + a_{(5,5)}\, I_{b\alpha}^{b} + a_{(5,6)}\, I_{b\beta}^{b}$$

$$+ a_{(5,7)}\, I_{a\alpha}^{cm} + a_{(5,8)}\, I_{a\beta}^{cm} + a_{(5,9)}\, i_{ad-} + a_{(5,10)}\, i_{aq-} + a_{(5,11)}\, I_{a\alpha}^{b} + a_{(5,12)}\, I_{a\beta}^{b}$$

$$+ a_{(5,13)}\, I_{b0}^{a\text{-}\alpha} + a_{(5,14)}\, I_{b0}^{a\text{-}\beta} + a_{(5,15)}\, I_{b\alpha}^{cm} + a_{(5,16)}\, I_{b\beta}^{cm} + a_{(5,17)}\, i_{bd-} + a_{(5,18)}\, i_{bq-} + P_5$$

(6th Row)

$$p_{\Delta\beta} = -\frac{v_b\, i_{a\beta}}{2} - 2\, v_{a\beta}\, i_{b0} - 2\, v_{a0}\, i_{b\beta} + v_{a\alpha}\, i_{b\beta} + v_{a\beta}\, i_{b\alpha}$$

$$= -\frac{1}{2} v_b\, i_{a\beta} - 2\, v_{a\beta}\, i_{b0} + \left(v_{a\alpha} - 2\, v_{cm}\right) i_{b\beta} + v_{a\beta}\, i_{b\alpha}$$

$$= -\frac{1}{2} v_b \left(\cos(\theta_a)\left(i_{aq+} + i_{aq-}\right) + \sin(\theta_a)\left(i_{ad+} - i_{ad-}\right) + \sqrt{2} I_{a\beta}^{cm} \cos(\theta_{cm}) + \sqrt{2}\, I_{a\beta}^{b} \cos(\theta_b)\right)$$

$$- 2\, v_{a\beta} \left(\sqrt{2} I_{b0}^{\perp b} \sin(\theta_b) + \sqrt{2} I_{b0}^{b} \cos(\theta_b) + \sqrt{2} I_{b0}^{cm} \cos(\theta_{cm}) + \sqrt{2} I_{b0}^{a\text{-}\alpha} \cos(\theta_a) + \sqrt{2} I_{b0}^{a\text{-}\beta} \sin(\theta_a)\right)$$

$$+ \left(v_{a\alpha} - 2\, v_{cm}\right) \left(\cos(\theta_a) i_{bq-} + \sin(\theta_a)\left(i_{bd+} - i_{bd-}\right) + \sqrt{2} I_{b\beta}^{cm} \cos(\theta_{cm}) + \sqrt{2}\, I_{b\beta}^{b} \cos(\theta_b)\right)$$

$$+ v_{a\beta} \left(\cos(\theta_a)\left(i_{bd+} + i_{bd-}\right) + \sin(\theta_a)\, i_{bq-} + \sqrt{2} I_{b\alpha}^{cm} \cos(\theta_{cm}) + \sqrt{2} I_{b\alpha}^{b} \cos(\theta_b)\right)$$

Now,

$$\overline{P_{\Delta\beta}} = a_{(6,1)}\, i_{ad+} + a_{(6,2)}\, I_{b0}^{b} + a_{(6,3)}\, i_{bd+} + a_{(6,4)}\, I_{b0}^{cm} + a_{(6,5)}\, I_{b\alpha}^{b} + a_{(6,6)}\, I_{b\beta}^{b}$$

$$+ a_{(6,7)}\, I_{a\alpha}^{cm} + a_{(6,8)}\, I_{a\beta}^{cm} + a_{(6,9)}\, i_{ad-} + a_{(6,10)}\, i_{aq-} + a_{(6,11)}\, I_{a\alpha}^{b} + a_{(6,12)}\, I_{a\beta}^{b}$$

$$+ a_{(6,13)}\, I_{b0}^{a\text{-}\alpha} + a_{(6,14)}\, I_{b0}^{a\text{-}\beta} + a_{(6,15)}\, I_{b\alpha}^{cm} + a_{(6,16)}\, I_{b\beta}^{cm} + a_{(6,17)}\, i_{bd-} + a_{(6,18)}\, i_{bq-} + P_6$$

A.6.3 General Expressions of the Elements of the Matrices $a_{6\times18}$ and $P_{6\times1}$.

Table A.6.1: General expression for the first three (1st to 3rd) columns of the matrix (a^T).

DOF_{18x1}	$\overline{P_{\Sigma 0}}$	$\overline{P_{\Delta 0}}$	$\overline{P_{\Sigma\alpha}}$
i_{ad+}	$\overline{\frac{1}{2}\left(v_{a\alpha}\cos(\theta_a) + v_{a\beta}\sin(\theta_a)\right)}$	0	$\overline{\frac{1}{2}\left(\left(2\, v_{cm} + v_{a\alpha}\right)\cos(\theta_a) - v_{a\beta}\sin(\theta_a)\right)}$
I_{b0}^{b}	$\overline{\sqrt{2}\, v_b \cos(\theta_b)}$	$\overline{-2\sqrt{2}\, v_{cm}\cos(\theta_b)}$	0
i_{bd+}	0	$\overline{-v_{a\alpha}\cos(\theta_a) - v_{a\beta}\sin(\theta_a)}$	$\overline{v_b\cos(\theta_a)}$
I_{b0}^{cm}	$\overline{\sqrt{2}\, v_b \cos(\theta_{cm})}$	$\overline{-2\sqrt{2}\, v_{cm}\cos(\theta_{cm})}$	0
$I_{b\alpha}^{b}$	0	$\overline{-\sqrt{2}\, v_{a\alpha}\cos(\theta_b)}$	$\overline{\sqrt{2}\, v_b\cos(\theta_b)}$
$I_{b\beta}^{b}$	0	$\overline{-\sqrt{2}\, v_{a\beta}\cos(\theta_b)}$	0
$I_{a\alpha}^{cm}$	$\overline{\frac{\sqrt{2}}{2} v_{a\alpha}\cos(\theta_{cm})}$	0	$\overline{\frac{\sqrt{2}}{2}\left(2\, v_{cm} + v_{a\alpha}\right)\cos(\theta_{cm})}$

$I^{cm}_{a\beta}$	$\overline{\frac{\sqrt{2}}{2} v_{a\beta} \cos(\theta_{cm})}$	0	$\overline{-\frac{\sqrt{2}}{2} v_{a\beta} \cos(\theta_{cm})}$
i_{ad-}	$\overline{\frac{1}{2}\left(v_{a\alpha} \cos(\theta_a) - v_{a\beta} \sin(\theta_a)\right)}$	0	$\overline{\frac{1}{2}\left(\left(2 v_{cm} + v_{a\alpha}\right) \cos(\theta_a) + v_{a\beta} \sin(\theta_a)\right)}$
i_{aq-}	$\overline{\frac{1}{2}\left(v_{a\alpha} \sin(\theta_a) + v_{a\beta} \cos(\theta_a)\right)}$	0	$\overline{\frac{1}{2}\left(\left(2 v_{cm} + v_{a\alpha}\right) \sin(\theta_a) - v_{a\beta} \cos(\theta_a)\right)}$
$I^{b}_{a\alpha}$	$\overline{\frac{\sqrt{2}}{2} v_{a\alpha} \cos(\theta_b)}$	0	$\overline{\frac{\sqrt{2}}{2}\left(2 v_{cm} + v_{a\alpha}\right) \cos(\theta_b)}$
$I^{b}_{a\beta}$	$\overline{\frac{\sqrt{2}}{2} v_{a\beta} \cos(\theta_b)}$	0	$\overline{-\frac{\sqrt{2}}{2} v_{a\beta} \cos(\theta_b)}$
$I^{a\text{-}\alpha}_{b0}$	$\overline{\sqrt{2} v_b \cos(\theta_a)}$	$\overline{-2\sqrt{2} v_{cm} \cos(\theta_a)}$	0
$I^{a\text{-}\beta}_{b0}$	$\overline{\sqrt{2} v_b \sin(\theta_a)}$	$\overline{-2\sqrt{2} v_{cm} \sin(\theta_a)}$	0
$I^{cm}_{b\alpha}$	0	$\overline{-\sqrt{2} v_{a\alpha} \cos(\theta_{cm})}$	$\overline{\sqrt{2} v_b \cos(\theta_{cm})}$
$I^{cm}_{b\beta}$	0	$\overline{-\sqrt{2} v_{a\beta} \cos(\theta_{cm})}$	0
i_{bd-}	0	$\overline{-v_{a\alpha} \cos(\theta_a) + v_{a\beta} \sin(\theta_a)}$	$\overline{v_b \cos(\theta_a)}$
i_{bq-}	0	$\overline{-v_{a\alpha} \sin(\theta_a) - v_{a\beta} \cos(\theta_a)}$	$\overline{v_b \sin(\theta_a)}$

Table A.6.2.: General expression for the last three (4th to 6th) columns of the matrix (a^T).

DOF_{18x1}	$\overline{P_{\Sigma\beta}}$	$\overline{P_{\Delta\alpha}}$	$\overline{P_{\Delta\beta}}$
i_{ad+}	$\overline{\frac{1}{2}\left(\left(2 v_{cm} - v_{a\alpha}\right) \sin(\theta_a) - v_{a\beta} \cos(\theta_a)\right)}$	$\overline{-\frac{v_b}{2} \cos(\theta_a)}$	$\overline{-\frac{v_b}{2} \sin(\theta_a)}$
I^{b}_{b0}	0	$\overline{-2\sqrt{2} v_{a\alpha} \cos(\theta_b)}$	$\overline{-2\sqrt{2} v_{a\beta} \cos(\theta_b)}$
i_{bd+}	$\overline{v_b \sin(\theta_a)}$	$\overline{-\left(2 v_{cm} + v_{a\alpha}\right) \cos(\theta_a) + v_{a\beta} \sin(\theta_a)}$	$\overline{\left(-2 v_{cm} + v_{a\alpha}\right) \sin(\theta_a) + v_{a\beta} \cos(\theta_a)}$
I^{cm}_{b0}	0	$\overline{-2\sqrt{2} v_{a\alpha} \cos(\theta_{cm})}$	$\overline{-2\sqrt{2} v_{a\beta} \cos(\theta_{cm})}$
$I^{b}_{b\alpha}$	0	$\overline{-\sqrt{2}\left(2 v_{cm} + v_{a\alpha}\right) \cos(\theta_b)}$	$\overline{\sqrt{2} v_{a\beta} \cos(\theta_b)}$
$I^{b}_{b\beta}$	$\overline{\sqrt{2} v_b \cos(\theta_b)}$	$\overline{\sqrt{2} v_{a\beta} \cos(\theta_b)}$	$\overline{\sqrt{2}\left(-2 v_{cm} + v_{a\alpha}\right) \cos(\theta_b)}$
$I^{cm}_{a\alpha}$	$\overline{-\frac{\sqrt{2}}{2} v_{a\beta} \cos(\theta_{cm})}$	$\overline{-\frac{\sqrt{2}}{2} v_b \cos(\theta_{cm})}$	0

$\boldsymbol{I_{a\beta}^{cm}}$	$\overline{\frac{\sqrt{2}}{2}\left(2\,v_{cm}-v_{a\alpha}\right)\cos(\theta_{cm})}$	0	$\overline{-\frac{\sqrt{2}}{2}\,v_b\cos(\theta_{cm})}$
$\boldsymbol{i_{ad-}}$	$\overline{-\frac{1}{2}\left(\left(2\,v_{cm}-v_{a\alpha}\right)\sin(\theta_a)+v_{a\beta}\cos(\theta_a)\right)}$	$\overline{-\frac{v_b}{2}\cos(\theta_a)}$	$\overline{\frac{v_b}{2}\sin(\theta_a)}$
$\boldsymbol{i_{aq-}}$	$\overline{\frac{1}{2}\left(\left(2\,v_{cm}-v_{a\alpha}\right)\cos(\theta_a)-v_{a\beta}\sin(\theta_a)\right)}$	$\overline{-\frac{v_b}{2}\sin(\theta_a)}$	$\overline{-\frac{v_b}{2}\cos(\theta_a)}$
$\boldsymbol{I_{a\alpha}^{b}}$	$\overline{-\frac{\sqrt{2}}{2}\,v_{a\beta}\cos(\theta_b)}$	$\overline{-\frac{\sqrt{2}}{2}\,v_b\cos(\theta_b)}$	0
$\boldsymbol{I_{a\beta}^{b}}$	$\overline{\frac{\sqrt{2}}{2}\left(2\,v_{cm}-v_{a\alpha}\right)\cos(\theta_b)}$	0	$\overline{-\frac{\sqrt{2}}{2}\,v_b\cos(\theta_b)}$
$\boldsymbol{I_{b0}^{a\text{-}\alpha}}$	0	$\overline{-2\sqrt{2}\,v_{a\alpha}\cos(\theta_a)}$	$\overline{-2\sqrt{2}\,v_{a\beta}\cos(\theta_a)}$
$\boldsymbol{I_{b0}^{a\text{-}\beta}}$	0	$\overline{-2\sqrt{2}\,v_{a\alpha}\sin(\theta_a)}$	$\overline{-2\sqrt{2}\,v_{a\beta}\sin(\theta_a)}$
$\boldsymbol{I_{b\alpha}^{cm}}$	0	$\overline{-\sqrt{2}\left(2\,v_{cm}+v_{a\alpha}\right)\cos(\theta_{cm})}$	$\overline{\sqrt{2}\,v_{a\beta}\cos(\theta_{cm})}$
$\boldsymbol{I_{b\beta}^{cm}}$	$\overline{\sqrt{2}\,v_b\cos(\theta_{cm})}$	$\overline{\sqrt{2}\,v_{a\beta}\cos(\theta_{cm})}$	$\overline{\sqrt{2}\left(-2\,v_{cm}+v_{a\alpha}\right)\cos(\theta_{cm})}$
$\boldsymbol{i_{bd-}}$	$\overline{-v_b\sin(\theta_a)}$	$\overline{-\left(2\,v_{cm}+v_{a\alpha}\right)\cos(\theta_a)-v_{a\beta}\sin(\theta_a)}$	$\overline{-\left(-2\,v_{cm}+v_{a\alpha}\right)\sin(\theta_a)+v_{a\beta}\cos(\theta_a)}$
$\boldsymbol{i_{bq-}}$	$\overline{v_b\cos(\theta_a)}$	$\overline{-\left(2\,v_{cm}+v_{a\alpha}\right)\sin(\theta_a)+v_{a\beta}\cos(\theta_a)}$	$\overline{\left(-2\,v_{cm}+v_{a\alpha}\right)\cos(\theta_a)+v_{a\beta}\sin(\theta_a)}$

Table A.6.3: General expression of the matrix $P_{6\times1}$.

		$\overline{\mathbf{P_{6\times1}}}$
$\overline{\boldsymbol{P_{\Sigma0}}}$	$\boldsymbol{P_1}$	$\overline{\frac{1}{2}\left(-v_{a\alpha}\sin(\theta_a)+v_{a\beta}\cos(\theta_a)\right)i_{aq+}+v_b\sqrt{2}I_{b0}^{\perp b}\sin(\theta_b)}$
$\overline{\boldsymbol{P_{\Delta0}}}$	$\boldsymbol{P_2}$	$\overline{\left(-2\,v_{cm}\sqrt{2}I_{b0}^{\perp b}\sin(\theta_b)\right)}$
$\overline{\boldsymbol{P_{\Sigma\alpha}}}$	$\boldsymbol{P_3}$	$\overline{\frac{1}{2}\left(-\left(2\,v_{cm}+v_{a\alpha}\right)\sin(\theta_a)-v_{a\beta}\cos(\theta_a)\right)i_{aq+}}$
$\overline{\boldsymbol{P_{\Sigma\beta}}}$	$\boldsymbol{P_4}$	$\overline{\frac{1}{2}\left(\left(2\,v_{cm}-v_{a\alpha}\right)\cos(\theta_a)+v_{a\beta}\sin(\theta_a)\right)i_{aq+}}$
$\overline{\boldsymbol{P_{\Delta\alpha}}}$	$\boldsymbol{P_5}$	$\overline{\frac{v_b}{2}\sin(\theta_a)\,i_{aq+}-2\sqrt{2}\,v_{a\alpha}\,I_{b0}^{\perp b}\sin(\theta_b)}$
$\overline{\boldsymbol{P_{\Delta\beta}}}$	$\boldsymbol{P_6}$	$\overline{-\frac{v_b}{2}\cos(\theta_a)\,i_{aq+}-2\sqrt{2}\,v_{a\beta}\,I_{b0}^{\perp b}\sin(\theta_b)}$

A.6.4 Elements of the Matrices $a_{6\times18}$ and $P_{6\times1}$ for Equal Frequency ($f_a = f_b \neq 0$) Operation.

Note: For equal frequency operation ($f_b = f_a \neq 0$). Here, $f_{cm} = 3f_a$ and the frequency for mean calculation is $f_{Mean} = f_a$.

(a) $\overline{\cos(\theta_a)\cos(\theta_b)} = \overline{\sin(\theta_a)\sin(\theta_b)} = \dfrac{\cos(\phi_b)}{2}$

(b) $\overline{\cos(\theta_a)\sin(\theta_b)} = \dfrac{\sin(\phi_b)}{2}$ and (c) $\overline{\cos(\theta_b)\sin(\theta_a)} = -\dfrac{\sin(\phi_b)}{2}$

Table A.6.4: Elements of the matrix a^T for equal frequency. Here, $f_{cm} = 3f_a$.

DOF_{18x1}	$\overline{P_{\Sigma 0}}$	$\overline{P_{\Delta 0}}$	$\overline{P_{\Sigma \alpha}}$	$\overline{P_{\Sigma \beta}}$	$\overline{P_{\Delta \alpha}}$	$\overline{P_{\Delta \beta}}$
i_{ad+}	$\frac{\sqrt{2}\,V_a}{2}$	0	0	0	$-\frac{V_b}{2\sqrt{2}}\cos(\phi_b)$	$\frac{V_b}{2\sqrt{2}}\sin(\phi_b)$
I_{b0}^{b}	V_b	0	0	0	$-2\,V_a\cos(\phi_b)$	$2\,V_a\sin(\phi_b)$
i_{bd+}	0	$-\sqrt{2}\,V_a$	$\frac{V_b}{\sqrt{2}}\cos(\phi_b)$	$-\frac{V_b}{\sqrt{2}}\sin(\phi_b)$	0	0
I_{b0}^{cm}	0	$-2\,V_{cm}$	0	0	0	0
$I_{b\alpha}^{b}$	0	$-V_a\cos(\phi_b)$	V_b	0	$-V_a\cos(\phi_b)$	$-V_a\sin(\phi_b)$
$I_{b\beta}^{b}$	0	$V_a\sin(\phi_b)$	0	V_b	$-V_a\sin(\phi_b)$	$V_a\cos(\phi_b)$
$I_{a\alpha}^{cm}$	0	0	V_{cm}	0	0	0
$I_{a\beta}^{cm}$	0	0	0	V_{cm}	0	0
i_{ad-}	0	0	$\frac{\sqrt{2}\,V_a}{2}$	0	$-\frac{V_b}{2\sqrt{2}}\cos(\phi_b)$	$-\frac{V_b}{2\sqrt{2}}\sin(\phi_b)$
i_{aq-}	0	0	0	$-\frac{\sqrt{2}\,V_a}{2}$	$\frac{V_b}{2\sqrt{2}}\sin(\phi_b)$	$-\frac{V_b}{2\sqrt{2}}\cos(\phi_b)$
$I_{a\alpha}^{b}$	$\frac{V_a}{2}\cos(\phi_b)$	0	$\frac{V_a}{2}\cos(\phi_b)$	$\frac{V_a}{2}\sin(\phi_b)$	$-\frac{V_b}{2}$	0
$I_{a\beta}^{b}$	$-\frac{V_a}{2}\sin(\phi_b)$	0	$\frac{V_a}{2}\sin(\phi_b)$	$-\frac{V_a}{2}\cos(\phi_b)$	0	$-\frac{V_b}{2}$
$I_{b0}^{a\text{-}\alpha}$	$V_b\cos(\phi_b)$	0	0	0	$-2\,V_a$	0
$I_{b0}^{a\text{-}\beta}$	$-V_b\sin(\phi_b)$	0	0	0	0	$-2\,V_a$

$\boldsymbol{I_{b\alpha}^{cm}}$	0	0	0	0	$-2\,V_{cm}$	0
$\boldsymbol{I_{b\beta}^{cm}}$	0	0	0	0	0	$-2\,V_{cm}$
$\boldsymbol{i_{bd-}}$	0	0	$\frac{V_b}{\sqrt{2}}\cos(\phi_b)$	$\frac{V_b}{\sqrt{2}}\sin(\phi_b)$	$-\sqrt{2}\,V_a$	0
$\boldsymbol{i_{bq-}}$	0	0	$-\frac{V_b}{\sqrt{2}}\sin(\phi_b)$	$\frac{V_b}{\sqrt{2}}\cos(\phi_b)$	0	$\sqrt{2}\,V_a$

Table A.6.5: General expression of the matrix $P_{6\times1}$ for equal frequency ($f_a = f_b \neq 0$) operation.

	$\overline{\mathbf{P_{6\times1}}}$	
$\overline{P_{\Sigma 0}}$	P_1	0
$\overline{P_{\Delta 0}}$	P_2	0
$\overline{P_{\Sigma\alpha}}$	P_3	0
$\overline{P_{\Sigma\beta}}$	P_4	0
$\overline{P_{\Delta\alpha}}$	P_5	$-\left(\frac{V_b\, i_{aq+}}{2\sqrt{2}} + 2\,V_a\, I_{b0}^{\perp b}\right)\sin(\phi_b)$
$\overline{P_{\Delta\beta}}$	P_6	$-\left(\frac{V_b\, i_{aq+}}{2\sqrt{2}} + 2\,V_a\, I_{b0}^{\perp b}\right)\cos(\phi_b)$

A.6.5 Elements of the Matrices $a_{6\times18}$ and $P_{6\times1}$ for Unequal Frequency Operation.

Note: For unequal frequency operation ($f_a = n\,f_b$, $f_b = n\,f_a$ and ($f_b = 0$ & $f_a \neq 0$)). Here, n = integer and $f_{cm} = \text{Max}(f_o, 3f_a)$ if $f_b \neq 3f_a$, or $f_{cm} = f_x$ if $f_b = 3f_a$. The frequency for mean calculation is $f_{Mean} = f_a$ if $f_b = 0$, and $f_{Mean} = \text{Min}(f_a, f_b)$ if $f_b \neq 0$.

(a) $\overline{\cos(\theta_a)\cos(\theta_b)} = \overline{\sin(\theta_a)\sin(\theta_b)} = \overline{\sin(\theta_a)\cos(\theta_b)} = \overline{\cos(\theta_a)\sin(\theta_b)} = 0$

Table A.6.6: Elements of the matrix a^T for unequal frequency operation. Here, $f_a = n\,f_b$, $f_b = n\,f_a$, or ($f_b = 0$ & $f_a \neq 0$). n = integer, and $f_{cm} = \text{Max}(f_o, 3f_a)$ if $f_b \neq 3f_a$, or $f_{cm} = f_x$ if $f_b = 3f_a$. **Note**: $V_b = V_{dc}$ if $f_b = 0$.

$\boldsymbol{DOF_{18x1}}$	$\overline{P_{\Sigma 0}}$	$\overline{P_{\Delta 0}}$	$\overline{P_{\Sigma\alpha}}$	$\overline{P_{\Sigma\beta}}$	$\overline{P_{\Delta\alpha}}$	$\overline{P_{\Delta\beta}}$
$\boldsymbol{i_{ad+}}$	$\frac{\sqrt{2}\,V_a}{2}$	0	0	0	0	0
$\boldsymbol{I_{b0}^{b}}$	V_b	0	0	0	0	0

$\boldsymbol{i_{bd+}}$	0	$-\sqrt{2}\,V_a$	0	0	0	0
$\boldsymbol{I_{b0}^{cm}}$	0	$-2\,V_{cm}$	0	0	0	0
$\boldsymbol{I_{b\alpha}^{b}}$	0	0	V_b	0	0	0
$\boldsymbol{I_{b\beta}^{b}}$	0	0	0	V_b	0	0
$\boldsymbol{I_{a\alpha}^{cm}}$	0	0	V_{cm}	0	0	0
$\boldsymbol{I_{a\beta}^{cm}}$	0	0	0	V_{cm}	0	0
$\boldsymbol{i_{ad-}}$	0	0	$\frac{\sqrt{2}\,V_a}{2}$	0	0	0
$\boldsymbol{i_{aq-}}$	0	0	0	$-\frac{\sqrt{2}\,V_a}{2}$	0	0
$\boldsymbol{I_{a\alpha}^{b}}$	0	0	0	0	$-\frac{V_b}{2}$	0
$\boldsymbol{I_{a\beta}^{b}}$	0	0	0	0	0	$-\frac{V_b}{2}$
$\boldsymbol{I_{b0}^{a\text{-}\alpha}}$	0	0	0	0	$-2\,V_a$	0
$\boldsymbol{I_{b0}^{a\text{-}\beta}}$	0	0	0	0	0	$-2\,V_a$
$\boldsymbol{I_{b\alpha}^{cm}}$	0	0	0	0	$-2\,V_{cm}$	0
$\boldsymbol{I_{b\beta}^{cm}}$	0	0	0	0	0	$-2\,V_{cm}$
$\boldsymbol{i_{bd-}}$	0	0	0	0	$-\sqrt{2}\,V_a$	0
$\boldsymbol{i_{bq-}}$	0	0	0	0	0	$\sqrt{2}\,V_a$

Table A.6.7: General expression of the matrix $P_{6\times1}$ for unequal frequency operation. Here, $f_a = n f_b$, $f_b = n f_a$, or ($f_b = 0$ & $f_a \neq 0$). n = integer and $f_{cm} = \text{Max}(f_o, 3f_a)$ if $f_b \neq 3f_a$, or $f_{cm} = f_x$ if $f_b = 3f_a$.

$\overline{\mathbf{P_{6\times1}}}$	$\mathbf{P_1 = P_2 = P_3 = P_4 = P_5 = P_6 = 0}$

A.7 Matrix A_{6x6} for Equal and Unequal Frequency Operations

A.7.1 Solution of the Average Arm Power Equations in the Steady State.

$$\left(\overline{P_{\Sigma/\Delta\alpha\beta 0}}\right)_{6x1} = A_{6x6}\, MI_{6x1} + \overline{P_{rem(6x1)}} = 0_{6x1} \tag{A7.1}$$

$$MI_{6x1} = -A_{6x6}^{-1}\ \overline{P_{rem(6x1)}} \tag{A7.2}$$

A.7.2 Matrix A_{6x6} for Energy Balancing Methods for Equal Frequency ($f_a = f_b \neq 0$) Operation.

Table A.7.1: Matrix A and its determinant (|A|) for the various energy balancing methods for equal frequency operation ($f_b = f_a \neq 0$).

Method	Matrix A and its determinant (|A|)
1	**A** = **a**(1:6,[1, 3, 5, 6, 17, 18]) $\begin{pmatrix} \frac{\sqrt{2}}{2}V_a & 0 & 0 & 0 & 0 & 0 \\ 0 & -\sqrt{2}\,V_a & -V_a\cos(\phi_b) & V_a\sin(\phi_b) & 0 & 0 \\ 0 & \frac{\sqrt{2}}{2}V_b\cos(\phi_b) & V_b & 0 & \frac{\sqrt{2}}{2}V_b\cos(\phi_b) & -\frac{\sqrt{2}}{2}V_b\sin(\phi_b) \\ 0 & -\frac{\sqrt{2}}{2}V_b\sin(\phi_b) & 0 & V_b & \frac{\sqrt{2}}{2}V_b\sin(\phi_b) & \frac{\sqrt{2}}{2}V_b\cos(\phi_b) \\ -\frac{\sqrt{2}}{4}V_b\cos(\phi_b) & 0 & -V_a\cos(\phi_b) & -V_a\sin(\phi_b) & -\sqrt{2}\,V_a & 0 \\ \frac{\sqrt{2}}{4}V_b\sin(\phi_b) & 0 & -V_a\sin(\phi_b) & V_a\cos(\phi_b) & 0 & \sqrt{2}\,V_a \end{pmatrix}$ **|A| = 0**
2	**A** = **a**(1:6,[1, 3, 5, 6, 11, 12]) $\begin{pmatrix} \frac{\sqrt{2}}{2}V_a & 0 & 0 & 0 & \frac{1}{2}V_a\cos(\phi_b) & -\frac{1}{2}V_a\sin(\phi_b) \\ 0 & -\sqrt{2}\,V_a & -V_a\cos(\phi_b) & V_a\sin(\phi_b) & 0 & 0 \\ 0 & \frac{\sqrt{2}}{2}V_b\cos(\phi_b) & V_b & 0 & \frac{1}{2}V_a\cos(\phi_b) & \frac{1}{2}V_a\sin(\phi_b) \\ 0 & -\frac{\sqrt{2}}{2}V_b\sin(\phi_b) & 0 & V_b & \frac{1}{2}V_a\sin(\phi_b) & -\frac{1}{2}V_a\cos(\phi_b) \\ -\frac{\sqrt{2}}{4}V_b\cos(\phi_b) & 0 & -V_a\cos(\phi_b) & -V_a\sin(\phi_b) & -\frac{1}{2}V_b & 0 \\ \frac{\sqrt{2}}{4}V_b\sin(\phi_b) & 0 & -V_a\sin(\phi_b) & V_a\cos(\phi_b) & 0 & -\frac{1}{2}V_b \end{pmatrix}$ $\lvert A\rvert = \frac{V_a^2}{16}\left(\cos^2(3\phi_b)\,V_a^2\,V_b^2\right) - \frac{V_a^2}{16}\left(2V_a^2 - V_b^2\right)^2$

3

$$\mathbf{A} = \mathbf{a}(1{:}6,[1, 3, 9, 10, 17, 18])$$

$$\begin{pmatrix} \frac{\sqrt{2}}{2} V_a & 0 & 0 & 0 & 0 & 0 \\ 0 & -\sqrt{2}\, V_a & 0 & 0 & 0 & 0 \\ 0 & \frac{\sqrt{2}}{2} V_b \cos(\phi_b) & \frac{\sqrt{2}}{2} V_a & 0 & \frac{\sqrt{2}}{2} V_b \cos(\phi_b) & -\frac{\sqrt{2}}{2} V_b \sin(\phi_b) \\ 0 & -\frac{\sqrt{2}}{2} V_b \sin(\phi_b) & 0 & -\frac{\sqrt{2}}{2} V_a & \frac{\sqrt{2}}{2} V_b \sin(\phi_b) & \frac{\sqrt{2}}{2} V_b \cos(\phi_b) \\ -\frac{\sqrt{2}}{4} V_b \cos(\phi_b) & 0 & -\frac{\sqrt{2}}{4} V_b \cos(\phi_b) & \frac{\sqrt{2}}{4} V_b \sin(\phi_b) & -\sqrt{2}\, V_a & 0 \\ \frac{\sqrt{2}}{4} V_b \sin(\phi_b) & 0 & -\frac{\sqrt{2}}{4} V_b \sin(\phi_b) & -\frac{\sqrt{2}}{4} V_b \cos(\phi_b) & 0 & \sqrt{2}\, V_a \end{pmatrix}$$

$$|\mathbf{A}| = -V_a^2 \left(V_a^2 - \frac{V_b^2}{4} \right)^2$$

4

$$\mathbf{A} = \mathbf{a}(1{:}6,[1, 3, 9, 10, 11, 12])$$

$$\begin{pmatrix} \frac{\sqrt{2}}{2} V_a & 0 & 0 & 0 & \frac{1}{2} V_a \cos(\phi_b) & -\frac{1}{2} V_a \sin(\phi_b) \\ 0 & -\sqrt{2}\, V_a & 0 & 0 & 0 & 0 \\ 0 & \frac{\sqrt{2}}{2} V_b \cos(\phi_b) & \frac{\sqrt{2}}{2} V_a & 0 & \frac{1}{2} V_a \cos(\phi_b) & \frac{1}{2} V_a \sin(\phi_b) \\ 0 & -\frac{\sqrt{2}}{2} V_b \sin(\phi_b) & 0 & -\frac{\sqrt{2}}{2} V_a & \frac{1}{2} V_a \sin(\phi_b) & -\frac{1}{2} V_a \cos(\phi_b) \\ -\frac{\sqrt{2}}{4} V_b \cos(\phi_b) & 0 & -\frac{\sqrt{2}}{4} V_b \cos(\phi_b) & \frac{\sqrt{2}}{4} V_b \sin(\phi_b) & -\frac{1}{2} V_b & 0 \\ \frac{\sqrt{2}}{4} V_b \sin(\phi_b) & 0 & -\frac{\sqrt{2}}{4} V_b \sin(\phi_b) & -\frac{\sqrt{2}}{4} V_b \cos(\phi_b) & 0 & -\frac{1}{2} V_b \end{pmatrix}$$

$$|\mathbf{A}| = 0$$

5

$$\mathbf{A} = \mathbf{a}(1{:}6,[2, 3, 5, 6, 17, 18])$$

$$\begin{pmatrix} V_b & 0 & 0 & 0 & 0 & 0 \\ 0 & -\sqrt{2}\, V_a & -V_a \cos(\phi_b) & V_a \sin(\phi_b) & 0 & 0 \\ 0 & \frac{\sqrt{2}}{2} V_b \cos(\phi_b) & V_b & 0 & \frac{\sqrt{2}}{2} V_b \cos(\phi_b) & -\frac{\sqrt{2}}{2} V_b \sin(\phi_b) \\ 0 & -\frac{\sqrt{2}}{2} V_b \sin(\phi_b) & 0 & V_b & \frac{\sqrt{2}}{2} V_b \sin(\phi_b) & \frac{\sqrt{2}}{2} V_b \cos(\phi_b) \\ -2\, V_a \cos(\phi_b) & 0 & -V_a \cos(\phi_b) & -V_a \sin(\phi_b) & -\sqrt{2}\, V_a & 0 \\ 2\, V_a \sin(\phi_b) & 0 & -V_a \sin(\phi_b) & V_a \cos(\phi_b) & 0 & \sqrt{2}\, V_a \end{pmatrix}$$

$$|\mathbf{A}| = 0$$

6	$\mathbf{A} = \mathbf{a}(1{:}6,[2, 3, 5, 6, 13, 14])$ $\begin{pmatrix} V_b & 0 & 0 & 0 & V_b \cos(\phi_b) & -V_b \sin(\phi_b) \\ 0 & -\sqrt{2}\, V_a & -V_a \cos(\phi_b) & V_a \sin(\phi_b) & 0 & 0 \\ 0 & \frac{\sqrt{2}}{2} V_b \cos(\phi_b) & V_b & 0 & 0 & 0 \\ 0 & -\frac{\sqrt{2}}{2} V_b \sin(\phi_b) & 0 & V_b & 0 & 0 \\ -2\, V_a \cos(\phi_b) & 0 & -V_a \cos(\phi_b) & -V_a \sin(\phi_b) & -2\, V_a & 0 \\ 2\, V_a \sin(\phi_b) & 0 & -V_a \sin(\phi_b) & V_a \cos(\phi_b) & 0 & -2\, V_a \end{pmatrix}$ $\lvert\mathbf{A}\rvert = 0$
7	$\mathbf{A} = \mathbf{a}(1{:}6,[1, 3, 5, 6, 15, 16])$ $\begin{pmatrix} \frac{\sqrt{2}}{2} V_a & 0 & 0 & 0 & 0 & 0 \\ 0 & -\sqrt{2}\, V_a & -V_a \cos(\phi_b) & V_a \sin(\phi_b) & 0 & 0 \\ 0 & \frac{\sqrt{2}}{2} V_b \cos(\phi_b) & V_b & 0 & 0 & 0 \\ 0 & -\frac{\sqrt{2}}{2} V_b \sin(\phi_b) & 0 & V_b & 0 & 0 \\ -\frac{\sqrt{2}}{4} V_b \cos(\phi_b) & 0 & -V_a \cos(\phi_b) & -V_a \sin(\phi_b) & -2\, V_{cm} & 0 \\ \frac{\sqrt{2}}{4} V_b \sin(\phi_b) & 0 & -V_a \sin(\phi_b) & V_a \cos(\phi_b) & 0 & -2\, V_{cm} \end{pmatrix}$ $\lvert\mathbf{A}\rvert = -2\, V_a^2\, V_b^2\, V_{cm}^2$
8	$\mathbf{A} = \mathbf{a}(1{:}6,[1, 3, 7, 8, 11, 12])$ $\begin{pmatrix} \frac{\sqrt{2}}{2} V_a & 0 & 0 & 0 & \frac{1}{2} V_a \cos(\phi_b) & -\frac{1}{2} V_a \sin(\phi_b) \\ 0 & -\sqrt{2}\, V_a & 0 & 0 & 0 & 0 \\ 0 & \frac{\sqrt{2}}{2} V_b \cos(\phi_b) & V_{cm} & 0 & \frac{1}{2} V_a \cos(\phi_b) & \frac{1}{2} V_a \sin(\phi_b) \\ 0 & -\frac{\sqrt{2}}{2} V_b \sin(\phi_b) & 0 & V_{cm} & \frac{1}{2} V_a \sin(\phi_b) & -\frac{1}{2} V_a \cos(\phi_b) \\ -\frac{\sqrt{2}}{4} V_b \cos(\phi_b) & 0 & 0 & 0 & -\frac{1}{2} V_b & 0 \\ \frac{\sqrt{2}}{4} V_b \sin_{(b)} & 0 & 0 & 0 & 0 & -\frac{1}{2} V_b \end{pmatrix}$ $\lvert\mathbf{A}\rvert = -\frac{1}{8} V_a^2\, V_b^2\, V_{cm}^2$

9

$$\mathbf{A} = \mathbf{a}(1{:}6,[1, 3, 7, 8, 15, 16])$$

$$\begin{pmatrix} \frac{\sqrt{2}}{2} V_a & 0 & 0 & 0 & 0 & 0 \\ 0 & -\sqrt{2}\, V_a & 0 & 0 & 0 & 0 \\ 0 & \frac{\sqrt{2}}{2} V_b \cos(\phi_b) & V_{cm} & 0 & 0 & 0 \\ 0 & -\frac{\sqrt{2}}{2} V_b \sin(\phi_b) & 0 & V_{cm} & 0 & 0 \\ -\frac{\sqrt{2}}{4} V_b \cos(\phi_b) & 0 & 0 & 0 & -2\, V_{cm} & 0 \\ \frac{\sqrt{2}}{4} V_b \sin(\phi_b) & 0 & 0 & 0 & 0 & -2\, V_{cm} \end{pmatrix}$$

$$|\mathbf{A}| = -4\, V_a^2\, V_{cm}^4$$

10

$$\mathbf{A} = \mathbf{a}(1{:}6,[1, 3, 7, 8, 17, 18])$$

$$\begin{pmatrix} \frac{\sqrt{2}}{2} V_a & 0 & 0 & 0 & 0 & 0 \\ 0 & -\sqrt{2}\, V_a & 0 & 0 & 0 & 0 \\ 0 & \frac{\sqrt{2}}{2} V_b \cos(\phi_b) & V_{cm} & 0 & \frac{\sqrt{2}}{2} V_b \cos(\phi_b) & -\frac{\sqrt{2}}{2} V_b \sin(\phi_b) \\ 0 & -\frac{\sqrt{2}}{2} V_b \sin(\phi_b) & 0 & V_{cm} & \frac{\sqrt{2}}{2} V_b \sin(\phi_b) & \frac{\sqrt{2}}{2} V_b \cos(\phi_b) \\ -\frac{\sqrt{2}}{4} V_b \cos(\phi_b) & 0 & 0 & 0 & -\sqrt{2}\, V_a & 0 \\ \frac{\sqrt{2}}{4} V_b \sin(\phi_b) & 0 & 0 & 0 & 0 & \sqrt{2}\, V_a \end{pmatrix}$$

$$|\mathbf{A}| = 2\, V_a^4\, V_{cm}^2$$

11

$$\mathbf{A} = \mathbf{a}(1{:}6,[1, 3, 9, 10, 15, 16])$$

$$\begin{pmatrix} \frac{\sqrt{2}}{2} V_a & 0 & 0 & 0 & 0 & 0 \\ 0 & -\sqrt{2}\, V_a & 0 & 0 & 0 & 0 \\ 0 & \frac{\sqrt{2}}{2} V_b \cos(\phi_b) & \frac{\sqrt{2}}{2} V_a & 0 & 0 & 0 \\ 0 & -\frac{\sqrt{2}}{2} V_b \sin(\phi_b) & 0 & -\frac{\sqrt{2}}{2} V_a & 0 & 0 \\ -\frac{\sqrt{2}}{4} V_b \cos(\phi_b) & 0 & -\frac{\sqrt{2}}{4} V_b \cos(\phi_b) & \frac{\sqrt{2}}{4} V_b \sin(\phi_b) & -2\, V_{cm} & 0 \\ \frac{\sqrt{2}}{4} V_b \sin(\phi_b) & 0 & -\frac{\sqrt{2}}{4} V_b \sin(\phi_b) & -\frac{\sqrt{2}}{4} V_b \cos(\phi_b) & 0 & -2\, V_{cm} \end{pmatrix}$$

$$|\mathbf{A}| = 2\, V_a^4\, V_{cm}^2$$

12

$$\mathbf{A} = \mathbf{a}(1{:}6,[2, 3, 5, 6, 15, 16])$$

$$\begin{pmatrix} V_b & 0 & 0 & 0 & 0 & 0 \\ 0 & -\sqrt{2}\,V_a & -V_a\cos(\phi_b) & V_a\sin(\phi_b) & 0 & 0 \\ 0 & \frac{\sqrt{2}}{2}V_b\cos(\phi_b) & V_b & 0 & 0 & 0 \\ 0 & -\frac{\sqrt{2}}{2}V_b\sin(\phi_b) & 0 & V_b & 0 & 0 \\ -2\,V_a\cos(\phi_b) & 0 & -V_a\cos(\phi_b) & -V_a\sin(\phi_b) & -2\,V_{cm} & 0 \\ 2\,V_a\sin(\phi_b) & 0 & -V_a\sin(\phi_b) & V_a\cos(\phi_b) & 0 & -2\,V_{cm} \end{pmatrix}$$

$$|\mathbf{A}| = -2\sqrt{2}\,V_a\,V_b^3\,V_{cm}^2$$

13

$$\mathbf{A} = \mathbf{a}(1{:}6,[2, 4, 5, 6, 13, 14])$$

$$\begin{pmatrix} V_b & 0 & 0 & 0 & V_b\cos(\phi_b) & -V_b\sin(\phi_b) \\ 0 & -2\,V_{cm} & -V_a\cos(\phi_b) & V_a\sin(\phi_b) & 0 & 0 \\ 0 & 0 & V_b & 0 & 0 & 0 \\ 0 & 0 & 0 & V_b & 0 & 0 \\ -2\,V_a\cos(\phi_b) & 0 & -V_a\cos(\phi_b) & -V_a\sin(\phi_b) & -2\,V_a & 0 \\ 2\,V_a\sin(\phi_b) & 0 & -V_a\sin(\phi_b) & V_a\cos(\phi_b) & 0 & -2\,V_a \end{pmatrix}$$

$$|\mathbf{A}| = 0$$

14

$$\mathbf{A} = \mathbf{a}(1{:}6,[2, 4, 5, 6, 15, 16])$$

$$\begin{pmatrix} V_b & 0 & 0 & 0 & 0 & 0 \\ 0 & -2\,V_{cm} & -V_a\cos(\phi_b) & V_a\sin(\phi_b) & 0 & 0 \\ 0 & 0 & V_b & 0 & 0 & 0 \\ 0 & 0 & 0 & V_b & 0 & 0 \\ -2\,V_a\cos(\phi_b) & 0 & -V_a\cos(\phi_b) & -V_a\sin(\phi_b) & -2\,V_{cm} & 0 \\ 2\,V_a\sin(\phi_b) & 0 & -V_a\sin(\phi_b) & V_a\cos(\phi_b) & 0 & -2\,V_{cm} \end{pmatrix}$$

$$|\mathbf{A}| = -8\,V_b^3\,V_{cm}^3$$

15	$\mathbf{A} = \mathbf{a}(1{:}6,[2, 4, 5, 6, 17, 18])$ $\begin{pmatrix} V_b & 0 & 0 & 0 & 0 & 0 \\ 0 & -2\,V_{cm} & -V_a\cos(\phi_b) & V_a\sin(\phi_b) & 0 & 0 \\ 0 & 0 & V_b & 0 & \frac{\sqrt{2}}{2}V_b\cos(\phi_b) & -\frac{\sqrt{2}}{2}V_b\sin(\phi_b) \\ 0 & 0 & 0 & V_b & \frac{\sqrt{2}}{2}V_b\sin(\phi_b) & \frac{\sqrt{2}}{2}V_b\cos(\phi_b) \\ -2\,V_a\cos(\phi_b) & 0 & -V_a\cos(\phi_b) & -V_a\sin(\phi_b) & -\sqrt{2}\,V_a & 0 \\ 2\,V_a\sin(\phi_b) & 0 & -V_a\sin(\phi_b) & V_a\cos(\phi_b) & 0 & \sqrt{2}\,V_a \end{pmatrix}$ $\lvert\mathbf{A}\rvert = V_a^2\,V_b^3\,V_{cm}$

A.7.3 Matrix A_{6x6} for Energy Balancing Methods for Unequal Frequency Operations.

Table A.7.2: Matrix A and its determinant (|A|) for the various energy balancing methods for unequal frequency operation ($f_b \neq f_a$). Here, $f_a = n f_b$, $f_b = n f_a$, or ($f_b = 0$ & $f_a \neq 0$). n = integer, $f_{cm} = \text{Max}(f_o, 3f_a)$ if $f_b \neq 3f_a$, $f_{cm} = f_x$ if $f_b = 3f_a$, and $V_b = V_{dc}$ if $f_b = 0$.

Method	Matrix A and its determinant (|A|)
1	$\mathbf{A} = \mathbf{a}(1{:}6,[1, 3, 5, 6, 17, 18])$ $\begin{pmatrix} \frac{\sqrt{2}}{2}V_a & 0 & 0 & 0 & 0 & 0 \\ 0 & -\sqrt{2}\,V_a & 0 & 0 & 0 & 0 \\ 0 & 0 & V_b & 0 & 0 & 0 \\ 0 & 0 & 0 & V_b & 0 & 0 \\ 0 & 0 & 0 & 0 & -\sqrt{2}\,V_a & 0 \\ 0 & 0 & 0 & 0 & 0 & \sqrt{2}\,V_a \end{pmatrix}$ $\lvert\mathbf{A}\rvert = 2\,V_a^4\,V_b^2$
2	$\mathbf{A} = \mathbf{a}(1{:}6,[1, 3, 5, 6, 11, 12])$ $\begin{pmatrix} \frac{\sqrt{2}}{2}V_a & 0 & 0 & 0 & 0 & 0 \\ 0 & -\sqrt{2}\,V_a & 0 & 0 & 0 & 0 \\ 0 & 0 & V_b & 0 & 0 & 0 \\ 0 & 0 & 0 & V_b & 0 & 0 \\ 0 & 0 & 0 & 0 & -\frac{1}{2}V_b & 0 \\ 0 & 0 & 0 & 0 & 0 & -\frac{1}{2}V_b \end{pmatrix}$ $\lvert\mathbf{A}\rvert = -\frac{1}{4}V_a^2\,V_b^4$

3	$\mathbf{A} = \mathbf{a}(1{:}6,[1, 3, 9, 10, 17, 18])$ $\begin{pmatrix} \frac{\sqrt{2}}{2} V_a & 0 & 0 & 0 & 0 & 0 \\ 0 & -\sqrt{2}\, V_a & 0 & 0 & 0 & 0 \\ 0 & 0 & \frac{\sqrt{2}}{2} V_a & 0 & 0 & 0 \\ 0 & 0 & 0 & -\frac{\sqrt{2}}{2} V_a & 0 & 0 \\ 0 & 0 & 0 & 0 & -\sqrt{2}\, V_a & 0 \\ 0 & 0 & 0 & 0 & 0 & \sqrt{2}\, V_a \end{pmatrix}$ $\lvert\mathbf{A}\rvert = -V_a^6$
4	$\mathbf{A} = \mathbf{a}(1{:}6,[1, 3, 9, 10, 11, 12])$ $\begin{pmatrix} \frac{\sqrt{2}}{2} V_a & 0 & 0 & 0 & 0 & 0 \\ 0 & -\sqrt{2}\, V_a & 0 & 0 & 0 & 0 \\ 0 & 0 & \frac{\sqrt{2}}{2} V_a & 0 & 0 & 0 \\ 0 & 0 & 0 & -\frac{\sqrt{2}}{2} V_a & 0 & 0 \\ 0 & 0 & 0 & 0 & -\frac{1}{2} V_b & 0 \\ 0 & 0 & 0 & 0 & 0 & -\frac{1}{2} V_b \end{pmatrix}$ $\lvert\mathbf{A}\rvert = \frac{1}{8} V_a^4 V_b^2$
5	$\mathbf{A} = \mathbf{a}(1{:}6,[2, 3, 5, 6, 17, 18])$ $\begin{pmatrix} V_b & 0 & 0 & 0 & 0 & 0 \\ 0 & -\sqrt{2}\, V_a & 0 & 0 & 0 & 0 \\ 0 & 0 & V_b & 0 & 0 & 0 \\ 0 & 0 & 0 & V_b & 0 & 0 \\ 0 & 0 & 0 & 0 & -\sqrt{2}\, V_a & 0 \\ 0 & 0 & 0 & 0 & 0 & \sqrt{2}\, V_a \end{pmatrix}$ $\lvert\mathbf{A}\rvert = 2\sqrt{2}\, V_a^3 V_b^3$
6	$\mathbf{A} = \mathbf{a}(1{:}6,[2, 3, 5, 6, 13, 14])$ $\begin{pmatrix} V_b & 0 & 0 & 0 & 0 & 0 \\ 0 & -\sqrt{2}\, V_a & 0 & 0 & 0 & 0 \\ 0 & 0 & V_b & 0 & 0 & 0 \\ 0 & 0 & 0 & V_b & 0 & 0 \\ 0 & 0 & 0 & 0 & -2\, V_a & 0 \\ 0 & 0 & 0 & 0 & 0 & -2 V_a \end{pmatrix}$ $\lvert\mathbf{A}\rvert = -4\sqrt{2}\, V_a^3 V_b^3$

7	$\mathbf{A} = \mathbf{a}(1{:}6,[1, 3, 5, 6, 15, 16])$ $\begin{pmatrix} \frac{\sqrt{2}}{2} V_a & 0 & 0 & 0 & 0 & 0 \\ 0 & -\sqrt{2}\, V_a & 0 & 0 & 0 & 0 \\ 0 & 0 & V_b & 0 & 0 & 0 \\ 0 & 0 & 0 & V_b & 0 & 0 \\ 0 & 0 & 0 & 0 & -2\, V_{cm} & 0 \\ 0 & 0 & 0 & 0 & 0 & -2\, V_{cm} \end{pmatrix}$ $\lvert\mathbf{A}\rvert = -4\, V_a^2\, V_b^2\, V_{cm}^2$
8	$\mathbf{A} = \mathbf{a}(1{:}6,[1, 3, 7, 8, 11, 12])$ $\begin{pmatrix} \frac{\sqrt{2}}{2} V_a & 0 & 0 & 0 & 0 & 0 \\ 0 & -\sqrt{2}\, V_a & 0 & 0 & 0 & 0 \\ 0 & 0 & V_{cm} & 0 & 0 & 0 \\ 0 & 0 & 0 & V_{cm} & 0 & 0 \\ 0 & 0 & 0 & 0 & -\frac{1}{2} V_b & 0 \\ 0 & 0 & 0 & 0 & 0 & -\frac{1}{2} V_b \end{pmatrix}$ $\lvert\mathbf{A}\rvert = -\frac{1}{4} V_a^2\, V_b^2\, V_{cm}^2$
9	$\mathbf{A} = \mathbf{a}(1{:}6,[1, 3, 7, 8, 15, 16])$ $\begin{pmatrix} \frac{\sqrt{2}}{2} V_a & 0 & 0 & 0 & 0 & 0 \\ 0 & -\sqrt{2}\, V_a & 0 & 0 & 0 & 0 \\ 0 & 0 & V_{cm} & 0 & 0 & 0 \\ 0 & 0 & 0 & V_{cm} & 0 & 0 \\ 0 & 0 & 0 & 0 & -2\, V_{cm} & 0 \\ 0 & 0 & 0 & 0 & 0 & -2\, V_{cm} \end{pmatrix}$ $\lvert\mathbf{A}\rvert = -4\, V_a^2\, V_{cm}^4$
10	$\mathbf{A} = \mathbf{a}(1{:}6,[1, 3, 7, 8, 17, 18])$ $\begin{pmatrix} \frac{\sqrt{2}}{2} V_a & 0 & 0 & 0 & 0 & 0 \\ 0 & -\sqrt{2}\, V_a & 0 & 0 & 0 & 0 \\ 0 & 0 & V_{cm} & 0 & 0 & 0 \\ 0 & 0 & 0 & V_{cm} & 0 & 0 \\ 0 & 0 & 0 & 0 & -\sqrt{2}\, V_a & 0 \\ 0 & 0 & 0 & 0 & 0 & \sqrt{2}\, V_a \end{pmatrix}$ $\lvert\mathbf{A}\rvert = 2\, V_a^4\, V_{cm}^2$

11	$\mathbf{A} = \mathbf{a}(1{:}6,[1, 3, 9, 10, 15, 16])$ $\begin{pmatrix} \frac{\sqrt{2}}{2} V_a & 0 & 0 & 0 & 0 & 0 \\ 0 & -\sqrt{2}\, V_a & 0 & 0 & 0 & 0 \\ 0 & 0 & \frac{\sqrt{2}}{2} V_a & 0 & 0 & 0 \\ 0 & 0 & 0 & -\frac{\sqrt{2}}{2} V_a & 0 & 0 \\ 0 & 0 & 0 & 0 & -2\, V_{cm} & 0 \\ 0 & 0 & 0 & 0 & 0 & -2\, V_{cm} \end{pmatrix}$ $\lvert\mathbf{A}\rvert = 2\, V_a^4\, V_{cm}^2$
12	$\mathbf{A} = \mathbf{a}(1{:}6,[2, 3, 5, 6, 15, 16])$ $\begin{pmatrix} V_b & 0 & 0 & 0 & 0 & 0 \\ 0 & -\sqrt{2}\, V_a & 0 & 0 & 0 & 0 \\ 0 & 0 & V_b & 0 & 0 & 0 \\ 0 & 0 & 0 & V_b & 0 & 0 \\ 0 & 0 & 0 & 0 & -2\, V_{cm} & 0 \\ 0 & 0 & 0 & 0 & 0 & -2\, V_{cm} \end{pmatrix}$ $\lvert\mathbf{A}\rvert = -4\sqrt{2}\, V_a\, V_b^3\, V_{cm}^2$
13	$\mathbf{A} = \mathbf{a}(1{:}6,[2, 4, 5, 6, 13, 14])$ $\begin{pmatrix} V_b & 0 & 0 & 0 & 0 & 0 \\ 0 & -2\, V_{cm} & 0 & 0 & 0 & 0 \\ 0 & 0 & V_b & 0 & 0 & 0 \\ 0 & 0 & 0 & V_b & 0 & 0 \\ 0 & 0 & 0 & 0 & -2\, V_a & 0 \\ 0 & 0 & 0 & 0 & 0 & -\sqrt{2}\, V_a \end{pmatrix}$ $\lvert\mathbf{A}\rvert = -8\, V_a^2\, V_b^3\, V_{cm}$
14	$\mathbf{A} = \mathbf{a}(1{:}6,[2, 4, 5, 6, 15, 16])$ $\begin{pmatrix} V_b & 0 & 0 & 0 & 0 & 0 \\ 0 & -2\, V_{cm} & 0 & 0 & 0 & 0 \\ 0 & 0 & V_b & 0 & 0 & 0 \\ 0 & 0 & 0 & V_b & 0 & 0 \\ 0 & 0 & 0 & 0 & -2\, V_{cm} & 0 \\ 0 & 0 & 0 & 0 & 0 & -2\, V_{cm} \end{pmatrix}$ $\lvert\mathbf{A}\rvert = -8\, V_b^3\, V_{cm}^3$

15	$\mathbf{A} = \mathbf{a}(1{:}6,[2, 4, 5, 6, 17, 18])$ $\begin{pmatrix} V_b & 0 & 0 & 0 & 0 & 0 \\ 0 & -2\,V_{cm} & 0 & 0 & 0 & 0 \\ 0 & 0 & V_b & 0 & 0 & 0 \\ 0 & 0 & 0 & V_b & 0 & 0 \\ 0 & 0 & 0 & 0 & -\sqrt{2}\,V_a & 0 \\ 0 & 0 & 0 & 0 & 0 & \sqrt{2}\,V_a \end{pmatrix}$ $\lvert\mathbf{A}\rvert = 4 V_a^2 V_b^3 V_{cm}$

A.8 Design of the Average Arm Energy Controllers of MMC

A.8.1 Design of the General Average Arm Energy Controller of MMC.

$$\overline{P_{(mn)}} = V_{\mathrm{MI}(mn)}\, I_{\mathrm{MI}(mn)} + \overline{P_{\mathrm{dis}(mn)}} \tag{A8.1}$$

Here, $m = \Sigma$ or Δ and $n = \alpha$, β or 0.

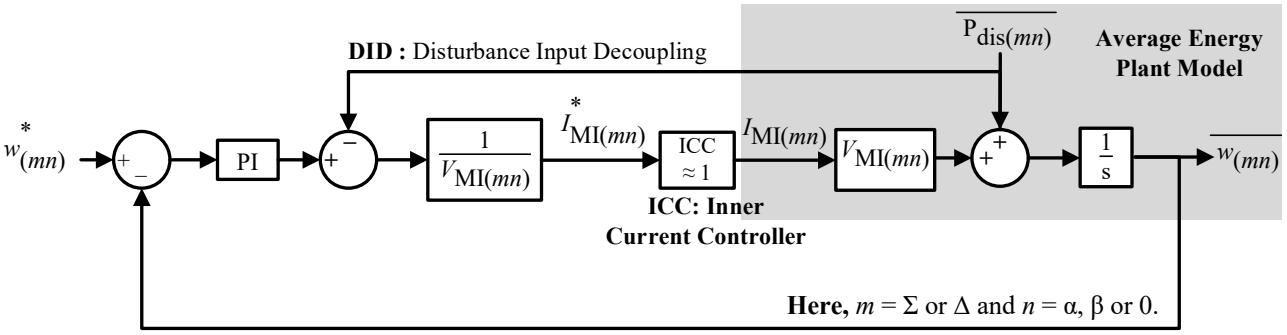

PI Tuning:

(a) Continuous-Time Domain	(b) Discrete-Time Domain
$K_{\mathrm{p}} = \dfrac{\left(1 - \mathrm{e}^{-2\pi(f_1+f_2)T_{\mathrm{s}}}\right)}{T_{\mathrm{s}}}$ $K_{\mathrm{I}} = \dfrac{1}{T_{\mathrm{s}}}\left(\dfrac{2 - \left(\mathrm{e}^{-2\pi f_1 T_{\mathrm{s}}} + \mathrm{e}^{-2\pi f_2 T_{\mathrm{s}}}\right)}{T_{\mathrm{s}}} - K_{\mathrm{p}}\right)$	$K_{\mathrm{p}} = 2\pi(f_1 + f_2)$ $K_{\mathrm{i}} = 4\pi^2 f_1 f_2$

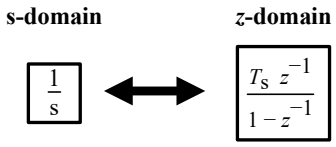

Figure A.8.1: Design of a general average outer arm energy control loop for MMC.

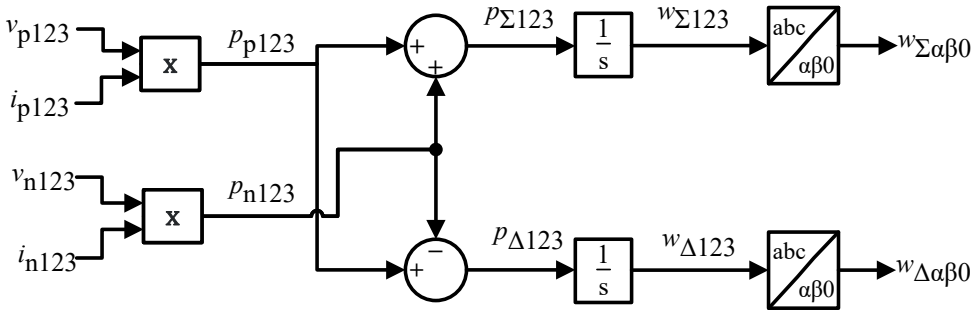

(a) Arm energies computation using the arm currents and voltages

$$w_{xy} = \frac{C_{\mathrm{SM}}}{2} \sum_{n=1}^{N} v_{\mathrm{c}xyn}^2$$

Here, x = p, or n

y = 1, 2, or 3

$v_{\mathrm{c}xyn}$ = DC-link voltage of n^{th} SM for the arm xy

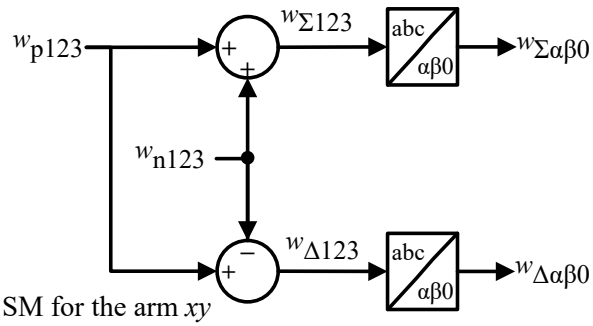

(b) Arm energies computation using the DC-link SM's capacitor voltages

Figure A.8.2: Computation of instantaneous arm energies using the arm powers and currents.

A.8.2 Coefficients of the General Average Arm Power Equation $\left(\overline{P_{(mn)}}\right)$ for the Equal Frequency Operation ($f_b = f_a \neq 0$).

Method	Average Arm Power	$I_{MI(mn)}$	$V_{MI(mn)}$	$\overline{P_{dis(mn)}}$
1	$\overline{P_{\Sigma 0}}$	i_{ad+}	$\frac{V_a}{\sqrt{2}}$	$\overline{v_b\, i_{b0}}$
	$\overline{P_{\Delta 0}}$	i_{bd+}	$-\sqrt{2}\, V_a$	$\overline{-v_{a\alpha}\, i^{b}_{b\alpha} - v_{a\beta}\, i^{b}_{b\beta}}$
	$\overline{P_{\Sigma \alpha}}$	$I^{b}_{b\alpha}$	V_b	$\overline{v_b \left(\left(i_{bd+} + i_{bd-} \right) \cos(\theta_a) + i_{bq-} \sin(\theta_a) \right)}$
	$\overline{P_{\Sigma \beta}}$	$I^{b}_{b\beta}$	V_b	$\overline{v_b \left(i_{bq-} \cos(\theta_a) + \left(i_{bd+} - i_{bd-} \right) \sin(\theta_a) \right)}$
	$\overline{P_{\Delta \alpha}}$	i_{bd-}	$-\sqrt{2}\, V_a$	$\overline{-\frac{v_b\, i_{a\alpha}}{2} - 2\, v_{a\alpha}\, i_{b0} - v_{a\alpha}\, i^{b}_{b\alpha} + v_{a\beta}\, i^{b}_{b\beta}}$
	$\overline{P_{\Delta \beta}}$	i_{bq-}	$\sqrt{2}\, V_a$	$\overline{-\frac{v_b\, i_{a\beta}}{2} - 2\, v_{a\beta}\, i_{b0} + v_{a\alpha}\, i^{b}_{b\beta} + v_{a\beta}\, i^{b}_{b\alpha}}$
2	$\overline{P_{\Sigma 0}}$	i_{ad+}	$\frac{V_a}{\sqrt{2}}$	$\overline{v_b\, i_{b0} + \frac{v_{a\alpha}\, i^{b}_{a\alpha}}{2} + \frac{v_{a\beta}\, i^{b}_{a\beta}}{2}}$
	$\overline{P_{\Delta 0}}$	i_{bd+}	$-\sqrt{2}\, V_a$	$\overline{-v_{a\alpha}\, i^{b}_{b\alpha} - v_{a\beta}\, i^{b}_{b\beta}}$
	$\overline{P_{\Sigma \alpha}}$	$I^{b}_{b\alpha}$	V_b	$\overline{v_b\, i_{bd+} \cos(\theta_a) + \frac{v_{a\alpha}\, i^{b}_{a\alpha}}{2} - \frac{v_{a\beta}\, i^{b}_{a\beta}}{2}}$
	$\overline{P_{\Sigma \beta}}$	$I^{b}_{b\beta}$	V_b	$\overline{v_b\, i_{bd+} \sin(\theta_a) - \frac{v_{a\alpha}\, i^{b}_{a\beta}}{2} - \frac{v_{a\beta}\, i^{b}_{a\alpha}}{2}}$
	$\overline{P_{\Delta \alpha}}$	$I^{b}_{a\alpha}$	$-\frac{V_b}{2}$	$\overline{-\frac{v_b\, i_{ad+}}{2} \cos(\theta_a) - 2\, v_{a\alpha}\, i_{b0} - v_{a\alpha}\, i^{b}_{b\alpha} + v_{a\beta}\, i^{b}_{b\beta}}$
	$\overline{P_{\Delta \beta}}$	$I^{b}_{a\beta}$	$-\frac{V_b}{2}$	$\overline{-\frac{v_b\, i_{ad+}}{2} \sin(\theta_a) - 2\, v_{a\beta}\, i_{b0} + v_{a\alpha}\, i^{b}_{b\beta} + v_{a\beta}\, i^{b}_{b\alpha}}$
3	$\overline{P_{\Sigma 0}}$	i_{ad+}	$\frac{V_a}{\sqrt{2}}$	$\overline{v_b\, i_{b0}}$
	$\overline{P_{\Delta 0}}$	i_{bd+}	$-\sqrt{2}\, V_a$	0
	$\overline{P_{\Sigma \alpha}}$	i_{ad-}	$\frac{V_a}{\sqrt{2}}$	$\overline{v_b\, i_{b\alpha}}$
	$\overline{P_{\Sigma \beta}}$	i_{aq-}	$-\frac{V_a}{\sqrt{2}}$	$\overline{v_b\, i_{b\beta}}$
	$\overline{P_{\Delta \alpha}}$	i_{bd-}	$-\frac{V_a}{\sqrt{2}}$	$\overline{-\frac{v_b\, i_{a\alpha}}{2} - 2\, v_{a\alpha}\, i_{b0}}$

	$\overline{P_{\Delta\beta}}$	$i_{\mathrm{bq}-}$	$\sqrt{2}\,V_{\mathrm{a}}$	$\overline{-\frac{v_{\mathrm{b}}\,i_{\mathrm{a}\beta}}{2} - 2\,v_{\mathrm{a}\beta}\,i_{\mathrm{b}0}}$
4	$\overline{P_{\Sigma 0}}$	$i_{\mathrm{ad}+}$	$\frac{V_{\mathrm{a}}}{\sqrt{2}}$	$\overline{v_{\mathrm{b}}\,i_{\mathrm{b}0} + \frac{v_{\mathrm{a}\alpha}\,\overset{\mathrm{b}}{i}_{\mathrm{a}\alpha}}{2} + \frac{v_{\mathrm{a}\beta}\,\overset{\mathrm{b}}{i}_{\mathrm{a}\beta}}{2}}$
	$\overline{P_{\Delta 0}}$	$i_{\mathrm{bd}+}$	$-\sqrt{2}\,V_{\mathrm{a}}$	0
	$\overline{P_{\Sigma\alpha}}$	$i_{\mathrm{ad}-}$	$\frac{V_{\mathrm{a}}}{\sqrt{2}}$	$\overline{v_{\mathrm{b}}\,i_{\mathrm{b}\alpha} + \frac{v_{\mathrm{a}\alpha}\,\overset{\mathrm{b}}{i}_{\mathrm{a}\alpha}}{2} - \frac{v_{\mathrm{a}\beta}\,\overset{\mathrm{b}}{i}_{\mathrm{a}\beta}}{2}}$
	$\overline{P_{\Sigma\beta}}$	$i_{\mathrm{aq}-}$	$-\frac{V_{\mathrm{a}}}{\sqrt{2}}$	$\overline{v_{\mathrm{b}}\,i_{\mathrm{b}\beta} - \frac{v_{\mathrm{a}\alpha}\,\overset{\mathrm{b}}{i}_{\mathrm{a}\beta}}{2} - \frac{v_{\mathrm{a}\beta}\,\overset{\mathrm{b}}{i}_{\mathrm{a}\alpha}}{2}}$
	$\overline{P_{\Delta\alpha}}$	$\overset{\mathrm{b}}{I}_{\mathrm{a}\alpha}$	$-\frac{V_{\mathrm{b}}}{2}$	$\overline{-\frac{v_{\mathrm{b}}}{2}\left(\left(i_{\mathrm{ad}+} + i_{\mathrm{ad}-}\right)\cos(\theta_{\mathrm{a}}) + i_{\mathrm{aq}-}\sin(\theta_{\mathrm{a}})\right) - 2\,v_{\mathrm{a}\alpha}\,i_{\mathrm{b}0}}$
	$\overline{P_{\Delta\beta}}$	$\overset{\mathrm{b}}{I}_{\mathrm{a}\beta}$	$-\frac{V_{\mathrm{b}}}{2}$	$\overline{-\frac{v_{\mathrm{b}}}{2}\left(i_{\mathrm{aq}-}\cos(\theta_{\mathrm{a}}) + \left(i_{\mathrm{ad}+} - i_{\mathrm{ad}-}\right)\sin(\theta_{\mathrm{a}})\right) - 2\,v_{\mathrm{a}\beta}\,i_{\mathrm{b}0}}$
5	$\overline{P_{\Sigma 0}}$	$\overset{\mathrm{b}}{I}_{\mathrm{b}0}$	V_{b}	$\frac{V_{\mathrm{a}}\,i_{\mathrm{ad}+}}{\sqrt{2}}$
	$\overline{P_{\Delta 0}}$	$i_{\mathrm{bd}+}$	$-\sqrt{2}\,V_{\mathrm{a}}$	$\overline{-v_{\mathrm{a}\alpha}\,\overset{\mathrm{b}}{i}_{\mathrm{b}\alpha} - v_{\mathrm{a}\beta}\,\overset{\mathrm{b}}{i}_{\mathrm{b}\beta}}$
	$\overline{P_{\Sigma\alpha}}$	$\overset{\mathrm{b}}{I}_{\mathrm{b}\alpha}$	V_{b}	$\overline{v_{\mathrm{b}}\left(\left(i_{\mathrm{bd}+} + i_{\mathrm{bd}-}\right)\cos(\theta_{\mathrm{a}}) + i_{\mathrm{bq}-}\sin(\theta_{\mathrm{a}})\right)}$
	$\overline{P_{\Sigma\beta}}$	$\overset{\mathrm{b}}{I}_{\mathrm{b}\beta}$	V_{b}	$\overline{v_{\mathrm{b}}\left(i_{\mathrm{bq}-}\cos(\theta_{\mathrm{a}}) + \left(i_{\mathrm{bd}+} - i_{\mathrm{bd}-}\right)\sin(\theta_{\mathrm{a}})\right)}$
	$\overline{P_{\Delta\alpha}}$	$i_{\mathrm{bd}-}$	$-\sqrt{2}\,V_{\mathrm{a}}$	$\overline{-\frac{v_{\mathrm{b}}\,i_{\mathrm{a}\alpha}}{2} - 2\,v_{\mathrm{a}\alpha}\,i_{\mathrm{b}0} - v_{\mathrm{a}\alpha}\,\overset{\mathrm{b}}{i}_{\mathrm{b}\alpha} + v_{\mathrm{a}\beta}\,\overset{\mathrm{b}}{i}_{\mathrm{b}\beta}}$
	$\overline{P_{\Delta\beta}}$	$i_{\mathrm{bq}-}$	$\sqrt{2}\,V_{\mathrm{a}}$	$\overline{-\frac{v_{\mathrm{b}}\,i_{\mathrm{a}\beta}}{2} - 2\,v_{\mathrm{a}\beta}\,i_{\mathrm{b}0} + v_{\mathrm{a}\alpha}\,\overset{\mathrm{b}}{i}_{\mathrm{b}\beta} + v_{\mathrm{a}\beta}\,\overset{\mathrm{b}}{i}_{\mathrm{b}\alpha}}$
6	$\overline{P_{\Sigma 0}}$	$\overset{\mathrm{b}}{I}_{\mathrm{b}0}$	V_{b}	$\overline{v_{\mathrm{b}}\left(\overset{\mathrm{a}\text{-}\alpha}{i}_{\mathrm{b}0} + \overset{\mathrm{a}\text{-}\beta}{i}_{\mathrm{b}0}\right)} + \frac{V_{\mathrm{a}}\,i_{\mathrm{ad}+}}{\sqrt{2}}$
	$\overline{P_{\Delta 0}}$	$i_{\mathrm{bd}+}$	$-\sqrt{2}\,V_{\mathrm{a}}$	$\overline{-v_{\mathrm{a}\alpha}\,\overset{\mathrm{b}}{i}_{\mathrm{b}\alpha} - v_{\mathrm{a}\beta}\,\overset{\mathrm{b}}{i}_{\mathrm{b}\beta}}$
	$\overline{P_{\Sigma\alpha}}$	$\overset{\mathrm{b}}{I}_{\mathrm{b}\alpha}$	V_{b}	$\overline{v_{\mathrm{b}}\,i_{\mathrm{bd}+}\cos(\theta_{\mathrm{a}})}$
	$\overline{P_{\Sigma\beta}}$	$\overset{\mathrm{b}}{I}_{\mathrm{b}\beta}$	V_{b}	$\overline{v_{\mathrm{b}}\,i_{\mathrm{bd}+}\sin(\theta_{\mathrm{a}})}$
	$\overline{P_{\Delta\alpha}}$	$\overset{\mathrm{a}\text{-}\alpha}{I}_{\mathrm{b}0}$	$-2\,V_{\mathrm{a}}$	$\overline{-\frac{v_{\mathrm{b}}\,i_{\mathrm{a}\alpha}}{2} - 2\,v_{\mathrm{a}\alpha}\,\overset{\mathrm{b}}{i}_{\mathrm{b}0} - v_{\mathrm{a}\alpha}\,\overset{\mathrm{b}}{i}_{\mathrm{b}\alpha} + v_{\mathrm{a}\beta}\,\overset{\mathrm{b}}{i}_{\mathrm{b}\beta}}$
	$\overline{P_{\Delta\beta}}$	$\overset{\mathrm{a}\text{-}\beta}{I}_{\mathrm{b}0}$	$-2\,V_{\mathrm{a}}$	$\overline{-\frac{v_{\mathrm{b}}\,i_{\mathrm{a}\beta}}{2} - 2\,v_{\mathrm{a}\beta}\,\overset{\mathrm{b}}{i}_{\mathrm{b}0} + v_{\mathrm{a}\alpha}\,\overset{\mathrm{b}}{i}_{\mathrm{b}\beta} + v_{\mathrm{a}\beta}\,\overset{\mathrm{b}}{i}_{\mathrm{b}\alpha}}$

7	$\overline{P_{\Sigma 0}}$	i_{ad+}	$\frac{V_a}{\sqrt{2}}$	$\overline{v_b\, i_{b0}}$
	$\overline{P_{\Delta 0}}$	i_{bd+}	$-\sqrt{2}\, V_a$	$\overline{-v_{a\alpha}\, i^{b}_{b\alpha} - v_{a\beta}\, i^{b}_{b\beta}}$
	$\overline{P_{\Sigma \alpha}}$	$I^{b}_{b\alpha}$	V_b	$\overline{v_b\, i_{bd+} \cos(\theta_a)}$
	$\overline{P_{\Sigma \beta}}$	$I^{b}_{b\beta}$	V_b	$\overline{v_b\, i_{bd+} \sin(\theta_a)}$
	$\overline{P_{\Delta \alpha}}$	$I^{cm}_{b\alpha}$	$-2\, V_{cm}$	$\overline{-\frac{v_b\, i_{a\alpha}}{2} - 2\, v_{a\alpha}\, i_{b0} - v_{a\alpha}\, i^{b}_{b\alpha} + v_{a\beta}\, i^{b}_{b\beta}}$
	$\overline{P_{\Delta \beta}}$	$I^{cm}_{b\beta}$	$-2\, V_{cm}$	$\overline{-\frac{v_b\, i_{a\beta}}{2} - 2\, v_{a\beta}\, i_{b0} + v_{a\alpha}\, i^{b}_{b\beta} + v_{a\beta}\, i^{b}_{b\alpha}}$
8	$\overline{P_{\Sigma 0}}$	i_{ad+}	$\frac{V_a}{\sqrt{2}}$	$\overline{v_b\, i_{b0} + \frac{v_{a\alpha}\, i^{b}_{a\alpha}}{2} + \frac{v_{a\beta}\, i^{b}_{a\beta}}{2}}$
	$\overline{P_{\Delta 0}}$	i_{bd+}	$-\sqrt{2}\, V_a$	0
	$\overline{P_{\Sigma \alpha}}$	$I^{cm}_{a\alpha}$	V_{cm}	$\overline{v_b\, i_{bd+} \cos(\theta_a) + \frac{v_{a\alpha}\, i^{b}_{a\alpha}}{2} - \frac{v_{a\beta}\, i^{b}_{a\beta}}{2}}$
	$\overline{P_{\Sigma \beta}}$	$I^{cm}_{a\beta}$	V_{cm}	$\overline{v_b\, i_{bd+} \sin(\theta_a) - \frac{v_{a\alpha}\, i^{b}_{a\beta}}{2} - \frac{v_{a\beta}\, i^{b}_{a\alpha}}{2}}$
	$\overline{P_{\Delta \alpha}}$	$I^{b}_{a\alpha}$	$-\frac{V_b}{2}$	$\overline{-\frac{v_b\, i_{ad+}}{2} \cos(\theta_a) - 2\, v_{a\alpha}\, i_{b0}}$
	$\overline{P_{\Delta \beta}}$	$I^{b}_{a\beta}$	$-\frac{V_b}{2}$	$\overline{-\frac{v_b\, i_{ad+}}{2} \sin(\theta_a) - 2\, V_{a\beta}\, i_{b0}}$
9	$\overline{P_{\Sigma 0}}$	i_{ad+}	$\frac{V_a}{\sqrt{2}}$	$\overline{v_b\, i_{b0}}$
	$\overline{P_{\Delta 0}}$	i_{bd+}	$-\sqrt{2}\, V_a$	0
	$\overline{P_{\Sigma \alpha}}$	$I^{cm}_{a\alpha}$	V_{cm}	$\overline{v_b\, i_{bd+} \cos(\theta_a)}$
	$\overline{P_{\Sigma \beta}}$	$I^{cm}_{a\beta}$	V_{cm}	$\overline{v_b\, i_{bd+} \sin(\theta_a)}$
	$\overline{P_{\Delta \alpha}}$	$I^{cm}_{b\alpha}$	$-2\, V_{cm}$	$\overline{-\frac{v_b\, i_{a\alpha}}{2} - 2\, v_{a\alpha}\, i_{b0}}$
	$\overline{P_{\Delta \beta}}$	$I^{cm}_{b\beta}$	$-2\, V_{cm}$	$\overline{-\frac{v_b\, i_{a\beta}}{2} - 2\, v_{a\beta}\, i_{b0}}$
10	$\overline{P_{\Sigma 0}}$	i_{ad+}	$\frac{V_a}{\sqrt{2}}$	$\overline{v_b\, i_{b0}}$
	$\overline{P_{\Delta 0}}$	i_{bd+}	$-\sqrt{2}\, V_a$	0
	$\overline{P_{\Sigma \alpha}}$	$I^{cm}_{a\alpha}$	V_{cm}	$\overline{v_b\, i_{b\alpha}}$

	$\overline{P_{\Sigma\beta}}$	$I_{a\beta}^{cm}$	V_{cm}	$\overline{v_b\, i_{b\beta}}$
	$\overline{P_{\Delta\alpha}}$	i_{bd-}	$-\sqrt{2}\, V_a$	$\overline{-\frac{v_b\, i_{a\alpha}}{2} - 2\, v_{a\alpha}\, i_{b0}}$
	$\overline{P_{\Delta\beta}}$	i_{bq-}	$\sqrt{2}\, V_a$	$\overline{-\frac{v_b\, i_{a\beta}}{2} - 2\, v_{a\beta}\, i_{b0}}$
11	$\overline{P_{\Sigma 0}}$	i_{ad+}	$\frac{V_a}{\sqrt{2}}$	$\overline{v_b\, i_{b0}}$
	$\overline{P_{\Delta 0}}$	i_{bd+}	$-\sqrt{2}\, V_a$	0
	$\overline{P_{\Sigma\alpha}}$	i_{ad-}	$\frac{V_a}{\sqrt{2}}$	$\overline{v_b\, i_{bd+} \cos(\theta_a)}$
	$\overline{P_{\Sigma\beta}}$	i_{aq-}	$-\frac{V_a}{\sqrt{2}}$	$\overline{v_b\, i_{bd+} \sin(\theta_a)}$
	$\overline{P_{\Delta\alpha}}$	$I_{b\alpha}^{cm}$	$-2\, V_{cm}$	$\overline{-\frac{v_b\, i_{a\alpha}}{2} - 2\, v_{a\alpha}\, i_{b0}}$
	$\overline{P_{\Delta\beta}}$	$I_{b\beta}^{cm}$	$-2\, V_{cm}$	$\overline{-\frac{v_b\, i_{a\beta}}{2} - 2\, v_{a\beta}\, i_{b0}}$
12	$\overline{P_{\Sigma 0}}$	I_{b0}^{b}	V_b	$\frac{V_a\, i_{ad+}}{\sqrt{2}}$
	$\overline{P_{\Delta 0}}$	i_{bd+}	$-\sqrt{2}\, V_a$	$\overline{-v_{a\alpha}\, i_{b\alpha}^{b} - v_{a\beta}\, i_{b\beta}^{b}}$
	$\overline{P_{\Sigma\alpha}}$	$I_{b\alpha}^{b}$	V_b	$\overline{v_b\, i_{bd+} \cos(\theta_a)}$
	$\overline{P_{\Sigma\beta}}$	$I_{b\beta}^{b}$	V_b	$\overline{v_b\, i_{bd+} \sin(\theta_a)}$
	$\overline{P_{\Delta\alpha}}$	$I_{b\alpha}^{cm}$	$-2\, V_{cm}$	$\overline{-\frac{v_b\, i_{a\alpha}}{2} - 2\, v_{a\alpha}\, i_{b0} - v_{a\alpha}\, i_{b\alpha}^{b} + v_{a\beta}\, i_{b\beta}^{b}}$
	$\overline{P_{\Delta\beta}}$	$I_{b\beta}^{cm}$	$-2\, V_{cm}$	$\overline{-\frac{v_b\, i_{a\beta}}{2} - 2\, v_{a\beta}\, i_{b0} + v_{a\alpha}\, i_{b\beta}^{b} + v_{a\beta}\, i_{b\alpha}^{b}}$
13	$\overline{P_{\Sigma 0}}$	I_{b0}^{b}	V_b	$\overline{v_b \left(i_{b0}^{a\text{-}\alpha} + i_{b0}^{a\text{-}\beta}\right)} + \frac{V_a\, i_{ad+}}{\sqrt{2}}$
	$\overline{P_{\Delta 0}}$	I_{b0}^{cm}	$-2\, V_{cm}$	$\overline{-v_{a\alpha}\, i_{b\alpha}^{b} - v_{a\beta}\, i_{b\beta}^{b}}$
	$\overline{P_{\Sigma\alpha}}$	$I_{b\alpha}^{b}$	V_b	0
	$\overline{P_{\Sigma\beta}}$	$I_{b\beta}^{b}$	V_b	0
	$\overline{P_{\Delta\alpha}}$	$I_{b0}^{a\text{-}\alpha}$	$-2\, V_a$	$\overline{-\frac{v_b\, i_{a\alpha}}{2} - 2\, v_{a\alpha}\, i_{b0} - v_{a\alpha}\, i_{b\alpha}^{b} + v_{a\beta}\, i_{b\beta}^{b}}$
	$\overline{P_{\Delta\beta}}$	$I_{b0}^{a\text{-}\beta}$	$-2\, V_a$	$\overline{-\frac{v_b\, i_{a\beta}}{2} - 2\, v_{a\beta}\, i_{b0} + v_{a\alpha}\, i_{b\beta}^{b} + v_{a\beta}\, i_{b\alpha}^{b}}$

14	$\overline{P_{\Sigma 0}}$	I_{b0}^{b}	V_b	$\frac{V_a\, i_{ad+}}{\sqrt{2}}$
	$\overline{P_{\Delta 0}}$	I_{b0}^{cm}	$-2\, V_{cm}$	$\overline{-v_{a\alpha}\, i_{b\alpha}^{b} - v_{a\beta}\, i_{b\beta}^{b}}$
	$\overline{P_{\Sigma \alpha}}$	$I_{b\alpha}^{b}$	V_b	0
	$\overline{P_{\Sigma \beta}}$	$I_{b\beta}^{b}$	V_b	0
	$\overline{P_{\Delta \alpha}}$	$I_{b\alpha}^{cm}$	$-2\, V_{cm}$	$\overline{-\frac{v_b\, i_{a\alpha}}{2} - 2\, v_{a\alpha}\, i_{b0} - v_{a\alpha}\, i_{b\alpha}^{b} + v_{a\beta}\, i_{b\beta}^{b}}$
	$\overline{P_{\Delta \beta}}$	$I_{b\beta}^{cm}$	$-2\, V_{cm}$	$\overline{-\frac{v_b\, i_{a\beta}}{2} - 2\, v_{a\beta}\, i_{b0} + v_{a\alpha}\, i_{b\beta}^{b} + v_{a\beta}\, i_{b\alpha}^{b}}$
15	$\overline{P_{\Sigma 0}}$	I_{b0}^{b}	V_b	$\frac{V_a\, i_{ad+}}{\sqrt{2}}$
	$\overline{P_{\Delta 0}}$	I_{b0}^{cm}	$-2\, V_{cm}$	$\overline{-v_{a\alpha}\, i_{b\alpha}^{b} - v_{a\beta}\, i_{b\beta}^{b}}$
	$\overline{P_{\Sigma \alpha}}$	$I_{b\alpha}^{b}$	V_b	$\overline{v_b \left(i_{bd-} \cos(\theta_a) + i_{bq-} \sin(\theta_a)\right)}$
	$\overline{P_{\Sigma \beta}}$	$I_{b\beta}^{b}$	V_b	$\overline{v_b \left(i_{bq-} \cos(\theta_a) - i_{bd-} \sin(\theta_a)\right)}$
	$\overline{P_{\Delta \alpha}}$	i_{bd-}	$-\sqrt{2}\, V_a$	$\overline{-\frac{v_b\, i_{a\alpha}}{2} - 2\, v_{a\alpha}\, i_{b0} - v_{a\alpha}\, i_{b\alpha}^{b} + v_{a\beta}\, i_{b\beta}^{b}}$
	$\overline{P_{\Delta \beta}}$	i_{bq-}	$\sqrt{2}\, V_a$	$\overline{-\frac{v_b\, i_{a\beta}}{2} - 2\, v_{a\beta}\, i_{b0} + v_{a\alpha}\, i_{b\beta}^{b} + v_{a\beta}\, i_{b\alpha}^{b}}$

A.9 Auxiliary Sheets

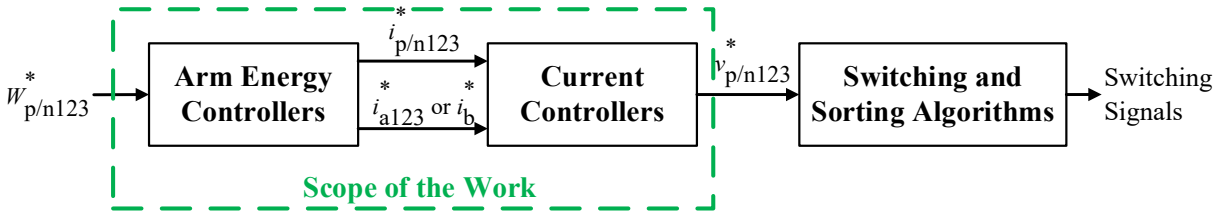

Figure 1.2: General control structure of MMC. **(Source:** Chapter-1**)**

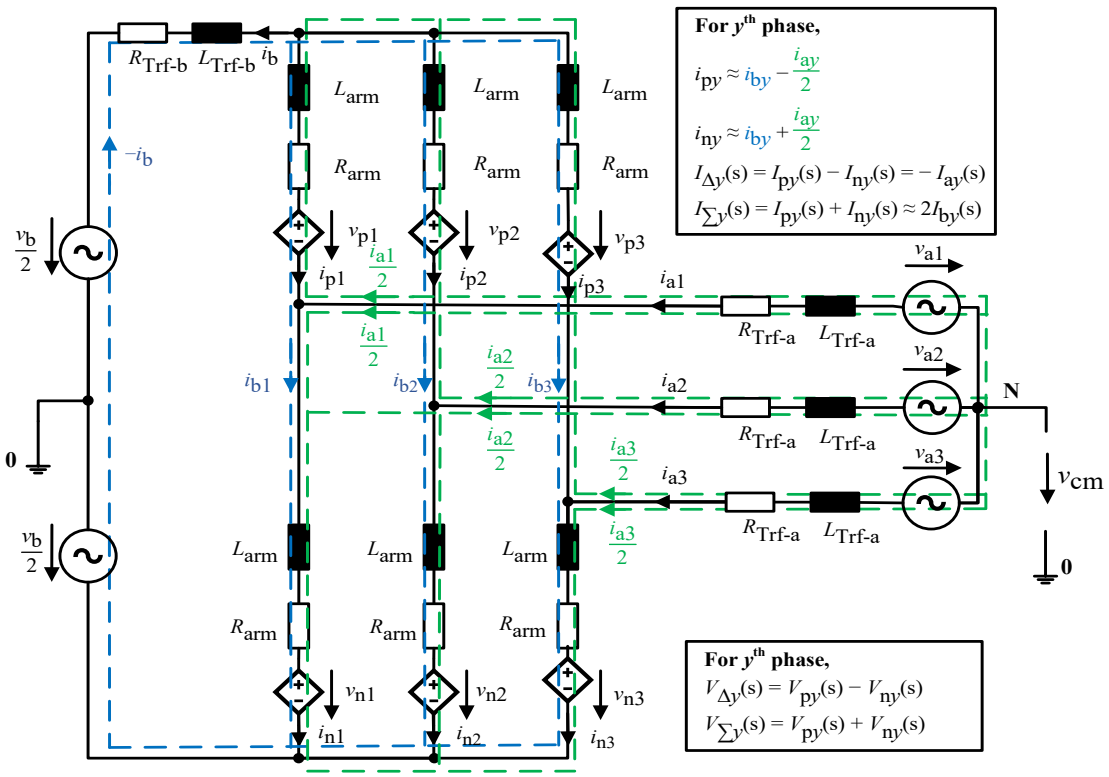

(a) Average Equivalent Circuit Diagram of MMC

1. **Total Arm Energy Regulation $(w_{\Sigma 0})$**
2. **Total Upper and Lower Arm Energies Regulation $(w_{\Delta 0})$**
3. **Summation Phase Energies Regulation $(w_{\Sigma\alpha\beta})$**
4. **Difference Phase Energies Regulation $(w_{\Delta\alpha\beta})$**

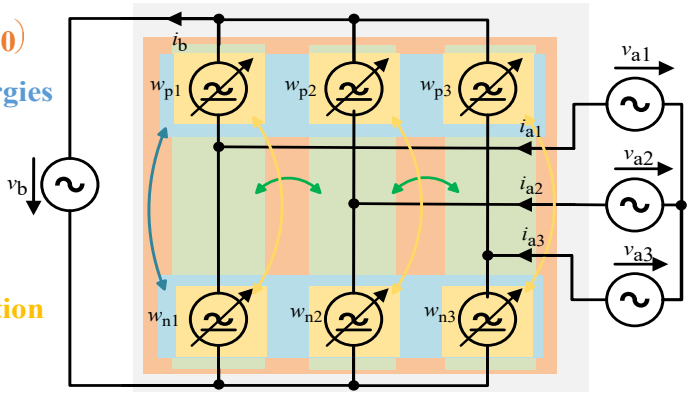

(b) Arm energy Model

Figure. 2.1: Electrical circuit diagram of MMC. (**Source**: Chapter-2)

A.9.1 Circuit Diagram of *Modular Multilevel Converter* (MMC) and Parameters

Fig. 2.1a presents the average circuit diagram of *Modular Multilevel Converter* (MMC). The circuit diagram parameters are defined below:

i_{p123}, and i_{n123}	Upper and Lower arm currents.
v_{p123}, and v_{n123}	Upper and Lower arm voltages.
i_{a123}, and v_{a123}	Three-phase currents and voltages.
$v_{cm} = v_{a0}$	Three-phase zero-sequence or common-mode voltage.
i_b, and v_b	Single-phase current and voltage.
i_{b123}	Circulating currents.
f_a, f_b, and f_{cm}	Three-phase, single-phase and common-mode voltage frequencies.
y (= 1, 2, or 3)	Phase y of MMC.
i_{py}, and i_{ny}	Upper and Lower arm currents of phase y of MMC.
v_{py}, and v_{ny}	Upper and Lower arm voltages of phase y of MMC.
i_{ay}, and i_{by}	Three-phase and circulating currents of phase y of MMC.
$F_{\Sigma y} = F_{py} + F_{ny}$	Summation system.
$F_{\Delta y} = F_{py} - F_{ny}$	Difference system.

(2.1) and (2.3) represents the arm currents (i_{py}, and i_{ny}) and voltages (v_{py}, and v_{ny}) of phase y of MMC. (2.2) represents the zero-sequence circulating current (i_{b0}), which is proportional to the single-phase current (i_b).

$$i_{py} = i_{by} - \frac{i_{ay}}{2}, \text{ and } i_{ny} = i_{by} + \frac{i_{ay}}{2} \tag{2.1}$$

$$i_{b0} = \frac{i_{b1} + i_{b2} + i_{b3}}{3} = -\frac{i_b}{3} \tag{2.2}$$

$$v_{py} = \frac{v_b}{2} - v_{ay}, \text{ and } v_{ny} = \frac{v_b}{2} + v_{ay} \tag{2.3}$$

A.9.2 Summation and Difference Arm Powers in the abc-Frame

(2.5) and (2.6) illustrate the arm currents ($i_{\Sigma y}$, and $i_{\Delta y}$) and voltages ($v_{\Sigma y}$, and $v_{\Delta y}$) in the summation (Σ) and difference (Δ) systems for phase y of MMC. $i_{\Sigma y}$ affects only the circulating current (i_{by}), and

$i_{\Delta y}$ influences only the three-phase current (i_{ay}). Similarly, $v_{\Sigma y}$ realizes the single-phase voltage (v_b), and $v_{\Delta y}$ affects the three-phase voltage (v_{ay}).

$$i_{\Sigma y} = i_{py} + i_{ny} = 2\, i_{by} \;\; ; \;\; i_{\Delta y} = i_{py} - i_{ny} = -\, i_{ay} \tag{2.5}$$

$$v_{\Sigma y} = v_{py} + v_{ny} = v_b \;\; ; \;\; v_{\Delta y} = v_{py} - v_{ny} = -\, 2\, v_{ay} \tag{2.6}$$

(2.7) and (2.8) presents the arm powers in the summation ($p_{\Sigma y}$) and difference ($p_{\Delta y}$) systems for phase y of MMC using the currents and voltages in the abc-frame.

$$p_{\Sigma y} = p_{py} + p_{ny} = v_{py}\, i_{py} + v_{ny}\, i_{ny} = v_b\, i_{by} + v_{ay}\, i_{ay} \tag{2.7}$$

$$p_{\Delta y} = p_{py} - p_{ny} = v_{py}\, i_{py} - v_{ny}\, i_{ny} = -\, 2\, v_{ay}\, i_{by} - \frac{i_{ay}}{2}\, v_b \tag{2.8}$$

A.9.3 Summation and Difference Arm Powers in the αβ0-Frame

Referring to Appendix A.5, (2.17) to (2.22) shows the summation and difference arm powers in the αβ0-frame using the currents and voltages in the αβ0-frame.

$$p_{\Sigma 0} = v_b\, i_{b0} + \frac{v_{a\alpha}\, i_{a\alpha} + v_{a\beta}\, i_{a\beta}}{2} \tag{2.17}$$

$$p_{\Delta 0} = -\, 2\, v_{cm}\, i_{b0} - v_{a\alpha}\, i_{b\alpha} - v_{a\beta}\, i_{b\beta} \tag{2.18}$$

$$p_{\Sigma \alpha} = v_b\, i_{b\alpha} + v_{cm}\, i_{a\alpha} + \frac{v_{a\alpha}\, i_{a\alpha} - v_{a\beta}\, i_{a\beta}}{2} \tag{2.19}$$

$$p_{\Sigma \beta} = v_b\, i_{b\beta} + v_{cm}\, i_{a\beta} - \frac{v_{a\alpha}\, i_{a\beta} + v_{a\beta}\, i_{a\alpha}}{2} \tag{2.20}$$

$$p_{\Delta \alpha} = -\frac{v_b\, i_{a\alpha}}{2} - 2\, v_{a\alpha}\, i_{b0} - 2\, v_{cm}\, i_{b\alpha} - v_{a\alpha}\, i_{b\alpha} + v_{a\beta}\, i_{b\beta} \tag{2.21}$$

$$p_{\Delta \beta} = -\frac{v_b\, i_{a\beta}}{2} - 2\, v_{a\beta}\, i_{b0} - 2\, v_{cm}\, i_{b\beta} + v_{a\alpha}\, i_{b\beta} + v_{a\beta}\, i_{b\alpha} \tag{2.22}$$

A.9.4 *Degrees of Freedom* (DOF)

Arm power equations from (2.17) to (2.22) contain general four terms (a) $v_{a\alpha}\, i_{x\alpha} + v_{a\beta}\, i_{x\beta}$, (b) $v_{a\alpha}\, i_{x\alpha} - v_{a\beta}\, i_{x\beta}$, (c) $v_{a\alpha}\, i_{x\beta} + v_{a\beta}\, i_{x\alpha}$, and (d) $v_g\, i_{x\alpha/\beta/0}$. Here, x = a or b; g = a, b, or cm; and $i_{x\alpha/\beta/0} = i_{x\alpha}$, $i_{x\beta}$, or i_{x0}. (2.28), (2.29), and (2.30) represent the general expressions of the average of the power terms: (a) $v_{a\alpha}\, i_{x\alpha} + v_{a\beta}\, i_{x\beta}$, (b) $v_{a\alpha}\, i_{x\alpha} - v_{a\beta}\, i_{x\beta}$, and (c) $v_{a\alpha}\, i_{x\beta} + v_{a\beta}\, i_{x\alpha}$, respectively. It is clear from (2.29) and (2.30) that even the negative sequence current components (i_{xd-}, and i_{xq-}) can influence the average arm powers ($\overline{v_{a\alpha}\, i_{x\alpha} - v_{a\beta}\, i_{x\beta}}$, and $\overline{v_{a\alpha}\, i_{x\beta} + v_{a\beta}\, i_{x\alpha}}$).

The voltage (v_g) and current ($i^g_{x\alpha/\beta/0}$) with the same frequency only can make average power. $i^g_{x\alpha/\beta/0}$ represents the component of the current $i_{x\alpha/\beta/0}$ in phase with the voltage v_g. (2.31) represents the average of the product of v_g and $i^g_{x\alpha/\beta/0}$. Here, V_g and $I^g_{x\alpha/\beta/0}$ are the RMS voltage and current values, respectively.

$$\overline{v_{a\alpha}\, i_{x\alpha} + v_{a\beta}\, i_{x\beta}} = \sqrt{2}\, V_a\, i_{xd+} \tag{2.28}$$

$$\overline{v_{a\alpha}\, i_{x\alpha} - v_{a\beta}\, i_{x\beta}} = \sqrt{2}\, V_a\, i_{xd-} \tag{2.29}$$

$$\overline{v_{a\alpha}\, i_{x\beta} + v_{a\beta}\, i_{x\alpha}} = \sqrt{2}\, V_a\, i_{xq-} \tag{2.30}$$

$$\overline{v_g\, i^g_{x\alpha/\beta/0}} = V_g\, I^g_{x\alpha/\beta/0} \tag{2.31}$$

Table 2.1: *Degrees of Freedom* (DOF) and six *Manipulated Inputs* ($MI_{1,2,3,4,5\&6}$) for regulating the corresponding arm energies of MMC.

5. Total Arm Energy ($\overline{w_{\Sigma 0}}$) Regulation using MI_1	**6. Total Upper and Lower Arms Energies ($\overline{w_{\Delta 0}}$) Regulation using MI_2**
DOF_1: Positive sequence three-phase currents in the d-axis (i_{ad+}).	**DOF_3**: Positive sequence circulating currents in the d-axis (i_{bd+}).
DOF_2: Zero sequence circulating current in phase with v_b $\left(i^{b}_{b0}\right)$.	**DOF_4**: Zero sequence circulating current in phase with v_{cm} $\left(i^{cm}_{b0}\right)$.
7. Summation Phase Energies ($\overline{w_{\Sigma\alpha\beta}}$) Regulation using $MI_{3\&4}$	**8. Difference Phase Energies ($\overline{w_{\Delta\alpha\beta}}$) Regulation using $MI_{5\&6}$**
$DOF_{5\&6}$: Circulating currents in phase with v_b $\left(i^{b}_{b\alpha\beta}\right)$.	**$DOF_{11\&12}$**: Three-phase currents in phase with v_b $\left(i^{b}_{a\alpha\beta}\right)$.
$DOF_{7\&8}$: Three-phase currents in phase with v_{cm} $\left(i^{cm}_{a\alpha\beta}\right)$.	**$DOF_{13\&14}$**: Single-phase currents in phase with $v_{a\alpha\beta}$ $\left(i^{a\text{-}\alpha\beta}_{b0}\right)$.
$DOF_{9\&10}$: Negative sequence three-phase currents (i_{adq-}).	**$DOF_{15\&16}$**: Circulating currents in phase with v_{cm} $\left(i^{cm}_{b\alpha\beta}\right)$.
Note: $i_{b0} = -\frac{i_b}{3}$	**$DOF_{17\&18}$**: Negative sequence circulating currents (i_{bdq-}).

Referring to Section 2.2, all discussed possible degrees of freedom corresponding to their energy controllers (also see Fig. 2.1b) are listed in Table. 2.1.

A.9.5 Arm Energy Balancing Methods Which do not Inject Harmonics into Load

Table 2.2: Stability analysis of all arm energies regulation techniques for direct AC-AC and DC-AC MMC topologies when no harmonics are injected into the load side of MMC. Here, n = integer, $f_{cm} = \text{Max}(f_o, 3f_a)$ if $f_b \neq 3f_a$, $f_{cm} = f_x$ if $f_b = 3f_a$, and $V_b = V_{dc}$ if $f_b = 0$. **Note**: v_{cm} can also be DC for AC-AC MMC application. Refer to section 2.4 to know about Matrix A and |A|.

Method	**Manipulated Inputs** (MI_1,MI_2,$MI_{3\&4}$, $MI_{5\&6}$)	**Determinant (|A|)** (Unstable if |A| = 0, otherwise stable)	
		$f_a = f_b \neq 0$	$f_a = n f_b, f_b = n f_a$, ($f_b = 0$ & $f_a \neq 0$).
1	i_{ad+}, i_{bd+}, $i^{b}_{b\alpha\beta}$, i_{bdq-}	0	$2\,V_a^4\,V_b^2$
2	i_{ad+}, i_{bd+}, $i^{b}_{b\alpha\beta}$, $i^{b}_{a\alpha\beta}$	$\frac{V_a^2}{16}\left(\cos^2(3\phi_b)\,V_a^2\,V_b^2 - \left(2V_a^2 - V_b^2\right)^2\right)$	$-\frac{1}{4}\,V_a^2\,V_b^4$
3	i_{ad+}, i_{bd+}, i_{adq-}, i_{bdq-}	$-V_a^2\left(V_a^2 - \frac{V_b^2}{4}\right)^2$	$-V_a^6$
4	i_{ad+}, i_{bd+}, i_{adq-}, $i^{b}_{a\alpha\beta}$	0	$\frac{1}{8}\,V_a^4\,V_b^2$
5	i^{b}_{b0}, i_{bd+}, $i^{b}_{b\alpha\beta}$, i_{bdq-}	0	$2\sqrt{2}\,V_a^3\,V_b^3$
6	i^{b}_{b0}, i_{bd+}, $i^{b}_{b\alpha\beta}$, $i^{a\text{-}\alpha\beta}_{b0}$	0	$-4\sqrt{2}\,V_a^3\,V_b^3$
7	i_{ad+}, i_{bd+}, $i^{b}_{b\alpha\beta}$, $i^{cm}_{b\alpha\beta}$	$-2\,V_a^2\,V_b^2\,V_{cm}^2$	$-4\,V_a^2\,V_b^2\,V_{cm}^2$
8	i_{ad+}, i_{bd+}, $i^{cm}_{a\alpha\beta}$, $i^{b}_{a\alpha\beta}$	$-\frac{1}{8}\,V_a^2\,V_b^2\,V_{cm}^2$	$-\frac{1}{4}\,V_a^2\,V_b^2\,V_{cm}^2$
9	i_{ad+}, i_{bd+}, $i^{cm}_{a\alpha\beta}$, $i^{cm}_{b\alpha\beta}$	$-4\,V_a^2\,V_{cm}^4$	$-4\,V_a^2\,V_{cm}^4$
10	i_{ad+}, i_{bd+}, $i^{cm}_{a\alpha\beta}$, i_{bdq-}	$2\,V_a^4\,V_{cm}^2$	$2\,V_a^4\,V_{cm}^2$
11	i_{ad+}, i_{bd+}, i_{adq-}, $i^{cm}_{b\alpha\beta}$	$2\,V_a^4\,V_{cm}^2$	$2\,V_a^4\,V_{cm}^2$
12	i^{b}_{b0}, i_{bd+}, $i^{b}_{b\alpha\beta}$, $i^{cm}_{b\alpha\beta}$	$-2\sqrt{2}\,V_a\,V_b^3\,V_{cm}^2$	$-4\sqrt{2}\,V_a\,V_b^3\,V_{cm}^2$
13	i^{b}_{b0}, i^{cm}_{b0}, $i^{b}_{b\alpha\beta}$, $i^{a\text{-}\alpha\beta}_{b0}$	0	$-8\,V_a^2\,V_b^3\,V_{cm}$
14	i^{b}_{b0}, i^{cm}_{b0}, $i^{b}_{b\alpha\beta}$, $i^{cm}_{b\alpha\beta}$	$-8\,V_b^3\,V_{cm}^3$	$-8\,V_b^3\,V_{cm}^3$

15	i^{b}_{b0}, i^{cm}_{b0}, $i^{b}_{b\alpha\beta}$, i_{bdq-}	$V_a^2\, V_b^3\, V_{cm}$	$4V_a^2\, V_b^3\, V_{cm}$

Arm energy balancing methods, that do not inject harmonics into the load current are listed in Table 2.2. Only four energy balancing methods (Method-1, 5, 7 & 12) are possible, which do not inject harmonics into both load and source currents. Among these four methods, only two methods (Method-7 and 12) are stable for equal frequency operation ($f_b = f_a \neq 0$), and v_{cm} is a must for equal frequency operation. And the other two methods (Method-1 and 5) are only stable for unequal frequency ($f_b \neq f_a$) operations.

A.9.6 Generalized Arm Currents Expressions Including all Degrees of Freedom

(2.23) and (2.24) present the definition of the three-phase voltage ($v_{a\alpha\beta}$) in the αβ-frame, single-phase voltage (v_b), and common-mode voltage (v_{cm}). (2.32) to (2.36) represent the general expression of the instantaneous three-phase current ($i_{a\alpha\beta}$), circulating current in the αβ-frame ($i_{b\alpha\beta}$), and circulating current in the 0-frame (i_{b0}), including all 18 degrees of freedom. Each current ($i_{a\alpha\beta}$, $i_{b\alpha\beta}$, and i_{b0}) consists of components in phase with the three-phase ($v_{a\alpha\beta}$), single-phase (v_b), and common-mode (v_{cm}) voltages. The three-phase current ($i_{a\alpha\beta}$) also includes the positive sequence three-phase current in the q-axis (i_{aq+}), which is responsible for the reactive power in the three-phase system (Q_a). Also, the circulating current in the 0-frame (i_{b0}) or the single-phase current $(i_b = -3\, i_{b0})$ includes the reactive power component $\left(i^{\perp b}_{b0}\right)$. $i^{\perp b}_{b0}$ is perpendicular to v_b. (2.37) shows the relationship between reactive powers (Q_b, and Q_a) and reactive current components ($i^{\perp b}_{b0}$, and i_{aq+}).

$$\theta_a = \omega_a t\ ;\ \theta_b = \omega_b t + \phi_b\ ;\ \theta_{cm} = \omega_{cm} t + \phi_{cm} \tag{2.23}$$

$$v_{a\alpha} = \sqrt{2} V_a \cos(\theta_a),\ v_{a\beta} = \sqrt{2} V_a \sin(\theta_a),\ v_b = \sqrt{2} V_b \cos(\theta_b) \text{ and } v_{cm} = \sqrt{2} V_{cm} \cos(\theta_{cm}) \tag{2.24}$$

$$i_{a\alpha} = \cos(\theta_a)\left(i_{ad+} + i_{ad-}\right) + \sin(\theta_a)\left(i_{aq-} - i_{aq+}\right) + \sqrt{2} I^{cm}_{a\alpha} \cos(\theta_{cm}) + \sqrt{2} I^{b}_{a\alpha} \cos(\theta_b) \tag{2.32}$$

$$i_{a\beta} = \cos(\theta_a)\left(i_{aq+} + i_{aq-}\right) + \sin(\theta_a)\left(i_{ad+} - i_{ad-}\right) + \sqrt{2} I^{cm}_{a\beta} \cos(\theta_{cm}) + \sqrt{2}\, I^{b}_{a\beta} \cos(\theta_b) \tag{2.33}$$

$$i_{b\alpha} = \cos(\theta_a)\left(i_{bd+} + i_{bd-}\right) + \sin(\theta_a)\, i_{bq-} + \sqrt{2} I^{cm}_{b\alpha} \cos(\theta_{cm}) + \sqrt{2} I^{b}_{b\alpha} \cos(\theta_b) \tag{2.34}$$

$$i_{b\beta} = \cos(\theta_a) i_{bq-} + \sin(\theta_a)\left(i_{bd+} - i_{bd-}\right) + \sqrt{2} I^{cm}_{b\beta} \cos(\theta_{cm}) + \sqrt{2}\, I^{b}_{b\beta} \cos(\theta_b) \tag{2.35}$$

$$i_{b0} = \sqrt{2} I^{\perp b}_{b0} \sin(\theta_b) + \sqrt{2} I^{b}_{b0} \cos(\theta_b) + \sqrt{2} I^{cm}_{b0} \cos(\theta_{cm}) + \sqrt{2} I^{a\text{-}\alpha}_{b0} \cos(\theta_a) + \sqrt{2} I^{a\text{-}\beta}_{b0} \sin(\theta_a) \tag{2.36}$$

$$I^{\perp b}_{b0} = -\frac{Q_b}{3\, V_b}\ ;\ i_{aq+} = -\frac{2\, Q_a}{3\, V_{ad}} \tag{2.37}$$

A.9.7 Compensating the Effect of the Load Reactive Power using the Source Reactive Power

Referring to Section 2.5 and Section 5.4, the MMC arm currents stress can be reduced significantly by compensating the average arm power term in the difference arm power equations in the αβ-frame ($\bar{p}_{\Delta\alpha\beta}$) due to the load reactive power using the source reactive power for equal frequency operation (also see Table 2.6). (2.68) is used if the three-phase system acts like a source ($MI_1 = i_{\mathrm{ad+}}$), and (2.69) is used if the single-phase system behaves like a source ($MI_1 = I_{\mathrm{b0}}^{\mathrm{b}}$).

$$i_{\mathrm{aq+}} = -\frac{4\sqrt{2}\,V_{\mathrm{a}}\,I_{\mathrm{b0}}^{\perp\mathrm{b}}}{V_{\mathrm{b}}} \text{ if } MI_1 = i_{\mathrm{ad+}}, \text{ or } \textbf{Source = 3Ph} \tag{2.68}$$

$$I_{\mathrm{b0}}^{\perp\mathrm{b}} = -\frac{V_{\mathrm{b}}\,i_{\mathrm{aq+}}}{4\sqrt{2}\,V_{\mathrm{a}}} \text{ if } MI_1 = I_{\mathrm{b0}}^{\mathrm{b}}, \text{ or } \textbf{Source = 1Ph} \tag{2.69}$$

(2.68) and (2.69) are irrelevant for the unequal frequency operation because the three-phase and single-phase voltages and currents do not make average arm powers or in other words the three-phase and single-phase systems are naturally decoupled.

A.9.8 Currents and Average Arm Powers for Method-7 and Method-12

The arm energy balancing Method-7 and Method-12 are the only two arm energy balancing methods that do not inject harmonics into source and load currents and are stable for both equal ($f_{\mathrm{b}} = f_{\mathrm{a}} \neq 0$) and unequal ($f_{\mathrm{b}} \neq f_{\mathrm{a}}$) input and output system frequencies.

Referring to Table 2.2, the selected six degrees of freedom or *Manipulated Inputs* (MI) for Method-7 and Method-12 are ($i_{\mathrm{ad+}}$, $i_{\mathrm{bd+}}$, $i_{\mathrm{b}\alpha\beta}^{\mathrm{b}}$, & $i_{\mathrm{b}\alpha\beta}^{\mathrm{cm}}$) and ($i_{\mathrm{b0}}^{\mathrm{b}}$, $i_{\mathrm{bd+}}$, $i_{\mathrm{b}\alpha\beta}^{\mathrm{b}}$, & $i_{\mathrm{b}\alpha\beta}^{\mathrm{cm}}$), respectively. Both methods use the same five degrees of freedom ($i_{\mathrm{bd+}}$, $i_{\mathrm{b}\alpha\beta}^{\mathrm{b}}$, & $i_{\mathrm{b}\alpha\beta}^{\mathrm{cm}}$) for regulation of the total upper and lower arms energies ($\bar{w}_{\Delta 0}$), summation phase energies ($\bar{w}_{\Sigma\alpha\beta}$), and difference phase energies ($\bar{w}_{\Delta\alpha\beta}$). Only the first manipulated input (MI_1) to regulate the total arm energy ($\bar{w}_{\Sigma 0}$) of MMC is different. The three-phase active power helps to balance $\bar{w}_{\Sigma 0}$ by controlling the positive sequence three-phase current in the d-axis ($i_{\mathrm{ad+}}$) for Method-7. The single-phase active power regulates $\bar{w}_{\Sigma 0}$ by controlling the zero-sequence circulating current in phase with v_{b} ($i_{\mathrm{b0}}^{\mathrm{b}}$) for Method-12.

(4.1) to (4.5) represent the general expressions of the instantaneous three-phase ($i_{\mathrm{a}\alpha\beta}$), circulating ($i_{\mathrm{b}\alpha\beta}$), and single-phase ($i_{\mathrm{b0}}$) currents for Method-7 and Method.12, including the selected six degrees

of freedom, the load active power component (i_{ad+} or i_{b0}^{b}), and two reactive current components (i_{aq+} and $i_{b0}^{\perp b}$), respectively.

$$i_{a\alpha} = i_{ad+}\cos(\theta_a) - i_{aq+}\sin(\theta_a) \tag{4.1}$$

$$i_{a\beta} = i_{aq+}\cos(\theta_a) + i_{ad+}\sin(\theta_a) \tag{4.2}$$

$$i_{b\alpha} = i_{bd+}\cos(\theta_a) + \sqrt{2}I_{b\alpha}^{cm}\cos(\theta_{cm}) + \sqrt{2}I_{b\alpha}^{b}\cos(\theta_b) \tag{4.3}$$

$$i_{b\beta} = i_{bd+}\sin(\theta_a) + \sqrt{2}I_{b\beta}^{cm}\cos(\theta_{cm}) + \sqrt{2}\,I_{b\beta}^{b}\cos(\theta_b) \tag{4.4}$$

$$i_{b0} = \sqrt{2}I_{b0}^{\perp b}\sin(\theta_b) + \sqrt{2}I_{b0}^{b}\cos(\theta_b) \tag{4.5}$$

(4.6) to (4.12) represents the simplified expression of the average arm power equations in the αβ0-frame for equal frequency operation ($f_b = f_a \neq 0$) considering only the selected six degrees of freedom, reactive current components (i_{aq+} and $i_{b0}^{\perp b}$), and load active power current component (i_{ad+} or i_{b0}^{b}). (4.6) to (4.12) are obtained by substituting (4.1) to (4.5) in the instantaneous arm power equations from (2.17) to (2.22), finding average and simplifying them. The frequency for mean calculation is $f_{Mean} = f_a$ for equal frequency operation ($f_b = f_a \neq 0$).

$$\overline{P_{\Sigma 0}} = \frac{V_a}{\sqrt{2}}i_{ad+} + \overline{v_b\, i_{b0}} \quad \text{for Method-7} \tag{4.6}$$

$$\overline{P_{\Sigma 0}} = V_b\, I_{b0}^{b} + \overline{\frac{v_{a\alpha}\, i_{a\alpha} + v_{a\beta}\, i_{a\beta}}{2}} \quad \text{for Method-12} \tag{4.7}$$

$$\overline{P_{\Delta 0}} = -\sqrt{2}\, V_a\, i_{bd+}\, \overline{-v_{a\alpha}\, i_{b\alpha}^{b} - v_{a\beta}\, i_{b\beta}^{b}} \tag{4.8}$$

$$\overline{P_{\Sigma\alpha}} = V_b\, I_{b\alpha}^{b} + \overline{v_b\, i_{bd+}\cos(\theta_a)} \tag{4.9}$$

$$\overline{P_{\Sigma\beta}} = V_b\, I_{b\beta}^{b} + \overline{v_b\, i_{bd+}\sin(\theta_a)} \tag{4.10}$$

$$\overline{P_{\Delta\alpha}} = -2\, V_{cm}\, I_{b\alpha}^{cm}\, \overline{-\frac{v_b\, i_{a\alpha}}{2} - 2\, v_{a\alpha}\, i_{b0} - v_{a\alpha}\, i_{b\alpha}^{b} + v_{a\beta}\, i_{b\beta}^{b}} \tag{4.11}$$

$$\overline{P_{\Delta\beta}} = -2\, V_{cm}\, I_{b\beta}^{cm}\, \overline{-\frac{v_b\, i_{a\beta}}{2} - 2\, v_{a\beta}\, i_{b0} + v_{a\alpha}\, i_{b\beta}^{b} + v_{a\beta}\, i_{b\alpha}^{b}} \tag{4.12}$$

A.10 Eidesstattliche Versicherung

Ich versichere eidesstattlich durch eigenhändige Unterschrift, dass ich die Arbeit selbstständig und ohne Benutzung anderer als der angegebenen Hilfsmittel angefertigt habe. Alle Stellen, die wörtlich oder sinngemäß aus Veröffentlichungen entnommen sind, habe ich als solche kenntlich gemacht.

Die Arbeit ist noch nicht veröffentlicht und ist in gleicher oder ähnlicher Weise noch nicht als Studienleistung zur Anerkennung oder Bewertung vorgelegt worden. Ich weiß, dass bei Abgabe einer falschen Versicherung die Prüfung als nicht bestanden zu gelten hat.

Rostock	15.12.2023	
	(Abgabedatum)	(Vollständige Unterschrift)

Thank you very much for reading this work